Liquid crystalline network phases for charge carrier materials

Dissertation

zur Erlangung des Doktorgrades der Naturwissenschaften
(Dr. rer. nat.)

der

Naturwissenschaftlichen Fakultät II
Chemie, Physik und Mathematik

der Martin-Luther-Universität
Halle-Wittenberg

vorgelegt von

Herrn Ohjin Kwon
geb. am 29.01.1985 in Seoul (Republik Korea)

Gutachter
1.) Prof. Dr. Carsten Tschierske
2.) Prof. Dr. Rudolf Zentel

Datum der Verteidigung: 29.09.2021

Acknowledgement

Here, I would like to appreciate the help, support and encouragement of people. Without them, it would have not been possible to finish this long journey.

First of all, I would like to thank my wife Vanesa Nuñez, my children, my parents and my parents in law for endless encouragement and support.

I sincerely appreciate my supervisor, Prof. Dr. Carsten Tschierske for giving me the opportunity to work under his supervision. It was a great honor. He gave me plenty of scientific knowledge and ideas through countless discussions.

I also appreciate Prof. Feng Liu (Xi'an Jiaotong University) for the discussions and the X-ray studies.

I am also grateful to Dr. Silvio Poppe for the additional XRD measurements, to Prof. Dr. Gorecka and Dr. Szydłowska for the TOF measurements and for advising me in this technique, to Prof. Dr. Dong Ki Yoon and Moon Jong Han for the OFET measurements, to Elke Neubauer and Roy Gyger for the DSC measurements, to Susanne Tanner for the ESI-MS measurements and to Matthias Wagner for the CD measurements.

Contents

Abbreviations

Φ	Twist angle between adjacent molecules in the networks of the Cub_{bi} phases
1D	One dimensional
2D	Two dimensional
3D	Three dimensional
a_{cub}	Lattice parameter of cubic phase
a_{hex}	Lattice parameter of hexagonal columnar phase
a_{tet}	Lattice parameter of tetragonal phase
BTBT	[1]Benzothieno[3,2-b]benzothiophene
BTBT-Br	2-Bromo[1]benzothieno[3,2-b][1]benzothiophene
BTBT-Br$_2$	2,7- Dibromo[1]benzothieno[3,2-b][1]benzothiophene
Col$_{hex}$	Hexagonal columnar phase
Col$_{biax}$	Biaxial columnar phase
Cr	Crystalline
Cr$_{Iso}$[*]	Optically isotropic crystalline mesophase with chiral conglomerate texture
Cub	Cubic
Cub$_{bi}$	Bicontinuous cubic phase
Cub$_{bi}$[*]	Bicontinuous cubic phase with chiral conglomerate texture
d_{net}	Lateral distance between the nets in the Ia3̄d phase
DCM	Dichloromathane
DMF	N,N-Dimethylformamide
DMSO	Dimethyl sulfoxide
DSC	Differential scanning calorimetry
EDM	Electron Density Map
Et$_2$O	Triethylamine
Iso	Isotropic phase
L_{net}	Total length of the netwoks per unit cell
LC	Liquid crystal
LCD	Liquid crystal display
M$_H$	Highly birefringent 3D mesophase
M$_L$	Lowly birefringent 3D mesophase
MeOH	Methanol
N	Nematic phase
n_{cell}	Number of molecules per unit cell

n_{raft}	Number of molecules organized in each tick raft of the columns
NMP	N-Methyl-2-pyrrolidone
OSC	Organic semiconductor
OPV	Organic photovoltaic
POM	Polarized optical microscopy
SAXS	Small angle X-ray scattering
SmA	Smectic A phase
SmC	Smectic C phase
SmC[*]	Smectic C phase showing a conglomerate of chiral domains
TBAI	Tetrabutylammonium iodide
THF	Tetrahydrofuran
V_{cell}	Volume of the unit cell
V_{mol}	Volume of the molecule
WAXS	wide angle X-ray scattering
XRD	X-ray powder diffraction

1. Introduction and motivation

1.1 Introduction

Liquid crystal (LC) science has been developed since Friedrich Reinitzer observed a double melting point of cholesterol benzoate in 1888. Due to its fascinating properties, it triggered numerous scientists. It resulted in a rapid development of liquid crystal displays (LCDs) which have totally replaced cathode ray tube displays. Nobody would deny that the development has completely revolutionized our society.[1] Besides LCDs, there are other promising application fields: organic semiconductor for photovoltaics,[2] steerable antennas in SATCOM and 5G communication systems,[3] responsive materials for biosensor applications,[4] active matter,[4] and photonic applications.[5,6] It is because liquid crystal is characterized by an extensive range of remarkable phenomena which depend on the subtle balance between its order and fluidity.[1]

The solar-cell is not only an eco-friendly but also renewable energy source which has a big potential to substitute petroleum and coal. The technology replacing petroleum and coal would give the Third World countries abilities to develop by themselves. Even though the solar cells have great potential as emission-free energy sources, the technology was still too expensive (inorganic based semiconductors) compared to fossil fuel-based energy generating system.[7] However, most of organic compounds can be efficiently produced with a continuous mass production through printing and coating from solution,[8] and furthermore, they can be modified easily and diversely based on organic chemistry.[7] In addition, organic semiconductors (OSCs) have not only inherent light weight and flexibility, but also possibility of tuning color and transparency, and thus, they can be applied in a much wider variety of places.

Since the first device incorporating an organic semiconductor with melanins in 1974,[9] materials for organic semiconductors have been investigated and have shown great performances and intriguing features.[10-14] As a new candidate, liquid crystals received a great attention as a self-organizing molecular semiconductor.[15-18] The potentials have been proved by studying calamitic and discotic liquid crystals forming smectic and columnar phases. In this research, we will focus on polycatenar mesogens using [1]benzothieno[3,2-b][1]benzothiophene (BTBT), leading to

mesogens with expanded π-conjugated systems, forming curious thermotropic bicountinuous cubic phases.

1.2 Liquid cystal self-assembly

Liquid crystalline phases occur at the transition from the highly ordered crystalline solid (Cr) to the disordered isotropic liquid state (Iso).[19] Therefore, the LC state can be defined as a disordered solid or an ordered liquid because LC occurring in distinct temperature ranges, combine the long range order of crystalline materials with the mobility of fluids.[20] Typical LC compounds are composed of rigid and flexible parts, resulting in both order and mobility of its structure at the same time. The rigid parts align in a preferred direction and due to the high mobility of the flexible part, its configuration can be changed by external stimuli (surfaces, electric, magnetic and mechanical fields).[21] Not only the molecules with rigid and flexible part, but also molecules composed of two mutually incompatible segments (amphiphilic mesogens: hydrophilic and hydrophobic) lead to the formation of distinct nanometer-scale order on a one-dimensional, two-dimensional, or three-dimensional periodic lattice.[21] Therefore, the rigidness, mobility, anisometricity and supramolecular structures influence the order of LCs. Based on the degree of order, it leads to orientational long-range order in the nematic phases or different types of liquid crystal phases such as smectic, columnar and cubic phases due to emerging positional long-range order.[19,22]

In general, the conventional LCs are observed when the molecular shape is a long rod or a flat disk. As the temperature decreases, the interaction forces between the molecules increase due to the decreased thermal motion. Then, the anisotropic LC molecules (rod-like molecules) tend to align parallel side by side to reduce the free space between them.[23] The figure 1.1 shows the models of organization in the different LC phases. When the molecules retain only orientational order without any positional order (Fig. 1.1b), the LC phase is called nematic phase (N). The molecules in a nematic phase are aligned in a specific direction, but there is no periodicity (positional order). Due to the lack of positional order, a nematic phase ordinarily appear with low viscosity like a liquid. The Fig. 1.2b shows a typical texture of a nematic phase exhibiting schlieren

texture with declinations and inversion walls. The point declinations appear with two or four brush defects in the nematic phase.[24]
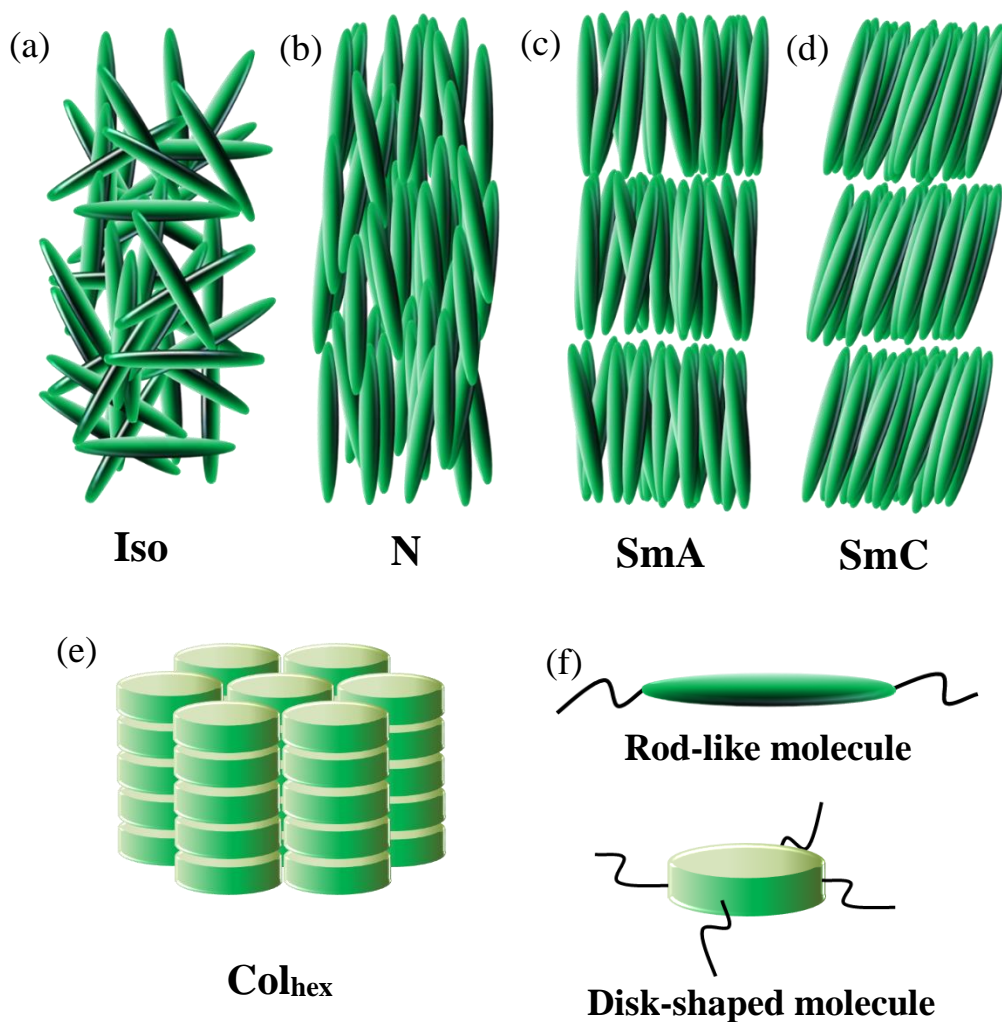
Figure 1.1 Models of the organization of conventional LC phases; a) isotropic liqud (Iso), b) nematic phase (N), c) smectic A phase (SmA) and d) smectic C phase (SmC) formed by rodlike (calamitic) molecules; e) hexagonal columnar phase (Col$_{hex}$) formed by disk shaped or polycatenar molecules. f) Models of rod-like and disk-shaped molecules with rigid aromatic core and flexible aliphatic chanis.

The addition of positional order leads to smectic phases.[19] Due to the chemically incompatible segments (rigid aromatic core and flexible aliphatic side chains) of the molecules, they preferably aggregate into layered structure when the volume ratio of the incompatible parts is in a certain range which allows their interfaces to develop. In the smectic A phase (SmA), the molecules are oriented on average along the layer normal (Fig. 1.1c) but the molecules in the

smectic C phase (SmC) are tilted with respect to the layer normal (Fig. 1.1d). The typical texture of SmA shows homeotropic regions (black areas) in which the orientation of the layers is parallel to the substrate (homeotropic alignment), focal-conics and polygonal defects in regions where the layers are organized perpendicular to the surfaces (planar alignment)[24](Fig. 1.2b). Instead, the texture of SmC shows broken focal-conic textures in planar alignment and schlieren texture with only four brush declinations in the homeotropic alignment.[24] (see figure 2d). In addition, some modifications of the molecular structure such as disk-like can lead to different phases. The disk-like structure helps the molecules to be stacked up, and thus, they predominantly form columns which align parallel and exhibit columnar phases in most cases with hexagonal 2D-lattice (Col_{hex}) (Fig. 1.1e). The typical texture of Col_{hex} contains birefringent spherulites and dark homeotropic regions (Fig. 1.2c). All of the textures are investigated by polarized optical microscopy (POM) with completely crossed polarizer to see the birefringence well. Chiral LC phases formed by chiral molecules show different textures, as for example known for the chiral nematic phase.[25] In recent work it was shown that chirality can also emerge spontaneously in LC phases of achiral molecules.[69] In this case a conglamerate of chiral domains is often observed. However, to confirm the chirality of these phases via POM, investigation with slightly uncrossed polarizer is used to detect chiral domains by a change of the brightness after rotating the analyzer either clockwise or anticlockwise out of the crossed orientation (see Fig 1.2e,f). Normally it is extremely difficult to investigate the chirality of any birefringent phase because the brightness from birefringence is much stronger than the effects of chirality. In contrast, the chirality of optically isotropic LC phases such as cubic phases, can be easily investigated because they exhibit no birefringence.
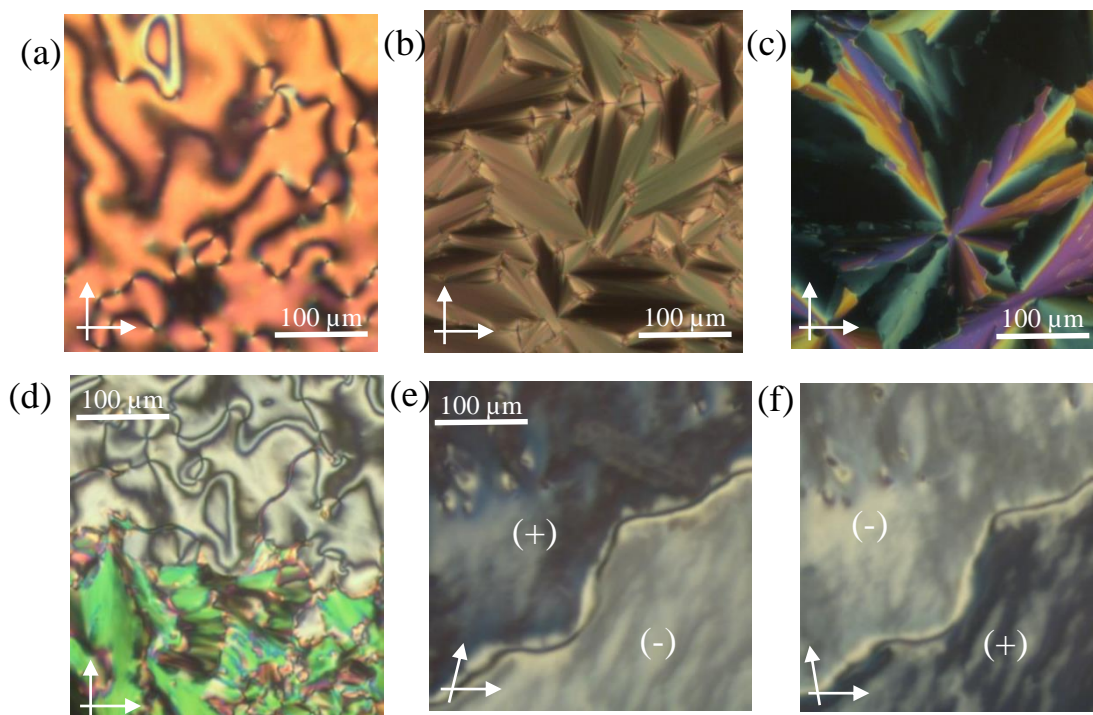
Figure 1.2 Representative textures; a) nematic (N); b) smectic A (SmA); c) hexagonal columnar phase (Col$_{hex}$); d-f) synclinic smectic C (SmC$^{[*]}$) phase showing a conglomerate of chiral domains in the low birefringent homeotropic areas with helical organization of the molecules (helix axis is parallel to the direction of view).[25]

1.3 Bicontinuous cubic phases

The structures of conventional LCs such as N, SmA, SmC and Col can be relatively easily understood because they are highly related to the molecular shape of their constituent molecules.[26] However, the structures of cubic (Cub) LCs are not simple to understand because they have a three-dimensional (3D) lattice and it is difficult to predict the change of the 3D structure derived from the molecular shape of their constituent molecules due to lack of knowledge.[26] The cubic phases mainly can be divided into two types.[26] One is the micellar type, which is discontinuous (Cub$_{sph}$) and made of arrangements of spherical or non-spherical micelles in a cubic lattice. The other one is a bicontinuous cubic phase (Cub$_{bi}$) which is made up of interpenetrating networks on a cubic lattice. It was first observed for lyotropic LC phases of amphiphilic molecules depending on the concentration of water or another solvent.[27,28] Cub$_{bi}$ phases can be also found in solvent free systems. Fig. 1.3 shows the phase sequence of amphiphiles by increasing the size of either polar or non-polar units. The volume ratio of the two incompatible segments (polar and non-polar)

determine the mesophase type by altering the curvature of the intefaces between the nano-segregated aggregates of the polar and apolar molecular segments. When the volume ratio is relatively close to one, it forms a lamellar phase (SmA). If the size of one segment becomes bigger, a curvature of these interfaces emerges. The curvature can be controlled by changing the volume ratio of incompatible segments which leads to the sequence SmA-Cub_{bi}-Col_{hex}-Cub_{dc} by the growth of curvature, i.e. the Cub_{bi} phases represent intermediate phases at the lamellar-columnar transitions.[27] Cub_{bi} phases contain nano-segregated networks of one component in the continuum of the other component,[29] and thus, it can build continuous conduction channels in all three spatial directions.[30] Thanks to the junctions in cubic phases, they can provide abundant transport routes for ions (ionic amphiphiles), electrons or holes (rod-like or disk-like LCs). Thus, these 3D-Networks minimize distortions induced by structural defects in lamellar (1D) and columnar strructures (2D), as recently demonstrated for ion carrying ionic amphiphiles.[31] This suggests that the Cub_{bi} phase involving π-conjugated units could have a high potential as a good candidate for organic semiconductors.
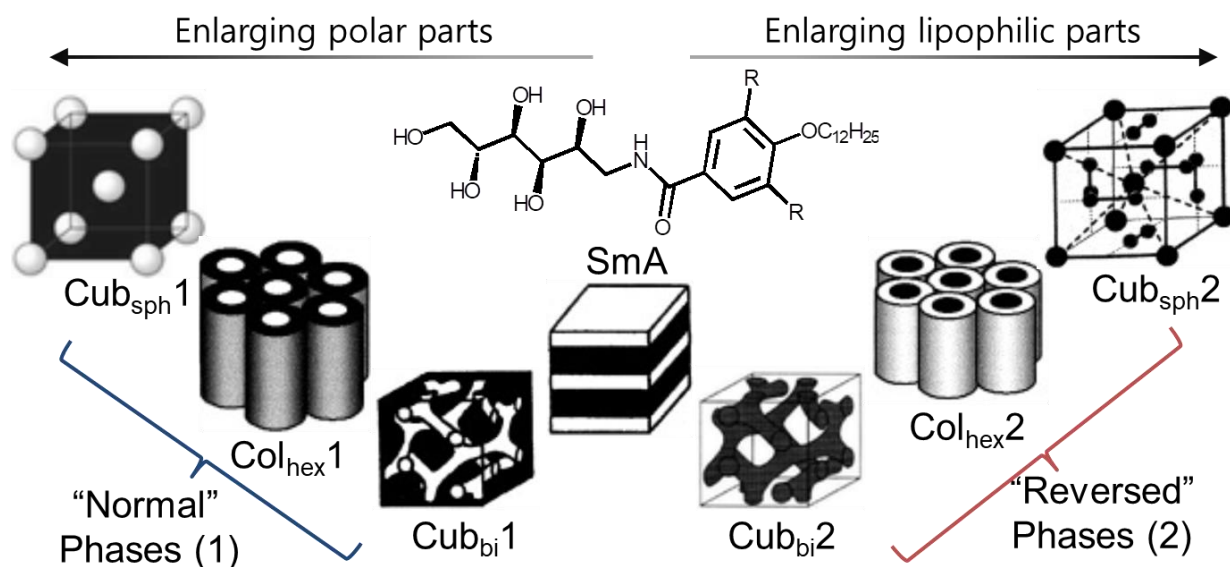
Figure 1.3 The general phase sequence of amphiphilic molecules as obtained by changing the volume fraction of the incompatible molecular segments (black indicates the polar parts, white the lipophilic parts)[27,32]; Cub_{bi} = bicontinuous cubic mesophase involving interpenetrating networks of branched columns, Cub_{sph} = discontinuous cubic mesophase formed by spheroidic aggregates; The formula shows an amphiphilic carbohydrates as example, which forms the sequence SmA → $Cub_{sph}2$. This was reproduced with permission from ref. 32, Copyright WILEY-VCH 2002.

Though thermotropic Cub_{bi} phases can be expected for taper-shaped amphiphiles, they were also found for rod-like mesogens in some cases. The history of thermotropic Cub_{bi} phases was started from the synthesis of 4′-n-alkoxy-3′-nitrobiphenyl-4-carboxylic acids ANBC-n with X=NO_2 by Gray et al. in 1957 [33] and the dibenzoylydrazines (BABH-ns) by Demus et al. in 1978, [40] (Fig. 1.4) even though their structures were not solved at that time.[34] The rod-like molecules such as ANBC-ns (**1**)[35-38,43] and BABH-ns (**2**)[39-43,] (Fig. 1.4) are consisted of aromatic and aliphatic units which are incompatible to each other and polar functional groups such as –NO_2, -CN or –COO- groups which induce a strong dipole moment. Since they retain rod-like molecular shape, smectic phases occur typically, but Cub_{bi} phase also appears due to the strong intermolecular interaction induced by the functional groups.[26] The aromatic cores are organized in the networks and the flexible alkyl chains are filled between them. Depending on the type of Cub_{bi} phases, there are one, two, or three continuous interwoven networks in a continuum. "Bicontinuous" stands for (continuous) networks + continuum, regardless of the number of networks.[43] The thermotropic Cub_{bi} phases will be the focus in this research. The most common thermotropic Cub_{bi} phase is with $Ia3d$ space group ($Cub_{bi}/Ia3d$).[26,43] In the $Cub_{bi}/Ia3d$ phase, molecules form two infinitive networks with three-way junctions with opposite chirality (the double gyroid, Fig. 1.5a,b), and thus, the $Cub_{bi}/Ia3d$ phase is always achiral and optically inactive.[43-47] Besides $Ia3d$ there is a second common Cub_{bi} phase, which was assumed to have the $Im3m$ space group which has a more complex structure and a larger lattice parameter than $Ia3d$.[29] Various models were suggested entailing three minimal surfaces, three networks or integrating spherical aggregates with two networks.[43,48-50] Recently a model with chiral $I23$ space group involving three networks was proposed.[51] All the networks have exclusively three way junctions as also found for the $Cub_{bi}/Ia3d$ phase. Single network structures have only recently been detected with bolapolyphiles.[52] Due to the cubic symmetry, Cub_{bi} phases are isotropic like ordinary liquids. Because they are optically isotropic, they do not show any linear birefringence, and thus, optical activity and mirror symmetry breaking could easily be discovered by the investigation under slightly uncrossed polarizer.[71] Cubic phases could be distinguished from the isotropic liquids by shearing the phase because the 3D-structured LCs such as Cub_{bi} phases, in contrast to the liquids, exhibit high viscosity. Moreover, the X-ray diffraction (XRD) patterns of Cub_{bi} phases show series of sharp small angle diffractions, whereas for a liquid there is only a diffuse small angle scattering.
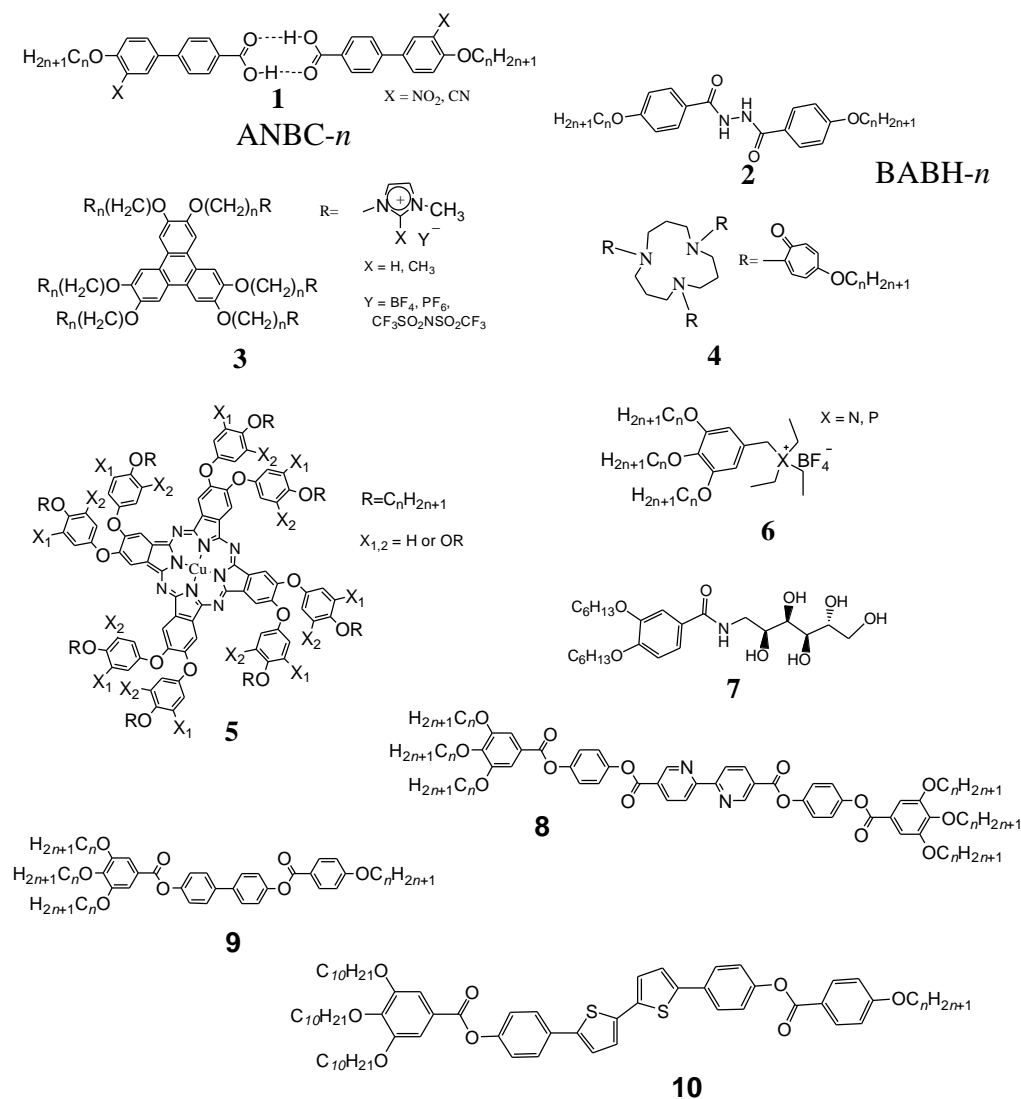
Figure 1.4 Representative molecules forming thermotropic Cub$_{bi}$ phases: **1,2** rod-like LCs, **3-5** disk-like molecules, **6,7** taper-shaped amphiphiles and **8-10** polycaternar molecules.
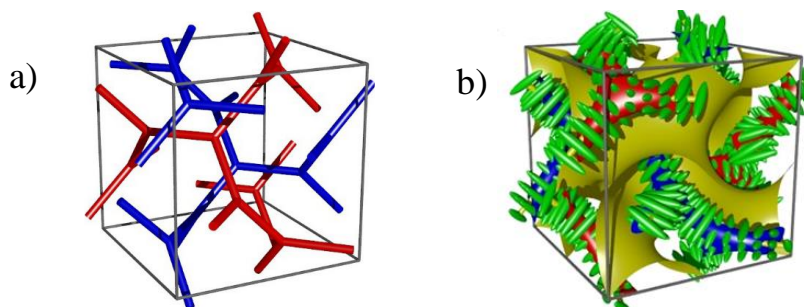
Figure 1.5 a) A schematic showing the networks of the Cub$_{bi}$/*Ia3d* phase; b) a model of the organization of the molecules (green rods) in the helical networks forming the Cub$_{bi}$/*Ia3d* phase in the saddle-splay minimal surface between the networks is shown in yellow.[51,53]

Disk-like molecules such as **3**[54-57], **4**[58,] **5**[59] in Fig. 1.4, predominantly tend to form columnar phases instead of smectic phases due to the shape of molecular structure. The molecular structure and the incompatibility of aromatic and aliphatic (the peripheral chains) units help the aromatic cores stacking up along the columns. Disk-like molecules also build another Cub_{bi} phase with *Pn*3*m* symmetry (Cub/*Pn*3*m*). The Cub/*Pn*3*m* phase compose of two pairs of interpenetrating networks involving four-way junctions[26,59] (see Fig. 1.6 a,b[59]), leading to the double diamond structure.

a)   b)
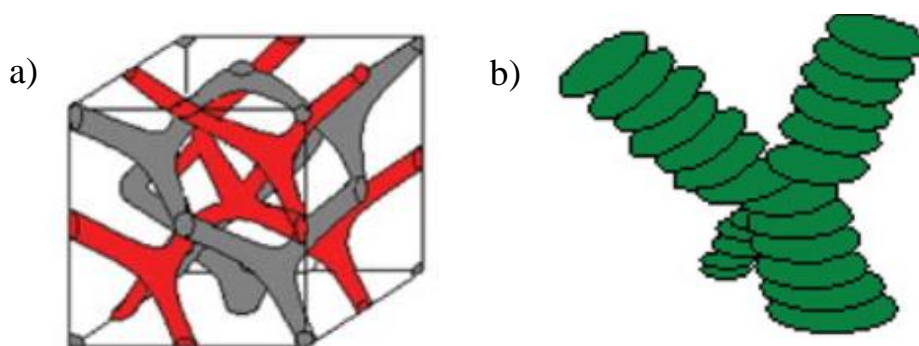
Figure 1.6 a) Schematic showing the double diamond networks and b) scaled up model of a junction in the Cub_{bi}/*Pn*3*m* phase. (a,b) were reproduced with permission from ref 59, Copyright Taylor & Francis 2007.

To investigate the Cub_{bi} phase more in detail, various new compounds were synthesized and analyzed such as fan-shaped molecules like **6**[31,60-62], **7**[63-65], symmetric hexacatenars **8**[66] and non-symmetric tetracatenars **9**[67,68] in Fig. 1.4. In addition, the newly designed bithiophene based non-symmetric achiral tetracatenar (**10**, Fig. 1.4) were reported[69] to form mirror symmetry broken $Cub_{bi}^{[*]}$ phases and isotropic liquids ($Iso_1^{[*]}$) forming conglomerates of chiral domains (see Fig. 1.7g,h). In the Cub_{bi} phases of the polycatenar molecules the aromatic cores show a tendency to organize themselves parallel to each other and perpendicular to the networks but they cannot align perfectly parallel because of the bulky terminal chains.[70,71] The collision of bulky terminal chains lead the achiral rod-like molecules to assume a helical twist along the networks (see Fig. 1.7a,b), resulting in spontaneous mirror symmetry breaking in some of the Cub_{bi} phases, namely in the *I*23 phase.[29,72] In contrast to the double network *Ia*3*d* phase where the chirality and helicity in the two networks is opposite and thus cancels out, the Cub_{bi} phase with *I*23 space group involves three

networks and therefore chirality cannot cancel, and therefore, it is intrinsically chiral (See Fig. 1.7c).[29,43,45,73,74]
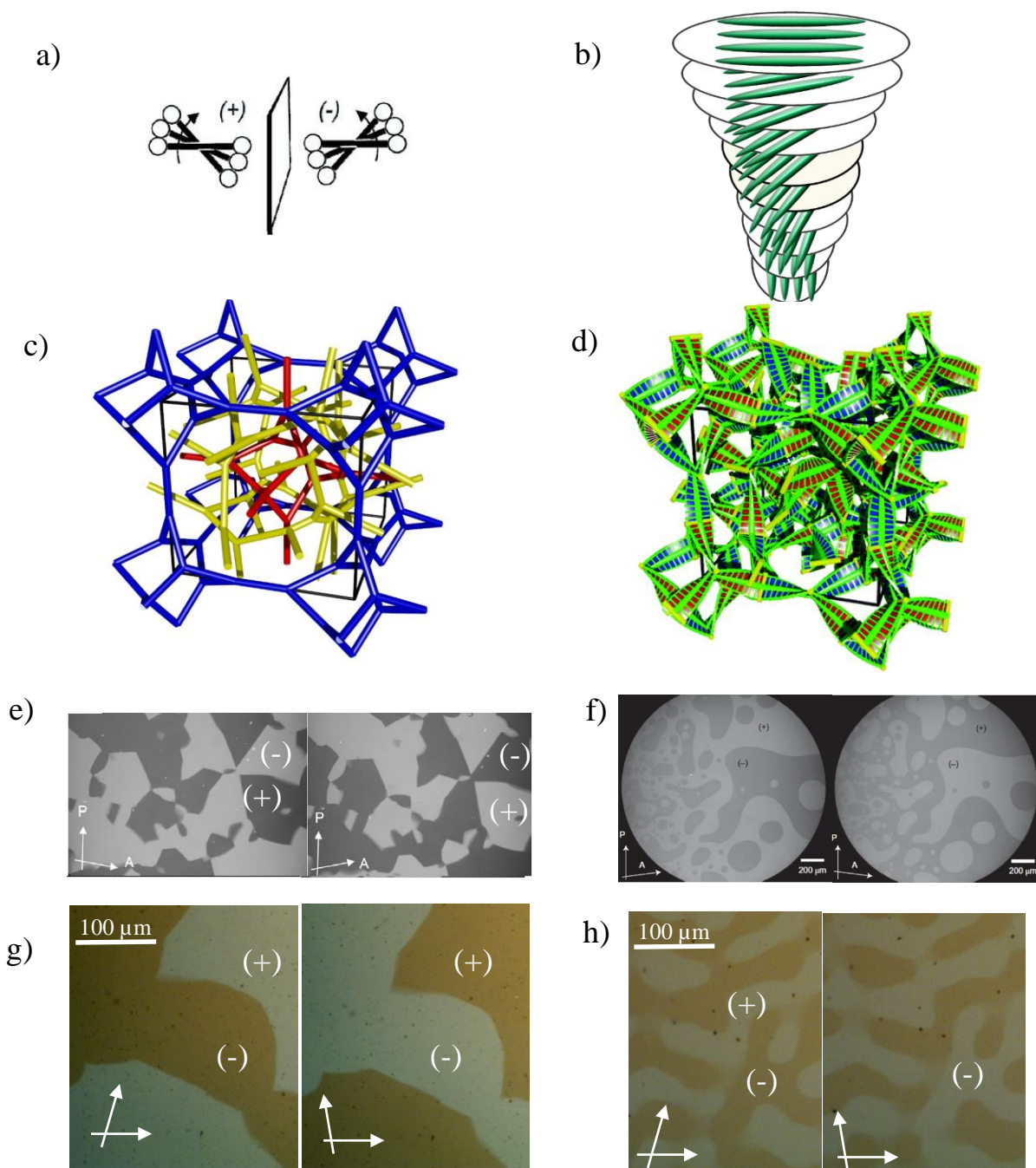
Figure 1.7 a) helical twist developing along the networks[45,53] caused by clashing of bulky aliphatic end units; b) helical structure of the rafts along the networks; c) a schematic showing the networks of the $Cub_{bi}^{[*]}/I23$ phase[51,53]; d) a model of the organization of the molecules (red and blue strips) in the helical networks forming the $Cub_{bi}^{[*]}/I23$ phase;[51,53] e-h) chiral domains of e[29],g) $Cub_{bi}^{[*]}/I23$ and f[69],h) $Iso_1^{[*]}$. e) was reproduced with permission from ref. 29, Copyright WILEY-VCH 2014.f) was reproduced with permission from ref 69, Copyright Nature Research 2014.

An especially exciting feature of polycatenars is their ability to show mirror symmetry breaking also in the isotropic liquid state. On heating the $I23$ phase the helical organization is retained in local clusters even during the transition to the isotropic liquid state, leading to a liquid polyamorphism involving a mirror symmetry broken liquid ($Iso_1^{[*]}$).[71,75] The other way around, cooling from the achiral Iso phase leads to the development of helical networks. At the transition to $Iso_1^{[*]}$ the chirality synchronization between the networks becomes long range, but without formation of a long range cubic lattice. Further cooling of $Iso_1^{[*]}$ then leads to an achiral $Cub_{bi}/Ia3d$ or a chiral $Cub_{bi}^{[*]}$ phase with $I23$ symmetry ($Cub_{bi}^{[*]}/I23$) depending on the aliphatic chain lengths.[29]

1.4 Mirror symmetry breaking in liquids and liquid crystals

Molecules are normally divided into chiral or achiral. Molecules which cannot be superimposed onto their mirror images are chiral.[76,77] Any molecule containing at least four different atoms can in principle adopt chiral conformations or configurations.[70,77] Molecules are counted as transiently chiral when the enantiomerisation barrier is low compared to kT, so that they coexist in a thermodynamic equilibrium. Molecules are counted as permanently chiral when the enantiomerisation barrier is sufficiently high ($>>kT$) that no enantiomerisation takes place at the given conditions.[70,77,78] For permanently chiral molecules it is known that in the crystalline state they can form racemate or conglomerates depending on the preferred inter-enantiomer interactions. Only in the case of a preferred packing of identical enantiomers conglomerate formation with local breaking of mirror symmetry can be observed.

As mentioned above, spontaneous mirror symmetry breaking and conglomerate formation was recently also found in the liquid state ($Iso_1^{[*]}$) and interpreted as a spontaneous chirality synchronization of chiral conformers in helical aggregates.[69,74,79] For polycatenars with a benzil unit **BD** (see Fig. 1.8a) the transition between the ordinary isotropic liquid state (Iso), assumed to be formed by individual molecules or small clusters, and the Cub_{bi} phases were studied in more detail. Distinct phase transitions from Cub_{bi} via Iso_1 to Iso on heating and from Iso via Iso_1 to $Iso_1^{[*]}$ to Cub_{bi} on cooling were observed, as indicated by endotherms and exotherms in the DSC traces of **BD** in Fig. 1.8b. On cooling from the isotropic liquid (Iso), nucleation of the molecules
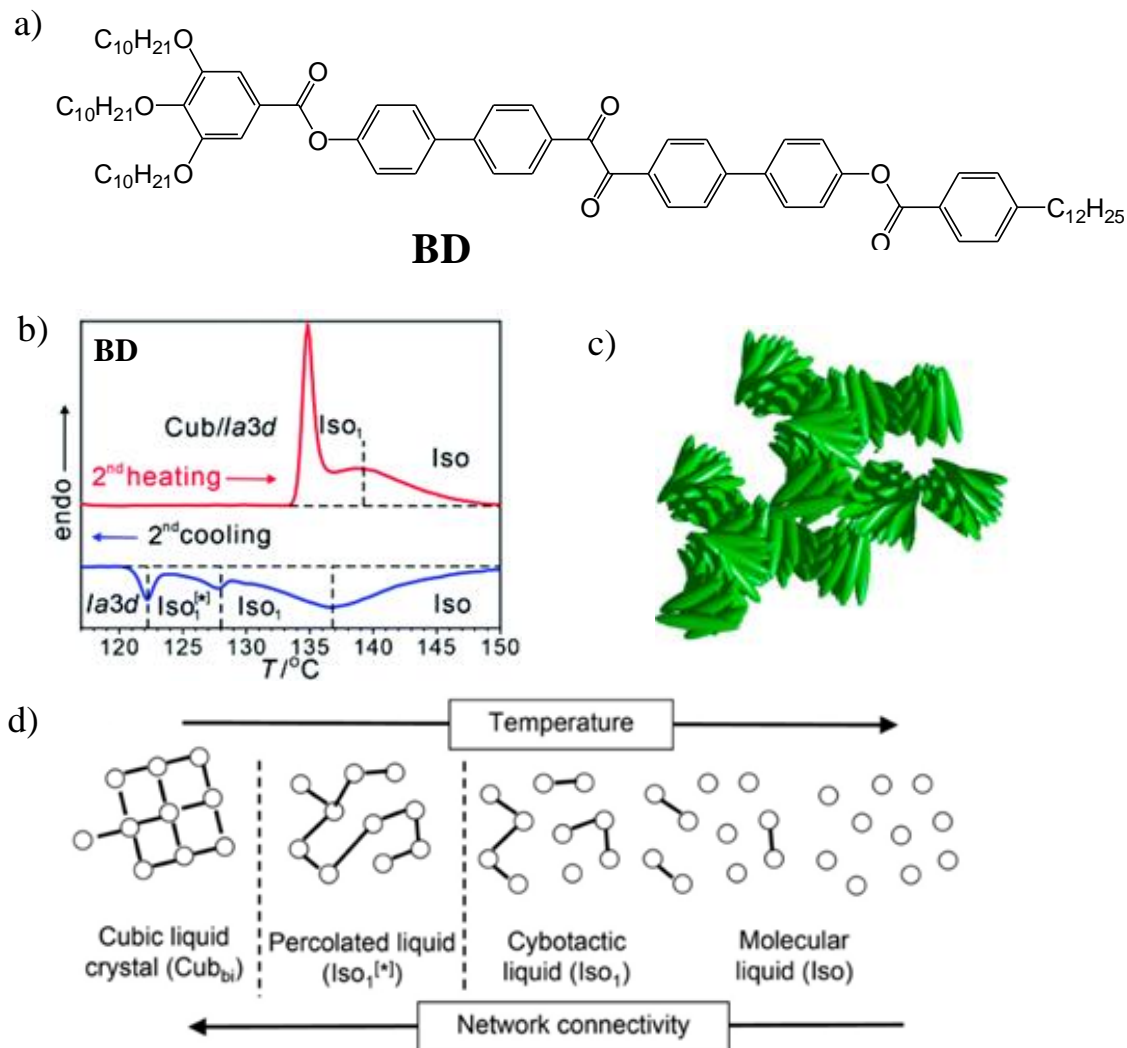
Figure 1.8 a) Molecular structure of polycatenar compound involving a benzil (**BD**); b) DSC traces of **BD** (10 K min^{-1}); c) sketch of the helical clusters in Iso$_1$[*] phase; d) schematic sketch of transition from Cub$_{bi}$ phase to the isotropic liquid state (Iso).[74] (b-d) were reproduced from ref 74, Copyright The Royal Society of Chemistry 2020.

occurs and they grow by forming small clusters of short helix fragment as Fig 1.8c shows.[71] This temperature rage below the broad DSC-feature is considered as cybotatctic isotropic liquid with a fluctuating local network structure (Iso$_1$)[74,79] (see Fig. 1.8d). By POM investigation, the cybotatic liquid Iso$_1$ has low viscosity and does not form any chiral domain like a normal liquid (Iso), and thus, it is impossible to distinguish it from Iso through POM. Further cooling leads to a small peak at the transition to the Iso$_1$[*] phase with mirror symmetry breaking.[74] It is proposed that at this transition the helical clusters fuse to dynamic networks in which chirality synchronization becomes long range in the liquid state. Upon further cooling the 3D-lattice develops at the

transition to Cub$_{bi}$.[71,74] It was suggested that the network formation is associated with transmission of helicity over macroscopic dimensions, leading to spontaneous mirror symmetry breaking in some of the isotropic liquid phase and in the triple-network Cub$_{bi}$[*] phase with $I23$ speace group.[29] As mentioned above, in the two networks of the $Ia3d$ phase the helix-sense is opposite and calcels out, thus the $Ia3d$ phase is achiral depite of the presence of a long range helical network structure.

1.5 Sequence of bicontinuous cubic phases

Further study related to the Cub$_{bi}$ phases showed an interesting phase transition sequence where the phase symmetry is changed upon increasing the aliphatic chain length or expansion of peripheral ring size as following: an achiral double gyroid $Ia3d$ phase, a chiral $I23$ phase and an achiral re-entrant $Ia3d$.[43,73]

Figure 1.9 a) Molecular structures of bithiophene based polycatenars with different ring structure; b,c,d,e) showing chiral domains of the $I23$ phase induced in the contact region between the two different $Ia3d$ phase types: $Ia3d_{(L)}$ and $Ia3d_{(S)}$; b,c) **R4** and **R12**[73], e) **A10** and **AH**[43]. (d,e) were reproduced with permission from ref. 43, Copyright WILEY-VCH 2020.

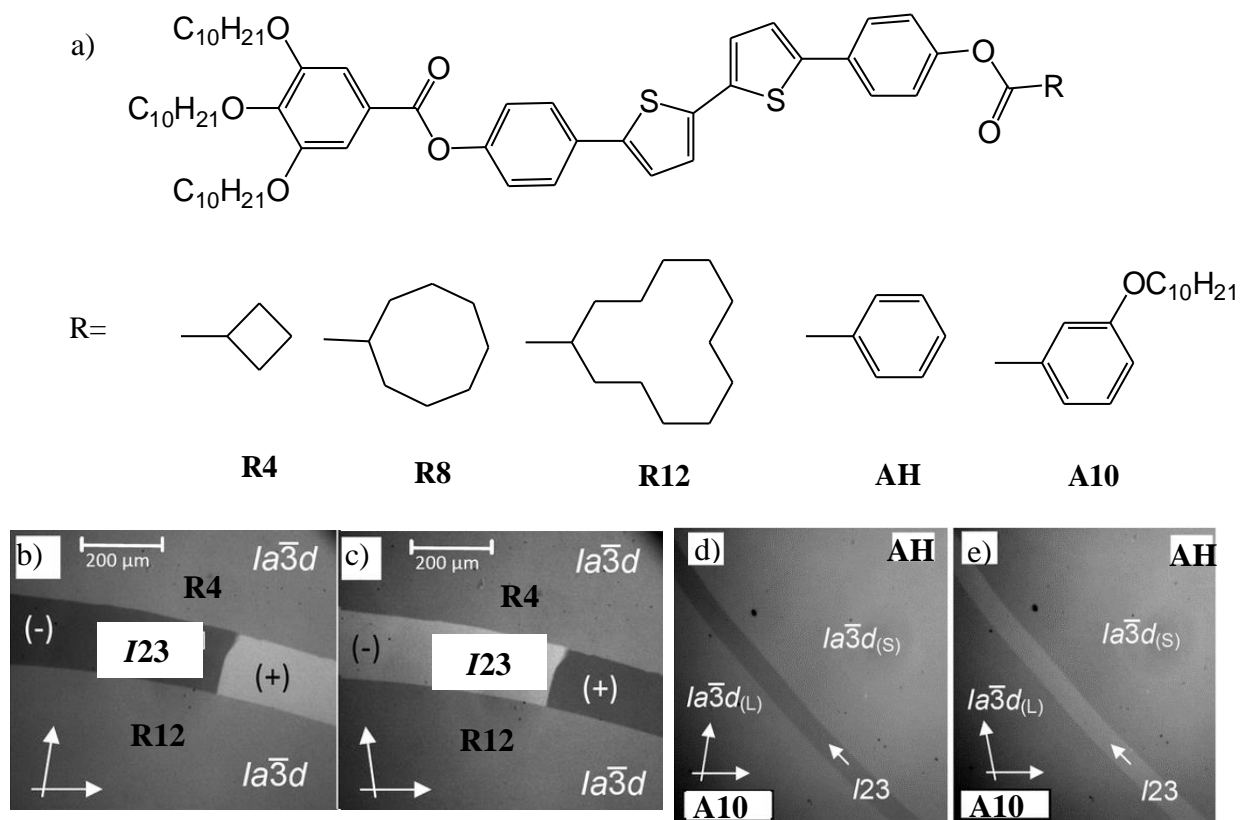Compound **R4** and **R12** in the series of **Rn**[73] exhibit $Cub_{bi}/Ia3d$ phases, in contrast, **R8** shows $Cub_{bi}^{[*]}/I23$. It proves that upon expanding volume of the peripheral unit, the phase sequence is changed as following: $Ia3d$ - $I23$ - $Ia3d$. Based on the XRD data, the lattice parameter of the $Ia3d$ phases of **R4** ($a_{cub} = 10.4$) and **R12** ($a_{cub} = 9.4$) are significantly different.[73] Moreover, in the contact region between the two compounds, chiral domains are formed, which are typical for an induced $Cub_{bi}^{[*]}/I23$ phase (see Fig. 1.9b,c). This proves that **R4** and **R12** form different $Ia3d$ phases: $Ia3d_{(L)}$ and $Ia3d_{(S)}$, respectively. The same phenomenon was reported between compounds **AH** ($a_{cub} = 10.8$) and **A10** ($a_{cub} = 9.8$) as shown in Fig. 1.9d,e.[43] Furthermore, based on the lattice parameter, the helical twist angle between adjacent molecules in the Cub_{bi} phases ($Ia3d^{29}$ and $I23^{51}$) can be calculated. The calculated twist angle Φ continuously increases with growth of apex volume of the peripheral units across the $Ia3d_{(L)}$-$I23$-$Ia3d_{(S)}$ transition.[43] While the helical twist becomes larger, the pitch length becomes shorter. As the helical pitch has to fit with the distance between the network junctions, this leads to a frustration of the $Ia3d_{(L)}$ phase, and thus, it is replaced by the triple network structure $I23$ phase. Upon further increasing helical twist, it leads to another mismatch in the $I23$ phase, and then it is replaced by another $Ia3d_{(S)}$ phase involving a shorter pitch.[43] Therefore, the sequence can be concluded as following: long pitch $Ia3d$ ($Ia3d_{(L)}$)-$I23$- short pitch $Ia3d$ ($Ia3d_{(S)}$).

1.6 Effect of fluorination on liquid crystals

In this research, fluorinated benzene is additionally studied to see the fluorination effect on Cub_{bi} and $Iso_1^{[*]}$ phase formation. Fluorinated benzene is an electron acceptor due to the high electronegativity and has increased bulkiness compared to the non-fluorinated. Thus, fluorine provides unusual properties to LC materials, for example, it can lead to ferroelectric nematic phase.[21,80] Due to the bigger size of fluorine compared to hydrogen, the flexibilities and molecule conformations are changed and the packing of the fluorinated molecules is affected by the increased steric hindrance.[21] Also the large dipole moment of the C-F bond has a significant influence.

Fig. 1.10 shows examples of non-fluorinated and fluorinated rod-like *p*-terphenyl-based liquid crystals. All the compounds have the same terminal chains at both ends. Compound **BF0**,

involving no fluoro-substituent, exhibits smectic A and B phases. **BF2** with two fluoro-substituents at each inner positions of the outer benzene rings, exhibits only a nematic mesophase. In case of **BF3**, containing three fluoro-substituents, smectic C and nematic mesophase were observed. Furthermore, all three compounds show very different melting and clearing temperature.[81]
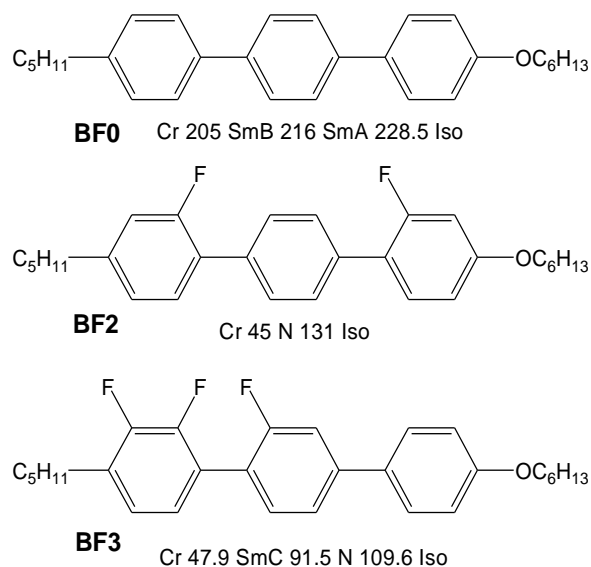
Figure 1.10 Examples of non-fluorinated (**BF0**) and fluorinated liquid crystal compounds (**BF2**, **BF3**).[81]

It was also shown in previous work that the position and number of fluorines at the aromatic core of polycatenar molecules can change their mode of self-assembly (see Fig. 1.11).[43] The compound with no fluorine (**AH**) shows only an $Ia3d$ phase on cooling from 156 to 69 °C. A fluorination at meta-position (**AF₃**) causes higher thermal stability of the $Ia3d$ phase while a fluorination at the ortho-position (**AF₂**) leads to a short range of the interesting Iso[*] phase. Though the thermal stability of the $Ia3d$ phase is reduced, it is stable even below room temperature. The Cub/$Ia3d$ phase is replaced by a Cub$_{bi}$[*]/$I23$ phase or SmC$_S$ phase when both meta-positions (**AF₃₅**) or both ortho-positions (**AF₂₆**) are fluorinated. Two meta-fluorine atoms (**AF₃₅**) lead to a stronger steric effect, resulting in a higher twist angle Φ leading to a transition to a $I23$ phase which is retained for compound **AF₂₃₄₅₆** with a perfluorinated apex. In contrast, two ortho-fluorine atoms (**AF₂₆**) cause a strong destabilizing effect on the Cub/$Ia3d$ phase which is replaced by a SmC$_S$ phase.[43] However, fluorination in the middle of the core of polycatenar mesogens removes the

Cub_bi phases and only lamellar phases were found.[82] Hence, there are very different effects of core fluorination which are not fully understood.
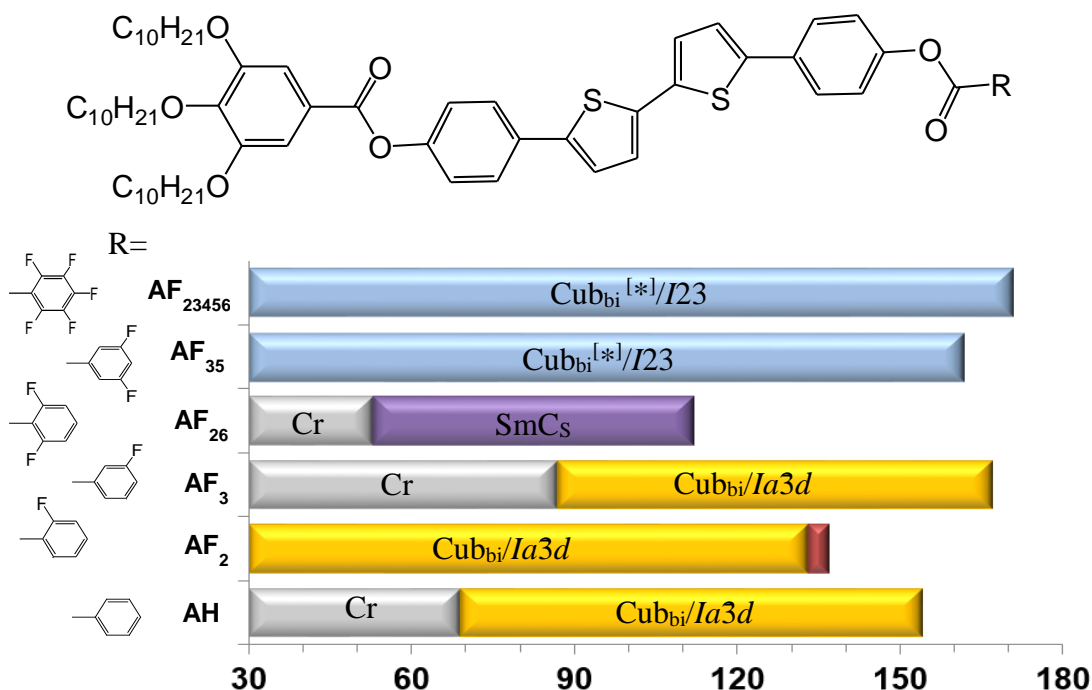
Figure 1.11 The effect of core fluorination on the LC phases of polycatenar compounds.[43]

1.7 Effect of bromination on LC self-assembly

In this research, brominated benzene is additionally studied to see the effect of bromination on LC self-assembly. There are only very few previous reports on the effects of core brominatnion on LC phases.[67] For example, the tetracatenar without bromine (**Br0**) involves three dodecyloxy chains at one end and one decyloxy chain at the other end and forms Cub_bi phase from 79 to 146 °C (see Fig.1.12). One brominated tetracatenar (**Br1**) involves three dodecyloxy chains at one end and one dodecyloxy chain at the other end and forms columnar phase from 85 to 141 °C. It is difficult to make a direct comparison between **Br0** and **Br1** because of the difference of chain lengths and molecular structures. However, the cubic phase of **Br0** is completely removed and replaced to the columnar phase by mono-bromination. Furthermore, one additional bromine substitution from **Br1** to **Br2** leads to a large lowering of the thermal stability of the columnar

phase. The effect of bromination is mainly attributed to the increased steric hindrance because of the much bigger size of bromine compared to hydrogen.

Br0   Cr 79 Cub 146 Iso

Br1   Cr 85 Col 141 Iso
Br2   Cr 71 Col 112 Iso   **Br1:** Y_1= Br, Y_2= H
                                       Br2: Y_1, Y_2= Br
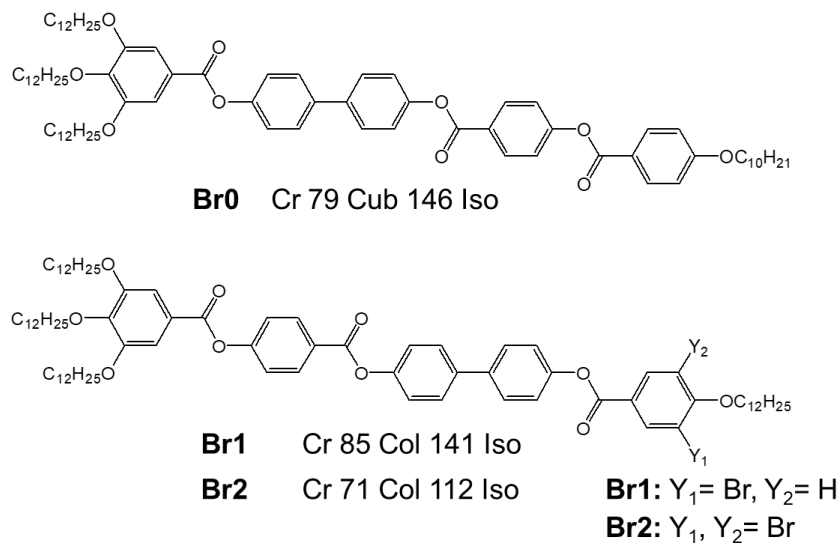
Figure 1.12 Examples of non-brominated (**Br0**) and polycatenar brominated liquid crystal compounds (**Br1** and **Br2**).[67]

1.8 Liquid crystals for organic semiconductors

Organic field effect transistor (OFET), organic light emitting diode (OLED) and organic photovoltaic (OPV) cells are fascinating device applications which can be easily prepared by solution-casting and printing. In addition, flexible electronic devices on a plastic substrate can be fabricated. OFETs, for example, uses organic semiconductors as its channel. The source (S) supplies the carrier, the gate controls the flow of current, and the drain (D) releases the carriers out of the device (see Fig. 1.13a).[83,84,85]

Diverse small-molecule materials for OFET such as 2,7-dioctyl[1]benzothieno[3,2-b][1]benzothiophen (C8-BTBT, **11**, Fig. 1.13)[11] and 2,9-didecyl-dinaphtho[2,3-b:2',3'-f]thieno[3,2-b]thiophene (C10-DNTT, **12**)[12] and polymer materials such as benzothiadiazole-cyclopentadithiophene based copolymers (CDT-BTZ-C16, **13**)[86] and diketopyrrolopyrrole based polymers (DPP polymer, **14**)[87] have been studied[16] as shown in Fig. 1.13. OFETs based on these crystalline films show great FET mobilities over 1 cm^2 Vs^{-1}.[16] By using small-molecules and polymers, it is not possible to control the molecular alignment, which causes the poor uniformity

11

12

13

14

15

16

a)

Device architecture for OFET

D: Drain

S: Source
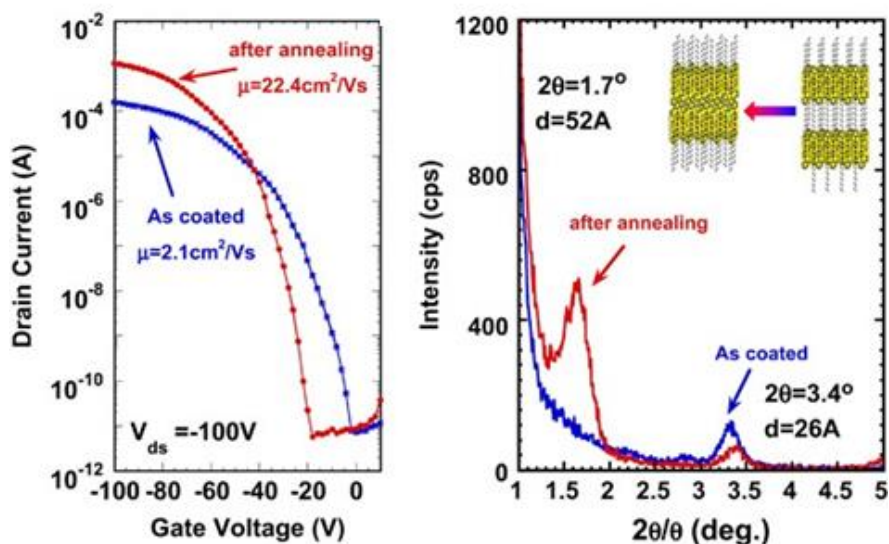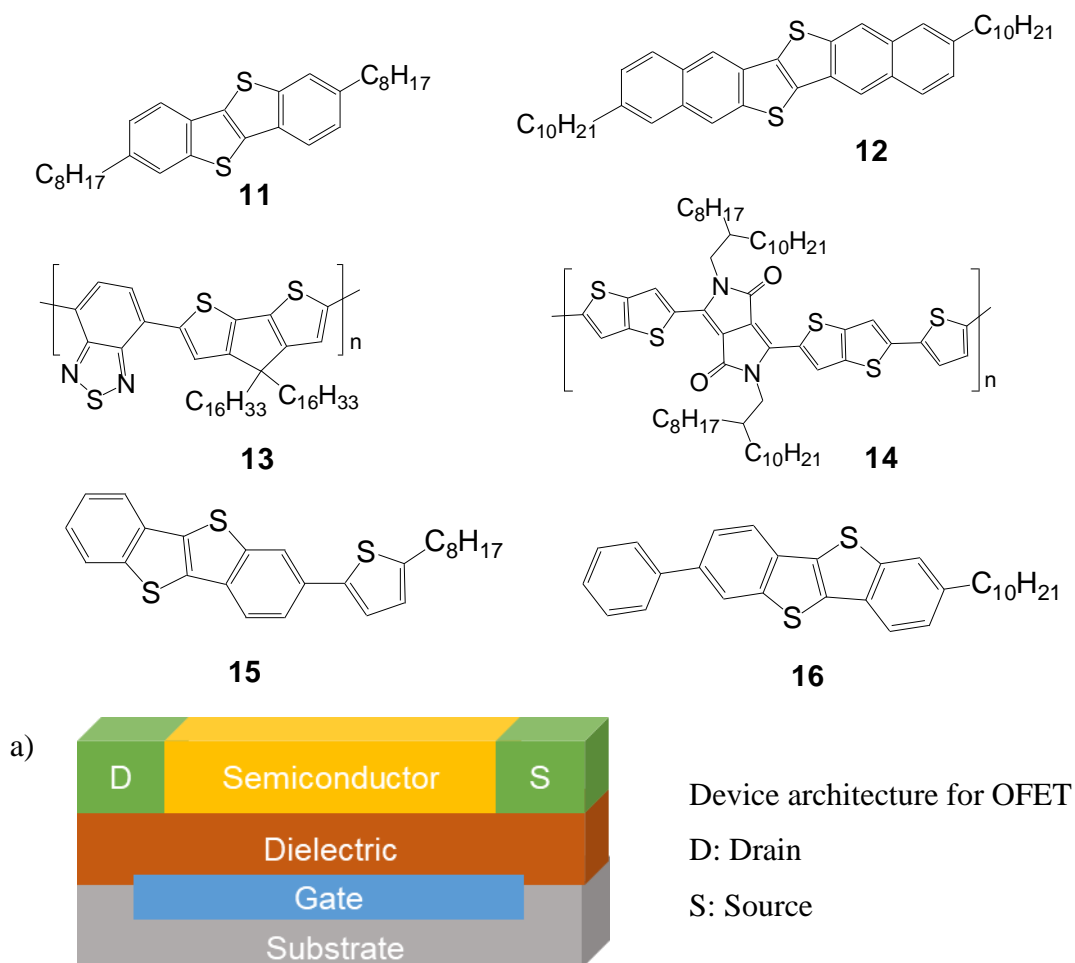
Figure 1.13 Molecular structure of the compounds for OFET: C8-BTBT (**11**)[11], DNBDT (**12**)[16], polymeric materials (**13,14**)[86,87], 8-Tp-BTBT (**15**)[16] and Ph-BTBT-10 (**16**)[15]; a) device architecture for OFET; b) transfer characteristics of FETs and small-angle XRD patterns for crystalline films both as coated and after thermal annealing.[15,16] (b,c) were reproduced with permission from ref 15, Copyright Nature Research 2015.

and surface morphology of crystalline films.[16] This obstructs the sustainability of FET performance. In addition, in case of polymer materials, it is almost impossible to reproduce the exactly same polymer due to the synthesis issue. The molecular weight and PDI (polydispersity index) of the polymers are controllable but only in a certain range.

Due to the limitation of the small-molecule and polymer materials, the use of liquid crystals for use as the organic semiconductor has been studied since 1990s.[16] LC molecules gained substantial attention for semiconductors due to their self-assembly ability. By utilizing LCs, self-assembled π-conjugated system can be induced which improves charge carrier transport properties significatly.[17] Various conventional LC phases such as smectic[15,16,88,89] and columnar[17,90,91] LCs have been investigated for organic semiconductor.[92-95]

Among them, Ph-BTBT-10 (**16**) forming a highly ordered SmE phase was introduced as a good candidate for OFET[15] (Fig. 1.13). The fabricated OFET shows a great performance with a high FET mobility of μ= 2.1cm^2/Vs. Furthermore, after annealing the OFET at 120 ℃ for 5 min, the FET mobility can be significantly enhanced up to 14.7[15] or 22.4[16] cm^2/Vs. The XRD results before and after annealing show that the layer thickness changes from 26 to 52 Å after annealing which indicates that the monolayer structure is transformed into a bilayer structure (Fig. 1.13).[15,16] This shows the importance of LC self-assembly on the performance of OFET devices.

1.9 Effects of fluorine and bromine substitution on photovoltaic efficiency

There have been many studies showing that fluorination of conjugated cyclic compounds can enhance the efficiency of organic photovoltaics.[96,97,98,99,100] Few of the various examples are selected and the corresponding molecular structures are shown in the Fig. 1.14. The polymers have been analyzed by cyclic voltammetry to determine the Highest Occupied Molecular Orbital (HOMO) and Lowest Unoccupied Molecular Orbital (LUMO) levels. As a result, the HOMO-LUMO gap of the polymer without fluorine (**17**) is 2.26eV (-5.40eV and -3.14eV) and the value of the polymer with fluorine (**18**) is 2.21eV (5.54eV and -3.33eV). Overall, not only HOMO and LUMO levels were decreased by fluorination, but **18** also has a lower HOMO-LUMO gap, which is very important value for conductivity.[99] In addition, organic solar cells were fabricated by using these two polymers and their Power Conversion Efficiency (PCE) was determined. As a result, the

PCE of organic solar cells with the polymer with fluorine atoms (**18**) is 7.2%, which is much higher than the one of the polymer without fluorine atom (**17**), 5.0%. As this result shows, fluorination has a high potential for better efficiency of organic solar cells.[99]

17: X= H   **18**: X= F

19: X_1, X_2= H   **20**: X_1 =Br, X_2= H   **21**: X_1, X_2= Br
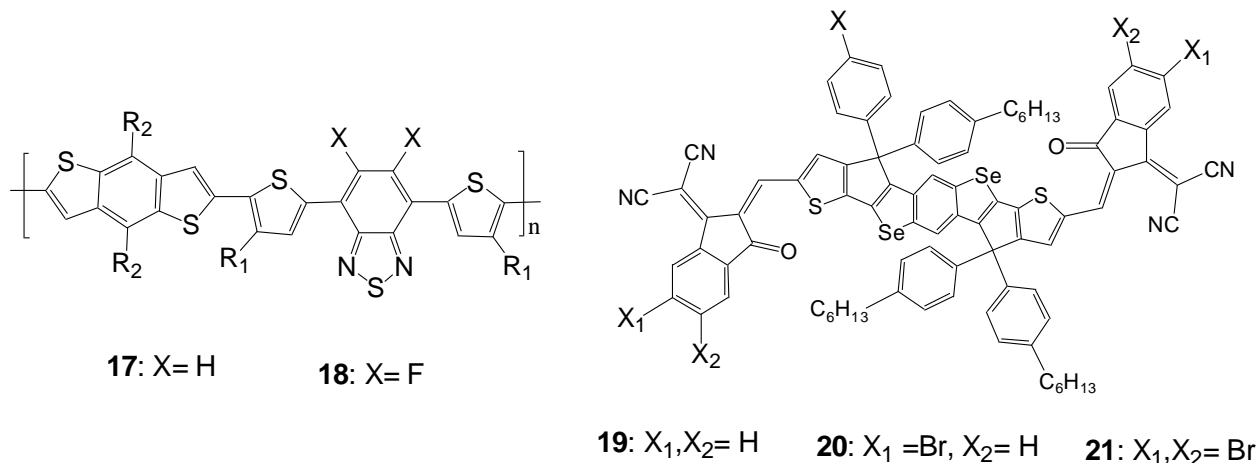
Figure 1.14 Molecular structures of π-conjugated polymers without (**17**) and with aromatic fluorine substituents (**18**) and selected small-molecule compounds without (BDSelC, **19**) and with two (BDSelC2Br, **20**) and four bromine atoms (BDSelC4Br, **21**) used for organic solar cells.[99,101]

Furthermore, bromine substitution of conjugated cyclic compounds can also enhance the properties of organic photovoltaics.[101,102] The changes of properties in organic photovoltaics according to the number of bromine substitution of a small-molecule compound are reported for BDSelC (**19**): without bromine, BDSelC2Br (**20**): with two bromines and BDSelC4Br (**21**): with four bromines (Fig. 1.14).[101] As the absorption spectra show, bromination leads to dramatic increases of the wavelength (redshift absorption) resulting in lowering the band gap 1.51 (**19**), 1.41(**20**) and 1.39 eV(**21**).[101] Also, the organic solar cells based on these compounds were fabricated and the device with the double brominated compound **20** showed a higher PCE (12.5%), compared to the PCE of the non-brominated compound **19** (7.1%) and the four-fold brominated compound **21** (9.6%). According to the result, bromination obviously has a great effect of enhancing the critical properties for organic photovoltaics.

1.10 Objectives

Liquid crystals have attracted substantial attention as organic semiconductor materials due to their ability of self-assembly. Especially Cub$_{bi}$ phases, involving nano-segregated network structures,[29] are highly promising candidates because they can form 3D conduction pathways, providing numorous routes for charge carriers, which can minimize the distortions by structural defects.[30,31] Additionally, the Cub$_{bi}$ phases show intriguing features as for example spontaneous mirror symmetry breaking, which is also of significant interest.[29,45,73,74]
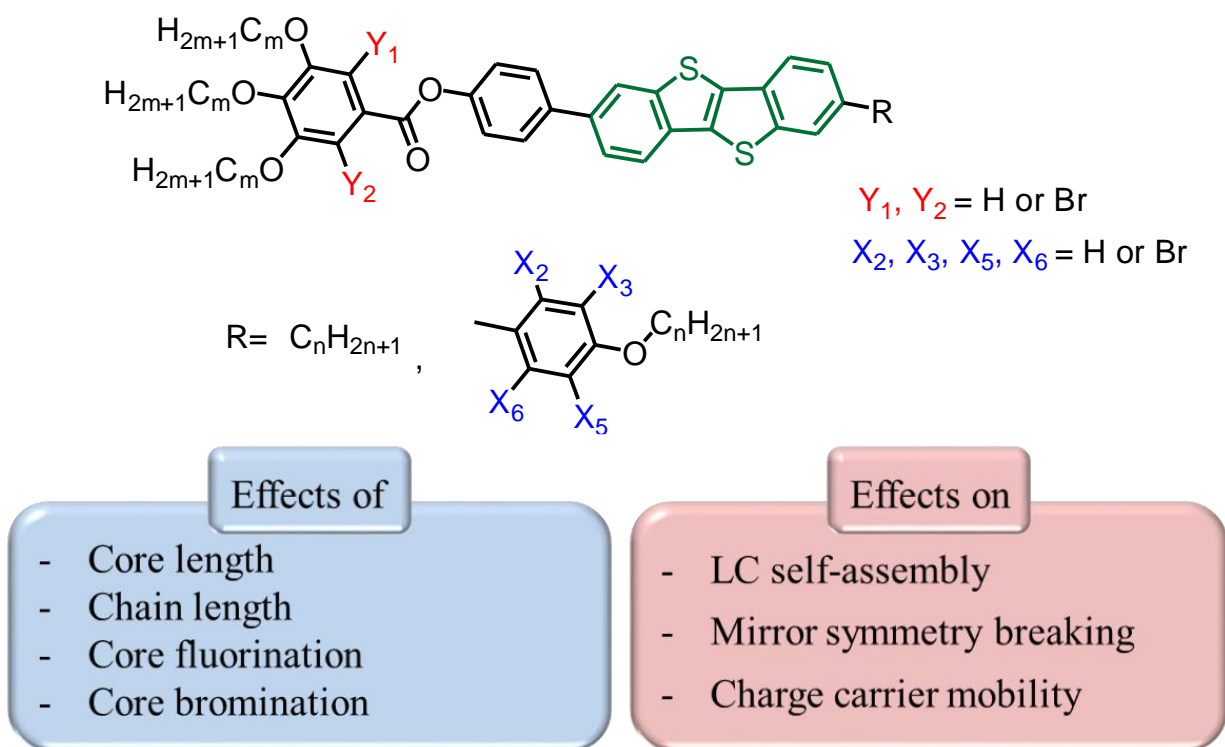
Figure 1.15 Molecular structures of the targeted BTBT based polycatenars.

The [1]benzothieno[3,2-b][1]benzothiophene (BTBT) unit was selected as a rigid core unit because it is known as a stable π-conjugated system with the ability of high charge carrier mobility and outstanding performance as an organic semiconductor material.[15,103,104,105,106] Therefore, the aim was to produce the first LC compounds involving the BTBT unit and forming cubic phases. Both liquid crystalline behavior and charge carrier mobility will be investigated. Special focus is

also on the aspect of mirror symmetry breaking in the cubic and the adjacent isotropic liquid phases. Moreover, by introducing bromine and fluorine atoms at different positions, the intriguing effects of bromination and fluorination on LC self-assembly, charge carrier mobility and mirror symmetry breaking are also to be studied. In all series of compounds, terminal alkyl chains and alkoxy chains will be varied from short to long to modify the LC phase types and investigate their effect on mirror symmetry breaking.

References

1   J.P.F Lagerwall and G. Scalia, *Current Applied Physics* **2012**, 12, 1387.
2   L. Schmidt-Mende, A. Fechtenkotter, K. Mullen, E. Moons, R. Friend and J. MacKenzie, *Science* **2001**, 293 (5532), 1119.
3   R. Jakoby, A. Gaebler and C. Weickkmann, *Crystals* **2020**, 10, 514.
4   E. Bukusoglu, M. B. Pantoja, P. C. Mushenheim, X. Wang and N. L. Abbott, Annu. *Rev. Chem. Biomol. Eng*. **2016**, 7, 163, 96.
5   Z.G. Zheng, Y.Q. Lu and Q. Li, *Adv. Mater*. **2020**, 1905318.
6   K. Bisoyi, T. J. Bunning and Q. Li, *Adv. Mater*. 2018, 1706512.
7   M. Dogru and T. Bein, *Chem. Commun*. 2014, 50, 5031.
8   J. Nelson, *Materials Today*, 2011, 14, 10, 462.
9   J. McGinness, P. Corry, P. Proctor, *Science*, 1974, 183, 4127, 853.
10   C. D. Sheraw, T. N. Jackson, D. L. Eaton and J. E. Anthony, *Adv. Mater*. **2003**, 15, 2009.
11   H. Ebata, T. Izawa, E. Miyazaki, K. Takimiya, M. Ikeda, H. Kuwabara and T. Yui, *J. Am. Chem.Soc*. **2007**, 129, 15732.
12   M. J. Kang, I. Doi, H. Mori, E. Miyazaki, K. Takimiya, M. Ikeda and H. Kuwabara, *Adv. Mater*. **2011**, 23, 1222.
13   T. Okamoto, C. Mitusi, M. Yamagishi, K. Nakahara, J. Soeda, Y. Hirose, K. Miwa, H. Sato, A. Yamano, T. Matsushita, T. Uemura, and J. Takeya, *Adv. Mater*. **2013**, 25, 6392.
14   C. Mitsui, T. Okamoto, M. Yamagishi, J. Tsurumi, K. Yoshimoto, K. Nakahara, J. Soeda, Y. Hirose, H. Sato, A. Yamano, T. Uemura, and J. Takeya, *Adv. Mater*. **2014**, 26, 4546.
15   H. Iino, T. Usui, and J. Hanna, *Nat.Commun*. **2015**, 6, 6828.
16   H. Iino and J. Hanna *Polymer Journal* **2017**, 49, 23.
17   M.Funahashi, *Polymer Journal* **2017**, 49, 75.
18   M, Kumar and S. Kumar, *Polymer Journal* **2017**, 49, 85.
19   C. Tschierske, *J. Mater. Chem*. **1998**, 8, 1485.
20   D. M. P. Mingos, *Structure and Bonding* **1999**, 94, 7.
21   C. Tschierske, *Top. Curr. Chem*. **2012**, 318, 1.
22   C. Tschierske, *Interface Focus* **2012**, 2, 680.
23   P. G. Gennes and J. Prost, The Physics of Liquid Crystals, 2nd ed. *Oxford University Press*, **1993**, New York.
24   J, Chen, W. Cranton, M. fihn, Handbook of Visual Display Technology, *Springer*, Cham, **2016**
25   I. Dierking, Textures of Liquid Crystals, *Wiley-VCH*, Weinheim, **2003**.
26   S. Kutsumuzu, *Isr. J. Chem*. **2012**, 52, 844.
27   C. Tschierske, *Chem. Soc. Rev.* **2007**, 36, 1930.

28   S. Hassan, W. Rowe and G. J. T. Tiddy, Handbook of Applied Surface and Colloid Chemistry, ed. K. Holmberg, *Wiley*, Chichester, **2002**.

29   C. Dressel, F. Liu, M. Prehm, X. Zeng, G. Ungar and C. Tschierske, *Angew. Int. Ed.* **2014**, 53, 13115.

30   T. Kato, *Angew. Chem. Int. Ed*. **2010**, 49, 7847.

31   T. Kato, M. Yoshio, T. Ichikawa, B. Soberats, H, Ohno and M. Funahashi, *Nat. Rev. Mater*. **2017**, 2, 17001.

32   P. Fuchs, C. Tschierske, K. Raith, K. Das and S. Diele, Angew. *Chem. Int. Ed*. **2002**, 41, 628.

33   G. W. Gray, B. Jones and F. Marson, *J. Chem. Soc*. **1957**, 393.

34   C. Dressel, Disseratioin, *Martin-Luther-Universitat Halle- Wittenberg*, Halle, **2015**.

35   D. Demus, G. Kunicke, J. Neelsen, H. Sackmann, *Zeitschrift Naturforsch*. **1968**, 23A, 84.

36   S. Kutsumizu, T. Ichikawa, M. Yamada, S. Nojima and S. Yano, *J. Phys. Chem*. B **2000**, 104, 10196.

37   S. Kutsumizu, K. Morita, T. Ichikawa, S. Yano, S. Nojima and T. Yamaguchi, *Liq. Cryst*. **2002**, 29, 1447.

38   S. Kutsumizu, K. Morita, S. Yano and S. Nojima, *Liq. Cryst*. **2002**, 29, 1459.

39   H. Schubert, J. Hauschild, D. Demus, S. Hoffmann, *Z. Chem*. 1978, 18, 256.

40   D. Demus, A. Gloza, H. Hartung, A. Hauser, I. Rapthel and A. Wiegeleben, *Cryst. Res. Technol*. **1981**, 16, 1445.

41   S. Kutsumizu, H. Mori, M. Fukatami, S. Naito, K. Sakajiri and K. Saito, *Chem. Mater*. **2008**, 20, 3675.

42   S. Kutsumizu, Y. Yamada, T. Sugimoto, N. Yamada, T. Udagawa and Y. Miwa, Phys. *Chem. Chem. Phys*. **2018**, 20, 7953.

43   C. Dressel, T. Reppe, S. Poppe, M. Prehm, H. Lu, X. Zeng, G. Ungar and C.Tschierske, *Adv. Funct. Mater*. **2020**, 30, 2004353.

44   Y. Cao, M. Alaasar, A. Nallapaneni, M. Salamończyk, P. Marinko, E. Gorecka, C. Tschierske, F. Liu, N. Vaupotič, and C. Zhu, *Phys. Rev. Lett*. **2020**, 125, 027801.

45   T. Reppe, S. Poppe and C. Tschierske, *Chem. Eur. J.* **2020**, 26, 16066.

46   A.H. Schoen, *Interface Focus* **2012**, 2, 658.

47   Y. Cao, C. Feng, A. Jaklic, C. Zhu, F. Liu, *Giant* **2020**, 2, 100018

48   A. M. Levelut and M. Clerc, *Liq. Cryst.* **1998**, 24, 105

49   X. Zeng, G. Ungar and M. Impror-Clerc, *Nat. Mater. Chem.* **2008**, 18, 2953

50   K. Saito, Y. Yamamura, Y. Miwa and S. Kutsumizu, *Phys. Chem. Chem. Phys.* **2016**, 18, 3280

51   X. B. Zeng and G. Ungar, *J. Mater. Chem.* C **2020**, 8, 5389.

52   S. Poppe, X. Cheng, C. Chen, X. Zeng, R.Zhang, F. Liu, G. Ungar, and C. Tschierske, *J. Am. Chem. Soc.* **2020**, 142, 7, 3296.

53   O. Kwon, X. Cai, W. Qu, F. Liu, J. Szydłowska, E. Gorecka, M. J. Han, D. K. Yoon S. Poppe and C. Tschierske, *Adv. Funct. Mater*, **2021**, 2102271

54   T. Ichikawa, M. Yoshio, A. Hamasaki, T. Mukai, H. Ohno and T. Kato, *J. Am. Chem. Soc.* **2007**, 129, 10662.

55   A. F. Frise, T. Ichikawa, M. Yoshio, H. Ohno, S. V. Dvinskikh, T. Kato and I. Fur, *Chem. Commun.* **2010**, 46, 728.

56   T. Ichikawa, M. Yoshio, A. Hamasaki, J. Kagimoto, H. Ohno and T. Kato, *J. Am. Chem. Soc.* **2011**, 133, 2163.

57   T. Ichikawa, M. Yoshio, A. Hamasaki, S. Taguchi, F. Lie, X.-B. Zeng, G. Ungar, H. Ohno and T. Kato, *J. Am. Chem. Soc.* **2012**, 134, 2634.

58   A. Mori, E. Yamamoto, K. Kubo, S. Ujiie, U. Baumeister and C. Tschierske, *Liq. Cryst.* **2010**, 37, 1059.

59   M. Ichihara, A. Suzuki, K. Hatsusaka and K. Ohta, *Liq. Cryst.* **2007**, 34, 555.

60   T. Ichikawa, *J. Am. Chem. Soc.* **2007**, 129, 10662.

61   A. E. Frise, *Chem. Commun.* **2010**, 46, 728.

62   T. Ichikawa, *J. Am. Chem. Soc.* **2012**, 134, 2634.

63   K. Borisch, S. Diele, P. Göring and C. Tschierske, *Chem.Commun.* **1996**, 237.

24

64	K. Borisch, S. Diele, P. Göring, H. Müller and C. Tschierske, *Liq. Cryst.* **1997**, 22, 427.
65	K. Borisch, S. Diele, P. Göring, H. Kresse and C. Tschierske, *J. Mater. Chem.* **1998**, 8, 529.
66	K. E. Rowe and D. W. Bruce, *J. Mater. Chem.* **1998**, 8, 331.
67	H. T. Nguyen, C. Destrade and J. Malthête, *Adv. Mater.* **1997**, 9, 375.
68	H. T. Nguyen, G. Sigaud, M. F. Achard, F. Hardouin, R. J. Twieg and K. Betterton, *Liq. Cryst.* **1991**, 10, 389.
69	C. Dressel, T. Reppe, M. Prehm, M. Brautzsch and C. Tschierske, *Nature Chemistry* **2014**, 6, 971.
70	C. Tschierske and G. Ungar, Chem. *Phys. Chem.* **2016**, 17, 9.
71	C. Tschierske and C. Dressel, *Symmetry* **2020**, 12, 1098.
72	H. Lu, X. Zeng, Goran Ungar, C. Dressel, and C. Tschierske, *Angew. Chem. Int. Ed.* **2018**, 57, 2835.
73	T. Reppe, C. Dressel, S. Poppe and C. Tschierske, *Chem. Commun.* **2020**, 56, 711
74	T. Reppe, S. Poppe, X. Cai, Y. Cao, F. Liu and C. Tschierske, *Chem. Sci.* **2020**, 11, 5902.
75	A. Ha, I. Cohen, X.L. Zhao, M. Lee, D, Kivelson, *J. Phys. Chem.* **1996**, 100, 1.
76	L. Pasteur, *Ann Chim Phys.* **1848**, 24, 442459.
77	C. Tschierske, *Liquid Crystals* **2018**, 45:13-15, 2221,
78	A. Zehnacker and M. A. Suhm, *Angew. Chem. Int. Ed.* **2008**, 47,6970.
79	J. W. Goodby, D. A. Dunmur and P. J. Collings, *Liquid Crystals* **1995**, 19, 5, 703.
80	H. Nishikawa, K. Shiroshita, H. Higuchi, Y. Okumura, Y. Haseba, S. Yamamoto, K. Sago and H. Kikuchi, *Adv. Mater.* **2017**, 29, 1702354.
81	J. W. Goodby, I. M. Saez, S. J. Cowling, J. S. Gasowska, R. A. MacDonald, S. Sia, P. Watson, K. J. Toyne, M. Hird, R. A. Lewis, S. Lee, and V. Vaschenko, *Liq. Cryst.* **2009**, 36, 6–7, 567.
82	A. I. Smirnova, B. Heinrich, B. Donnio, D. W. Bruce, *RSC Adv.* **2015**, 5, 75149.
83	A. Salleo, M.L. Chabinyc and M.S. Yang, Street, *Applied Physics Letters* **2002**, 81 (23), 4383..
84	J. Mei, *J. Am. Chem.Soc*. **2013**, 135, 6724.
85	A. Köhler, and H. Bässler, Electronic Processes in Organic Semiconductors, *Wiley*, Weinheim, **2015**.
86	H. N. Tsao, D. M. Cho, I. Park, M. R. Hansen, A. Mavrinskiy, D. Y. Yoon, R. Graf, W. Pisula, H. W. Spiess and K. Mullen, *J. Am. Chem. Soc.* **2011**, 133, 2605.
87	H. Bronstein, Z. Chen, R. S. Ashraf, W. Zhang, J. Du, J. R. Durrant, P. S. Tuladhar, K. Song, S. E. Watkins, Y. Geerts, M. M. Wienk, R. A. J. Janssen, T. Anthopoulos, H. Sirringhaus, M. Heeney and I. McCulloch, *J. Am. Chem. Soc.* **2011**, 133, 3272.
88	Y. He, M. Sezen, D. Zhang, A. Li, L. Yan, H. Yu, C. He, O. Goto, Y.-L. Loo and H. Meng, *Adv. Electron. Mater.* **2016**, 2, 1600179.
89	C. Ruzie, J. Karpinska, A. Laurent, L. Sanguinet, S. Hunter, T. D. Anthopoulos, V. Lemaur, J. Cornil, A. R. Kennedy, O. Fenwick, P. Samorı, G. Schweicher, B. Chattopadhyay and Y. H. Geerts, *J. Mater. Chem. C* **2016**, 4, 4863.
90	C.-X. Liu, H. Wang, J.-Q. Du, K.-Q. Zhao, P. Hu, B.-Q. Wang, H. Monobe, B. Heinrich, *J. Mater. Chem. C* **2018**, 6, 4471.
91	S. Mery, D. Haristoy, J.-F. Nicoud, D. Guillon, S. Diele, H. Monobe and Y. Shimizu, *J. Mater. Chem*. **2002**, 12, 37.
92	M. Funahashi, *Polym.* J. **2009**, 41, 459.
93	W. Pisula, M. Zorn, J. Y. Chang, K. Müllen and R. Zentel, *Macromol. Rapid Commun.* **2009**, 30, 1179.
94	M. O'Neill, and S. M. Kelly, *Adv. Mater*. **2011**, 23, 566.
95	A. Seki and M.Funahashi, *Heterocycles* **2016**, 92, 3.
96	H. Chang, L. Li, C. Zhu, H. Peng and Y. Zou, *Chem. Phys.* **2020**, 528, 110529.
97	J. You, L. Dou, K. Yoshimura, T. Kato, K. Ohya, T. Moriarty, K. Emery, C.C. Chen, J. Gao, G. Li and Y. Yang, *Nat. Commun*. **2013**, 4, 1446, 2411.

98   H. Hu, K. Jiang, J. H. Kim, G. Yang, Z. Li, T. Ma, G. Lu, Y. Qu, H. Ade and H. Yan, *J. Mater. Chem A*, **2016**, 4, 5039.

99   H. Zhou, L. Yang, A.C. Stuart,S. C. Price, S. Liu and W. You, *Angew. Chem.* **2011**, 123, 3051.

100   H. Medlej, A. Nourdine, H. Awada, M. Abbas, C. Dagron-Lartigau, G. Wantz and L. Flandin, *European Polymer Journal*, **2014**, 59, 25.

101   S. Wan, C. Chang, J. Wang, G. Yuan, Q. Wu, M. Zhang and Y. Li, Sol. RRL **2019**, 3, 1800250.

102   K. Chum, B. R. Henry and J. Mol. *Spectrosc.* **1976**, 60, 150.

103   G. Tarsoly, Y. Choi, Y. You, S. Jhang and S. Pyo, *Adv. Electron. Mater*. **2021**, 2000973.

104   A. Babuji, F. Silvestri, L. Pithan, A. Richard, Y. H. Geerts, N. Tessler, O. Solomeshch, C. Ocal, and E. Barrena *ACS Appl. Mater. Interfaces* **2020**, 12 (51), 57578.

105   T. Salzillo, A. Campos, A. Babuji, R. Santiago, S. T. Bromley, C. Ocal, E. Barrena, R. Jouclas, C. Ruzie, G. Schweicher, Y. H. Geerts and M. Mas-Torrent, *Adv. Funct. Mater*. **2020**, 30, 2006115.

106   H. H. Choi, A. F. Paterson, M. A. Fusella, J. Panidi, O. Solomeshch, N. Tessler, M. Heeney, K. Cho, T. D. Anthopoulos, B. P. Rand, V. Podzorov, *Adv. Funct. Mater.* **2020**, 30, 1903617.

2. Synthesis

The synthetic routes to the target compounds derived from BTBT are shown in Scheme 2.1. Mainly three different routes were used to synthesize the polycatenars with a fan-shaped 3,4,5-trialkoxybenzoate moiety.
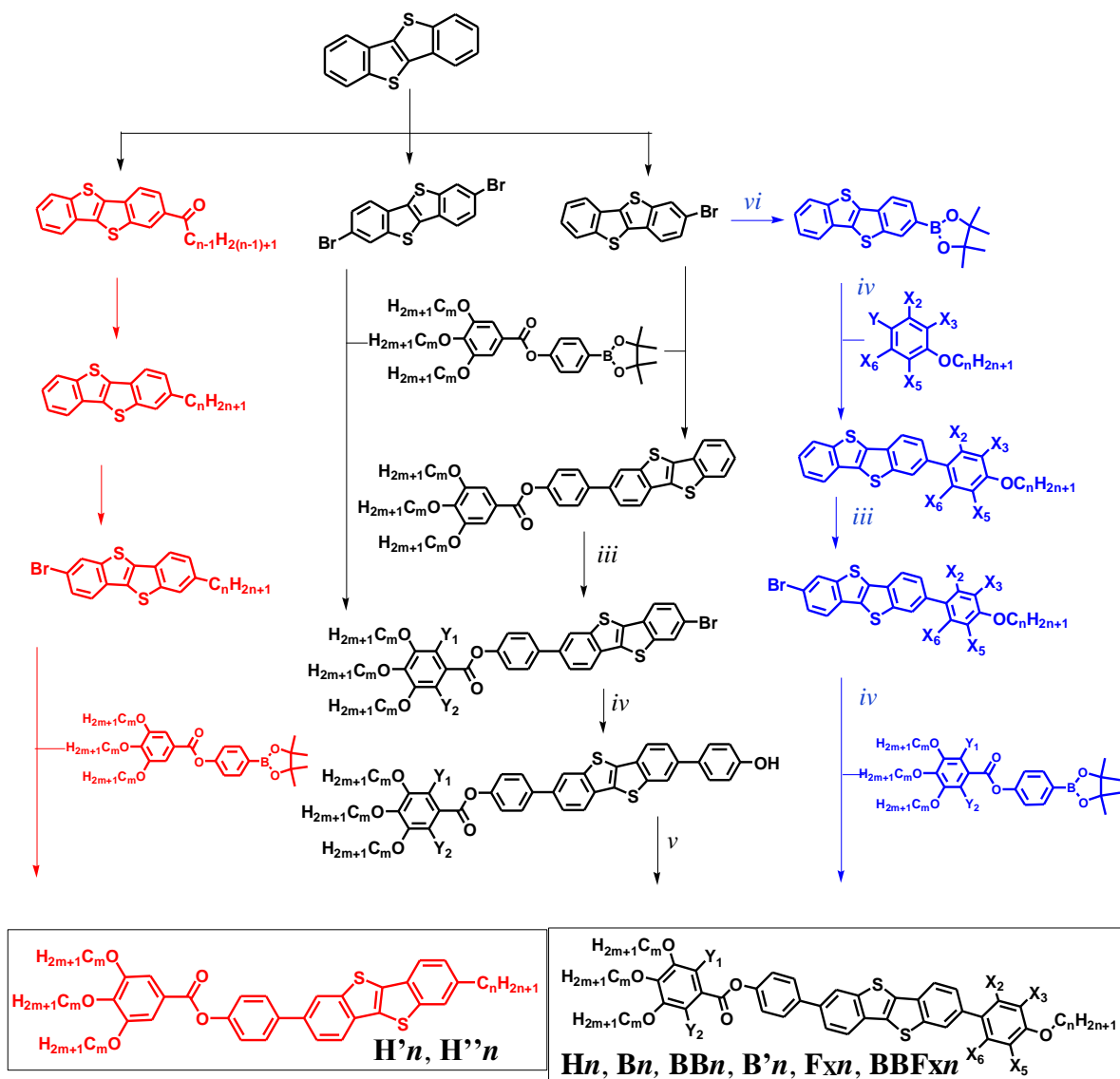
Scheme 2.1 Overall synthetic scheme for the investigated BTBT based polycatenars. Reagents and conditions: i) $AlCl_3$, dry DCM, acyl chloride, -5 °C; ii) $AlCl_3$, $NaBH_4$, dry THF, reflux; iii) Br_2, DCM, RT; iv) THF, sat. $NaHCO_3$ solution, $Pd(PPh_3)_4$, reflux; v) dry 2-butanone, K_2CO_3, TBAI, reflux; vi) Bis(pinacolato)diboron, CH_3CO_2K, DMSO, $PdCl_2(dppf)$. For the meaning of X and Y, see Fig. 1.15.

2.1 Synthesis of [1]benzothieno[3,2-b][1]benzothiophene (BTBT) and BTBT derivatives with different functional groups
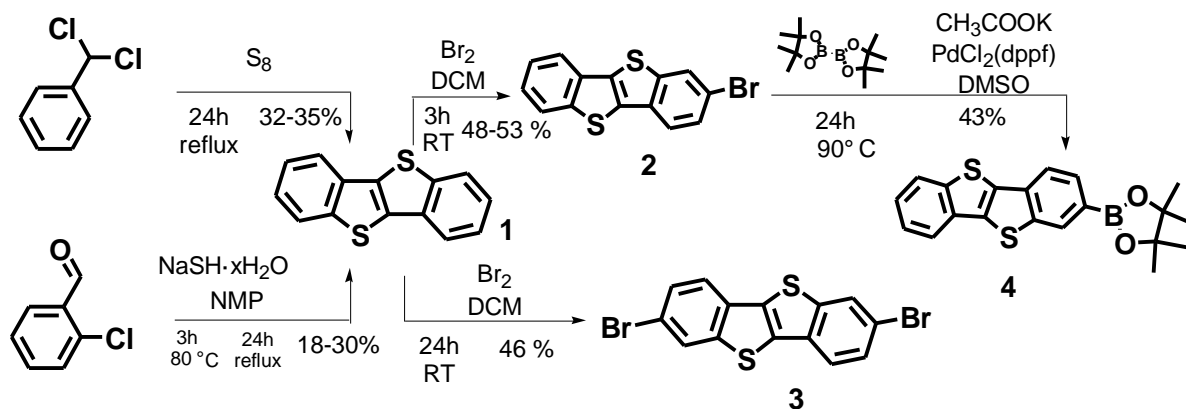
Scheme 2.2 Synthesis of BTBT(**1**), BTBT-Br(**2**), BTBT-Br$_2$(**3**) and BTBT-BO(**4**); abbreviations: DCM = dichlormethan, NMP = N-Methyl-2-pyrrolidone, DMSO = Dimethyl sulfoxide.

For the synthesis of the BTBT (**1**) unit, two different methods were used. For the first method, benzal chloride and sulfur were used without any extra solvent.[1] The mixture was refluxed for 24 hours and the yield was 32 to 35 %. For the second method, 2-chlorobenzaldehyde, sodium hydrogensulfide hydrate and NMP were used.[2] Even though the yield is from 18 to 30%, which is lower than in the first method, the second method is still better due to its more convenient purification. Then 2-bromo BTBT (**2**)[3] and 2,7-dibromo BTBT(**3**)[2] were synthesized by bromination of BTBT unit using bromine in DCM. To selectively produce either 2-bromo BTBT or 2,7-dibromo BTBT, different equivalent of bromine and reaction time were used; 1.1 or 2.2 eq. and 3 or 24h each. Finally Miyaura borylation[4] was used to synthesize the BTBT boronate (**4**). BTBT-Br and bis(pinacolato)diboron in DMSO as solvent, CH$_3$COOK as base and PdCl$_2$(dppf) as catalyst were used for the reaction based on the reported procedure. It is essential to use 3eq. of bis(pinacolato)diboron and CH$_3$COOK as the reaction does not occur if only 1.5 eq. of bis(pinacolato)diboron and CH$_3$COOK was used.

2.2 Synthesis of 4-(3,4,5-tri-n-alkoxybenzoyloxy)phenylboronic acid pinacol ester and bromination
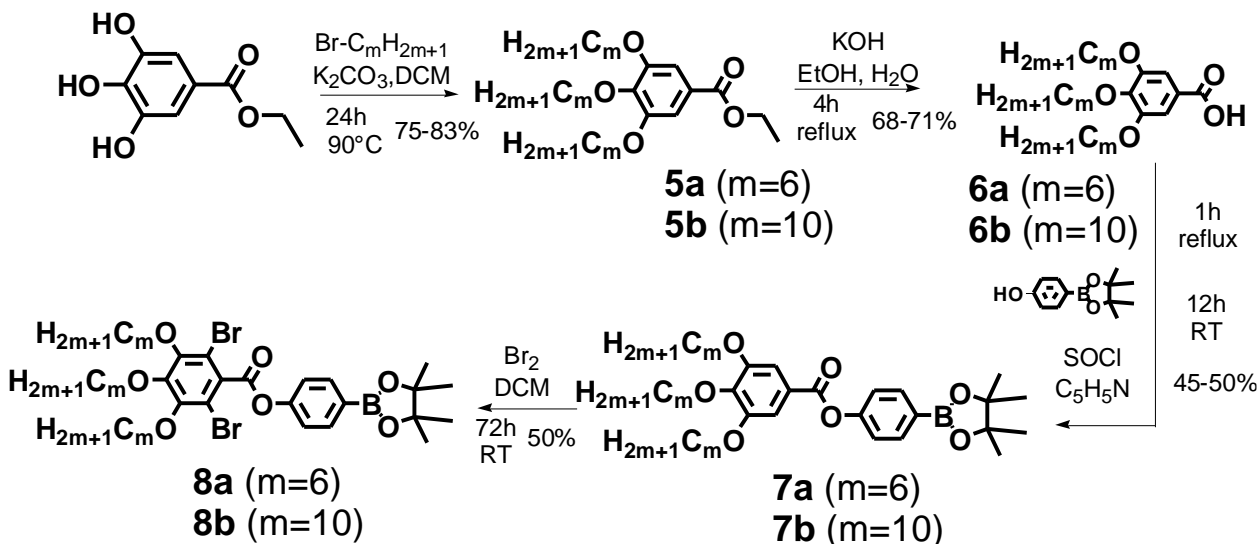
Scheme 2.3 Synthesis of **7** and **8**.

Ethyl gallate was used as a starting material to synthesize the boronates **7** and **8**. Alkylation of ethyl gallate was carried out as a first step by using Williamson ether synthesis according to the reported procedure.[5] 3.3 eq. of n-alkylbromide was used in the reaction to induce a higher yield and avoid one and two alkylated compounds as side products. Then, the ethoxycarbonyl group was converted to the carboxylic acid using KOH in EtOH and H_2O.[5] After converting the carboxylic acid to the acid chloride using $SOCl_2$, the 4-benzoyloxyphenylboronic acid pinacol ester **7** was synthesized by esterification in the presence of pyridine as base. The obtained boronate **7** was used for the synthesis of the non-brominated compounds **H***n*, and the 2,6-dibromiated compound **8** was obtained by double bromination of **7**. 2.2 eq. of bromine was used, and reaction for 72 hours was required to obtain a high yield of the double brominated compound.

2.3 Synthesis of polycatenar compounds based on BTBT unit and selective bromination
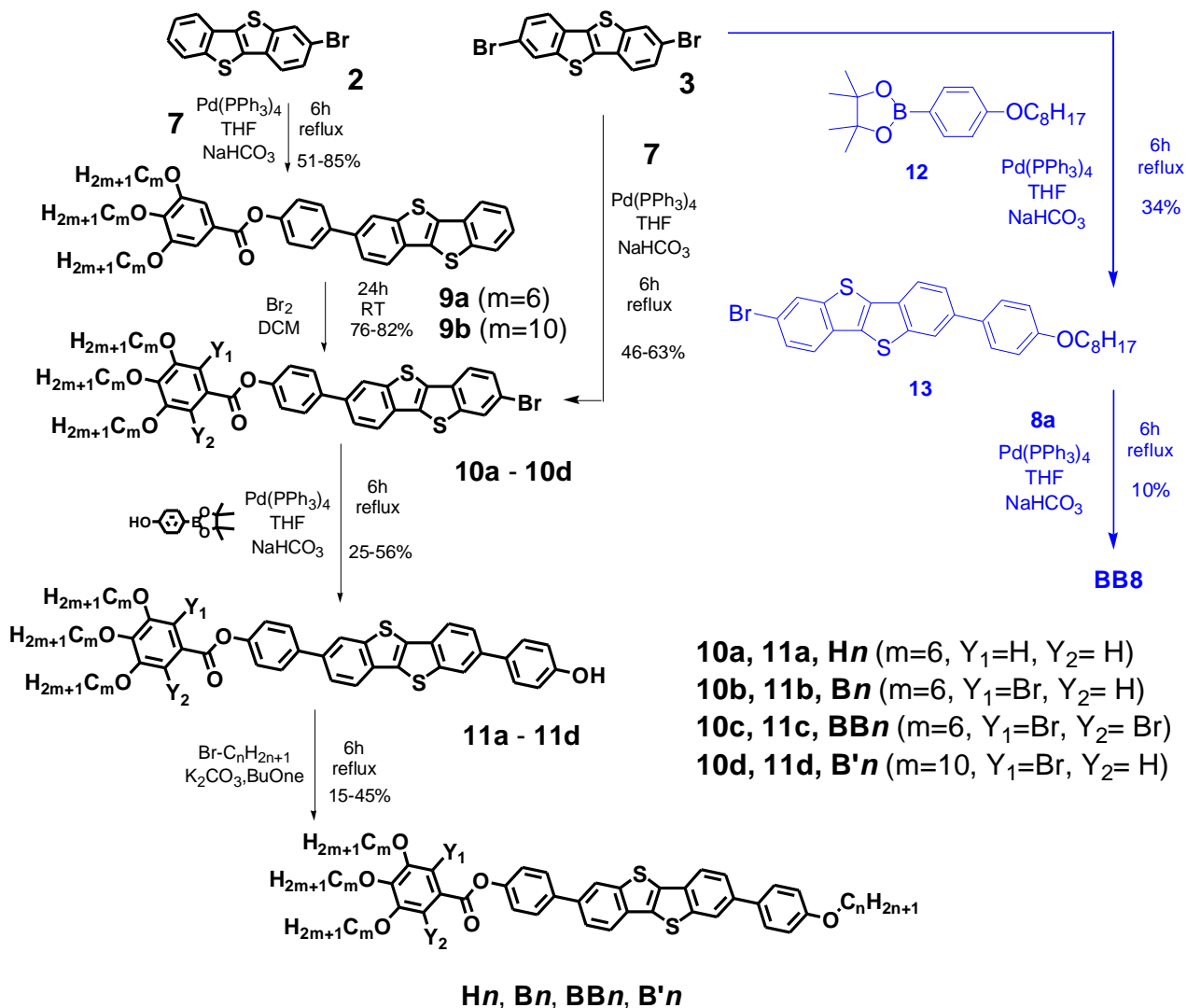
Scheme 2.4 Synthesis of **H*n***, **B*n***, **BB*n*** and **B'*n***

For the synthesis of polycatenars **9**, 2-bromo BTBT **2** and the boronate **7** were coupled via Suzuki coupling reaction.[6] From compound **9**, mono-bromination was attempted at the periphery of the BTBT unit, but failed because the electron-rich benzene with three alkoxy chains has reactive sites as well. Therefore, it is not possible to obtain **10a** directly from **9a**. To obtain the arylbromide **10a** without bromine at the benzoate unit, it is essential to start with the dibrominated BTBT (**3**) which is coupled with one eq. of the boronate **7**. The dibromianted compound **10b** and

the tribrominated compound **10c** can be obtained by bromination of **9a,b** and by adjusting the amount of bromine (2.2 eq. and 3.3 eq., respectively). The bromoarenes **10** were coupled with 4-hydroxyphenylboronic acid pinacol ester using the Suzuki coupling reaction.[6] This reaction works very well for the benzoate **10a**, but for the 2,6-dibromobenzoate **10C** it works only with Pd[PPh$_3$]$_4$ catalyst prepared according to reference.[7] However, the Pd[PPh$_3$]$_4$ catalyst commercially available from TCI is too reactive and leads to competitive coupling at the benzoate unit. In this case another synthetic route can be chosen as marked in blue in scheme 2.4 by coupling the dibrominated boronate **8a** with the BTBT bromide **13**. As a final step, for all other compounds alkylation of the phonols **11** was conducted with the appropriate alkyl bromide by using Williamson ether synthesis. The final compounds **Hn**, **Bn**, **BBn** and **B'n** were all purified by column chromatography with n-hexane/CHCl$_3$, and furthermore, by recrystallization with THF/MeOH and THF/EtOH.

2.4 Synthesis of short core polycatenar compounds based on BTBT unit
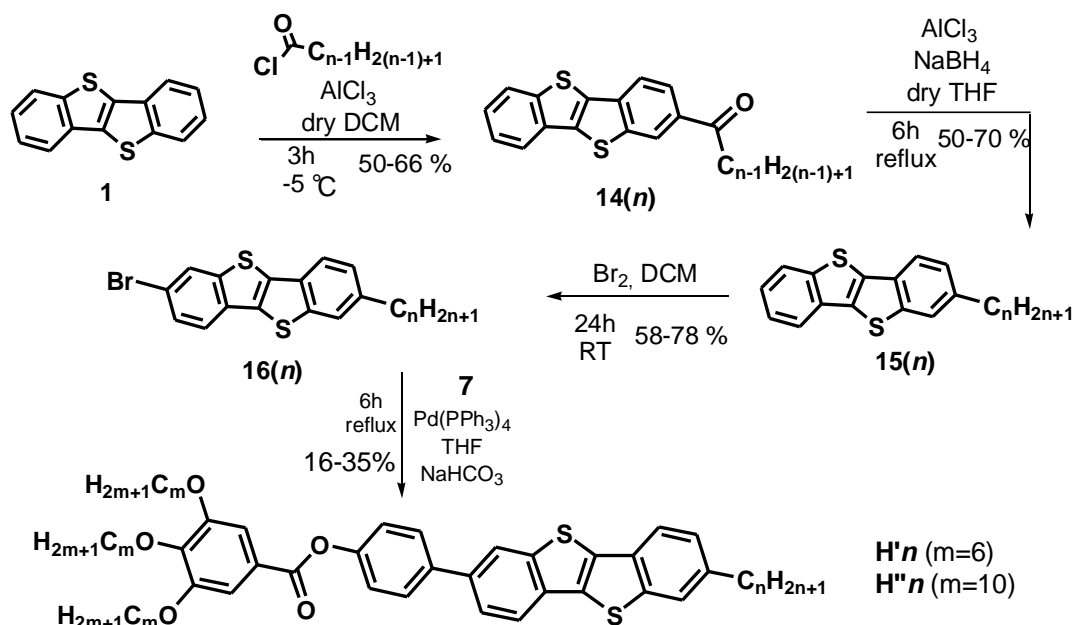
Scheme 2.5 Synthesis of **H'n** and **H''n**.

For the synthesis of short core polycatenar compounds based on the BTBT unit (**H'n** and **H''n**), Friedel-Crafts acylation was carried out using **BTBT** (**1**), the appropriate acyl chloride and AlCl$_3$ as the first reaction. Reductive deoxygenation of the acylated compounds **14(n)** with

NaBH$_4$/AlCl$_3$ removed the oxygen and replaced it by two hydrogen atoms. The resulting 2-alkysubstituted BTBT **15(n)** was brominated on the 7-position of the BTBT unit using bromine in DCM. For the final step, compounds **7** and **16(n)** were coupled via Suzuki coupling reaction,[6] resulting in **H'n** and **H''n**. The final compounds **H'n** and **H''n** were all purified by column chromatography with n-hexane/CHCl$_3$, and repeated recrystallization with THF/MeOH, *n*-hexane and *n*-pentane.

2.5 Synthesis of polycatenar compounds based on BTBT unit with a fluorinated benzene at the monoalkylated end
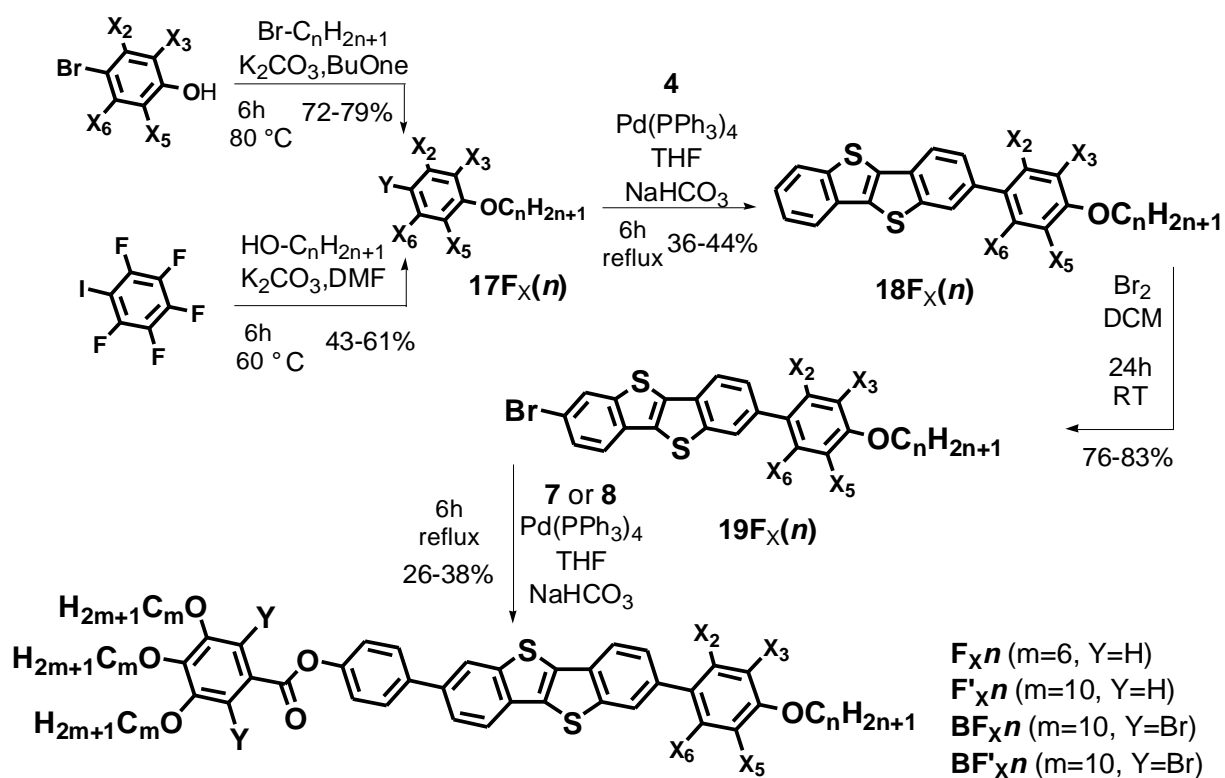
Scheme 2.6 Synthesis of **Fxn**, **F'xn**, **BFxn** and **BF'xn**.

For the synthesis of mono or difluorinated compounds the appropriate bromofluorophenols were selected as starting materials and iodopentafluorobenzene was used for the synthesis of tetrafluorinated compounds. Thus, bromofluorophenols were alkylated with appropriate n-alkylbromides while iodopentafluoro-benzene was alkylated by nucleophilic substitution with

appropriate n-alcanols. The resulting compounds **17F$_X$(n)** were coupled with an excess of BTBT boronate **4** through the Suzuki coupling reaction to give the 2-phenyl BTBT, **18F$_X$(n)**.[6] After monobromination of **18F$_X$(n)** in the 7-position, another Suzuki coupling reaction was carried out between the resulting compounds **19F$_X$(n)** and the boronates **7** or **8** using Pd[PPh$_3$]$_4$, THF and aqueous NaHCO$_3$ solution. The final compounds **F$_X$$n$**, **F'$_X$$n$**, **BF$_X$$n$** and **BF'$_X$$n$** were all purified by column chromatography with n-hexane/CHCl$_3$, and furthermore, by recrystallization with THF/MeOH and THF/EtOH.

For all compounds correct ^{1}H-NMR, ^{13}C-NMR, ^{19}F-NMR, HR-MS spectra and elemental analysis data were obtained confirming the proposed structure (chapter 11.Experimental section).

References

1   B. Košata, V. Kozmík, J. Svoboda, *Coll. Czech. Chem. Commun*. **2002**, 67, 645.

2   A. Sanzone, S. Mattiello, G. M. Garavaglia, A. M. Calascibetta, C. Ceriani, M. Sassi, L. Beverina, *Green Chem*., **2019**, 21, 4400.

3   S. Inoue, H. Minemawari, J. Tsutsumi, M. Chikamatsu, T. Yamada, S. Horiuchi, M. Tanaka, R. Kumai, M. Yoneya, and T. Hasegawa *Chem.Mater.* **2015** *27*, 11, 3809.

4   J. Takagi, K. Takahashi, T. Ishiyama, and N. Miyaura *J. Am. Chem. Soc.* **2002**, 124, 27, 8001.

5   V. A. Piunova, G. M. Miyake, C. S. Daeffler, R. A. Weitekamp, and R. H. Grubbs, *J. Am. Chem. Soc.* **2013**, 135, 15609.

6   N. Miyaura and A. Suzuki, *J. Chem. Soc. Chem. Commun.,* **1979**, 19, 866.

7   S. O. Mihigo, W. Mammo, M. Bezabih, K. Andrae-Marobela and B. M. Abegaz, *Bioorg. Med. Chem*., **2010**, **18**, 2464.

3. Investigation

All synthesized compounds were analyzed by differential scanning calorimetry (DSC), polarized optical microscopy (POM) and X-ray scattering (SAXS and WAXS) to characterize the liquid crystalline phases. Mirror symmetry breaking was investigated by POM and circular dichroism (CD). Furtherrmore, the charge carrier mobilities were investigated by TOF (time of flight) experiments and in OFET cells.

3.1 Characterization of the mesophases

Optical investigation. Phase transitions were observed by polarizing microscopy (Leica DMR XP) in conjunction with a heating stage (FP 82 HT, Mettler) and controller (FP 90, Mettler). Optical investigation was carried out under equilibrium conditions between glass slides which were used without further treatment, sample thickness was ~15 µm. A full wavelength retardation plate was used to determine the sign of birefringence. Optical micrographs were taken using a Leica MC120HD camera.

Calometric investigation. DSC measurements were carried out by means of DSC-7 and DSC-8000 (Perkin Elmer) at heating/cooling rates of 10 K min^{-1}. If not otherwise noted transition temperatures and –enthalpies were taken from the second heating and cooling curve and refer to the peak temperatures.

XRD. In-house XRD investigations were carried out by Dr. Silvio Poppe, at the Department of Chemistry, Martin Luther University of Halle-Wittenberg and were conducted at Cu K$_\alpha$ line (λ = 1.54 Å) using a standard Coolidge tube source with Ni-filter on powder-like samples. The samples were prepared on a glass plate and were heated to the isotropic state. The powder-like samples were obtained upon fast cooling into the LC phase and were measured in a temperature-controlled heating stage. The distance between sample and the detector was 9 cm (wide angle X-ray scattering - WAXS) or 26.8 cm (small angle X-ray scattering - SAXS) and the exposure time was 15 min for

WAXS and 30 min for SAXS. The diffraction patterns were recorded with a 2D detector (Vantec 500, Bruker), transformation to θ-scan was performed using GADDS.

High-resolution small/wide-angle powder diffraction experiments were performed by Prof. Feng Liu group at the Shaanxi International Research Center for Soft Matter, Xi'an Jiaotong University. They were recorded on Beamline BL16B1 at Shanghai Synchrotron Radiation Facility, SSRF. Experiments were carried out on samples in 1 mm glass capillaries under the control of modified Linkam hot stage with a thermal stability within 0.2 °C. The Pilatus 2M detector was applied in the experiments. q calibration and linearization were testified by using several orders of layer reflections from silver behenate and a series of n-alkanes.

Electron density calculation. Electron density calculations were also performed by our collaborators at Xi'an Jiaotong University. The diffraction peaks were indexed on the basis of their peak positions, and the lattice parameters and the plane/space groups were subsequently determined. Once the diffraction intensities are measured and the corresponding plane/space group determined, 3D electron density maps can be reconstructed, on the basis of the general formula

$$E(xyz) = \Sigma_{hkl}F(hkl) \exp[i2\pi(hx+ky+lz)] \tag{Eqn. 1}$$

Here $F(hkl)$ is the structure factor of a diffraction peak with index (hkl). It is normally a complex number and the experimentally observed diffraction intensity

$$I(hkl) = K \cdot F(hkl) \cdot F^*(hkl) = K \cdot |F(hkl)|^2 \tag{Eqn. 2}$$

Here K is a constant related to the sample volume, incident beam intensity, etc. In this paper we are only interested in the relative electron densities, hence this constant is simply taken to be 1. Thus, the electron density for 3D space groups is:

$$E(xyz) = \Sigma_{hkl} \text{sqrt}[I(hkl)] \exp[i2\pi(hx+ky+lz)+\phi_{hkl}] \tag{Eqn. 3}$$

As the observed diffraction intensity $I(hkl)$ is only related to the amplitude of the structure factor $|F(hkl)|$, the information about the phase of $F(hkl)$, ϕ_{hkl}, can not be determined directly from the experiment. However, the problem is much simplified when the structure of the ordered phase is centrosymmetric, and hence the structure factor $F(hkl)$ is always real and ϕ_{hkl} is either 0 or π. In the case of the centrosymmetric phase it is possible for a trial-and-error approach, where candidate electron density maps are reconstructed for all possible phase combinations, and the "correct"

phase combination is then selected on the merit of the maps, helped by prior physical and chemical knowledge of the system.

However, for non-centrosymmetric phase, such as I23, ϕ_{hkl} is arbitrary between 0 and π. Taking the model from a relevant work,[1] we applied similar phases and intensity distributions on the phases we studied in this work.

Investigation of cubic phases. The cubic phase types were distinguished by their typical SAXS patterns and by chiroptical investigations by POM between slightly uncrossed polarizer. The cubic phases are optically isotropic under all alignment conditions and distinguished from the isotropic liquid state by a much lighter viscosity. Cubic phases do not flow, but only can be deformed upon application of mechanical stress. The *Ia*3*d* phase is indicated by the absence of a chiral conglomerate structure, meaning that independent of the position of the polarizers there is a uniform brightness/darkness of the sample. Moreover, the SAXS pattern shows two strong scattering peaks which can be indexed as (211) and (220) scatterings of the *Ia*3*d* lattice.[2] In contrast the *I*23 phase is characterized by a conglomerate of dark and bright domains if investigated between slightly uncrossed polarizers; the brightness is reversed by inverting the rotation direction of the analyzer with respect to the crossed orientation (see Fig 1.7).[2,3] In this case the SAXS pattern shows three main scattering peaks which can be indexed to (321), (400) and (420) of the *I*23 lattice. [1,2] In both cubic phases there are additional smaller SAXS peaks which fit with the indexation of the main scattering peaks. In the WAXS range there is only a diffuse scattering with the maximum at $d = 0.45$ nm (or maximum at 0.45 and a second maximum as a shoulder at 0.34-0.39 nm) indicating the absence of fixed positions of the individual molecules and thus confirming the LC state of the mesophases. The additional maxima around 0.34-0.35 nm result from face-to-face π-stacking interactions. The Cub$_{bi}$-Iso transition is indicated by a sudden transition from a viscoelastic solid to a fluid state, associated with a small endotherm in the DSC traces, while the material remains optically isotropic. On cooling, this transition is easily supercooled and takes place at about 10-20 K lower temperature and often is accompanied by the formation of metastable and birefringent intermediate phases.

3.2 Charge carrier mobility

TOF measurements. The TOF experiments were carried out by myself and by Dr. Jadwiga Szydłowska at the Faculty of Chemistry, University of Warsaw. They were performed in a conventional setup, similar to those described in reference.[4] The 10 micron thick cell was used with ITO electrodes covered with homogeneously aligning surfactant, the cells were filled using capillary forces and the applied voltage was in the range of 11-117 V. All wire connections had grounded screens. The transient photocurrent was measured over 50 kΩ resistor and recorded with 300 MHz digitizing oscilloscope (Agilent Technologies DSO6034A) triggered by the laser pulse. The estimated response time of the whole setup was less than 2.5 μs. The charges (holes and electrons) were generated by a short light pulse (355 nm wavelength, ~8 ns pulse width) coming from a solid-state laser EKSPLA NL202. The sample was illuminated by a single pulse manually triggered to give the sample enough time for relaxation. To reduce the noise the data were collected over 16 runs and averaged. For the studied material the hole current was stronger, more stable and reproducible than the electron current. The registered hole photocurrent curves were non-dispersive, with clear cut-off enabling precise determination the transient time, τ. The transient time τ was determined as the intersection of two lines tangential to the plateau and 'current tail'. Form the transient time τ the charge (hole) mobility was calculated according to the formula: $\mu = d/(\tau E)$, where d is the sample thickness (in cm), E – the strength of electric field (in Vcm^{-1}) and τ – time-of-flight (τ/s). The charge mobility generally follows the linear relation $\log\mu \sim aE^{1/2}$, with the slope a decreasing with increasing temperature.[5] The hole mobility μ was further analyzed assuming one dimensional charge carrier hopping transport, using the formula with temperature (in K) and field (in V/cm) dependence:

$$\mu = \mu_0 \exp\left[-\left(0.9\frac{\sigma}{kT}\right)^2\right] exp\left\{C\left[\frac{\sigma}{kT} - \Sigma\right]\sqrt{E}\right\} \quad (1)$$

where prefactor μ_0 is charge mobility at T→∞, $E = 0$, k – Boltzman constant (8.617 × 10^{-3} eV/K); σ is a standard deviation of Gaussian distribution of energy levels ('diagonal disorder') that are available as hopping sites in holes transport process. The parameter Σ ('off-diagonal disorder')

reflects a coupling between transport sites. The parameter μ_0 and σ (standard deviation of energy levels) were obtained by extrapolating the linear dependence $\ln\mu(E^{1/2})$ to $E = 0$ at each temperature and using for $\ln\mu(E = 0)$ the formula:

$$b = ln\mu(E = 0) = ln\mu_0 - \left(0.9\sigma/_{kT}\right)^2 \text{ with:} \quad (2)$$

$$b' = ln\mu_0; \quad a' = -\left(0.9\sigma/_{k}\right)^2$$

The parameter b as a function of T^{-2} are plotted below and b' and a' parameter of this function are taken from linear fitting. The value of and μ_0 and σ parameters are given in Figure 5. Similarly, other coefficients C and Σ describing the charge transport process are calculated from the slopes a of the lines $\ln\mu \sim aE^{1/2}$. Writing $a = C[(\sigma/kT) - \Sigma]$ (formula (1)) and drawing a as a function of T^{-1} the fitted linear parameters are $a'' = C(\sigma/k)$ and $b'' = -C\Sigma$. The found C and Σ are shown in Figure 5.

OFET cells. The OFET experiments were carried out by Moon Jong Han at the Graduate School of Nanoscience and Technology, Korea Advanced Institute of Science and Technology. The OFETs with a bottom-gate top-contact configuration were fabricated on a heavily n-doped silicon wafer as the gate electrode. A 300 nm thick layer of thermally grown SiO_2 served as the gate dielectric layer. The device substrates were cleaned in an ultrasound cleaning bath and sequential rinsing with acetone, ethanol, and deionized water for 15 min each. The 50 nm Au source and drain electrodes with 3 nm Ti as the adhesion layer were both deposited via thermal evaporation using a shadow mask. For a uniform cell gap, the silicon particle with a 1 μm diameter was deposited on the edges of the bottom substrates using UV-curable polymer (NOA 63, Norland Products). The prepared top substrates which are coated with polyimide (PI) were combined with the bottom substrates following UV exposure. The **B22** crystalline powder was prepared on the entrance of the gap, and then heated to around the isotropic phase temperature of **B22** (T_{iso} = 220 °C) to fill the sandwich cell by capillary action. The transfer characteristics of bottom-gate top-contact FETs based on the semiconductor were studied with a Keithley 4200A-SCS semiconductor parameter analyzer. The charge carrier mobility (μ) was calculated by using the following equation from the saturated region in the transfer curve,

$$I_{DS} = (W C_i/2L)\mu(V_{GS} - V_{th})^2$$

where W and L refer to the channel width (500 μm) and length (50 μm), respectively. C_i is the areal capacitance of the SiO_2 gate dielectric (1.04×10^{-8} F cm^{-2}), and V_{th} is threshold voltage. V_{th} was extracted via a linear fitting of versus V_G, which is based on the linear transfer data. To avoid mobility attenuation depending on V_G, we selected a sufficient V_G to ensure that the saturation region $V_{GS} \leq V_{th}$ and $V_{DS} \leq V_{GS} - V_{th}$ is satisfied.[6]

References

1   X. Zeng, G. Ungar, *J. Mater. Chem. C*, **2020**, 8, 5389.

2   C. Dressel, T. Reppe, S. Poppe, M. Prehm, H. Lu, X. Zeng, G. Ungar, C. Tschierske, *Adv. Funct. Mater.* **2020**, 2004353.

3   a) C. Dressel, F. Liu, M. Prehm, X. Zeng, G. Ungar, C. Tschierske, *Angew.Chem. Int. Ed.* **2014**, 53, 13115; b) Y. Cao , M. Alaasar, A. Nallapaneni, M. Salamończyk, P. Marinko, E. Gorecka, C. Tschierske, F. Liu, N. Vaupotič, C. Zhu, *Phys.Rev.Lett.* **2020**, 125, 027801.

4   P. M. Borsenberg, L. Pautmeier, H. Bässler, *J. Chem. Phys.,* **1991**, 95, 1258.

5   H. Bässler, *Physica Status Solidi*, **1993**, 175, 15; *Phys. Chem. Chem. Phys*., **2014**, 16, 7754; M. Kastler, F. Laquai, K. Müllen, G. Wegner, *Appl. Phys. Lett.,* **2006**, 89, 252103.

6   M. J. Han, M. McBride, B. Risteen, G. Zhang, B. V. Khau, E. Reichmanis, D. K. Yoon, *Chem. Mater.* **2020**, 32, 688.

4. Charge transportation and chirality in liquid crystalline helical network phases of the first achiral BTBT-derived polycatenar molecules
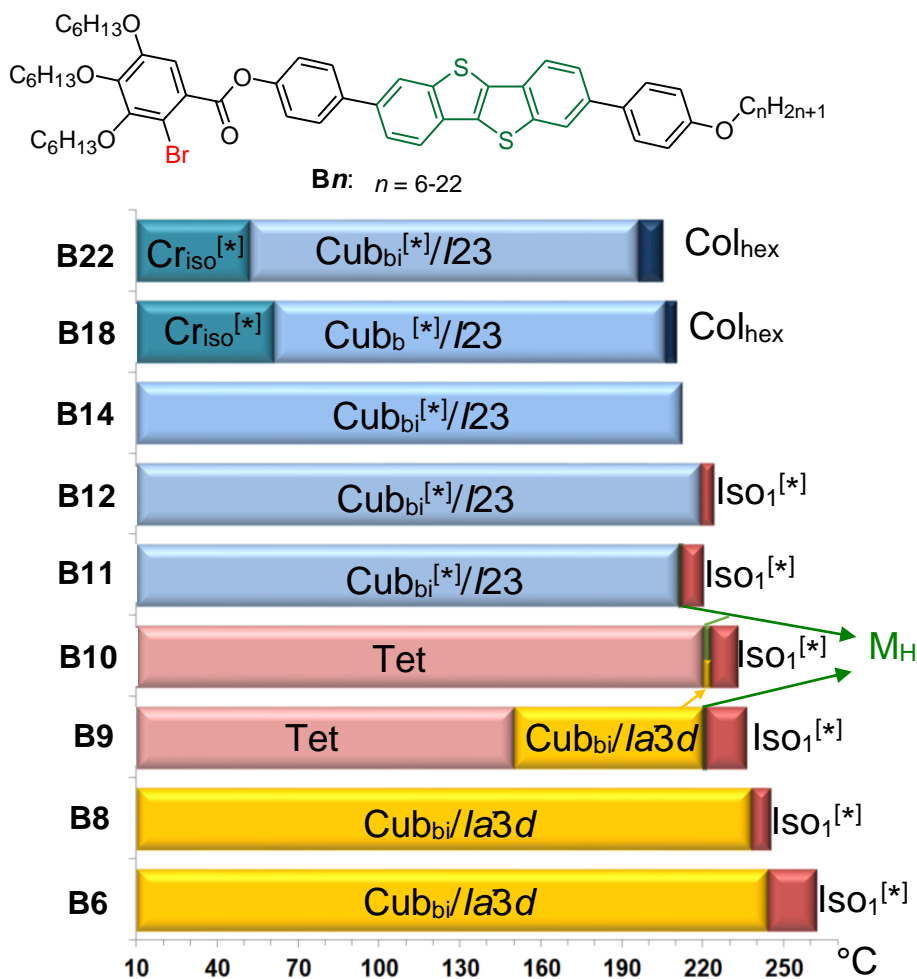
Figure 4.1 LC phases and phase transitions of compounds **Bn** as observed on cooling (DSC, rate 10 K min^{-1}); abbreviations: Cr$_{Iso}$[*] = optically isotropic crystalline mesophase with chiral conglomerate texture; Cub$_{bi}$/$Ia3d$ = bicontinuous cubic phase with double gyroid structure; Cub$_{bi}$[*]/$I23$ = mirror symmetry broken tricontinuous cubic phase with $I23$ space group; Tet = tetragonal phase, Col$_{hex}$ = hexagonal columnar LC phase; Iso$_1$[*] = mirror symmetry broken isotropic liquid and M$_H$ = metastable highly birefringent 3D mesophase (for **B10** either Cub$_{bi}$/$Ia3d$ or M is formed depending on the conditions; for data on heating and for numerical data with transition enthalpies, see Table 4.1

An especially wide range of different chain length was investigated for the monobrominated compounds **B***n* (and **B'***n*, see Section 6). This series of compounds will be described first and all structurally related compounds will be discussed in relation to this series further below. The mesophases and phase transitions of the series of compounds **B***n* on cooling are shown in Fig. 4.1; the numerical data with associated enthalpy values are collated in Table 4.1. In the following the soft self-assembly of compounds **B***n*, with a focus on their ability of network formation, is described first. Then the charge transportation properties are reported.

4.1 Two types of bicontinuous cubic network phases

Depending on the chain length two different Cub_{bi} phases, separated by a birefringent tetragonal phase (Tet) can be observed as the dominating mesophases (Fig. 4.1). The small angle X-ray scattering (SAXS) pattern of the Cub_{bi} phase of the short chain compounds **B6**-**B9** is typical for a cubic lattice with *Ia*3*d* space group (the double gyroid, Cub_{bi}/*Ia*3*d*, see Fig. 4.2d and Table 4.1). For **B6** the lattice parameter is $a_{cub} = 10.1$ nm at 190 °C (for numerical data, see Table 4.2) and about 700 molecules are organized in each unit cell (n_{cell}) with 3-4 molecules are arranged in the cross section of the networks (n_{raft}, see Table 4.2). On cooling **B6** and **B8** with the shortest chains, the double gyroid phase is retained from 244/238 °C down to 0 °C (see Figs. 4.1, 4.2a and Table 4.1), thus leading to a wide Cub_{bi} phase range of about 240 K. No melting is observed in the second and all following heating scans, meaning that the samples do not crystallize. Only after 2 years storage at room temperature the sample of **B6** has partly crystallized and a melting of the crystallized parts of the sample of **B6** can be observed at 87 °C.

The Cub_{bi}/*Ia*3*d* phase is observed for all compounds **B8**-**B10** with slightly *decreasing* lattice parameter upon chain *elongation* from $a_{cub} = 10.1$ nm for **B6** to 9.85 nm for **B10** (Table 4.2). This inverted chain length dependence of a_{cub} is in line with an increasing helical twist Φ with growing chain volume (8.8 ° to 9.1°). As the helical twist between two adjacent junctions of the network is fixed to 70.5° also the angle between the rod-like cores at the junctions have to be twisted by this fixed angle. Therefore, an increasing intermolecular twist reduces the distance between the junctions, thus shrinking the cubic lattice (see Fig 4.3d). [1,2] A similar shrinkage of a_{cub} is also observed by rising temperature (for **B8**, as example, from 10.2 nm at 100 °C to 9.9 nm at 240 °C, see Fig. 4.3c), in this case due to the increasing helical twist caused by thermal alkyl chain

Table 4.1 Transition temperatures and corresponding enthalpies of compounds **B6-B22** as measured on heating and cooling at 10K/min.[a]

Comp.	T/°C [ΔH /kJ·mol^{-1}]
B6	Heating: Cr 87 [3.8] Cub$_{bi}$/$Ia3d$ 266 [1.8] Iso Cooling: Iso 262 [-1.0] Iso$_1$[*] 244 [-1.0] Cub$_{bi}$/$Ia3d$ <20 Cr
B8	Heating: Cr <20 Cub$_{bi}$/$Ia3d$ 247 [2.0] Iso Cooling: Iso 245 [-0.1] Iso$_1$[*] 238 [-1.2] Cub$_{bi}$/$Ia3d$ <20 Cr
B9	Heating: Cr <20 Tet 155 [-] Cub$_{bi}$/$Ia3d$ 236 [1.7] Iso Cooling: Iso 236 [-0.2] Iso$_1$[*] 221 [-] M 220 [-0.7][b] Cub$_{bi}$/$Ia3d$ 150 [-] Tet <20 Cr
B10	Heating: Cr 90 [16.8] Tet 226 [-] Cub$_{bi}$/$Ia3d$ 227 [1.7] Iso$_1$[*] 233 Iso Cooling: Iso 233 [-0.1] Iso$_1$[*] 223 M [-] 220 [-0.7][b] Tet <20 Cr
B11	Heating: Cr <20 Cub$_{bi}$[*]/$I23$ 160 [-] Tet 180 [-] Cub$_{bi}$[*]/$I23$ 227 [1.8] Iso Cooling: Iso 220 [-0.1] Iso$_1$[*] 212 M 211 [-0.9][b] Cub$_{bi}$[*]/$I23$ <20 Cr
B12	Heating: Cr 98 [8.0] Cub$_{bi}$[*]/$I23$ 231 [2.5] Iso Cooling: Iso 224 [-0.2] Iso$_1$[*] 219 [-1.7] Cub$_{bi}$[*]/$I23$ <20 Cr
B14	Heating: Cr 60 [23.0] Cub$_{bi}$[*]/$I23$ 227 [2.5] Iso Cooling: Iso 212 [-1.9] Cub$_{bi}$[*]/$I23$ <20 Cr
B18	Heating: Cr 98 [36.7] Cub$_{bi}$[*]/$I23$ 220 [2.9] Iso Cooling: Iso 210 [-1.6] Col$_{hex}$ 206 [-0.5] Cub$_{bi}$[*]/$I23$ 61 [-33.8] Cr$_{Iso}$[*] 2nd Heating: Cr$_{Iso}$[*] 95 [34.3] Cub$_{bi}$[*]/$I23$ 220 [2.9] Iso
B22	Heating: Cr$_1$ 99 [64.9] Cub$_{bi}$[*]/$I23$ 211 [2.9] Iso Cooling: Iso 205 [-1.9] Col$_{hex}$ 196 [-0.5] Cub$_{bi}$[*]/$I23$ 52 [-26.4] Cr$_{Iso}$[*] 2nd Heating: Cr$_{Iso}$[*] 74 [-7.1] Cr$_2$ 88 [33.5] Cub$_{bi}$[*]/$I23$ 212 [2.8] Iso

[a] Determined by DSC, 10 K min^{-1}; all heating data were recorded for the first heating of a previously molten sample (after more than two years storage, except compound **B18** which was obtained by the first heating of the crystallized sample); the cooling data were obtained for the following cooling scan; transitions without enthalpy were determined by POM; abbreviations: Cr, Cr$_1$ and Cr$_2$ = birefingent crystalline phases, for the other abbreviations, see Figure 4.1. [b]Enthalpy involves both transitions.
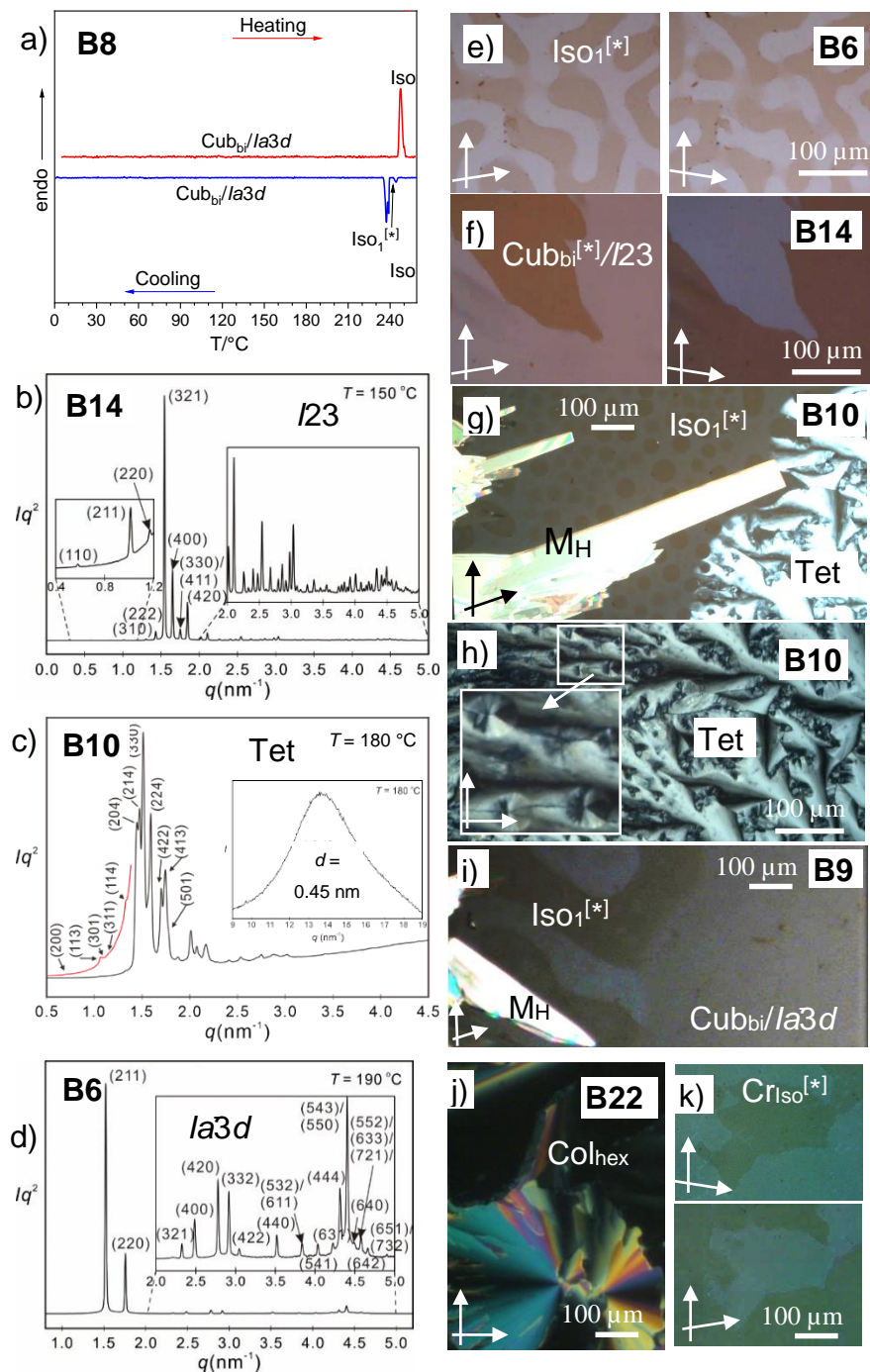
Figure 4.2 Characterization of the mesophases of compounds **B***n*. (a) DSC heating and cooling traces (10 K min⁻¹) of **B8**. (b-d) SAXS patterns of b) **B14**, c) **B10** (the inset shows the diffuse WAXS) and d) **B6** in the distinct phases at the given temperatures with indexation. (e-j) Representative textures; (e) chiral domains of the Iso₁[*] phase of **B6** at 262 °C; f) chiral domains of the Cub_bi[*]/*I*23 phase of **B14** at 150 °C; (g) Iso₁[*]-M_H-Tet transition of **B10** at 220 °C; (h) fully developed Tet phase of **B10** at 180 °C; (i) Iso₁[*]-M_H-Cub_bi/*Ia*3*d* transition of **B9** at 221 °C and (j) Col_hex phase of **B22** at 203 °C; (k) conglomerate of the Cr_Iso[*] phase of **B22** at 20 °C as observed between slightly uncrossed polarizers.
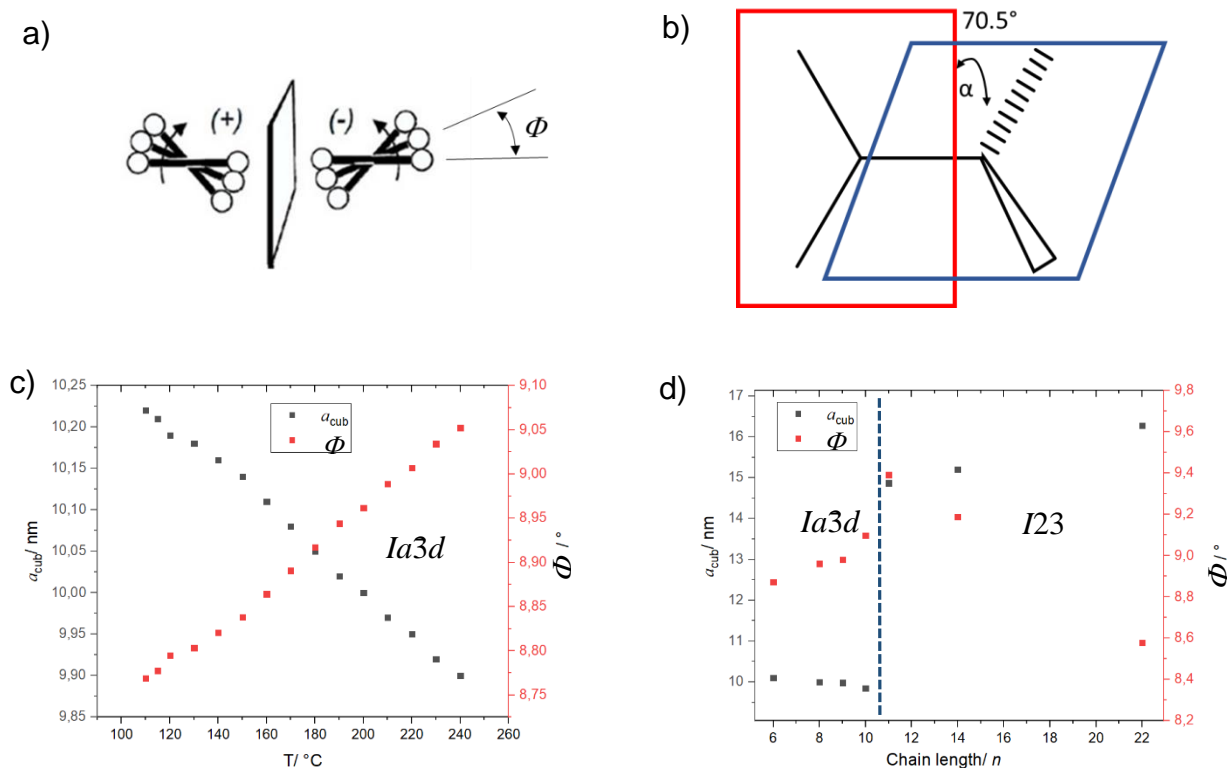
Figure 4.3 a) Intermolecular twist along the networks; b) twist between the two adjacent junctions of the networks in the $Ia3d$ phase; c) T-dependence of a_{cub} and Φ for the $Ia3d$ phase of compound **B8** and d) chain length dependence of a_{cub} and Φ in the series **Bn**.

expansion. At a certain pitch length, the double gyroid structure becomes instable and is replaced by other LC phases, as follows. For all compounds with $n = 11$-22 the SAXS pattern of the Cub$_{bi}$ phase can be indexed to the $I23$ space group. The SAXS pattern of compound **B14** is shown as example in Fig. 4.2b. Representative examples of the reconstructed electron density maps of the Cub$_{bi}$/$Ia3d$ phase of **B9** and the Cub$_{bi}$/$I23$ phase of **B22** are shown in Fig. 4.4. In accordance with a transition from a double network to a triple network the lattice parameter for the Cub$_{bi}$[*]/$I23$ phase is about 50% larger than that in the Cub$_{bi}$/$Ia3d$ phase (Table 4.2). This Cub$_{bi}$ phase is mirror symmetry broken and forms a conglomerate composed of chiral domains, as identified by investigations between polarizers being rotated by a few (1~5°) degrees out of the exactly 90° orientation (Fig. 4.2f). Inverting the direction of the rotation inverts the brightness of the domains, thus indicating an optical rotation being in line with the chiral $I23$ lattice.[3] In the $Ia3d$ phase range the effect of elongation of the relatively short chains is mainly a chain volume effect, increasing the steric distortion at the molecular ends and thus increasing the helical twist. In contrast, in the

*I*23 phases, formed by long chain compounds, chain elongation reduces the helical twist (from 9.4°
for **B11** to 8.6° for **B22**, see Table 4.2 and Fig. 4.3d). Besides the steric effect, chain elongation
simultaneously elongates the molecules, especially if the contribution of *all-trans* segments
increases. The elongation of the molecule (at constant chain volume) reduces the twist. For the
long chain compounds **B*n*** the contribution of chain elongation on the molecular length has
obviously a stronger twist-reducing effect than the twist-increasing effect provided by the
simultaneously growing chain volume.[4] Therefore no transition to a second *Ia*3*d* phase with larger
twist (*Ia*3*d*(S), as obtained for other tetracatenars[5,6]) can be achieved, even for the compounds **B18**
and **B22** with very long alkyl chains.
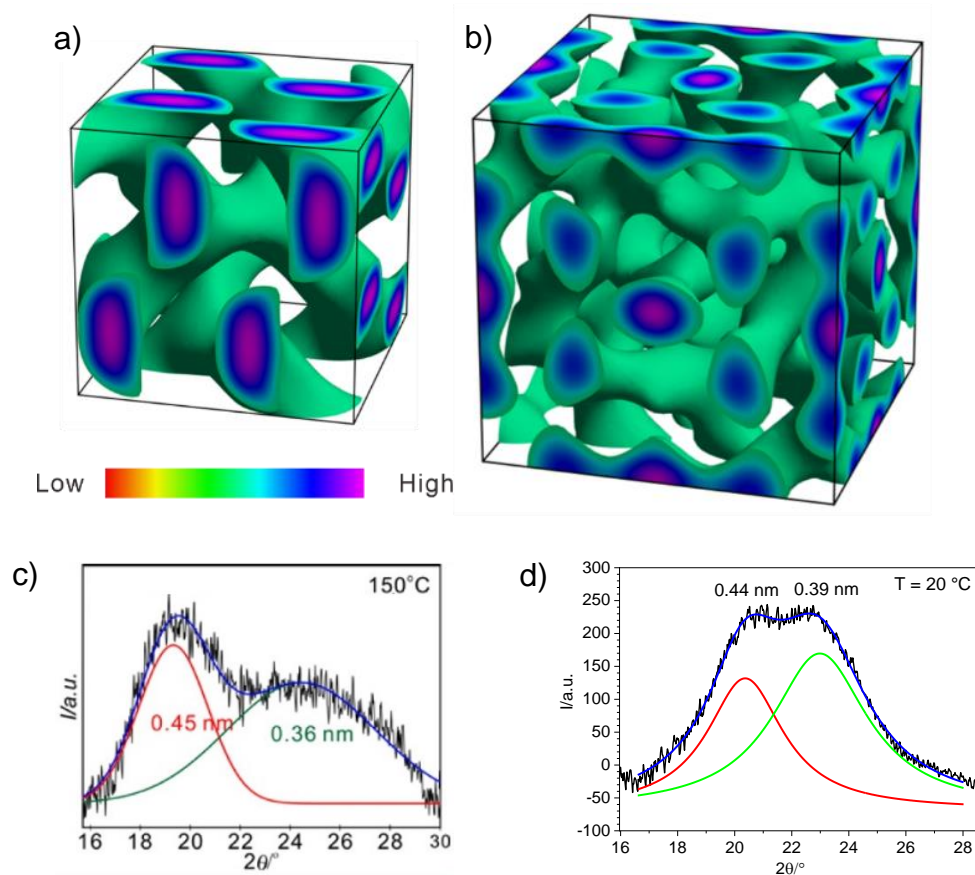
Figure 4.4 a, b) Reconstructed electron density map of (a) the Cub$_{bi}$/ $Ia\overline{3}d$ phase of **B9** and (b)
the Cub$_{bi}$[*]/*I*23 phase of **B22**. The green iso-surfaces enclose the high electron density
(blue/purple, aromatic cores) regions of the 3D electron density map. The low electron density
(red/yellow) alkyl chains regions are omitted for clarifying the networks; (c,d) show the WAXS
diffractogram of (c) the Cub$_{bi}$[*]/*I*23 phase of **B12** and (d) the Cr$_{Iso}$[*] phase of **B22** with
deconvolution into two scattering maxima.

Table 4.2 Structural data of the mesophases of the investigated compounds.

Compd.	Phase	T/°C	a_{cub} or c/nm	V_{cell}/nm^3	V_{mol}/nm^3	n_{cell}	d_{net}/nm	L_{net}/nm	n_{raft}	Φ/°
B6	Cub$_{bi}$/$Ia3d$	210	10.10	1030	1.284	717	4.37	85.70	3.76	8.87
B8	Cub$_{bi}$/$Ia3d$	200	10.00	1000	1.334	670	4.33	84.85	3.55	8.96
B9	Cub$_{bi}$/$Ia3d$	190	9.98	994	1.358	653	4.32	84.68	3.47	8.98
B9	Tet	180	17.80 20.12	6375	1.358	4191	-	-	-	-
B10	Cub$_{bi}$/$Ia3d$	230	9.85	956	1.383	617	4.27	83.58	3.32	9.10
B10	Tet	130	17.74 20.32	6395	1.383	4129	-	-	-	-
B11	Tet	170	17.80 20.12	6361	1.408	4034	-	-	-	-
B11	Cub$_{bi}$ [*]/$I23$	200	14.87	3288	1.408	2085	-	307.51	3.05	9.39
B14	Cub$_{bi}$ [*]/$I23$	150	15.20	3512	1.482	2116	-	314.34	3.03	9.19
B22	Cub$_{bi}$ [*]/$I23$	150	16.28	4315	1.681	2292	-	336.67	3.06	8.58
B22	Col$_{hex}$/$p6mm$	205	4.65	8.43	1.681	4.5	-	-	4.5	-

[a] Abbreviations: $V_{cell} = a_{cub}^3$ = volume of the unit cell; for the tetragonal phase $V_{cell} = a^2$ x c, for Col$_{hex}$ phases a height h of 0.45 nm is assumed: $V_{cell} = h(\sqrt{3}a_{hex}^2/2)$; V_{mol} = volume of the molecule as calculated with the crystal volume increments of Immirzi;[7] n_{cell} = number of molecules per unit cell, calculated according to 0.893 V_{cell}/V_{mol}, where the factor 0.893 is a correction for the different packing density in the crystalline and the LC state; d_{net} = lateral distance between the nets in the $Ia3d$ phase, calculated according to: $d_{net} = \sqrt{3}(a_{cub}/4)$, this value is in good agreement with the molecular length, shown in Fig. S9 for **B10** and considering the conformational disorder of the alkyl chains; L_{net} = total length of the netwoks per unit cell ($L_{net} = 8.485a_{Ia3d}$ and $L_{net} = 20.68a_{I23}$, respectively;[8] n_{raft} = number molecules organized in each 0.45nm tick raft of the networks or columns, calculated according to $n_{raft} = n_{cell}/(L_{net}/0.45)$; for Col$_{hex}$: $n_{raft} = n_{cell}$; Φ = twist angle between adjacent molecules (or rafts of molecules) in the networks of the Cub$_{bi}$ phases; $\Phi(Ia3d$) = 70.5°/[0.354a_{cub}/0.45nm], $\Phi(I23)$ = 90°/[0.290a_{cub}/0.45nm] [8].

4.2 Non-cubic 3D phases

At the transition between the two cubic phases two additional birefringent mesophases were observed. For the compounds **B9-B11** a small range of a highly birefringent mesophase (M$_H$) with mosaic texture develops on cooling at the transition from the Iso$_1$[*] phase and disappears together with the developing Cub$_{bi}$ phase (see Fig. 4.2g, i). However, due to metastability, its investigation was not possible. In addition, a weakly birefringent mesophase with unique texture is observed (see Fig. 4.2g, h); for **B9** it appears on cooling below the Cub/$Ia3d$ phase at 150 °C and for the next homologue **B10** it replaces the Cub/$Ia3d$ phase almost completely. For **B11** it

interrupts the $Cub_{bi}^{[*]}/I23$ phase between 160 and 180 °C upon heating whereas on cooling exclusively the $Cub_{bi}^{[*]}/I23$ phase is found (see Table 4.1). The formation of birefringent mesophases with non-cubic 3D lattice[9] is obviously associated with the $Ia3d-I23$ transition and compound **B10**, located in the middle of this transition forms the broadest region. The SAXS pattern of **B10** can be indexed to a tetragonal lattice with the lattice parameters $a_{squ} = 17.74$ nm and $b = 20.32$ nm based on the possible highest symmetry space group $P4_2/nnm$ (Fig. 3c, see Table 4.2). Similar values were found for the related phase of compounds **B9** and **B11** (Table 4.2). Both lattice parameters are even larger than those of the $I23$ phase and the number of molecules per unit cell (n_{cell}) is approximately doubled from about 2100-2300 in $I23$ to 4050-4650 in Tet (Table 4.2). As also observed in the adjacent $Ia3d$ phase n_{cell} decreases with growing chain length, suggesting that this tetragonal phase is likely to be a helical network phase, too, but assuming a distorted non-cubic lattice. Further investigations are required to fully understand these intermediate phases.

4.3 Columnar phase of B22

For the compounds with the longest chains ($n = 18, 22$) the $Cub_{bi}/I23$ phase occurs below a small range of a hexagonal columnar (Col_{hex}) phase (for $n = 22$: $a_{hex} = 4.65$ nm, see Fig. 4.2j). The formation of a columnar phase is in line with the growing interface curvature achieved for compounds with longer chains above a certain temperature. However, the columnar phase is metastable, as it can only be found in the cooling cycles, whereas on heating in all cases a direct Cub_{bi}-Iso transition is observed. It appears that on cooling the chain mobility can be retained at the transition to Col_{hex}, which requires alkyl chain disorder to efficiently fill the space around the columns. In the Cub_{bi} phase, having less mean curvature, a larger reduction of chain disorder is required. This might lead to an entropic penalty for the direct Iso-Cub_{bi} transition on cooling. On the other hand, a larger fraction of *all-trans* chain conformations can be retained in the Cub_{bi} phase which stabilizes the Cub_{bi} phase energetically by denser intermolecular contacts and thus cooperatively inhibits the transition to Col_{hex} on heating. This provides hysteresis and pathway complexity.

4.4 Crystalline network phase of B22
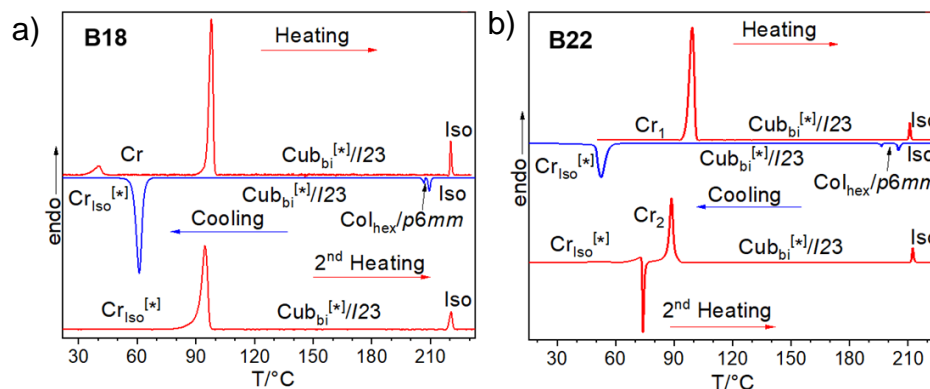
Figure 4.5 DSC heating and cooling traces (10 K min^{-1}) of (a) **B18** and (b) **B22**.

In addition, for the two long chain compounds **B18** and **B22** the transition to an optically isotropic crystalline mesophase with conglomerate texture (Cr_{Iso}[*], see Fig. 4.2k)[11] is observed on cooling the Cub_{bi}/$I23$ phase, associated with a significant transition enthalpy ($\Delta G \sim$ 30 kJ mol^{-1}, see Table 4.1 and Fig. 4.5). The WAXS splits into two maxima at $d = 0.44$ and 0.39 nm (Fig. 4.4d), the latter is attributed to π-π-stacking of the crystallized aromatics, whereas the alkyl chains remain in the disordered state, thus retaining the scattering around 0.45 nm; the SAXS becomes a single diffuse scatter at $d = 3.2$ nm which is interpreted as a loss of the cubic lattice, though, chirality synchronization and network structure are obviously retained. Though the Cr_{Iso}[*] phase is metastable with respect to the birefringent crystalline phase (Cr), once formed it is long time stable (>2 years) at ambient temperature (Fig. 4.2k). The slow kinetics of the transition Cr_{Iso}[*] to Cr might result from a combination of reduced molecular mobility at lower temperature and the cooperativity, provided by the long range synchronized helical network structure, providing a significant energetic barrier for the transition to the structurally different birefringent crystalline (Cr) phase.

4.5 Mirror symmetry broken isotropic liquid network phase

Another interesting feature of compounds **Bn** is the formation of a mirror symmetry broken isotropic liquid (Iso_1[*])[10,11,12] between the achiral isotropic liquid (Iso) and the Cub_{bi} phases of

compounds **B6**-**B12** (Fig. 4.1 and Table 4.1). For compound **B10** it is a thermodynamically stable (enantiotropic) phase, whereas for the other homologues it is only observed as a monotropic (metastable) phase on cooling before the Cub_{bi} phase is formed. The $Iso_1^{[*]}$ phase is considered as a percolated liquid formed by a dynamic chirality synchronized helical network without long range periodic lattice.[10,11] It results from the ordinary isotropic liquid (Iso) by a growing number of network junctions with decreasing temperature. After reaching a critical density of the junctions, chirality synchronization sets in at the Iso-$Iso_1^{[*]}$ transition and mirror symmetry breaking (conglomerate formation, see Fig. 4.2e) is observed.[12] Further cooling then leads to the development of a cubic lattice with long range periodicity, either *Ia*3*d* with loss of mirror symmetry breaking, or *I*23 by retaining mirror symmetry breaking (see Fig. 4.1 and Table 4.1).

4.6 Charge carrier mobility depending on the phase type

The charge carrier mobility of selected compounds was determined by time of flight (TOF) measurements as well as in an organic field effect transistor (OFET) device, as described in the Section 3 and Experimental Section.

*4.6.1 Time of flight experiments in the I23 phase of **B12***

The charge carrier mobility in the cubic network phases was measured by TOF experiments for the *I*23 phase of **B12** to be between 1.7×10^{-5} to 1.3×10^{-4} cm^2 V^{-1} s^{-1}, increasing with rising temperature from 110 to 180 °C (Figs. 4.6a). Remarkably, the character of hole current vs. time is non-dispersive with very well-defined cut–off (see Fig. 4.6d, e), such features are only rarely observed for LC materials,[13] suggesting a considerably lower number of defects in the structure and lower molecular mobility, than in the other LC phases, thus allowing propagation of the charge wave through the sample without dissipation. Due to the absence of long range π-stacking interaction between the aromatic cores (indicated by the diffuse wide-angle X-ray scattering with a maximum at 0.45 nm, see Fig. 4.4c as example) and the longer path of the channels transporting the holes/electrons between the electrodes in the complex 3D structure of the Cub_{bi} phases compared to the linear channels in a well aligned Col_{hex} phase of the same material,[13] the charge

carrier mobility is still limited, but it can be significantly enhanced at the transition to a soft crystalline network phase as shown below.
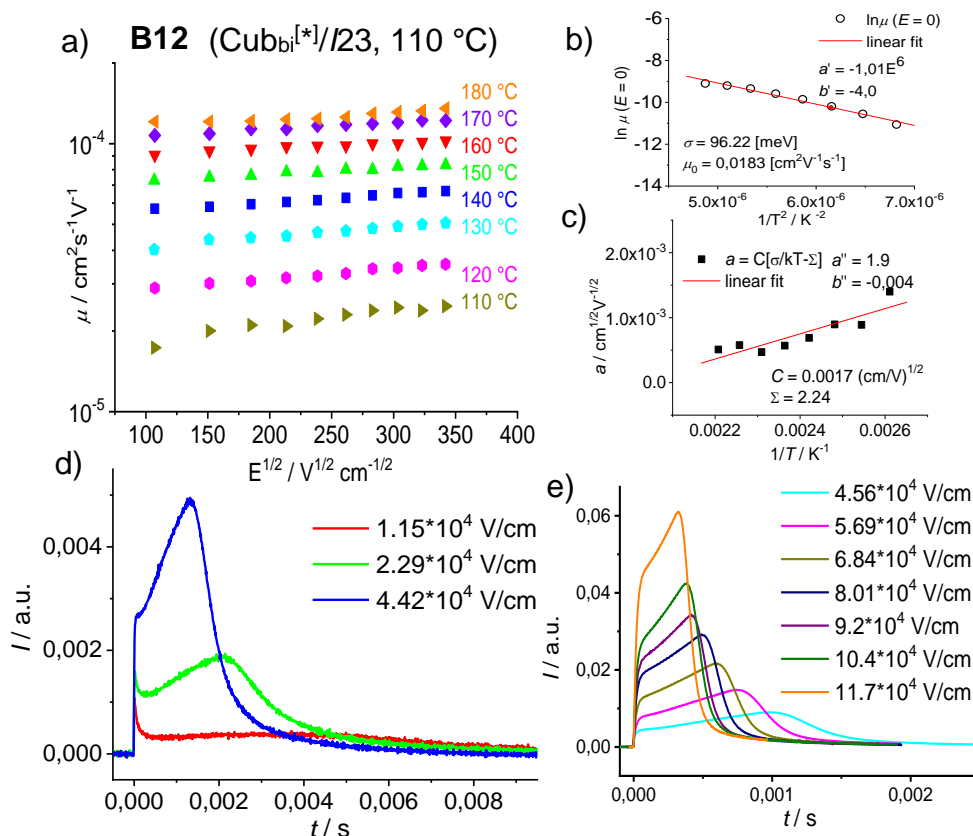
Figure 4.6 TOF investigation of **B12** in $Cub_{bi}^{[*]}/I23$ phase at 110 °C. (a) Field dependence of hole mobility, (b) slope a of the $\ln\mu(E^{1/2})$ dependence and (c) zero-field hole mobility b and $a = C[(\sigma/kT) - \Sigma]$; (d, e) TOF transient current of holes at different fields, for details of calculations, see Experimental Section.

*4.6.2 Investigation of OFET cells of **B22***

The charge carrier mobility of **B22** was measured in modified OFET sandwich cells with bottom-gate bottom-contact (BGBC) configuration (Fig. 4.7a), which were prepared as described in Section 3 and the Experimental Section. The OFETs shows highly uniform and smooth surface morphology, which improves reproducibility and reliability of the device performance. The electrical properties of the *p-type* **B22**-based OFETs were measured as shown in Fig. 4.7b which allowed the investigation of the relationship between the molecular ordering and charge-carrier (hole) mobility. Figure 4.7b shows the transfer characteristics of OFETs in the different phases

which were simultaneously observed by polarized optical microscopy (POM) (Fig. 4.7c). In the columnar phase at $T = 208$ °C the sample appears almost isotropic and therefore the dominating alignment of the columns should be perpendicular to the substrate surfaces (Fig. 4.7c, left). Only the small brighter spots indicate some defects due to a not fully perfectly uniform alignment of the columns. With decrease in temperature, the hole mobility increases from 5×10^{-3} cm^2 V^{-1} s^{-1} in Col$_{hex}$ to 8.2×10^{-2} in the Cub$_{bi}$ phase and to 0.56 cm^2 V^{-1} s^{-1} in the Cr$_{Iso}$[*] phase at lowest temperature (Fig. 4.7b). This shows that the 3D network structure allows an enhanced charge carrier mobility compared to (imperfectly aligned) columnar phases. Moreover, the charge carrier mobility can be further improved by π-stacking of the crystallized BTBT cores along the networks in Cr$_{Iso}$[*].

Phase (T/°C)	Mobility (cm^{2}V^{-1}s^{-1})	I_{ON}/I_{OFF}	V_{th} (V)	Subthreshold Slope (V/dec)
Col (208)	$(5 \pm 2.2) \times 10^{-3}$	$\sim 10^3$	$- (32 \pm 8.2)$	~ 9
Cub$_{bi}$[*]/I23 (90)	$(8.2 \pm 2.8) \times 10^{-2}$	$\sim 10^4$	$- (22 \pm 5.3)$	~ 5
Cr$_{Iso}$[*] (30)	$(5.6 \pm 3.2) \times 10^{-1}$	$\sim 10^5$	$- (15 \pm 3.5)$	~ 4
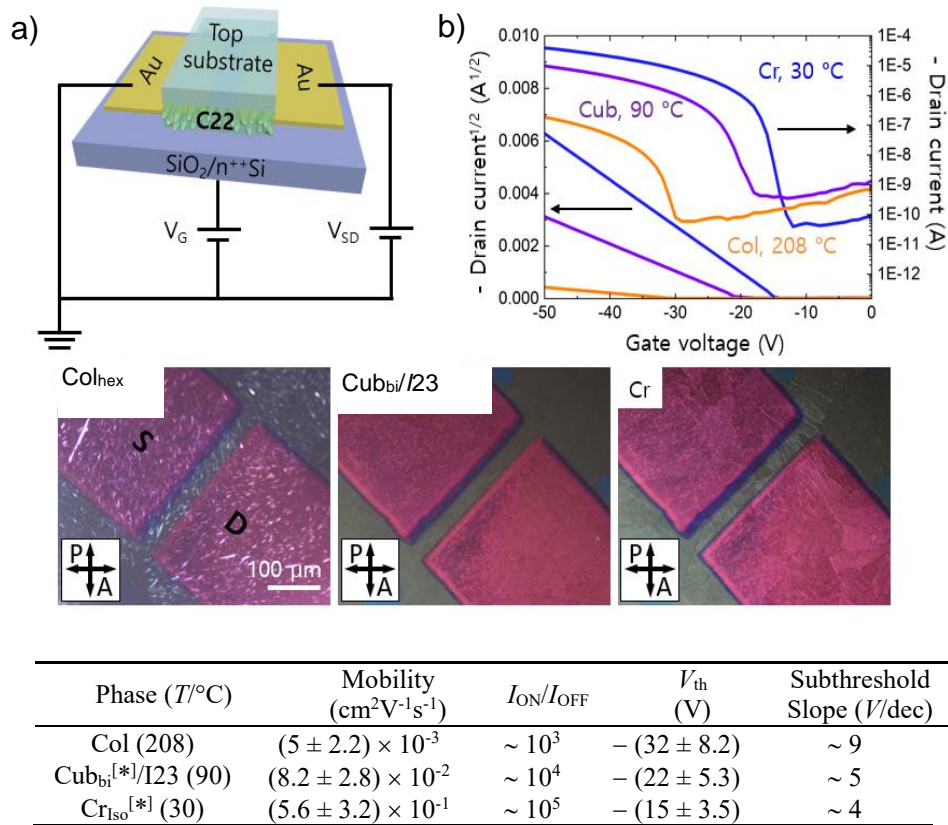
Figure 4.7 Electrical properties of **B22**-based organic field effect transistors (OFETs) prepared by sandwich cell. (a) Bottom-gate bottom-contact OFETs configuration, (b) transfer ($V_{DS} = - 50$ V) curves in the different phases, (c) POM images and numerical data shown at the bottom, including the average charge carrier mobility, I_{ON}/I_{OFF}, the threshold voltage (V_{th}), and the subthreshold slope (V/dec) which are average values from 10 devices.

4.7 Summary and Conclusions

Overall, it is shown that the functional BTBT unit can be incorporated into polycatenar molecules with a tapered 2-bromo-3,4,5-trialkoxybenzoyloxy end and that these compounds can form a wide variety of different helical network phases, ranging from soft crystalline via bicontinuous cubic and non-cubic 3D phases to mirror symmetry broken isotropic liquids. The Cub_{bi} phases cover amazingly wide temperature ranges including ambient temperature and the phase type (*Ia*3*d* or *I*23) can be controlled by adjusting the intermolecular twist along the networks by chain length modification. As proof of the concept, the investigation of OFET cells indicates that the capability of the Cub_{bi} phase for charge transport in all three spatial directions can be advantageous over the 1D transport in the columnar phases and that it can be further enhanced at the transition from LC to crystalline network phases. We expect that further tuning of the molecular structure and blending will improve the charge transport properties in these bicontinuous networks. This provides a new concept for (semi)conducting LCs, complementing the previously known 2D conducting lamellar and 1D conducting columnar systems by the new concept of 3D networks. [14]

In addition, the mirror symmetry broken helical arrays of achiral π-conjugated molecules in the *I*23 phase, initially formed as conglomerate, can assume uniform chirality, either induced by external chirality sources[10] or even spontaneously,[12] and thus can provide uniformly helical soft matter structures and chiral liquids from achiral BTBT derived functional molecules. These spontaneously chiral systems, formed by small molecules and comprising well organized functional π-conjugated units, provide additional applications going beyond their use as charge carrier materials, for example, as soft and stimuli responsive materials for photophysical applications like aggregation induced polarized emission and light harvesting.[15]

The work in this chapter has been published and support information is available online for further information.[16]

References

1   C. Dressel, T. Reppe, S. Poppe, M. Prehm, H. Lu, X. Zeng, G. Ungar, C. Tschierske, *Adv. Funct. Mater.* **2020**, 2004353.

2   S. Mery, D. Haristoy, J.-F. Nicoud, D. Guillon, S. Diele, H. Monobe, Y. Shimizu, *J. Mater. Chem.,* **2002**, *12*, 37.

3   X. Zeng, G. Ungar, *J. Mater. Chem*. C **2020**, *8*, 5389.

4   Though in other cases a re-entrance of the Cubbi/$Ia\bar{3}d$ phase is observed upon chain elongation beyond the existence region of the $I23$ phase 11 this is not found in this case. It appears that the increased molecular length, expanding the lattice, does not allow the transition to a short pitch $Ia\bar{3}d_{(S)}$ phase and would require even smaller twist angles for the alternative transition back to a long pitch $Ia\bar{3}d_{(L)}$ phase.

5   C. Dressel, T. Reppe, S. Poppe, M. Prehm, H. Lu, X. Zeng, G. Ungar and C.Tschierske, Adv. Funct. Mater. **2020**, 30, 2004353.

6   T. Reppe, C. Dressel, S. Poppe and C. Tschierske, Chem. Commun. **2020**, 56, 711

7   A. Immirzi and B. Perini, *Acta Cryst.* A **1977**, 33, 216.

8   X. Zeng, G. Ungar, Spontaneously chiral cubic liquid crystal: three interpenetrating networks with a twist, *J. Mater. Chem*. C **2020**, *8*, 5389.

9   A.-M. Levelut, M. Clerc, *Liq. Cryst*. **1998**, *24*, 105; H. Lu, X. Zeng, G. Ungar, C. Dressel, C. Tschierske, *Angew. Chem. Int. Ed.* **2018**, *57,* 2835-2840; J. Matraszek, D. Pociecha, N. Vaupotic, M. Salamonczyk, M. Vogrine, E. Gorecka, *Soft Matter*, **2020**, *16*, 3882.

10   C. Dressel, T. Reppe, M. Prehm, M. Brautzsch, C. Tschierske, *Nat. Chem*. **2014**, *6*, 971.

11   T. Reppe, S. Poppe, X. Cai, Y. Cao, F. Liu, C. Tschierske, *Chem. Sci*., **2020**, *11,* 5902.

12   C. Tschierske, C. Dressel, *Symmetry*, **2020**, 12, 1098.

13   a) H. Iino and J. Hanna, *Appl. Phys. Lett*. **2005**, 87, 132102; b) M. Kastler, F. Laquai, K. Müllen, G. Wegner, *Appl. Phys. Lett*. **2006**, *89*, 252103.

14   To the best of our knowledge, the only Cubbi material which was investigated with respect to charge carrier mobility is based on a bis(4-alkoxybenzoyl)hydrazine core with relatively short π-conjugation length.

15   Z.-G. Zheng, Y.-Q. Lu, Q. Li, *Adv. Mater*. 2020, 1905318; X. Bai, Y. Sun, Y. Jiang, G. Zhao, J. Jiang, C. Yuan, M. Liu, *Angew. Chem. Int. Ed*. **2021**, 60, 3745.

16   O. Kwon, X. Cai, W. Qu, F. Liu, J. Szydłowska, E. Gorecka, M. J. Han, D. K. Yoon S. Poppe and C. Tschierske, *Adv. Funct. Mater*, **2021**, 2102271

5. 2,6-Dibromogallates as a new building blocks for controlling π-stacking, network formation and mirror symmetry breaking
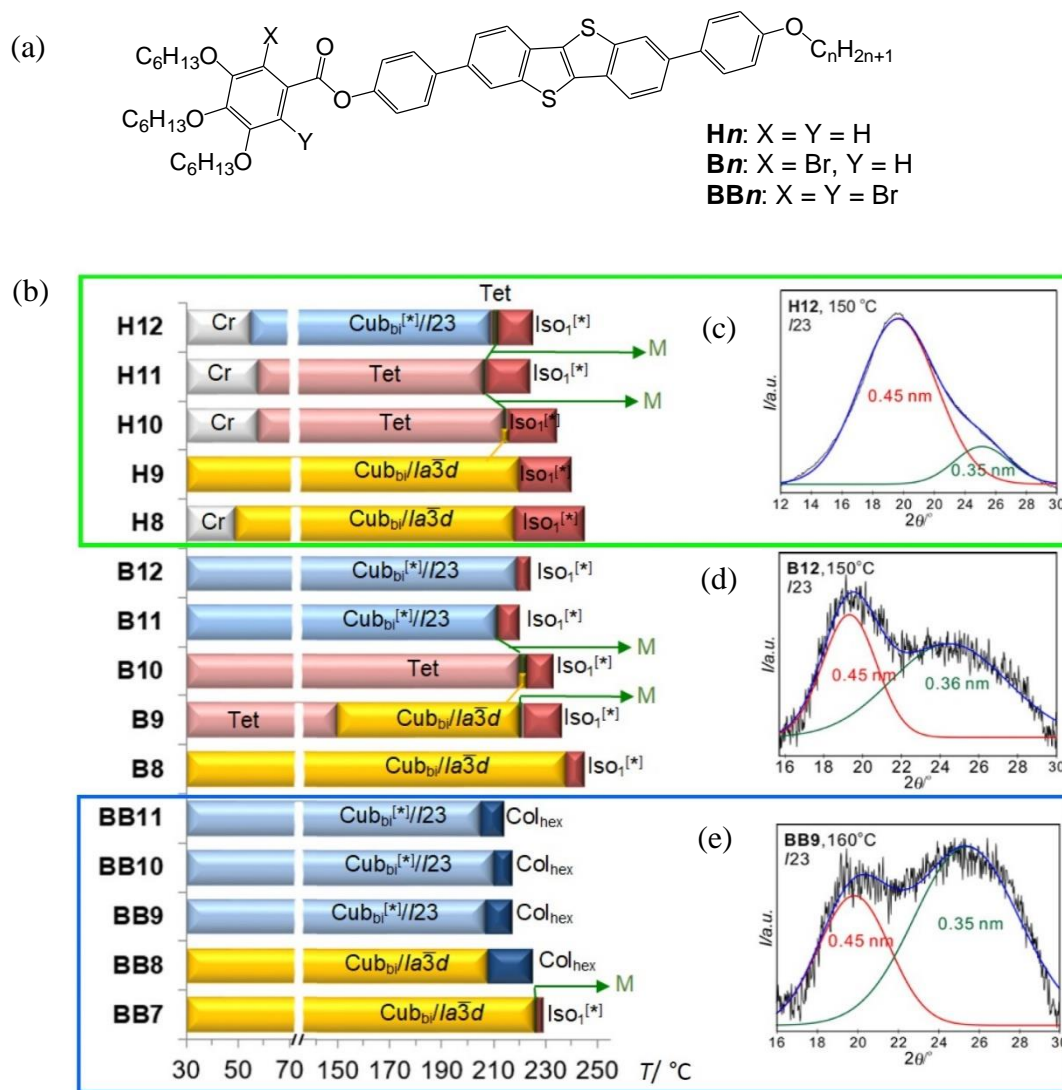
Figure 5.1 a) Molecular structures of **H***n*, **B***n* and **BB***n*, b) phase transitions as observed by DSC on cooling (10 K min⁻¹); The related transitions on heating, the numerical data and transition enthalpy values are collated in Table 5.1, and for structural data Table 5.2; abbreviations: Col$_{hex}$ = hexagonal columnar phase; c-e) representative WAXS patterns of selected compounds from each series at the indicated temperatures.

Table 5.1 Transition temperatures and corresponding enthalpies of compounds **H***n* and **BB***n* as measured on heating and cooling at 10 K/min.

Comp.	T/°C [ΔH /kJ·mol^{-1}]
H8	Heating: Cr 50 [2.9] Cub$_{bi}$/*Ia*3*d* 246 [1.9] Iso Cooling: Iso 245 [0.4] Iso$_1$[*] 218 [0.7] Cub$_{bi}$/*Ia*3*d* 49 [3.6] Cr
H9	Heating: Cr <20 Cub$_{bi}$/*Ia*3*d* 240 [1.8] Iso Cooling: Iso 240 [0.1] Iso$_1$[*] 220 [0.7] Cub$_{bi}$/*Ia*3*d* <20 Cr
H10	Heating: Cr 136 [29.9] Cub$_{bi}$/*Ia*3*d* +Tet 180 Tet 229 Iso$_1$[*] 234 [1.36] Iso Cooling: Iso 234 [0.2] Iso$_1$[*] 215 Cub$_{bi}$/*Ia*3*d* 214 [0.5] M 214 Tet 58 [7.0] Cr
H11	Heating: Cr 136 [4.8] Tet 221 [1.4] Iso$_1$[*] 225 [0.1] Iso Cooling: Iso 224 [0.2] Iso$_1$[*] 207 [0.7] M 206 Tet 58 [5.0] Cr
H12	Heating: Cr 51 [4.5] Cub$_{bi}$[*]/*I*23 175 Tet 223 Iso$_1$[*] 225 [1.7] Iso Cooling: Iso 225 [0.4] Iso$_1$[*] 212 [0.7] M 210 Tet 209 Cub$_{bi}$[*]/*I*23 55 [4.8] Cr
BB7	Heating: Cr 118 [13.5] Cub$_{bi}$/*Ia*3*d* 236 [1.9] Iso Cooling: Iso$_2$ 229 Iso$_1$* 227 [1.3] M 226 Cub$_{bi}$/*Ia*3*d* <20 Cr
BB8	Heating: Cr 127 [12.7] Cub$_{bi}$/*Ia*3*d* 230 [1.4] Iso Cooling: Iso 225 [0.9] Col$_{hex}$ 208 [1.3] Cub$_{bi}$/*Ia*3*d* <20 Cr
BB9	Heating: Cr 117 [12.2] Cub$_{bi}$[*]/*I*23 227 [2.1] Iso Cooling: Iso 217 [1.4] Col$_{hex}$ 207 [0.1] Cub$_{bi}$[*]/*I*23 <20 Cr
BB10	Heating: Cr 115 [9.4] Cub$_{bi}$[*]/*I*23 229 [2.1] Iso Cooling: Iso 217 [1.8] Col$_{hex}$ 210 [0.3] Cub$_{bi}$[*]/*I*23 <20 Cr
BB11	Heating: Cr 99 [11.0] Cub$_{bi}$[*]/*I*23 224 [2.7] Iso Cooling: Iso$_2$ 214 [1.6] Col$_{hex}$ 205 [0.5] Cub$_{bi}$[*]/*I*23 <20 Cr

In a next step the effect of bromination on the self-assembly is investigated. In all three series of compounds (Fig. 5.1a) there are two different types of optically isotropic Cub$_{bi}$ phases which can be distinguished by their small angle X-ray scattering (SAXS) patterns and chiroptical properties (see Fig. 5.2). The dibrominated compound **BB7** with the shortest apex chain shows an *Ia*3*d* lattice with a_{cub} = 9.80 nm (Fig. 5.2a). The reconstructed electron density (ED) map confirms a double gyroid structure, where the aromatic cores with the highest ED (purple→green) form the networks and the alkyl chains form the continuum around them (Fig. 5.2b). The same network phase is found for **BB8**, but the Cub$_{bi}$ phases of the longer homologues have three main SAXS peaks which can be indexed to the (321), (400) and (420) reflections of the *I*23 lattice (a_{cub} = 14.7

nm for **BB9,** Fig. 5.2c). This cubic phase with a lattice parameter being about 50 % larger than in the *Ia*3*d* phase has a triple network structure, again with the aromatic cores forming the networks and the alkyl chains in the continuum (Fig. 5.2d). The lattice parameters are collated in Table 5.2.

Table 5.2 Structural data of the mesophases of compounds **H***n*, **B***n* and **BB***n*.

Comp.	Phase	T/°C	a,c/ nm	V_{cell}/ nm³	V_{mol}/ nm³	n_{cell}	d_{net}	L_{net}	n_{raft}	Φ/°
H8	Cub$_{bi}$/*Ia*3*d*	180	10.19	1058	1.308	723	4.41	86.46	3.76	8.79
H10	Cub$_{bi}$/*Ia*3*d*	232	9.95	985	1.357	648	4.31	84.43	3.45	9.01
H10	Tet	200	17.72 15.84	4974	1.357	3273				
H12	Cub$_{bi}$[*]/*I*23	220	14.83	3262	1.407	2070		306.68	3.04	9.42
BB7	Cub$_{bi}$/*Ia*3*d*	170	9.8	941	1.335	630	4.24	83.15	3.41	9.14
BB9	Cub$_{bi}$[*]/*I*23	170	14.72	3190	1.385	2057		304.41	3.04	9.49
BB11	Cub$_{bi}$[*]/*I*23	210	14.69	3170	1.434	1974		303.79	2.92	9.51
BB11	Col$_{hex}$/*p*6*mm*	235	4.33	7.469	1.434	5.21			5.21	

The Cub$_{bi}$ phase of **BB7** and **BB8** is achiral (Fig. 5.3a), in line with the *Ia*3*d* lattice (Fig. 5.1c). In contrast, the Cub$_{bi}$ phase of **BB9-BB11** shows a conglomerate of dark and bright domains (Fig. 5.3d), if observed by optical microscopy between polarizers rotated by a small angle out of the precise 90° orientation. The domain brightness is inverted by changing the sense of rotation, thus indicating that this optically isotropic Cub$_{bi}$ phase is chiral, confirming a triple network *I*23 structure. [1,2,3,4] At a certain critical twist angle ($\Phi > 9.2$ nm, see Table 5.2) the transition from *Ia*3*d* to *I*23 takes place in all three series of compounds. However, the *Ia*3*d*→*I*23 transition is shifted by bromination to shorter chain length **H***n*: 9→12; **B***n*: 8→11 **BB***n*: 8→9, see Fig. 5.1a). This means that the bromines obviously contribute to the expansion of the molecular periphery and thus favour mirror symmetry breaking by favouring the *Ia*3*d*→*I*23 transition. Thus, addition of Br has a similar effect as an elongation of the apex chain by one additional CH$_2$ unit, being in line with the similar volumes of Br (3.3 x 10^{-3} nm³) and CH$_2$ (2.5 x 10^{-3} nm³).[5] Though the melting temperatures are almost the same in all three series (see Table 5.1 and 4.1), there is a reduction of the crystallization tendency, leading to an improved supercooling of the crystallization with growing number of bromines, allowing the formation of long time persistent Cub$_{bi}$ phases down to ambient temperature (Fig. 5.1a).
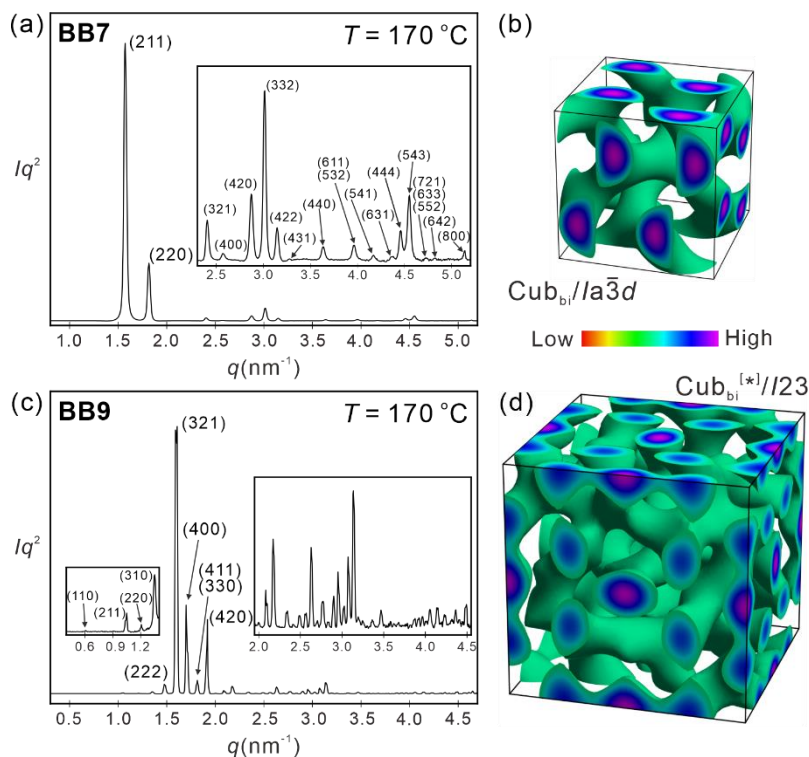
Figure 5.2 SAXS patterns at the indicated temperatures. a) $Cub_{bi}/Ia3d$ phase of **BB7** and c) the $Cub_{bi}^{[*]}/I23$ phase of compound **BB9** with b, d) the corresponding ED maps reconstructed from the diffraction patterns, the aromatic cores are located in the networks formed by the green iso-surfaces, the space in between is filled by the alkyl chains; for the network models, see Fig. 5.1c, d; for numerical values and additional XRD date, Tables 5.2.

At the transition between the two different cubic phases two types of birefringent mesophases occur (Tet, M, Fig. 5.3). Comparison of the three series shows that an increasing degree of bromination reduces the Tet and M_H phase ranges and even completely eliminates the Tet phase for compounds **BB**n (Fig. 5.1a). The Tet phases of **H**n and **B**n have very similar low birefringent optical textures (Fig. 5.3c) and a-parameters (a = 17.7 and 17.8 nm, respectively) of the tetragonal lattices, and therefore both should belong to the same kind. Only the parameter c is increased by bromination from c = ~16 nm for **H10** to c = ~20-22 nm for **B**n (Table 5.2).[6] The metastable mesophase M, growing as highly birefringent platelets, which rapidly transform into Cub_{bi} or Tet with time or upon cooling (Fig. 5.3a, b). This mesophase is observed in all three series of compounds in a very small temperature range during the transition from $Iso_1^{[*]}$ to $Cub_{bi}/Ia3d$ or Tet on cooling. It is metastable and rapidly removed by the Cub_{bi} or Tet phase with time or upon

further cooling. It appears to be associated with the *Ia*3*d*→(Tet)→*I*23 transition upon chain elongation and it is removed as soon as either the Cub$_{bi}$[*]/*I*23 or the *Ia*3*d* phase becomes the dominating phase type. Double bromination removes the M$_H$ phase in most cases.
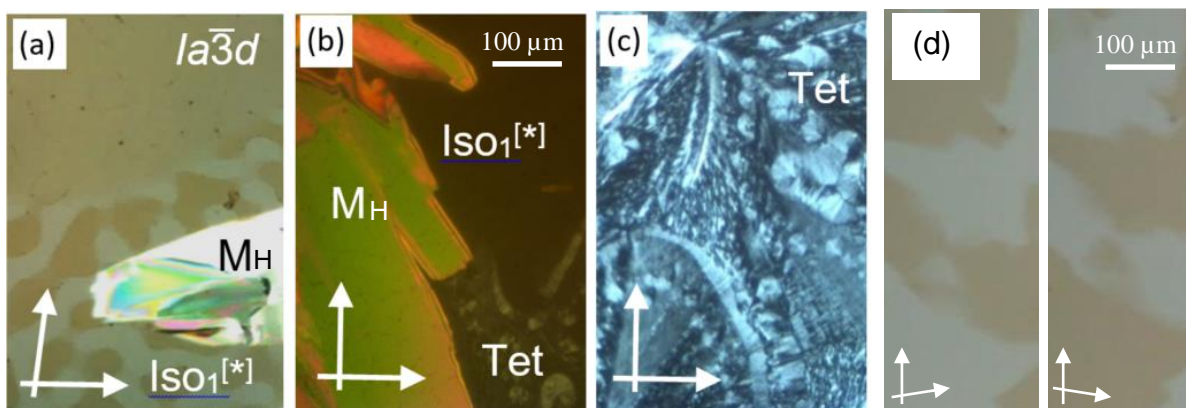
Figure 5.3 Optical textures of a) **BB7** at 226 °C as observed on cooling between two polarizers slightly rotated out of the 90 ° twisted configuration (arrows) and showing the transition from the Iso$_1$[*] phase (chiral conglomerate) to Cub$_{bi}$/*Ia*3*d* with simultaneous growth of the M$_H$-phase and b, c) of **H10** between fully crossed polarizers; b) high birefringent M phase developing from the Iso$_1$[*] phase and the co-developing low birefringent Tet phase (bottom, right) at 215 °C and c) fully developed texture of the Tet phase at 205 °C (longer exposure time); d) chiral domains of the Cub$_{bi}$[*]/*I*23 phase from **BB9** at 205 °C.

In all mesophases (Cub$_{bi}$, Tet, M$_H$, Col$_{hex}$), the wide-angle scattering (WAXS) is diffuse with a maximum around 0.45 – 0.46 nm, as typical for LC phases (Figs. 5.1b, c). For **H10** there is a very weak shoulder at larger 2θ values which for **B*n*** and **BB*n*** becomes a second diffuse scattering with increased intensity around 0.35-0.37 nm. (Fig. 5.1d). This is independent on the phase type, but decreases in intensity with rising temperature. We attribute this additional scattering to a change of the self-assembly of the π-conjugated rods. For **H*n*** the preferred average organization is edge-to-face, leading to a dominating WAXS maximum at 0.45-0.46 nm, whereas bromination disfavour this arrangement and supports a parallel face-to-face stacking of the π-systems of compounds **B*n*** and **BB*n*** with a mean distance of 0.35-0.37 nm.[7] It appears that the face-to-face packing is mainly caused by the increased aspect ratio of the brominated compounds (**H*n*** << **B*n*** < **BB*n***). This disfavours the edge-to-face and supports the face-to-face packing of the aromatic cores, which then allows the overlapping of adjacent π-systems.[7] However, the coherence length of the face-to-face stacking is still relatively short, as indicated by the diffuse WAXS.

For all investigated compounds the viscoelastic 3D mesophases are accompanied by additional highly fluid mesophases. One is a mirror symmetry broken isotropic liquid $Iso_1^{[*]}$ phase which is observed on cooling from the achiral isotropic liquid (Iso). [8,9] Its width is the largest for **Hn** and it decreases with increasing bromination in the order **Hn** > **Bn** >> **BBn**. In the series **BBn** it is only observed in a small temperature range on cooling the shortest compound **BB7** before the transition to the M_H and $Ia3d$ phases, whereas for all compounds **BBn** with longer chains it is replaced by a Col_{hex} phase (Fig. 5.1). This effect of bromination could be attributed to the increase of interface curvature by the bulky bromines, which is additionally supported by the change of the preferred mode of packing from edge-to-face to face-to-face (see above), thus supporting a taper-like molecular shape. In this Col_{hex} phase the lattice parameter $a_{hex} = 4.33$ nm (**B11**) is in good agreement with the total molecular length $L_{mol} = 4.8$ nm after considering the chain folding in the columnar LC phases. The calculated number of ~4.5 molecules per 0.46 nm thick raft of the columns (n_{raft}, see Table 5.2) is close to the number of molecules organized in the rafts of the networks of the $Ia3d$ phases, ranging from 3 (**BB11**) to 4 (**H8**) molecules (Table 5.2). Thus, this is an antiparallel organization of the molecules in the aggregates (Fig. 5.4)

In both series **Hn** and **Bn** the $Iso_1^{[*]}$ phase is found at the high temperature side besides the $I23$, $Ia3d$ and Tet phases. The proximity to the chiral $I23$ phase suggests a local $I23$-like structure of these $Iso_1^{[*]}$ phases showing long range chirality synchronization, even after loss of the long range cubic lattice in the liquid state.[2] Because the $I23$ phase can develop from the $Ia3d$ phase upon increasing twist along the networks, [1-4] it is likely that thermal chain expansion can increase the helical twist (see Fig. 4.3c) and transform the $Cub_{bi}/Ia3d$ lattice into a local $I23$-like structure in the adjacent $Iso_1^{[*]}$ phase.

Remarkably, the LC→Iso/$Iso_1^{[*]}$ transition temperatures are almost the same in all three series of compounds if the same chain lengths are compared (Table 5.2). This is surprising, as it is known from previous work, that bulky substituents in the 2,6-positions at opposite sides of the aromatic core have a dramatic destabilizing effect on LC phases.[10] Hence, it appears that the unfavourable steric effect of bromination is compensated by mesophase stabilizing effects. Besides the different π-stacking modes, the increased London dispersion interactions of the highly polarizable bromines could stabilize the LC phases. Moreover, the bromines can in an antiparallel

arrangement efficiently fill the free space around the adjacent ester linkage, and this increases the contact area between the molecules, thus strengthening the dispersion interactions (Fig. 5.5).
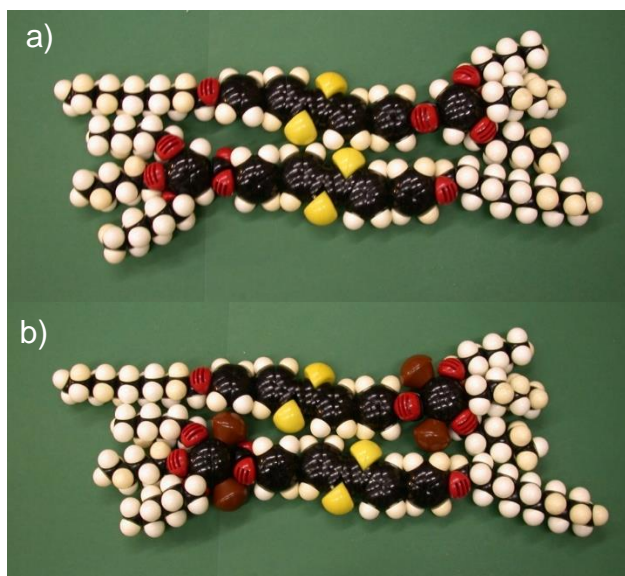
Figure 5.4 Space filling CPK models of compounds a) **H10** and b) **BB10** (L_{mol} = 4.8 nm). In b) the bromines fill the void space around the COO groups.
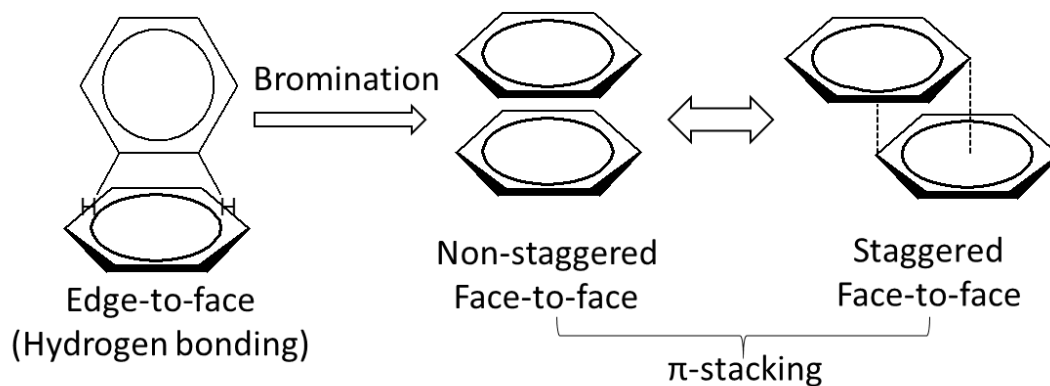
Figure 5.5 Scheme showing the transition from edge-to-face to face-to-face stacking of aromatic cores by increasing bromination.

Overall, peripheral double bromination of the tapered end of π–conjugated polycatenars allows the formation of broad regions of mirror symmetry broken network phases, even covering ambient temperature. It also leads to a removal of birefringent 3D phases occurring at the *Ia*3*d*-*I*23 transition and hinders the crystallization. These surprising effects of double-bromination are in contrast to the effect observed for halogenation at other positions. Especially, halogenation in

the centre of the core unit of polycatenars is known to supress Cub$_{bi}$ phase formation.[11] Remarkable is the support of a parallel alignment of the π-faces of the aromatic cores which is important for the tailoring of photophysical properties and expected to support charge transportation. Hence, the work provides general guidelines for the controlled design of helical network forming and mirror symmetry broken soft materials based on π-conjugated rods. These are of current interest for numerous applications, as for example, in organic electronics, for light harvesting and polarized emission.

The work in this chapter has been published and support information is available online for further information.[12]

References

1   C. Dressel, T. Reppe, S. Poppe, M. Prehm, H. Lu, X. Zeng, G. Ungar and C. Tschierske, *Adv. Funct. Mater*., **2020**, 202004353.

2   T. Reppe, C. Dressel, S. Poppe and C. Tschierske, *Chem. Commun.,* **2020**, 56, 711; T. Reppe, S. Poppe, X. Cai, Y. Cao, F. Liu and C. Tschierske, *Chem. Sci.,* **2020**, 11, 5902; M. Alaasar, S. Poppe, Q. Dong, F. Liu and C. Tschierske, *Angew. Chem. Int. Ed.,* **2017**, 56, 10801.

3   X. B. Zeng and G. Ungar, *J. Mater. Chem.* C, **2020**, 8, 5389.

4   C. Dressel, F. Liu, M. Prehm, X. B. Zeng, G. Ungar and C. Tschierske, *Angew. Chem. Int. Ed.,* 2014, **53**, 1115; H. Lu, X. Zeng, Goran Ungar, C. Dressel, and C. Tschierske, *Angew. Chem. Int. Ed.,* **2018**, 57, 2835.

5   A. Immirzi and B. Perini, *Acta Cryst*. A, **1977**, 33, 216.

6   O. Kwon, X. Cai, W. Qu, F. Liu, J. Szydłowska, E. Gorecka, M. J. Han, D. K. Yoon S. Poppe and C. Tschierske, *Adv. Funct. Mater*, **2021**, 2102271.

7   C. A. Hunter and J. K. M. Sanders, J. Am. Chem. Soc., 1990, 112, 5525; C. R. Martinez and B. L. Iverson, Chem. Sci. **2012**, 3, 2191.

8   C. Tschierske, *Liqu. Cryst.,* **2018**, 45, 2221; b) C. Tschierske and G. Ungar, C*hemPhysChem*, **2016**, 17, 9; C. Tschierske and C. Dressel, *Symmetry*, 2020, **12**, 1098.

9   C. Dressel, T. Reppe, M. Prehm, M. Brautzsch and C. Tschierske, *Nat. Chem*., **2014**, 6, 971.

10   D. W. Bruce and S. A. Hudson, *J. Mater. Chem.,* **1994**, 4, 479; J. W. Goodby, I. M. Saez, S. J. Cowling, J. S. Gasowska, R. A. MacDonald, S. Sia, P. Watson, K. J. Toyne, M. Hird, R. A. Lewis, S.-E. Lee and V. Vaschenko, *Liq. Cryst.,* **2009**, 36, 567.

11   A. I. Smirnova, B. Heinrich, B. Donnio and D. W. Bruce, *RSC Adv.*, **2015**, 5, 75149.

12   O. Kwon, X. Cai, A. Saeed, F. Liu, S. Poppe and C. Tschierske, *Chem. Comm.* **2021** accepted.

6. Controlling the formation of cubic network and columnar phase by chain elongation at the tapered end

a)

b)
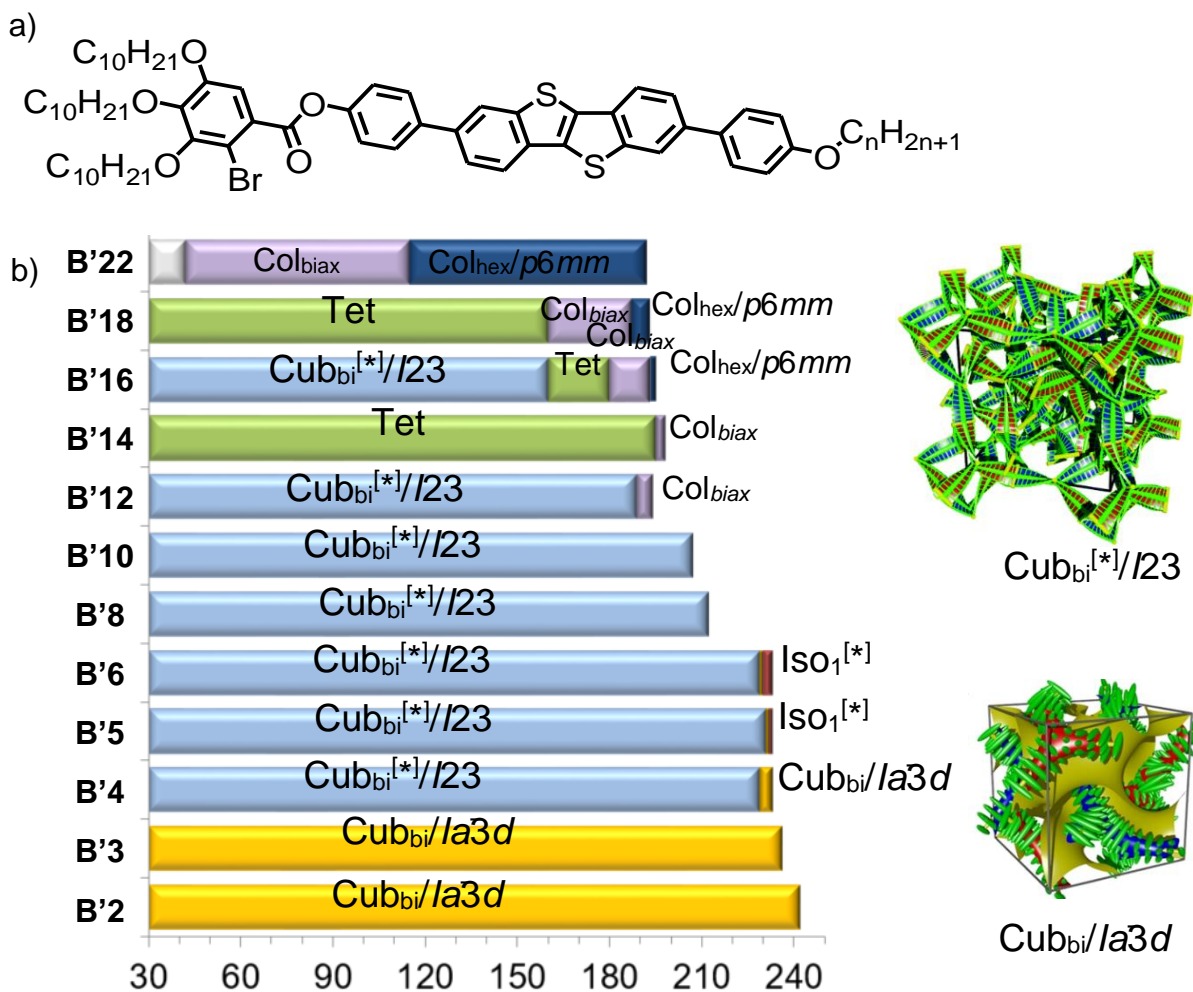
Figure 6.1 a) Chemical structure of compounds **B'n** and b) phase transitions as observed on cooling (rate 10 K min⁻¹); Col_{biax} = a biaxial columnar LC phase with either rectangular or oblique lattice. The models of $Cub_{bi}/Ia3d$ and $Cub_{bi}^{[*]}/I23$.[1,3]

Here, we report the effect of elongation of the three alkoxychains at the tapered end from $m = 6$ to $m = 10$ and the effect of elongation of the single chain at the monosubstituted end from $n = 2$ –22. The phase transitions are collected in the Tab. 6.1 and in Fig. 6.1 shown graphically for the cooling cycles. Overall the thermal stability of the mesophases becomes lower by replacing the hexyloxy groups (**Bn**) by decyloxy groups (**B'n**). When the alkoxy chain is short ($n = 6$), the

mesophase of **B6** appears from 262 °C upon cooling while the same of **B'6** from 233 °C . When the compounds have a long chain (*n*=22), the mesophase of **B22** forms from 205 °C upon cooling while the same of **B'22** from 192 °C. This indicates that with increasing length of the apex end chains (*m*) the difference between compounds **B*n*** and **B'*n*** decreases.

6.1 Bicontinuous cubic phases with *Ia*3*d* and *I*23 lattice

Compounds **B'2** to **B'12** show a similar sequence of *Ia*3*d* and *I*23 phases as formed for compounds **B6 – B22** (Figs 4.1 and 6.1). The shift of the *Ia*3*d* → *I*23 transition to shorter chain length *m* shows the strong effect of the elongation of all three chains at the tapered end. Because elongation of these chains (*m*) leads to 3 times the volume increase compared to the elongation of the single chain at the apex (*n*), this observation is not surprising. Nevertheless, the total chain volume required for the *Ia*3*d* → *I*23 transition is larger for the compounds **B'*n*** with a larger tapered end (Table 6.3) meaning that there is a stronger effect of apex chain elongation per single CH_2-unit., For compounds **B'*n*** there is no birefrengent phase associated with the *Ia*3*d* - *I*23 transition. In this respect the effect of chain elongation at the tapered end is similar to the effect of 2,6-dibromination. The WAXS results of the mesophases of **B'*n*** are characterized by a single scattering maximum around 0.46 nm (see Fig. 6.2c). In contrast, introduction of additional bromine atoms causes two diffuse WAXS maxima; one at 0.46 nm and a shoulder around 0.35 nm, indicating π -π stacking.[3] Thus, elongation of alkyl chains at the tapered end can eliminate unfavorable birefringent mesophase at the transition from *Ia*3*d* to *I*23 without inducing π -π stacking.
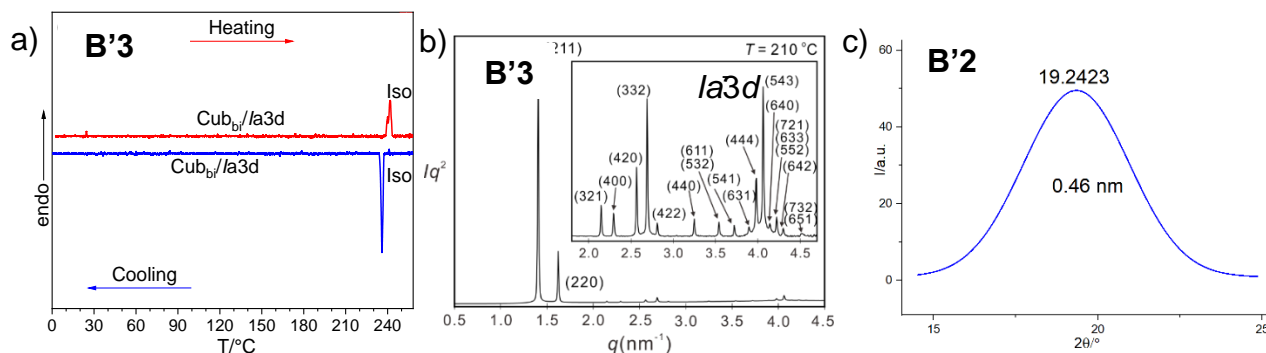
Figure 6.2 a) DSC traces of **B'3**; b) SAXS diffractograms of the Cub$_{bi}$/*Ia*3*d* of **B'3**;[2] c) WAXS diffractograms of the Cub$_{bi}$/*Ia*3*d* phase of **B'2** at 180°C.

Table 6.1 Transition temperatures and corresponding enthalpies of compounds **B'2**-**B'22** as measured on heating and cooling at 10 K/min.

	T/°C [ΔH /kJ·mol^{-1}]
B'2	H: Cr <20 Cub$_{bi}$/$Ia3d_{(L)}$ 251 [2.2] Iso
	C: Iso 242 [1.6] Cub$_{bi}$/$Ia3d_{(L)}$ <20 Cr
B'3	H: Cr <20 Cub$_{bi}$/$Ia3d_{(L)}$ 242 [3.3] Iso
	C: Iso 236 [1.5] Cub$_{bi}$/$Ia3d_{(L)}$ <20 Cr
B'4	H: Cr$_1$ 87 [30.1] Cr$_2$ 111 [16.8] Cub$_{bi}$[*]/$I23$ 240 [0.3] Cub$_{bi}$/$Ia3d_{(L)}$ 243 [2.4] Iso
	C: Iso 233 [1.6] Cub$_{bi}$/$Ia3d_{(L)}$ 229 [0.1] Cub$_{bi}$[*]/$I23$ <20 Cr
B'5	H: Cr1 81 [35.9] Cr2 101 [8.4] Cub$_{bi}$[*]/$I23$ 238 [2.8] Iso
	C: Iso 233 Iso$_1$[*] 232 [1.7]^a Cub$_{bi}$/$Ia3d$ 231 [-] Cub$_{bi}$[*]/$I23$ <20 Cr
B'6	H: Cr 87 [12.8] Cub$_{bi}$[*]/$I23$ 237 [2.8] Iso
	C: Iso 233 Iso$_1$[*] 230 [1.7]^a Cub$_{bi}$/$Ia3d$ 229 [-] Cub$_{bi}$[*]/$I23$ <20 Cr
B'8	H: Cr$_1$ 55 [16.0] Cr$_2$ 90 [34.5] Cub$_{bi}$[*]/$I23$ 223 [2.9] Iso
	C: Iso 212 [1.7] Cub$_{bi}$[*]/$I23$ <20 Cr
B'10	H: Cr <20 Cub$_{bi}$[*]/$I23$ 213 [2.1] Iso
	C: Iso 207 [1.8] Cub$_{bi}$[*]/$I23$ <20 Cr
B'12	H: Cr 75 [3.7] Cub$_{bi}$[*]/$I23$ 204 [2.1] Iso
	C: Iso 194 [1.3] Col$_{biax}$ 189 [0.3] Cub$_{bi}$[*]/$I23$ <20 Cr
B'14	H: Cr 70 [5.4] Tet 200 [-] Cub$_{bi}$/$Ia3d_{(S)}$ 203 [1.9] Iso
	C: Iso 198 [1.5] Col$_{biax}$ 195 [0.1] Tet <20 Cr
B'16	H: Cr 70 [24.4] Cr$_2$ 79 [5.1] Cr$_3$ 85 [0.7] Cub$_{bi}$[*]/$I23$ 150 [-] Tet 195 [-] Cub$_{bi}$/$Ia3d_{(S)}$ 200 [2.5] Iso
	C: Iso 195 [1.5] Col$_{hex}$/$p6mm$ 193 [0.1] Col$_{biax}$ 180 [-] Tet 160 [-] Cub$_{bi}$[*]/$I23$ <20 Cr
B'18	H: Cr 83 [24.1] Tet 180 Cub$_{bi}$/$Ia3d_{(S)}$ 195 [-] Col$_{biax}$ 197 [2.4] Iso
	C: Iso 193 [1.8] Col$_{hex}$ /$p6mm$ 187 [0.1] Col$_{biax}$ 160 [-] Tet <20 Cr
B'22	H: Cr 88 [28.0] Col$_{biax}$194 [2.1] Iso
	C: Iso 192 [2.2] Col$_{hex}$ /$p6mm$ 115 [-] Col$_{biax}$ 42 [23.2] Cr

^{a}Enthalpy involves both transitions.

Table 6.2 Structural data of the Cub$_{bi}$ phases of the investigated compounds.

Comp.	Phase	a/nm	V_{cell}/nm³	V_{mol}/nm³	n_{cell}	d_{net}	L_{net}	n_{raft}	Φ/°	T/°C
B'18	Cub/*Ia3d*	10.50	1157.6	1.8792	550	4.5	89.09	2.78	8.54	210
B'16	Cub/*Ia3d*	10.39	1121.6	1.8296	547	4.5	88.16	2.79	8.63	214
B'16	Cub/*I23*	16.75	4699.4	1.8296	2294	7.3	346.39	2.98	8.34	150
B'14	Cub/*Ia3d*	10.36	1111.9	1.7800	558	4.5	87.90	2.86	8.65	220
B'12	Cub/*I23*	16.84	4775.6	1.7304	2465	7.3	348.25	3.18	8.29	140
B'10	Cub/*I23*	16.49	4484.0	1.6808	2382	7.1	341.01	3.14	8.47	180
B'8	Cub/*I23*	16.53	4516.7	1.6312	2473	7.2	341.84	3.26	8.45	180
B'6	Cub/*I23*	16.61	4582.6	1.5816	2587	7.2	343.49	3.39	8.41	170
B'5	Cub/*I23*	16.41	4419.0	1.5568	2535	7.1	339.36	3.36	8.51	180
B'4	Cub/*I23*	16.47	4467.7	1.5320	2604	7.1	340.60	3.44	8.48	200
B'3	Cub/*Ia3d*	10.95	1312.9	1.5072	778	4.7	92.91	3.77	8.18	210
B'2	Cub/*Ia3d*	10.94	1309.3	1.4824	789	4.7	92.83	3.82	8.19	180
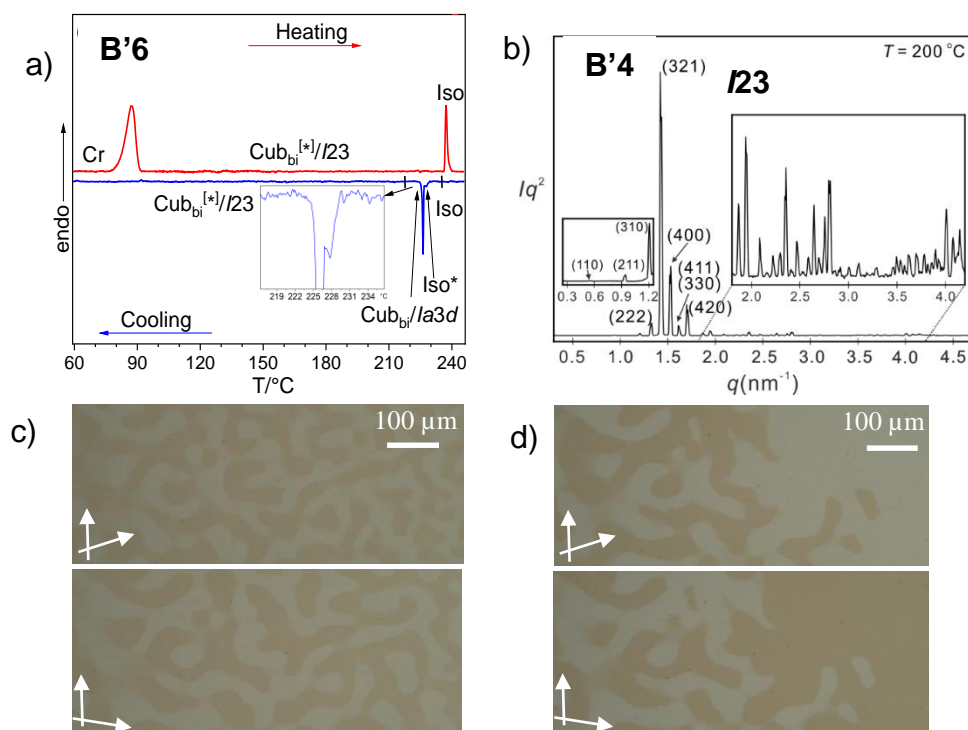
Figure 6.3 a) DSC heating and cooling traces (10 K min^{-1}) of **B'6**; b) SAXS diffractograms of the Cub$_{bi}$/*I23* of **B'4**;[2] c) Chiral domains of the Iso$_1$[*] phase at 232 °C amd (d) the Cub$_{bi}$[*]/*I23* phase at 200°C under slightly decrossed polarizers after rotation in clockwise and anticlockwise from **B'6**.

Moreover, only a small range of the Iso$_1$[*] phase can be observed for **B'5** and **B'6**. However, it appears that the Iso$_1$[*] phase of compound **B'6** is separated by a small range of the achiral Cub$_{bi}$/$Ia3d$ phase from the chiral $I23$ phase. As a proof, when the cooling rate is 5K/min, the chiral domains in Iso$_1$[*] disappear completely at the transition to $Ia3d$, and subsequently, another type of chiral domains is formed in the $I23$ phase. When the cooling rate is 20K/min, some part of the chiral domains from Iso$_1$[*] remain the same and some other part of the chirality is erased and formed again (Fig. 6.3c,d). By chain elongation from **B'6** to **B'8** the Iso$_1$[*] is removed.
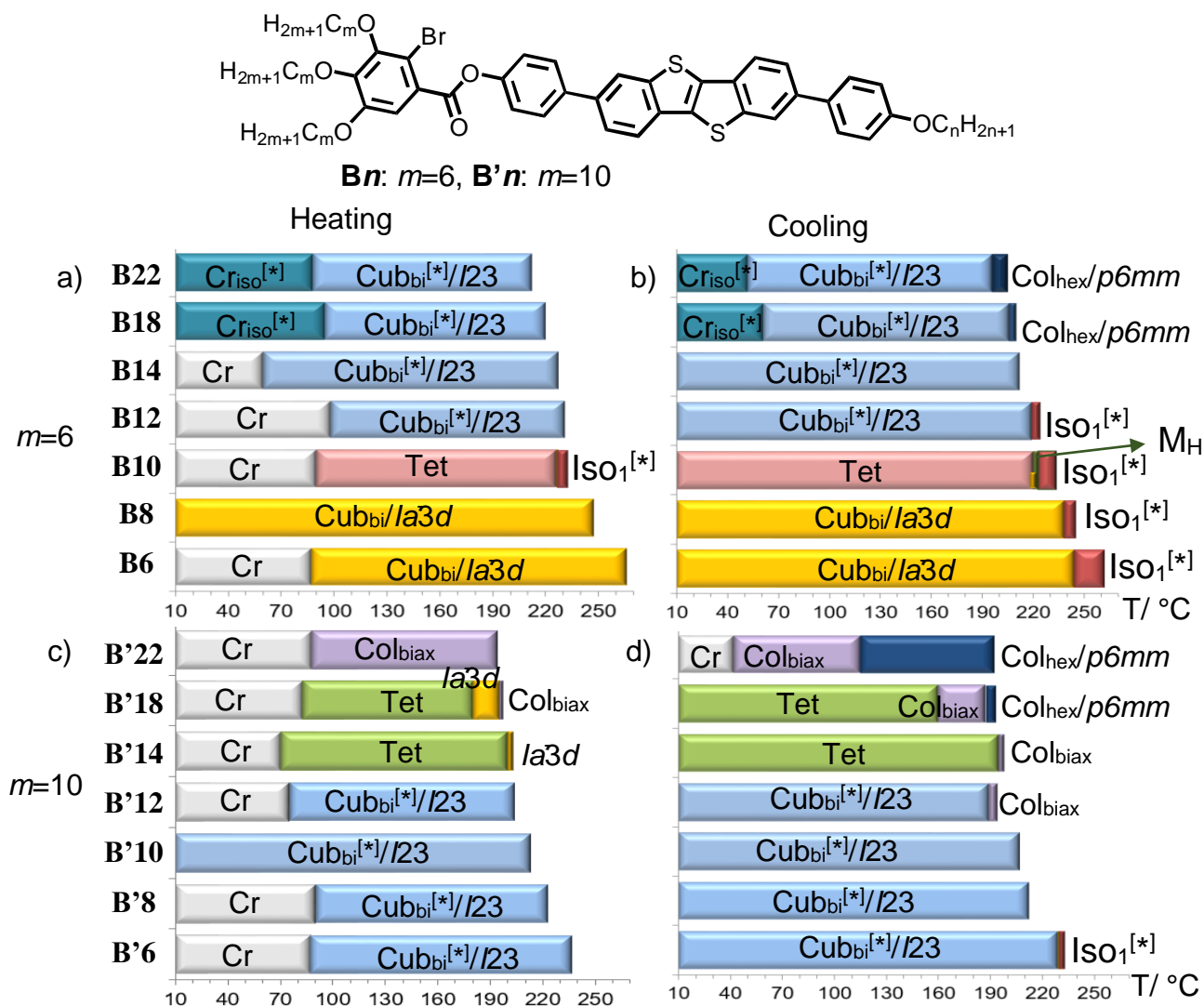
Figure 6.4 Comparison of the mesophases and transition temperatures of a,b) the tri-decyloxy substituted compounds **B'n** with c,d) the tri-hexyloxy substituted compounds **Bn**[3] observed on a,c) heating and b,d) on cooling.

Table 6.3 Total chain volume of the compounds at the transition between $Ia3d$ and $I23$ phase.

	N_{n+m}	$T/°C$ $[\Delta H /kJ \cdot mol^{-1}]$
B'3	33	H: Cr <20 Cub$_{bi}$/$Ia3d$ 242 [3.3] Iso
B'4	34	H: Cr$_1$ 87 [30.1] Cr2 111 [16.8] Cub$_{bi}$[*]/$I23$ 240 [0.3] Cub$_{bi}$/$Ia3d$ 243 [2.4] Iso
B9	27	H: Cr <20 Tet 155 [-] Cub$_{bi}$/$Ia3d$ 236 [1.7] Iso
B11	29	H: Cr <20 Cub$_{bi}$[*]/$I23$ 160 [-] Tet 180 [-] Cub$_{bi}$[*]/$I23$ 227 [1.8] Iso

abbreviations: N_{n+m} = total number of CH$_2$ groups in the alkyl chains of the compounds

6.2 Phase sequence $Ia3d_{(L)}$ – $I23$ – $Ia3d_{(S)}$

Increasing the length of the single chain (n) from 12 to 14 leads to the replacement of the $I23$ phase by an achiral $Ia3d$ phase and additional birefrigent mesophases. Compounds from **B'14** to **B'18** form a relatively low birefringent phase on both heating and cooling which is estimated as a tetragonal phase (Fig. 6.6c,d,f,g). It exhibits a high viscosity as a cubic phase, and therefore, it can be considered as a 3D phase. More investigation is needed to clarify the structure and alignment of molecules of the phase. In addition, the 3D phase (**B'14 - B'18**) is replaced by Cub$_{bi}$/$Ia3d$ phase on heating. The $Ia3d$ phase can only be observed on heating whereas on cooling it is completely replaced by the birefringent mesophases. The range of Cub$_{bi}$/$Ia3d$ phase becomes broader on elongating the chain lengths; **B'14** (200 – 203 °C), **B'16** (195 – 200 °C) and **B'18** (180 – 195 °C). However further elongation of to n= 22 removes the $Ia3d$ phase, and it is completely replaced by columnar phases. (**B'22**, Fig. 6.1, Table 6.1).

The lattice parameters range of the $Ia3d$ phases for these long chain compounds (**B'14 - B'18**) is from 10.35 to 10.50 nm which is smaller than found for the short chain compounds (**B'2 - B'3**) from 10.94 to 10.95 nm (Table 6.2). The calcalated helical twist Φ changes from 8.2° for **B'2 - B'3** to 8.6° for **B'14 - B'18**. Based on these result the Cub$_{bi}$/$Ia3d$ phases can be devided into long pitch ($Ia3d_{(L)}$, **B'2 – B'3**) and short pitch types ($Ia3d_{(S)}$, **B'14 – B'18**) in line with the phase sequence $Ia3d_{(L)}$ – $I23$ – $Ia3d_{(S)}$.[4] Contact preparation between **B'2** and **B'18** was conducted to confirm the phase sequence between two different Cub$_{bi}$/$Ia3d$ phase types (Fig. 6.5). Upon heating

both **B'2** and **B'18** exhibit *Ia*3*d* at 190 ℃. In the contact region between these two achiral *Ia*3*d* phases a ribbon of a chiral conglomerate texture, as typical for *I*23 emerges (Fig. 6.5) and furthermore, a birefringent phase appears in the contact region between the induced *I*23 phase and the *Ia*3*d*(S) phase of **B'18**.
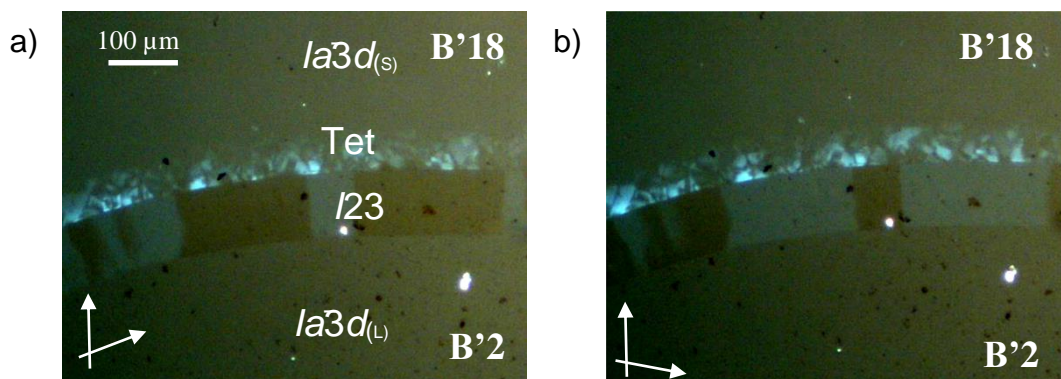
Figure 6.5 Contact region between the achiral *Ia*3*d* phase of **B'18** and **B'2** at 190 ℃ on heating as observed between a) left hand and b) right hand uncrossed polarizers.

Elongaition of the three alkyloxy chains at the tapered end can have two different effects on mesophase formation. First one is a lateral expansion which leads to more steric distortion, thus leading to the *Ia*3*d*(S) – *I*23 – *Ia*3*d*(L) sequence by increasing helical twist. Elongation of the taper-end-chains mainly contributes to lateral expansion whereas apex-chain elongation also contributes to longitudinal expansion. The first gives rise to the *Ia*3*d*(S) – *I*23 – *Ia*3*d*(L) sequence. The second is an increased molecular length which tends to lead to a reduced helical twist. In the *I*23 phase range the twist-reducing and –increasing effects compete with each other as the apex chain length increases, leading to a decrease of the helical twist in the *I*23 phase range. (from 8.48° for **B'4** to 8.34° for **B'16**, see Table 6.2). This competition might also be the reason that the *Ia*3*d*(S) phase is formed only on heating while the development of birefringent mesophases is observed on cooling.

68
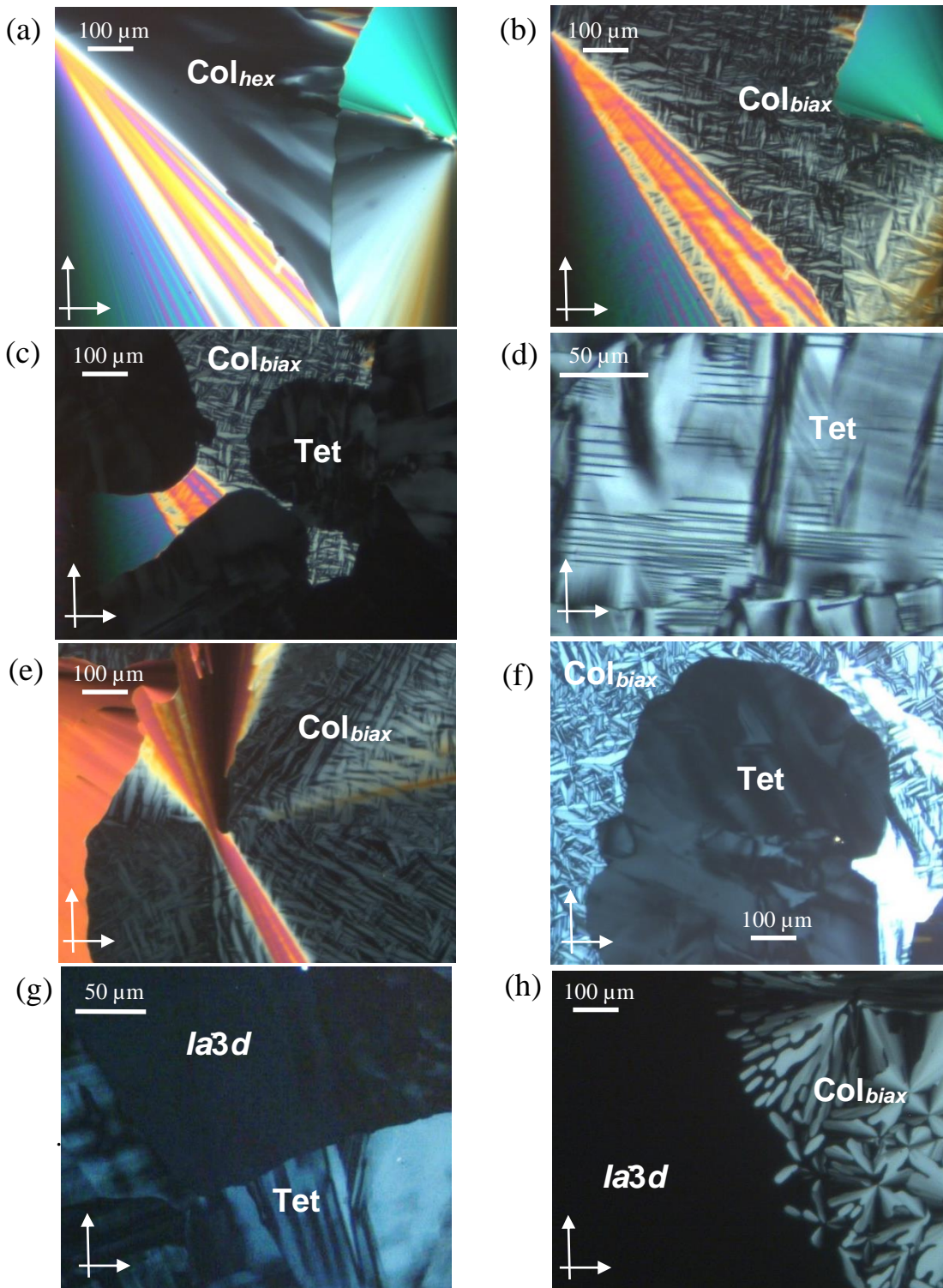
Figure 6.6 a-d) Textures of **B'16**; a) Col$_{hex}$/ *p6mm* 195 ℃, b) Col$_{biax}$ phase at 190 ℃, c) Col$_{biax}$ phase to Tet transition at 180 ℃, d) Tet phase at 160 ℃ on cooling, e-h) textures of **B'18** e) Col$_{biax}$ phase at 170 ℃, f) Col$_{biax}$ to Tet transition at 160 ℃ on cooling, g) Tet to $Ia\bar{3}d$ transition at 180 ℃ on heating, h) $Ia\bar{3}d$ to Col$_{biax}$ phase transition at 196 ℃ on heating.

6.3 Birefringent mesophases of the long chain compounds

Compounds from **B'12** to **B'22** show different types of birefingent phases 3D tetragonal and 2D columnar phases depending on the chain length. In case of **B'18**, a birefrengent texture is detected at 193 °C on cooling via POM investigation (see Fig. 6.6a). The POM texture contains dark areas, which indicates a uniaxial mesophase in homeotropic alignment of the molecules, and moreover, spherulitic areas are detected in the texture (Fig. 6.6a). This is typical texture for an optical uniaxial columnar phase. The $1/d$ values of sharp SAXS reflections with a ratio $1:\sqrt{3}:2:\sqrt{7}$, indicate a hexagonal columnar phase with $p6mm$ lattice (Col$_{hex}$ /$p6mm$) and a = 4.73 nm (Fig. 6.7a,c). The temperature range of the Col$_{hex}$ /$p6mm$ phase becomes broader with longer alkyloxy chain. **B'16** shows the Col/$p6mm$ from 195 to 193 °C while **B'22** shows it from 192 to 115 °C on cooling (see Table 6.1). This indicates that longer alkyl chain stabilize the hexagonal columnar phase due to its higher space filling.
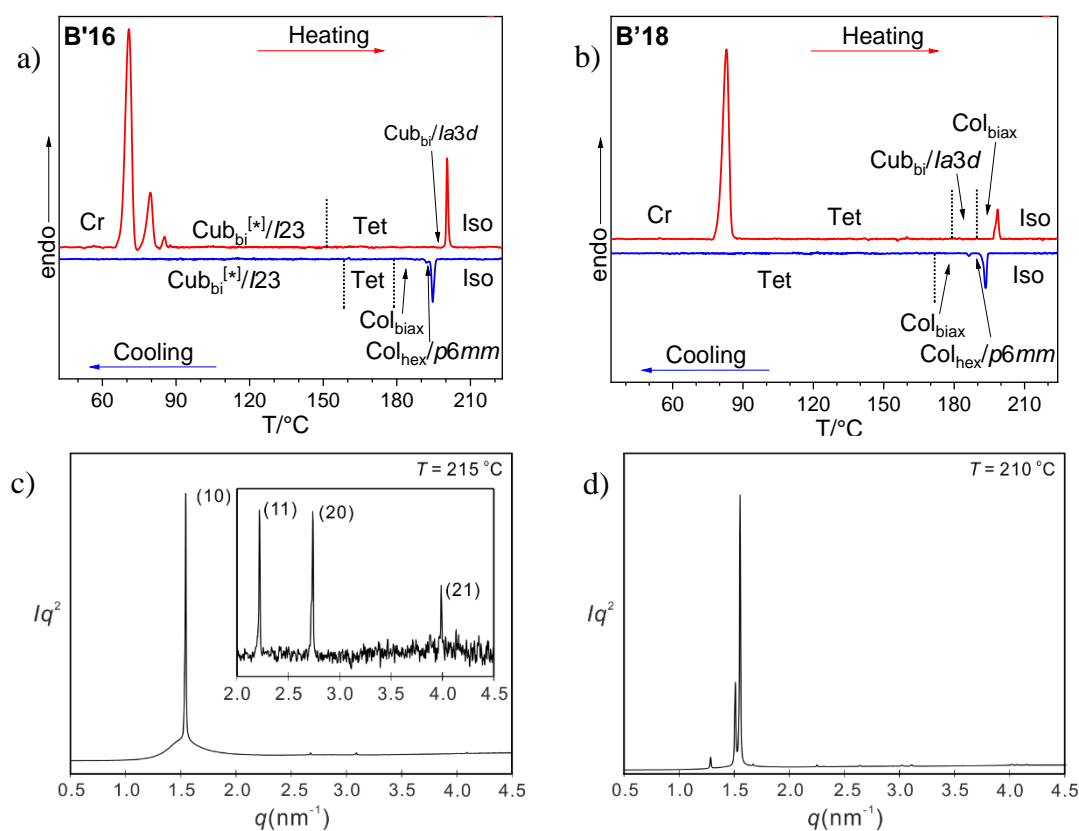
Figure 6.7 DSC heating and cooling traces (10 K min^{-1}) (a) **B'16** and (b) **B'18**; SAXS diffractograms[2] of (c) $p6mm$ phase of **B'16** at 215 °C and (d) Col$_{biax}$ of **B'16** at 210 °C upon cooling.

Further cooling of the Col/$p6mm$ of **B'18** converts it to a biaxial columnar phase at 187 ℃, which is associated with a small transition enthalpy of $\Delta H = 0.1$ kJ mol^{-1} (Table 6.1). At the same time the homeotropic region from Col$_{hex}$/$p6mm$ phase is filled with strip-shaped birefringent texture in Fig. 6.6b,e. In the SAXS pattern the position of the scattering peaks changes. Though indexations to a $p2gg$ (compound **B'16**) or a $c2mm$ lattice (compound **B'18**) would be possible (Fig. 6.7d), the reconstructed electron densirty maps cannot be assigned to a reasonable organization of the moelcules. Therefore, we cannot give a sure model of the organization of compounds **B'n** in these Col phases. We assume that the molecules are organized in ribbons which are rotationally disordered in the Col$_{hex}$ phase (Fig. 6.10, right). At the transition to the biaxial columnar phase the rotation becomes restricted and a rectangular or oblique lattice is formed. These biaxial columnar phases with unknown 2D-lattice are designed as Col$_{biax}$. Since the Col$_{biax}$ phases are shearable, the possibility of being 3D phase can be ruled out (see Fig. 6.8). It is likely that in the Col$_{hex}$ and Col$_{biax}$ phases the long range synchronized helical organization as in the Cub$_{bi}$ phase is lost, because the network structure is removed at the Cub$_{bi}$ – Col transition and any helical pitch has only short range correlation in the non-branched columnar aggregates.
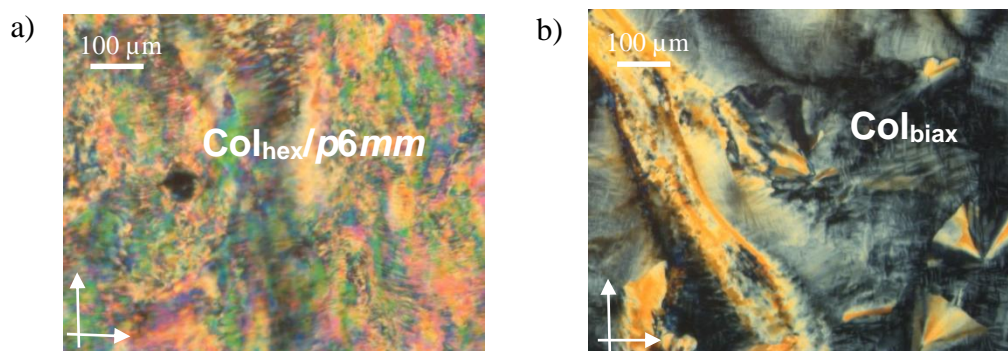
Figure 6.8 Textures of the columnar phases; a) Col$_{hex}$/$p6mm$ (**B'22**, 192 ℃) and b) biaxial Col$_{biax}$ phase (**B'18**, 180 ℃) phase after shearing.

Furthermore, the long chain compounds **B'14** to **B'18** form additional highly viscous birefringent mesophases. Upon further cooling the Col$_{biax}$ phase the low birefringence, biaxiality and high viscosity are features which are very similar to the tetragonal phases. These mesophases are designated as Tet. (Fig. 6.6c,d,f,g). The phase range recorded on cooling decrease with growing chain lengths (from 195 → 0 ℃ for **B'14**, 180 → 0 ℃ for **B'16** and 160 → 0 ℃ for **B'18**). This

observation is in line with a deformed network structure of the Tet phases because longer chains increases the interface curvature and support the transition from Cub_{bi}-like to columnar self-assembly. In case of **B'16**, SAXS result shows that Cub_{bi}[*]/$I23$ replaces the tetragonal phase at 160 ℃ on cooling though it is not detected by POM investigation (see Fig.6.9). This indicates that the Tet phase might represent slightly distorted version of the triple network $I23$ phase.
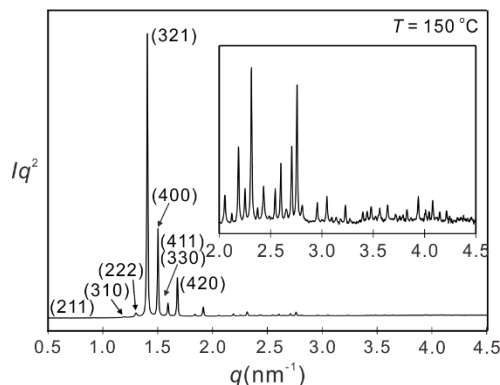
Figure 6.9 SAXS diffractogram of the Cub_{bi}[*]/$I23$ phase of **B'16** at 150 ℃[2]

6.4 Conclusion

In this series due to the bulky alkyl chains there is no additional Tet phase at the transition from $Ia\overline{3}d_{(L)}$ to $I23$ without inducing $\pi-\pi$ stacking which is different from applying additional bromine atom. It is shown that elongation of the length of the alkyl chains at the tapered end shifts the $Ia\overline{3}d_{(L)}$ - $I23$ transition to shorter chain length, suppresses Tet phase formation at the $Ia\overline{3}d$ - $I23$ transition and leads to a reentrance of the $Ia\overline{3}d$ phase by elongation of the apex-chain. However this $Ia\overline{3}d_{(S)}$ phase is only formed on heating in a short T-range below the transition to the isotropic liquid and it is replaced by 3D phases with deformed networks and by biaxial and uniaxial columnar phase (Col_{biax}, Col_{hex}) with non-branched abd non-helical columnar aggregates.
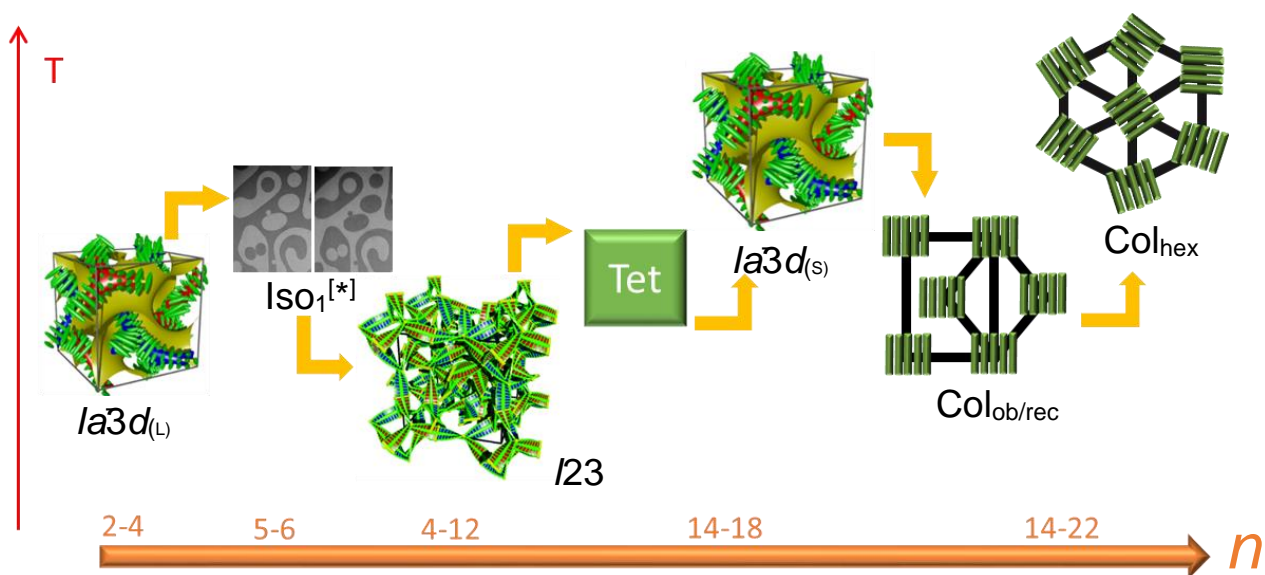
Figure 6.10 Overall phase sequence of compounds **B'*n*** on increasing the apex chain length.

References

1   X. B. Zeng and G. Ungar, J. Mater. Chem. C **2020**, 8, 5389.

2   F. Liu, Xi'an Jiaotong University, P. R. China 710049, unpublished results

3   O. Kwon, X. Cai, W. Qu, F. Liu, J. Szydłowska, E. Gorecka, M. J. Han, D. K. Yoon S. Poppe and C. Tschierske, *Adv. Funct. Mater*. **2021**, 2102271.

4   C. Dressel, T. Reppe, S. Poppe, M. Prehm, H. Lu, X. Zeng, G. Ungar, C.Tschierske, *Adv. Funct. Mater.* **2020**, 30, 2004353.

7. Controlling the formation of cubic network phases and mirror symmetry breaking by core fluorination
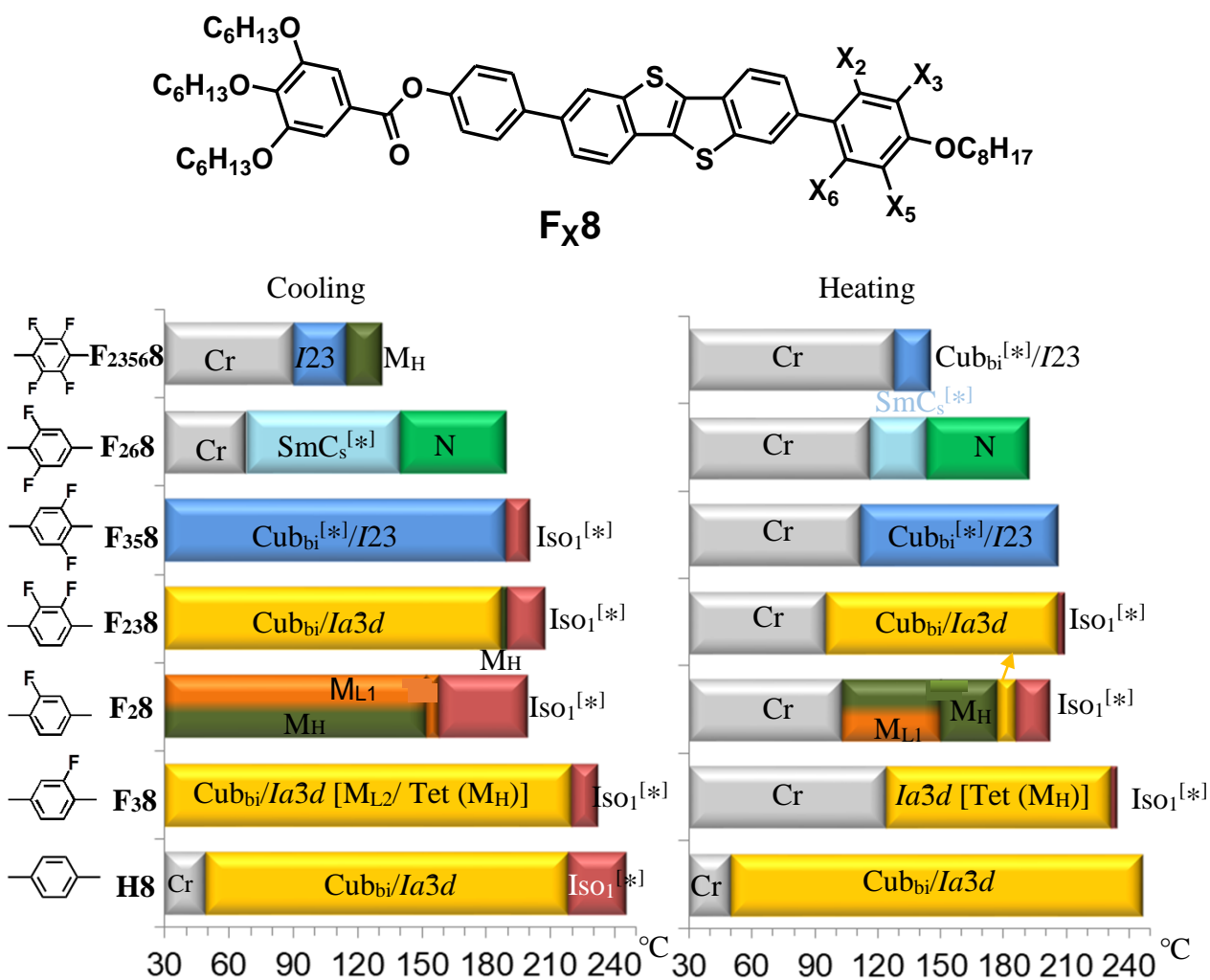
Figure 7.1 a) Structure of the compounds **Fₓ8** and b) their phases and phase transitions observed on cooling (left) and heating (right, rate 10 K min⁻¹); M = mesophases with 3D lattice; M_H = highly birefringent M phase (mosaic texture), M_{L1} = low birefringent (gray) M-phase with mosaic texture; M_{L2} = low birefringent M phase with "triangular mosaic texture"; $SmC_s^{[*]}$ = synclinic tilted smectic phase, showing a conglomerate of chiral domains in cells with homeotropic alignment; N = nematic LC phase; the numerical values with transition enthalpies are collated in Table 7.1.

Herein we report series of new 2,7-diphenyl BTBT derived tetracatenar compounds having a tapered 3,4,5-trialkoxybenzoate (in most cases hexyloxy chains) end and a 4-monoalkylated (in most cases octyloxylated) apex at the opposite end, being additionally fluorinated in different

positions at the apex-ring (compounds F_x8). It is shown that increasing fluorination of this terminal benzene ring from 1 to 4 fluorines and variation of the positions of the fluorines leads to a transition from achiral *Ia*3*d* to chiral *I*23 type bicontinuous cubic mesophases and simultaneously destabilizes the mirror symmetry broken isotropic liquid ($Iso_1^{[*]}$). The subscript(s) x in the compounds designations indicate(s) the positions of each of the fluorines.

Table 7.1 Transition temperatures and –enthalpies of compounds F_x8 on heating and cooling at 10 K/min.

	T/°C [ΔH /kJ·mol^{-1}]
H8	H: Cr 50 [2.9] Cub$_{bi}$/*Ia*3*d* 246 [1.9] Iso C: Iso$_2$ 245 [0.4] Iso$_1^{[*]}$ 218 [0.7] Cub$_{bi}$/*Ia*3*d* 49 [3.6] Cr
F$_3$8	H: Cr 124 [7.7] Cub$_{bi}$/*Ia*3*d* or Tet/*I*4$_1$/*acd* 231 [1.4] Iso$_1^{[*]}$ 234 [0.1] Iso C: Iso 232 [0.1] Iso$_1^{[*]}$ 220 [2.2] Cub$_{bi}$/*Ia*3*d*, Tet/*I*4$_1$/*acd* or M$_{L2}$ <20 Cr
F$_2$8	H: Cr 73 [19.7] Cr$_2$ 103[3.3] M$_{L1}$ and M$_H$ 165 [-] Cub$_{bi}$/*Ia*3*d* 176 [0.8] Iso$_1^{[*]}$ 202 [0.2] Iso C: Iso 200 [0.1] Iso$_1^{[*]}$ 152 [0.2] Tet <20 Cr
F$_{23}$8	H: Cr 95 [25.9] Cub$_{bi}$/*Ia*3*d* 206 [1.7] Iso$_1^{[*]}$ 209 Iso C: Iso 207 [0.8] Iso$_1^{[*]}$ 190 [0.7] M$_H$ 187 [-] Cub$_{bi}$/*Ia*3*d* <20 Cr
F$_{35}$8	H: Cr 112 [33.7] Cub$_{bi}$/*I*23 206 [2.1] Iso C: Iso 200 [0.1] Iso$_1^{[*]}$ 189 [1.5] Cub$_{bi}$/*I*23 <20 Cr
F$_{26}$8	H: Cr$_1$ 106 [28.2] Cr$_2$ 116 [17.7] SmCs$^{[*]}$ 143 [0.2] N 192 [0.6] Iso C: Iso 190 [0.9] N 140 [0.2] SmCs$^{[*]}$ 68 [21.6] Cr
F$_{2356}$8	H: Cr 126 [25.7] Cub$_{bi}$/*I*23 145 [1.6] Iso C: Iso 131 [0.9] M$_H$ 115 [-] Cub$_{bi}$/*I*23 90 [1.2] Cr 78 [20.7] Cr

7.1 Monofluorinated compounds F$_2$8 and F$_3$8 in comparison to the non-fluorinated compound H8

The non-fluorinated compound **H8**, shows a broad region of an achiral cubic phase with *Ia*3*d* lattice, being stable between 50 and 246 °C. Upon cooling from Iso a mirror-symmetry

broken $Iso_1^{[*]}$ phase is formed first between 245 to 218 °C before the *Ia3d* phase develops on further cooling, no additional birefringent mesophase was observed at the $Iso_1^{[*]}$-*Ia3d* transition.[1] The thermal stability of the mesophases ($Iso_1^{[*]}$ and LC) is reduced by mono-fluorination. The fluorination in the inside directed 2-position (F_28) has a larger destabilizing effect than the peripheral 3-position (F_38). This is similar to observations made with smectic phases of rod-like molecules and it is considered as being due to a stronger steric distortion of inside directed substituent on the parallel packing of rod-like molecules.[2]
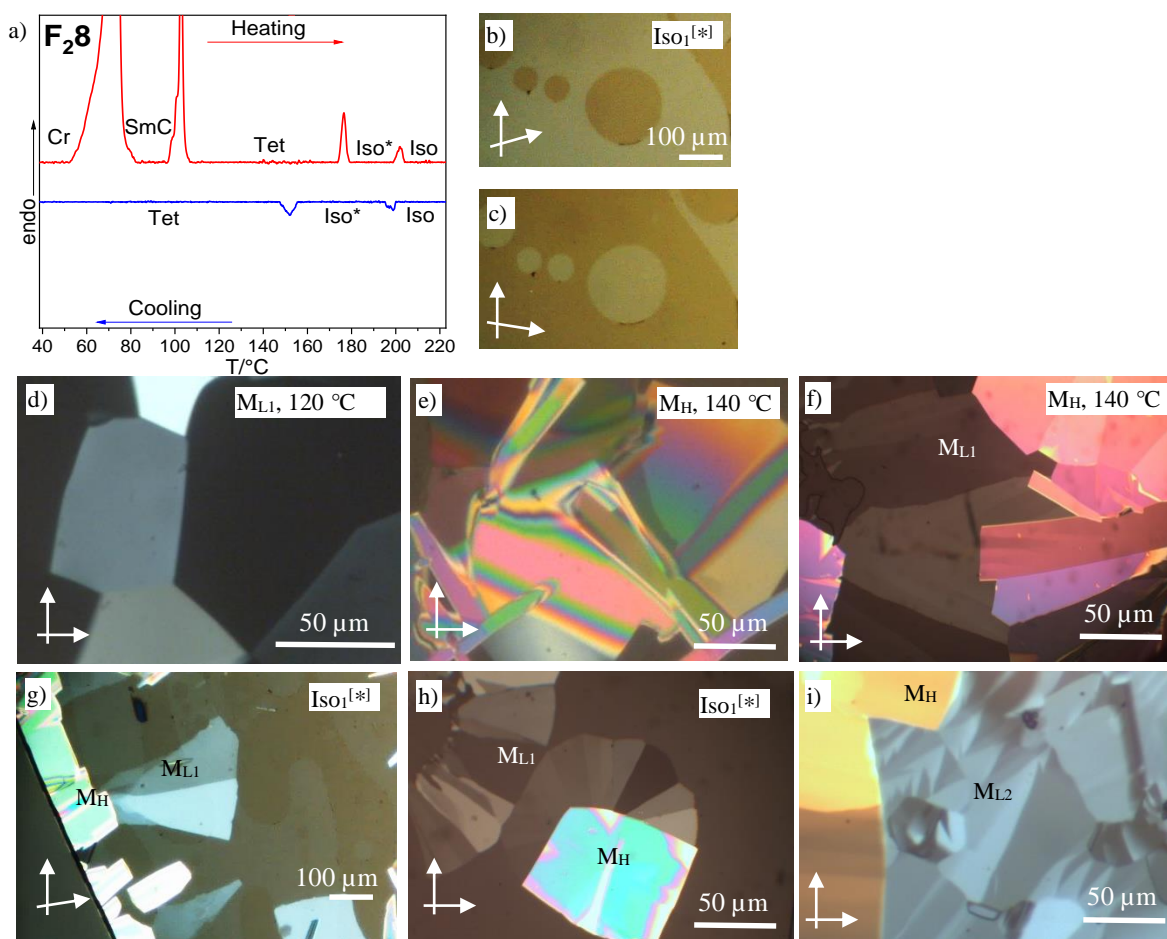
Figure 7.2 Compound F_28. a) DSC heating and cooling traces (10 K min⁻¹), b,c) chiral domains of the $Iso_1^{[*]}$ phase as observed by POM between slightly uncrossed polarizers at 170 °C; d) low birefringent phase (M_{L1}) observed on cooling at 120 °C and e) highly birefringent M_H-phase observed on heating at 140 °C; f,g,h,i) shows the coexistence of the two birefringent 3D phases with the chiral domains of the $Iso_1^{[*]}$ phase at 140 °C on cooling in g) between slightly uncrossed polarizers and in h) between 90° crossed polarizers.

In contrast to **H8**, having exclusively the *Ia*3*d* phase, the monofluorinated compounds **F₂8** and **F₃8** show very complicated phase sequences of coexisting *Ia*3*d* and high and low-birefringent non-cubic phases (M_H and M_{L1}, M_{L2}). For both compounds the achiral *Ia*3*d* phase of **H8** is retained in certain temperature range. The mirror symmetry broken isotropic liquid ($Iso_1^{[*]}$) is formed besides the cubic phase on cooling as well as on heating, whereas for the non-fluorinated compound **H8** it is only observed on cooling. This means that by monofluorination the $Iso_1^{[*]}$ phase range becomes enantiotropic in a certain temperature range (Fig. 7.1, Table 7.1). Remarkable is also the strong effect of the position of fluorine on the $Iso_1^{[*]}$ phase range. In both cases **F₂8** (inside-directed) and **F₃8** (outside directed, peripheral) the temperature range of the $Iso_1^{[*]}$ phase is shifted to lower temperatures compared to **H8**, but, only the peripheral substitution in **F₃8** reduces the $Iso_1^{[*]}$ phase width, whereas it is significantly expanded by the inside directed fluorination in **F₂8**. This provides a broad range of the $Iso_1^{[*]}$ phase with a thermodynamic stable (enantiotropic) range of 26 K. On cooling it can even be retained down to ambient temperature when it apparently gasifies around 20-30 ℃, though it is always accompanied by coexisting areas of birefringent mesophases (Fig. 7.2f). The complete phase sequence of **F₂8** is schematically shown in Scheme 7.1.

Both birefringent mesophases are highly viscous, similar to the cubic phase; one of them has a highly birefringent (colorful) mosaic texture and is designated as M_H. The other one appears gray, indicating a low birefringent mesophase with mosaic texture (M_{L1}). The thermodynamic stability of the phases decreases in the order $Ia3d > M_H > M_{L1}$, as indicated by the phase transition temperatures and the slow transitions $M_{L1} \rightarrow M_H \rightarrow Ia3d$. Obviously the *Ia*3*d* phase is the thermodynamically most stable phase, but formation of the *Ia*3*d* phase is kinetically hindered. It probably cannot from directly from the chiral domains of the $Iso_1^{[*]}$ phase, because this would require helix inversion for half of the helical networks. Based on the textural features it is possible that the low birefringent M_{L1} phase represents a SmQ phase ($P4_122$) which is composed of two interwoven networks with 90° junctions and identical chirality in the networks, and hence it is chiral, too, not requiring any helix inversion during its formation. [3] From previous work it is known that the *Ia*3*d* phase can indeed easily develop form the SmQ phase,[3] in our case taking place as a phase transition on heating to 169 ℃. Alternatively, the M_{L1} phase can slowly transforms into the high birefringent M_H phase, and then forms the *Ia*3*d* phase already above 165 ℃. After the *Ia*3*d*

phase is formed it melts into $\text{Iso}_1{}^{[*]}$ at 185 °C upon further heating. When the formed *Ia3d* phase is cooled, it does not convert to one of the M phases. Rapid cooling of the $\text{Iso}_1{}^{[*]}$ phase leads to only partial transition of the $\text{Iso}_1{}^{[*]}$ phase into M_{L1} and M_H, while a large part of the $\text{Iso}_1{}^{[*]}$ phase is retained. At low temperature (<150 °C) all transitions become extremely slow and the phases are long time persistent.

Thus, the observed phases and phase sequences are strongly dependent on the conditions and sample history, providing pathway complexity. It also appears that there is a sensitivity of the birefringent mesophase to thermal aging, for **F₂8** it leads to a shift from M_H to M_{L1} as the dominating birefringent 3D phase, whereas the Cub_{bi} and $\text{Iso}_1{}^{[*]}$ phase ranges are obviously not affected.
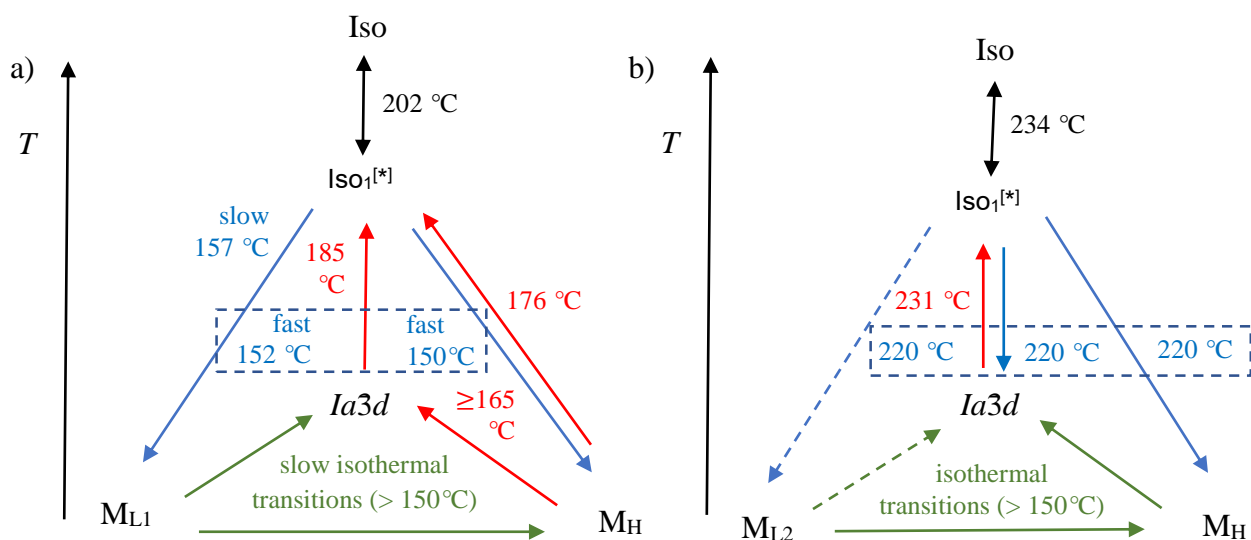
Scheme 7.1 Phase transitions of compounds a) **F₂8** and b) **F₃8** on second heating (red) and the following cooling (blue), green indicates isothermal transitions and black indicates reversible phase transitions (crystalline phases are not shown).

Overall, the *Ia3d* phase is the preferred cubic lattice of compound **F₂8**, meaning that its single inside directed fluorine does not lead to the alternative chiral *I23* phase. This is an indication for a local network structure of the $\text{Iso}_1{}^{[*]}$ phase which is not *I23*-like, but should be SmQ-like.[3] Because exclusively lamellar phases were observed for the 2,6-disubstituted compound **F₂₆8**, having two inside directed fluorines (see below), a slight shift towards lamellar self-assembly could in the case of **F₂8** lead to the stabilization of the noncubic 3D phases and the $\text{Iso}_1{}^{[*]}$ phase.
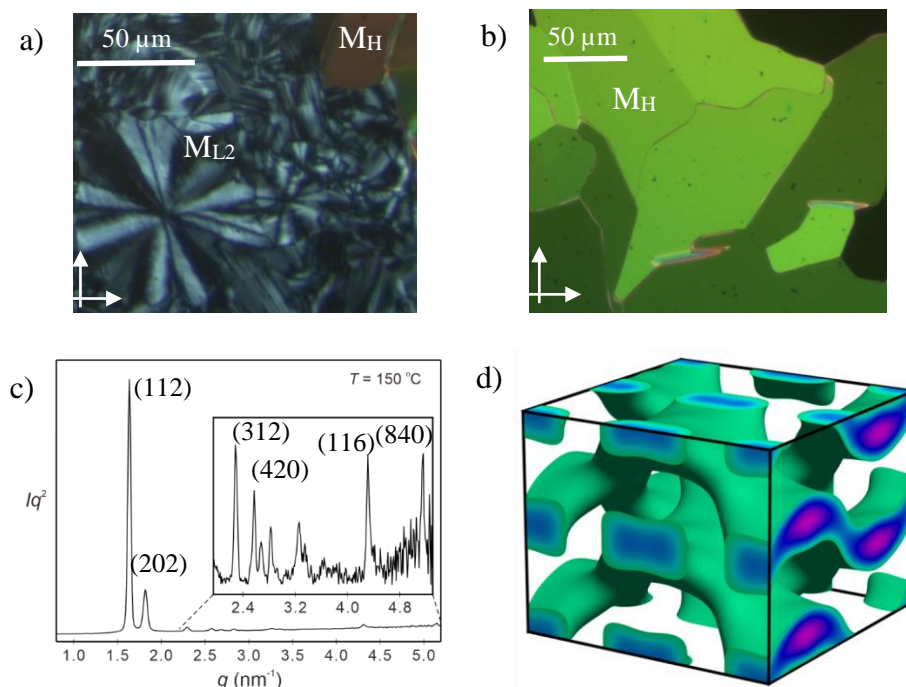
Figure 7.3 Compound **F₃8** a) texture of lowly birefringent M_L phase and highly birefringent M phase M_H observed on fast cooling at 210 °C; b) texture of highly birefringent M_H observed on slow cooling at 210 °C; c) SAXS patterns of Tet/ $I4_1/acd$ at 150 °C;[4] d) the corresponding ED maps reconstructed from the diffraction patterns, the aromatic cores are located in the networks formed by the green iso-surfaces, the space in between is filled by the alkyl chains.[4]

Also for the peripheral 3-fluorinated compound **F₃8** the $Ia3d$ phase of **H8** is retained as thermodynamically stable mesophase and two additional birefringent mesophases, a high birefringent and a low birefringent, are formed as metastable phases as well (Fig. 7.2, 7.3). The high birefringent phase has the same texture as M_H of compound **F₂8**, whereas the low birefringent phase is different and shows a unique texture involving regular arrays of triangular shaped domains (Figs. 7.2i, 7.3a). Thus, it is likely that it is different from the M_{L1} phase of **F₂8** and therefore we designate it as M_{L2}. Exclusively the high birefringent M_H phase is observed in the very first heating. Both birefringent mesophases are formed simultaneously during first cooling, whereas M_{L2} is observed only with fast cooling rate (>20 K min⁻¹). The M_H phase is dominating and the low birefringent M_{L2} phase is slowly replaced by the high birefringent M_H phase. This indicates that the two textures indeed represent different phases, not only different modes of alignment of a single mesophase, and that the high birefringent M_H phase is again the more stable phase compared to the low birefringent one. Based on XRD result, the M_H phase appear to be tetragonal phase with $I4_1/acd$ symmetry, which is a distorted $Ia3d$ phase (Tet/ $I4_1/acd$) (Fig. 7.3c). The Tet/ $I4_1/acd$ phase

changes its lattice parameter with temperature, showing an increase in distortion on decreasing temperature. The lattice parameter at 210 °C (a_{tet} = 10.76 nm, c_{tet} = 8.92 nm) are shifted at 130 °C (a_{tet} = 11.16 nm, c_{tet} = 8.79 nm, see Fig. 7.3 and Tab. 7.2). During the distortion of $Ia3d$ phase, the vertical axis (c) is shortened and the horizontal axis (a) is lengthened, and additional cooling increases the degree of distortion. The lattice parameter of the Cub_{bi}/$Ia3d$ phase is a_{cub-} = 9.44 nm at 230 °C (see Tab. 7.3).

Table 7.2 Lattice parameters of **F₃8** upon 3rd cooling from 250 °C. [4]

T/°C	Lattice parameters/nm	V_{cell}/nm^3
210	a_{tet} = 10.76, c_{tet} = 8.92	1032.7
190	a_{tet} = 10.77, c_{tet} = 8.93	1035.8
170	a_{tet} = 11.05, c_{tet} = 8.87	1083.0
160	a_{tet} = 11.07, c_{tet} = 8.85	1084.5
130	a_{tet} = 11.16, c_{tet} = 8.79	1094.8

The Tet/$I4_1$/acd and M_{L2} phases are slowly replaced by the achiral Cub_{bi}/$Ia3d$ phase, again representing the thermodynamic minimum structure. The formation of the Cub_{bi} phase starts in the the Tet/$I4_1$/acd regions and grows into the region of the M_{L2} phase. On heating this transition becomes faster and all birefringent phases transform into the optically isotropic Cub_{bi} phase followed by a transition from Cub_{bi} to $Iso_1^{[*]}$ at 231 °C and to the achiral isotropic liquid at 234 °C. If heating is stopped slightly above the Cub_{bi} - $Iso_1^{[*]}$ phase transition, i.e. within the $Iso_1^{[*]}$ range, then exclusively the formation of the Cub_{bi} phase is observed on cooling which is retained until crystallization. The same is observed if the Cub_{bi} phase was formed from the birefringent phases. Formation of the M phases requires rapid cooling (>10 K min^{-1}) from the achiral Iso phase from at least 20 K above the Cub-$Iso_1^{[*]}$ transition temperature. In this case residual surface layers of the Cub_{bi} phase are obviously removed and as the formation of the $Ia3d$ phase from $Iso_1^{[*]}$ is slow, only the rapidly growing M phases are observed. However, once the Cub_{bi} phase has formed, it always replaces the birefringent phases on cooling and remains as the only mesophase (Scheme 7.1b).

Overall, it appears that the peripheral fluorine of **F₃8** does not modify the self-assembly of **H8** significantly, it only leads to a slight shift towards the $Ia3d$-$I23$ transition range, thus leading

to non-cubic intermediate phases appearing before the mirror symmetry broken $I23$ phase is formed. This is supported by the formation of exclusively the $I23$ phase in the case of the double peripheral substituted compound **F$_{35}$8** (see below). Comparison of **F$_3$8** with **F$_2$8** and **H8** shows that the $Ia3d$ phase is retained, though in the sequence **H8** < **F$_3$8** < **F$_2$8** the birefringent phases become more dominating and the Iso$_1$[*] phase range expands. Furthermore, compound **F$_3$6**, which contains a shorter side chain than **F$_3$8**, forms only the Iso$_1$[*] phase and the $Ia3d$ phase, both upon heating and cooling. It supports that the birefringent phases appear at the transition from $Ia3d$ to $I23$ (see Table. 7.1).

The low birefringent 3D phases observed for the two monofluorinated compounds are likely to represent network phases with a deformed cubic lattice, deformed in one (Tet) or two spatial directions (Orh) or by a deviation of the angles from 90 ° (Rho). Though several tetragonal, orthorhombic and even a rhomohedral 3D phase are known from polycatenar mesogens, their structures are still unclear.[5,6] Only the SmQ phase with tetragonal $P4_222$ lattice has recently been solved and understood as a result of the geometric frustration provided by the helical organization along the networks.[3] The orthorhombic $Fddd$ and $Pnma$ networks (O^{70}, O^{53}), as another examples, are known for block copolymer morphologies.[7] However, these networks are formed by flexible polymers and do not experience the chirality induced frustrations of the helical networks of the polycatenrs. Moreover, there are numerous network structures with other structures than the gyroid as for example the simple, double diamond and "primitive" networks.[8]

Whereas the textures of M$_{L1}$ and M$_{L2}$ are clearly different, suggesting different structures, the high birefringent mesophases of **F$_2$8** and **F$_3$8** show almost identical textures and therefore are assumed to be very similar or identical. The high birefringence of the M$_H$ phase suggests either a strongly deformed network structure or a kind of mesh phase, formed by stacking of square nets (see Fig. 8.5d).

7.2 Difluorinated compounds F$_{26}$8 and F$_{35}$8

Substituents at both sides of an aromatic core are known to strongly distort the parallel alignment of rod-like units and hence, mesophase formation.[9] Though a cubic phase is retained by peripheral double fluorination (compound **F$_{35}$8**) its stability is reduced compared to **H8** and **F$_3$8** and the cubic lattice has changed to $I23$, thus leading to a broad range of a mirror symmetry broken

cubic phase. This is in line with the increase of the bulkiness of the periphery. Thus this double fluorination has a similar effect as chain elongation.
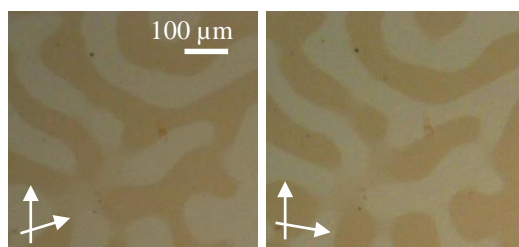
Figure 7.4 Texture of the mirror symmetry broken $I23$ phase of $F_{35}8$ at 160 °C.

Only a lamellar and a nematic phase were observed for $F_{26}8$ with two inside directed fluorines and in this case all network phases (Cub_{bi} and $Iso_1^{[*]}$) are completely suppressed (Fig. 7.1). This is in line with the core widening effect of inside directed fluorination, reducing the interfacial curvature and shifting the phase type from Cub_{bi} to lamellar. The nematic phase of $F_{26}8$ is a cybotactic nematic phase with a relatively strong diffuse small angle scattering at $d = 4.2$ nm (see Fig. 7.5e). The smectic phase occurring below 147 °C on cooling (Fig. 7.5d), shows a weakly birefringent schlieren texture with exclusively 4-brush disclinations in homeotropic alignment as typical for synclinic tilted SmC phases (SmC_s). In planar samples with fan texture an optical tilt in the range of about 30-40° can be deduced from the orientation of the extinctions being inclined with the directions of polarizer and analyzer.

In the SAXS pattern there is only one sharp scattering at $d = 4.38$ nm (130 °C). This layer distance in the lamellar phase is only slightly smaller than the molecular length in the most stretched conformation ($L_{mol} = 4.6$ nm), which in a fully intercalated antiparallel organization (see Fig. 8.3) would not allow the relatively large optically determined tilt of 30-40°. An intercalated double layer structure with overlapping apex chains and aromatic cores, as previously reported for tricatenars.[10] It would lead to a length of these pairs of 5.2 nm, which is in line with the measured tilt angle and d-value. This intercalation supports a reduction of the interface curvature (two cores vs 3 chains) compared to the antiparallel monolayer structure (two cores vs 4 chains, see Fig. 8.3) and thus the transition from the bicontinuous networks to flat layers in SmC_s. The partial mixing of aliphatic chains and aromatics rods in this organization provides a layer destabilizing effect on the lamellae, especially at elevated temperature. This is supported by the steric distortion of lamellar packing due to the substitution in the inside directed positions at both sides of the core

units and leads to the loss of long-range positional order while retaining orientational order due to the long rod-like cores, thus leading to a cybotactic nematic phase composed of SmC$_s$ clusters.
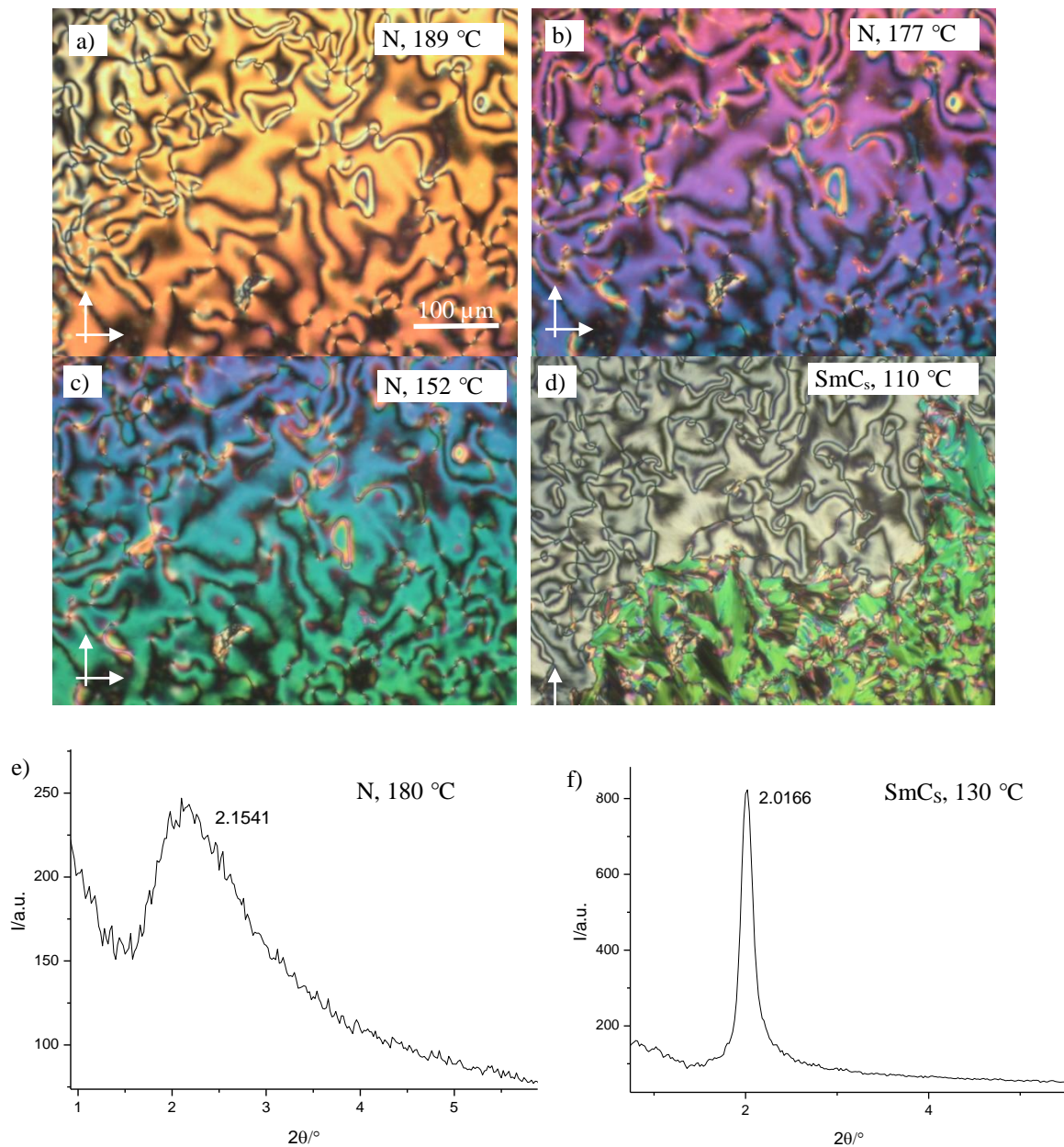
Figure 7.5 Textures of compound **F$_{26}$8** (same area) as observed between two non-treated microscopy glass plates. a-c) Schlieren textures of the nematic phase as observed on cooling at a) 189 °C, b) 177 °C and c) 152 °C showing increasing birefringence, and d) SmC$_s$ phase at 130 °C, showing homeotropic (top/left) areas with Schlieren texture and planar aligned regions (bottom/right) with fan-like texture; SAXS diffractogram of e) N at 180 °C and f) SmC$_s$ at 130 °C.
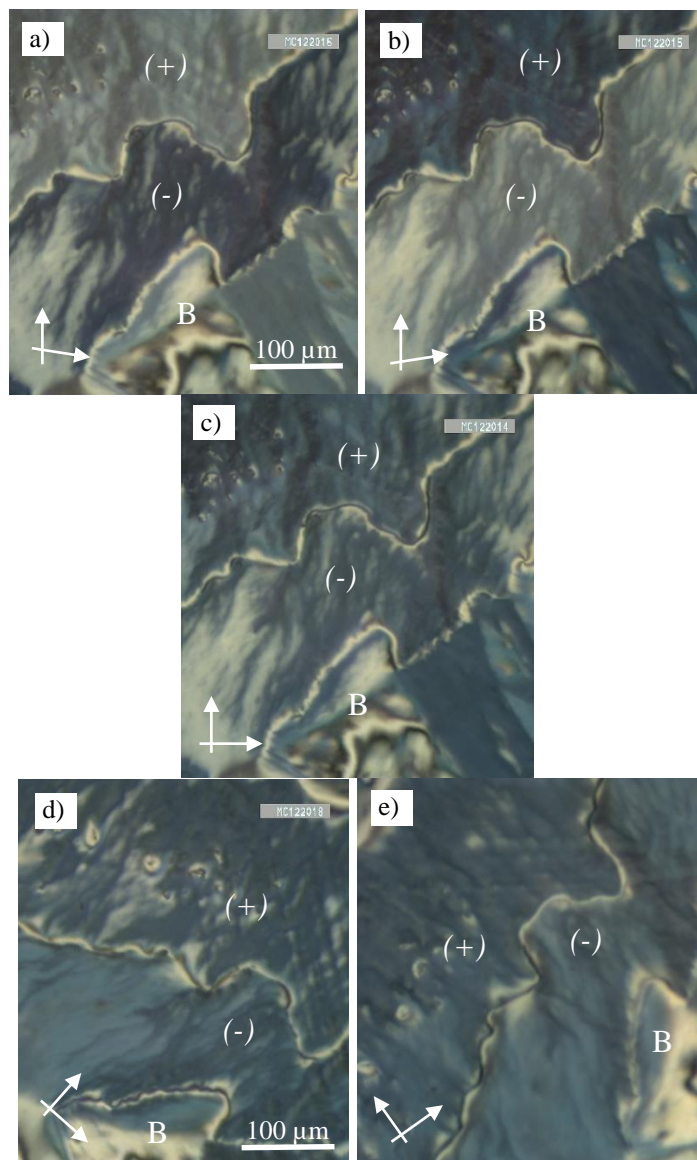
Figure 7.6 Chiral domains as observed for the $SmC_s^{[*]}$ phase of compound **F$_{26}$8** in a thin homeotropic sample as obtained after shearing (T = 130 °C); a, b) domain textures as observed between slightly uncrossed polarizers, showing inverted brightness of the domains after rotating the analyzer in clockwise or anticlockwise direction; c-e) show the same texture between crossed polarizers, in d, e) with the sample rotated between the crossed polarizers either in d) clockwise or e) anti-clockwise direction. That the brightness of the majority of domains (except area B) in d, e) is identical and does not change by rotating the sample means that a simple alignment of the SmC director is not the origin of the differences observed in a) and b). The almost isotropic appearance of the strongly tilted synclinic SmC_s phase thus results from a heliconical superstructure (indicated by [*]) with the helix axis perpendicular to the layers, which are organized parallel to the substrate surfaces in the homeotropic alignment. This structure is assumed to be surface stabilized. B indicates an achiral area.

An additional unusual feature of the SmC$_s$ phase of **F$_{26}$8** is the formation of chiral domains in thin homeotropic aligned samples arranged between two glass plates (Fig. 7.6). Development of a heliconical twist between the surfaces is assumed to be responsible for the spontaneous emergence of surface stabilized chirality in this case. Related phenomena have been observed for nematic [11] and SmC phases of bent-core mesogens[12], benzoate based rod-like molecules[13] and more recently for a tricatenar compound **AF$_{26}$** with a 2,6-difluorinated apex (see Fig. 1.11). [14] The major difference between **AF$_{26}$** and **F$_{26}$8** is the presence of an additional alkyl chain at the apex. In contrast to the heliconical smectic phases of bent molecules,[15,16] which have a very short pitch, the heliconical organization of the polycatenars is of the long pitch type, similar to the SmC* phases [17] and requires surface stabilization to occur. [18] It appears that the inside directed 2,6-substitution supports the intramolecular twist, leading to a stabilization of helical conformations which then support the heliconical twist between the layers. Simultaneously, the inside directed fluorination (**F$_2$8**, **F$_{26}$8**) reduces the interaggregate interface curvature and removes the Cub$_{bi}$ phases and replaces them by long-range (SmC$_s$) or short-range (N$_{CybC}$) lamellar phases. In contrast, peripheral fluorination (**F$_3$8**, **F$_{35}$8**) supports the intermolecular helical twist for steric reasons which then supports the formation of the mirror symmetry broken *I*23 phase instead of the achiral *Ia*3*d* phase requiring a smaller intermolecular twist.[14] The next question concerns the effects of combination of the competing inside- and outside directed substitution patterns.

7.3 Compounds F$_{23}$8 and F$_{2356}$8 combining fluorination in peripheral and inner positions
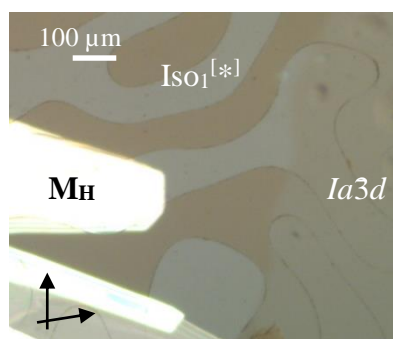
Figure 7.7 Iso$_1$[*]-M$_H$/Cub$_{bi}$/*Ia*3*d* transition of **F$_{23}$8** at 187 °C as observed on cooling.

Compounds **F$_{23}$8** and **F$_{2356}$8** provide combination of inside and peripheral substitution. **F$_{23}$8** behaves very similar to **H8**, characterized by a sequence Iso[*]-*Ia*3*d* with only a very short

range of the metastable birefringent M_H phase at the transition between them (see Fig. 7.1 and Tab. 7.1). The tetrafluorinated compound $F_{2356}8$ has the lowest phase transition temperature in the series of fluorinated compounds (Fig. 7.1). For example, the non-fluorinated compound $H8$ the transition to the isotropic liquid (Iso) takes place at 246 °C while for $F_{2356}8$ it is more than 100 K lower, at 145 °C. Obviously the mesophase stabilizing effect of reduction of the electron density of the π–system, which is expected to increases the strength of the core-core interactions, is more than compensated by the steric effect provided by the tetrafluorination.[19,20]
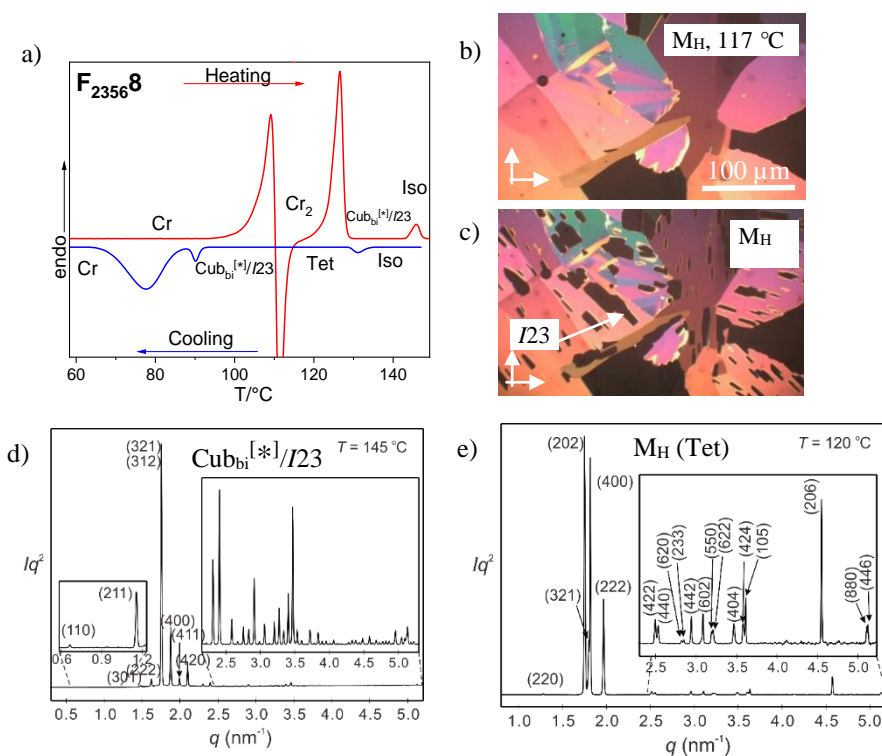
Figure 7.8 Investigation of compound $F_{2356}8$. a) DSC heating and cooling traces (10 K min^{-1}), b, c) POM textures of the mesophases of as observes between crossed polarizers; b) highly birefringent M_H phase at 117 °C (dark mosaics become birefringent by rotation of the sample between the crossed polarizers) and c) M_H-to-Cub_{bi}[*]/$I23$ transition after ~1 minute at 115 °C; d, e) SAXS patterns of d) the Cub_{bi}[*]/$I23$ phase[4] and e) the M-phase with indexation to a tetragonal 3D lattice. [4]

On cooling $F_{2356}8$ from Iso the highly birefringent M_H phase is formed at 131 °C (Figure 7.8b), it becomes instable below 117 °C and is replaced by the growing Cub_{bi}[*]/$I23$ phase (Figure 7.8c). On heating exclusively the Cub_{bi}[*]/$I23$ phase can be found with a Cub→Iso transition at ~147 °C. This means that the Cub_{bi} phase again represents the thermodynamically stable

mesophase whereas the M_H phase is metastable. The XRD pattern of the cubic phase shows the typical SAXS pattern of the $I23$ space group with a lattice parameter of $a_{cub} = 13.32$ nm at 145 °C. The SAXS pattern changes significantly in the M_H phase, observed on cooling, which can be indexed to a tetragonal lattice with $a = 13.90$ nm and $c = 8.45$ nm (Fig. 7.8 d,e).

Table 7.3 Structural data of the 3D mesophases of the investigated compounds depending on the number and position of fluorination. [4]
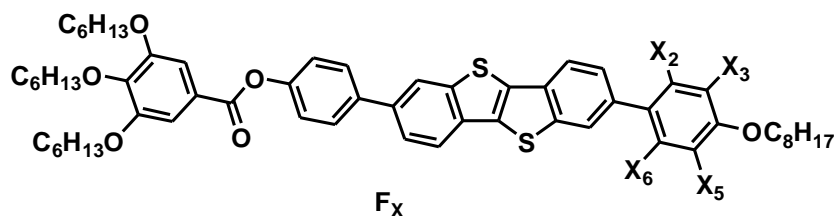
Comp.	Phase	Temp.	a/nm	V_{cell}/ nm^3	V_{mol}/ nm^3	n_{cell}	d_{net}	L_{net}	n_{raft}	Φ/°
H	Cub$_{bi}$/$Ia3d$	180	10.19	1058.1	1.308	723	4.41	86.46	3.76	8.79
F$_3$8	Cub$_{bi}$/$Ia3d$	230	9.44	841.2	1.313	572	4.09	80.10	3.21	9.49
F$_3$8	Tet/ $I4_1$/acd	210	10.88, 8.94	1058.3	1.313	720				
F$_2$38**	Cub$_{bi}$/$Ia3d$	150	9.32	809.6	1.319	548	4.04	79.08	3.12	9.62
F$_{35}$8	Cub$_{bi}$[*]/$I23$	150	13.48	2449.5	1.319	1658	5.84	278.77	2.68	10.36
F$_{2356}$8	Cub$_{bi}$[*]/$I23$	145	13.32	2363.3	1.331	1585	5.77	275.46	2.59	10.48

7.4 Summary and Conclusions

Whereas peripheral fluorination of the apex leads to a transition from the achiral $Ia3d$ phase to the chiral $I23$ phase, in line with an increasing helical twist caused by the peripheral fluorination, the inside directed fluorination removes the cubic phases and shifts the self-assembly towards the lamellar phases. The tetrafluorinated compound, combining peripheral and inside directed fluorination have the lowest mesophase stability and the strongest tendency to form the mirror symmetry broken $I23$ phase instead of the achiral double gyroid $Ia3d$ phase.

As typical for polycatenars the transition between the $Ia3d$ phase and the $I23$ phase is accompanied by the formation of different types of high and low birefringent 3D phases which are considered as tetragonal phases resulting from different modes and strength of deformation of the

cubic lattice. One of the highly birefringent mesophases is a tetragonal phase with $I4_1/acd$ symmetry, which is caused by one peripheral fluorination and it is considered as being derived by deformation of the $Ia3d$ phase. These 3D-mesophases are formed at relatively high temperatures and are associated with the transition from the chiral or achiral Iso phases to the cubic phases on cooling. They are often metastable and their precise structure as well as their relation to the helical twist along the networks needs to be investigated in ongoing work.

References

1   O. Kwon, X. Cai, W. Qu, F. Liu, J. Szydłowska, E. Gorecka, M. J. Han, D. K. Yoon, S. Poppe and C. Tschierske, *Adv. Func. Mater*. **2021**, 2102271

2   J. W. Goodby, I. M. Saez, S. J. Cowling, J. S. Gasowska, R. A. MacDonald, S. Sia, P. Watson, K. J. Toyne, M. Hird, R. A. Lewis, S.-E. Lee, V. Vaschenko, *Liq. Cryst*. **2009**, 36, 567.

3   H. Lu, X. Zeng, G. Ungar, C. Dressel, C. Tschierske, *Angew. Chem. Int. Ed.* **2018**, 57, 2835.

4   F. Liu, Xi'an Jiaotong University, P. R. China 710049, unpublished results

5   D. Demus, L. Richter, Textures of Liquid Crystals, VEB Deutscher Verlag für Grundstoffindustrie, Leipzig 1978, pp. 91, 92,178; A. Levelut, B. Donnio and D. W. Bruce, *Liq. Crys.*, **1997**, 22, 6, 753.

6   a) J. Matraszek, D. Pociecha, N. Vaupotic, M. Salamon´czyk, M. Vogrine and E. Gorecka, *Soft Matter* **2020**, 16, 3882; b) M. Imperor-Clerc, P. Sotta and M. Veber, *Liq. Cryst.*, **2000**, 27, 1001; c) J. Kain, S. Diele, G. Pelzl, C. Lischka and W. Weissflog, *Liq. Cryst.*, **2000**, 27, 1, 11.

7   A. J. Meuler, M. A. Hillmyer, F. S. Bates, *Macromolecules* **2009**, 42, 7221; L. Agosta, A. Metere, P. Oleynikov, and M. Dzugutov, *J. Chem. Phys.* **2020**, 152, 191101; E. L. Thomas, *Sci. China Chem.* **2018**, 61, 25.

8   a) C. Chen, M. Poppe, Dr. S. Poppe, C. Tschierske, F. Liu, Angew. *Chem. Int. Ed.* **2020**, 59, 20820; b) S. Poppe, X. Cheng, C. Chen, X. Zeng, R.Zhang, F. Liu, G. Ungar, and C. Tschierske, *J. Am. Chem. Soc.* **2020**, 142, 7, 3296; c) X. Zeng, S. Poppe, A. Lehmann, M. Prehm, C. Chen, F. Liu, H. Lu, G. Ungar, C. Tschierske, *Angew. Chem.* **2019**, 131, 7453.

9   a) D. W. Bruce and S. A. Hudson, *J. Mater. Chem.,* **1994**, 4, 479; b) J. W. Goodby, I. M. Saez, S. J. Cowling, J. S. Gasowska, R. A. MacDonald, S. Sia, P. Watson, K. J. Toyne, M. Hird, R. A. Lewis, S.-E. Lee and V. Vaschenko, *Liq. Cryst.,* **2009**, 36, 567.

10   T. Reppe, C. Dressel, S. Poppe, A. Eremin, and C. Tschierske, *Adv. Optical Mater.* **2020**, 2001572.

11   V. Görtz, *Liq. Cryst. Today*, **2010** 19:2, 37.

12   M. Alaasar, M. Prehm, M. G. Tamba, N. Sebastian, A. Eremin and C. Tschierske, *ChemPhysChem* **2016**, 17, 278.

13   M. Inukai, T. Fukushima, Y. Hijikata, N. Ogiwara, S. Horike and S. Kitagawa, *J. Am. Chem. Soc.* **2015**, 137, 38, 12183.

14   C. Dressel, T. Reppe, S. Poppe, M. Prehm, H. Lu, X. Zeng, G. Ungar, C. Tschierske, *Adv. Funct. Mater.* **2020**, 2004353.

15   a) M. Alaasar, M. Poppe, S. Poppe, M. Prehm, M. Nagaraj, S. P. Sreenilayam, Y. P. Panarin, J. K. Vij, and C. Tschierske; *Chem. Eur. J.* **2020**, 26, 4714; b) S. P. Sreenilayam, Y. P. Panarin, J. K. Vij, V. P. Panov, A. Lehmann, M. Poppe, M. Prehm and C. Tschierske, *Nature Comm.* **2016**, 7:11369; c)A. A. S. Green, M. R. Tuchband, R. Shao, Y. Shen, R. Visvanathan, A. E. Duncan, A. Lehmann, C. Tschierske, E. D. Carlson, E.

Guzman, M. Kolber, D. M. Walba, C. S. Park, M. A. Glaser, J. E. Maclennan, and N. A. Clark, *Physical Rreview Letters* **2019**, 122, 107801.

16   J.P. Abberley, R. Killah, R. Walker, J. M. D. Storey, C. T. Imrie, M. Salamończyk, C. Zhu, E. Gorecka and D. Pociecha, *Nat. Comm*. **2018,** 9, 228.

17   J. P. F. Lagerwall and G. Scalia, Liquid Crystals with Nano and Microparticles, *World Scientific,* **2016**

18   M. Alaasar, M. Prehm, M. Nagaraj, J. K. Vij and C. Tschierske, *Adv. Mater.* **2013**, 25, 2186.

19   a) K. Kishikawa, *Isr. J. Chem*. **2012**, 52, 800; b) M. Hird, *Chem. Soc. Rev.* **2007**, 36, 2070; c) D. Pauluth, K. Tarumi, *J. Mater. Chem.,* **2004**, 14, 1219; d) C. Tschierske, *Top. Curr. Chem.* **2012**, 318, 1; e) M. Spengler, R. Y. Dong, C. A. Michal, M. Pfletscher and M. Giese, *J. Mater. Chem. C.* **2017**, 5, 2235.

20   J. Wen, M. Tian and Q. Chen, *J. Fluorine Chem.* **1994**, 68, 117–120; Y. Xu, Y. Hu, Q. Chen and J. Wen, *J. Mater. Chem*. **1995**, 5, 219–221.

8. Controlling mirror symmetry breaking and charge carrier mobility by fluorination and brominaton of BTBT-derived polycatenar molecules

$BF'_{2356}n$: $m=10$, Y=Br
$F'_{2356}n$: $m=10$, Y=H
$F_{2356}n$: $m=6$, Y=Br
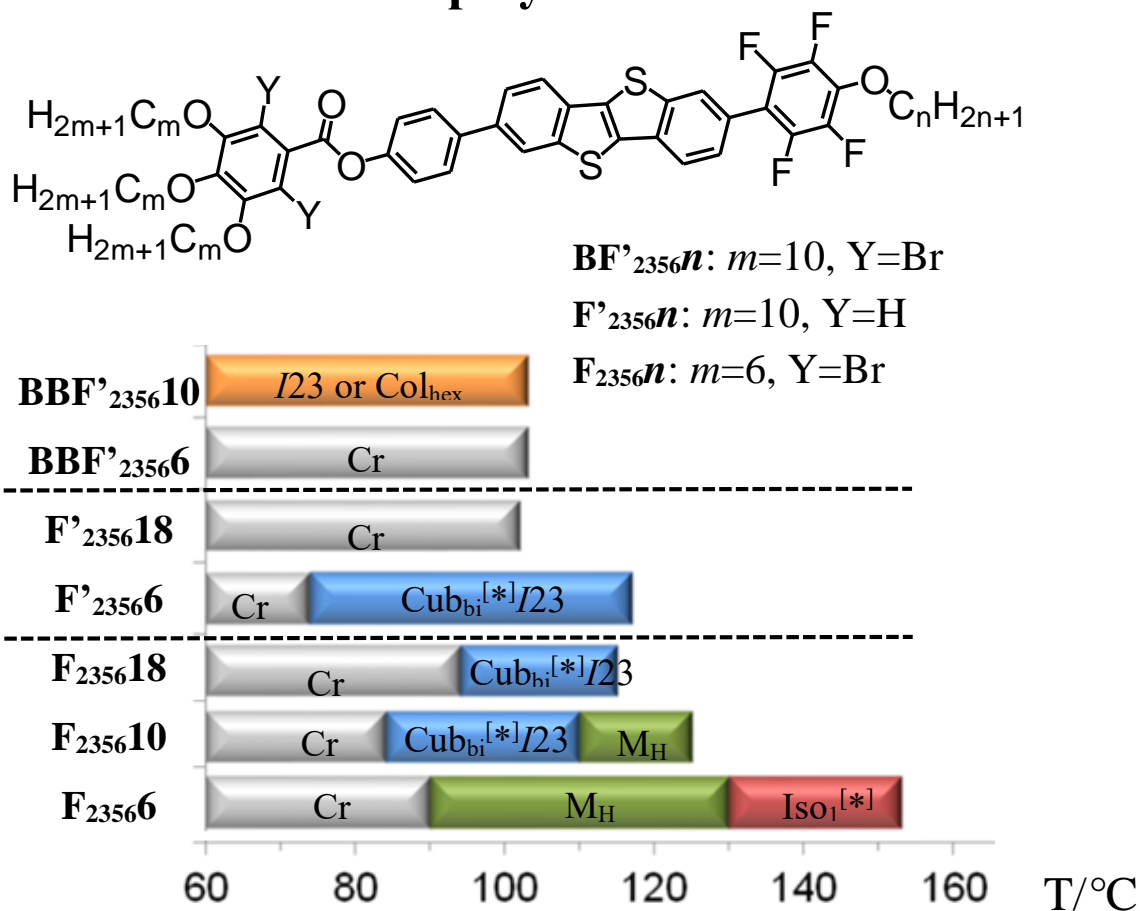
Figure 8.1. Molecular structures, mesophases and transition temperatures of the tetrafluorinated compounds with trihexyloxy chains $F_{2356}n$, tetrafluorinated compounds with tridecyloxy chains $F'_{2356}n$, brominated and tetrafluorinated compounds with tridecyloxy chains $BF'_{2356}n$.

Table 8.1 Transition temperatures and –enthalpies of compounds **Fx and BBFx** on heating and cooling at 10 K/min.

	T/°C [ΔH /kJ·mol^{-1}]
F$_{2356}$4	H: Cr 170 [32.5] SmA 201 [1.1] Iso$_2$ C: Iso$_2$ 198 [1.1] SmA 130 [27.8] Cr
F$_{2356}$6	H: Cr 127 [21.2] Tet 140 [-] Cub$_{bi}$/*Ia*3*d* 151[1.0] Iso* 160 [0.1] Iso$_2$ C: Iso 155 [0.1] Iso*132 [0.5] Tet 90 [13.7] Cr
F$_{2356}$8	H: Cr 126 [25.7] Cub$_{bi}$$^{[*]}$/*I*23 145 [1.6] Iso C: Iso 131 [0.9] Tet 115 [-] Cub$_{bi}$$^{[*]}$/*I*23 90 [1.2] Cr [20.7] Cr
F$_{2356}$10	H: Cr 106 [20.1] Cub$_{bi}$$^{[*]}$/*I*23 141 [1.6] Iso C: Iso 125 [1.3] Tet 117 [-] Cub$_{bi}$$^{[*]}$/*I*23 84 [20.8] Cr
F$_{2356}$14	H: Cr 111 [16.7] Cub$_{bi}$$^{[*]}$/*I*23 139 [1.3] Iso$_2$ C: Iso$_2$ 122 [1.4] Cub$_{bi}$$^{[*]}$/*I*23 88 [18.8] Cr
F$_{2356}$18	H: Cr 105 [17.5] Cub$_{bi}$$^{[*]}$/*I*23 118 [1.2] Iso$_2$ C: Iso$_2$ 115 [1.2] Cub$_{bi}$$^{[*]}$/*I*23 94 [18.6] Cr
F'$_{2356}$6	H: Cr 101 [14.0] Cub$_{bi}$$^{[*]}$/*I*23 132 [1.3] Iso2 C: Iso 117 [1.1] Cub$_{bi}$$^{[*]}$/*I*23 74 [14.8] Cr
F'$_{2356}$18	H: Cr 59 [3.9] Cr$_2$ 101 [0.9] Cr$_3$ 114 [11.1] Iso C: Iso 101 [13.3] Cr
BBF'$_{2356}$6	H: Cr 127 [29.2] Iso C: Iso 103 [26.6] Cr
BBF'$_{2356}$10	H: Cr 106 [3.0] Cub$_{bi}$$^{[*]}$/*I*23 111 [1.3] Iso C: Iso 103 [1.1] Col$_{hex}$ (metastable, Cub$_{bi}$$^{[*]}$/*I*23 appears slowly with slow cooling) >20 Cr
BBF$_{26}$8	H: Cr 88 [12.2] (SmC$_s$ 86 [0.6]) Cub$_{bi}$/*Ia$\overline{3}$d* 90 [-] N 134 [0.2] Iso C: Cooling: Iso 132 [-0.2] N 85 [-0.6] SmC$_s$ >20 Cr

Herein we report series of 2,7-diphenyl BTBT derived tetracatenar compounds having a tapered 3,4,5-trialkoxybenzoat (hexyloxy and decyloxy chains) end and a 4-monoalkylated (*n*) apex at the opposite end, being additionally tetra fluorinated at the apex-ring (compounds **F$_{2356}$*n*,**

F'$_{2356}$n) and the related 2,6-dibromo-3,4,5-trialkoxybenzoates (**BBF'$_{2356}$n**). For the tetrafluorinated compounds **F$_{2356}$n** a homologous series with increasing apex chain length (compounds with hexyloxy chains **F$_{2356}$n** with n = 4-18 and compounds with decyloxy chains **F'$_{2356}$n** with n = 6 and 18) was synthesized and investigated. The effects of bromination and tetrafluorination on the charge carrier mobility is also investigated with selected examples.

8.1 Effect of apex chain length on the self-assembly of the tetrafluorinated compounds F$_{2356}$n
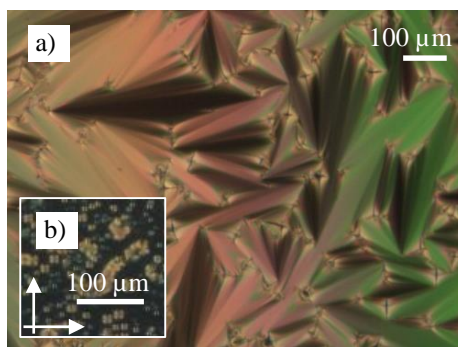
Figure 8.2 SmA phase of **F$_{2356}$4** at 190 ℃ a) planar fan texture and b) isotropic homeotropic texture after shearing with developing oily streaks and Maltese crosses.

The tetrafluorinated compounds **F$_{2356}$n** are of interest due to their relatively low transition temperatures of their mirror symmetry broken Cub$_{bi}$$^{[*]}$/$I$23 phase and, in addition, the alternating donor-acceptor structure of their core, being of interest for use in n-channel and ambipolar charge carrier materials.[1] Therefore, for this series of compounds the effects of chain length on the self-assembly was investigated. The shortest compound **F$_{2356}$4** forms exclusively a SmA phase with a d-value (d = 4.37 nm) which is a bit larger than the molecular length (L_{mol} = 4.2 nm), thus being in line with the partly intercalated bilayer model, as proposed for the SmC$_s$ phase of **F$_{26}$8** (Fig. 8.3).

Remarkably, there is only one (even numbered) homologue showing the Cub$_{bi}$/Ia3d phase (**F$_{2356}$6**) whereas all following homologues have the mirror symmetry broken Cub$_{bi}$/$I$23 phase (Fig. 8.4b). Compared to the series **Hn** (Fig. 8.4a) there is a significant shift of the Ia3d-$I$23 transition to shorter chain lengths. Even this single compound showing the Ia3d phase forms this phase only on cooling in a small temperature range besides the M$_H$ phase. The M$_H$ phases of all

Figure 8.3 CPK space filling models showing the organization of pairs of compound a,b) **F$_{26}$8** and c) **BBF$_{26}$8** in the the SmC$_s$ phases. a) antiparallel organization in the hypothetical monolayer structure; b) partly intercalated double layer organization with the apex chains between the aromatic cores, thus providing a reduced interfacial curvature; c) the bromines reduce the degree of intercalation of the apex chains, thus elongating the pairs.

three compounds **F$_{2356}$n** with n = 6-10 are characterized by the same typical high birefringent mosaic and fern-like texture (see Fig. 8.5) However, only for compounds **F$_{2356}$n** with n = 8 and 10 the M$_H$ phase was sufficiently broad and not distorted by the presence of other competing mesophases that SAXS pattern can be recorded. The X-ray scattering indicates a tetragonal phase with lattice parameters of a = 13.9, c = 8.45 nm for n = 8 and a = 9.94, c = 10.75 nm for n = 10. (Table 8.1). The c-parameter corresponds to about twice the molecular length (L_{mol} = 4.6 and 4.8 nm, respectively). The detailed structure is not yet clear, but it could be related to the tetragonal phase with $I4_1/acd$ symmetry of **F$_3$8** introduced in chapter 7 (Fig. 7.3d). Considering the position of this phase at the transition from SmA via $Ia3d$ to $I23$, a square mesh phase (Fig. 8.5d) known to appear at the lamellar - Cub$_{bi}$ transition in some lyotropic systems appears to be another likely

model of the M_H phase formed by compounds $\mathbf{F_{2356}n}$. The parameter c increases with growing chain length n as expected, whereas the parameter a decreases, leading to very different lattice parameters for these two homologues compounds. This opposite development of a and c with growing chain length is very unusual and provides a key for the understanding of the phase structure of the M_H phase. Because the intermolecular helical twist increases with growing n the helical pitch becomes shorter. The twist along each segment between the junctions of the square nets should be 180°, thus allowing an almost parallel alignment of all rods upon approaching the junctions. The twist between adjacent rafts of molecules $\mathbf{F_{2356}n}$ is calculated to be 5.8° for $n = 8$ and 7.8° for $n = 10$, both are in the range usually observed for the Cub_{bi} phases of polycatenar molecules (5-10°). An increased twist reduces the helical pitch and thus the distance between the nodes, and this leads to the experimentally observed shrinkage of the lattice by chain elongation. The number of molecules in the rafts stacked along the columns is between about 8 ($n = 10$) and 9 ($n = 8$). Though these values are about twice the numbers found in the Cub_{bi} phases, it still allows an almost circular column cross section ($9 \times 0.45 = 4.05$ nm, $L_{mol} = 4.6$ nm).

It is noted, that the M_H phase occurs in the same phase sequence and with the same birefringence and optical texture as the so-called S4 phase, already found long ago for the 4'-alkyloxy-3'-nitrobiphenyl carboxylic acids as a metastable phase at the transition from SmA to Cub_{bi} on cooling[2] and being ubiquitous in polycatenar systems, but has not yet been solved. A crystalline body centered tetragonal based on a square mesh was also reported for rod-coil molecules by Lee et al[2]

Remarkably, the mirror symmetry broken liquid phase ($Iso_1^{[*]}$) can be observed for only one of the even numbered homologues and the appearance of the $Iso_1^{[*]}$ phase coincides with the transition SmA $\rightarrow Ia3d \rightarrow I23$. It is completely removed as soon as the mirror symmetry broken $I23$ phase emerges. Based on the position of the $Iso_1^{[*]}$ phase adjacent to the achiral $Ia3d$ phase we propose a SmQ-like local structure in this network liquid as already discussed above.

Figure 8.4 shows the structure with labels:

Heating   [X = H]   Cooling

a) **H12**, **H11**, **H10**, **H9**, **H8**

b) [X = F]   **F2356 18**, **F2356 14**, **F2356 10**, **F2356 8**, **F2356 6**, **F2356 4**

Figure 8.4 Comparison of mesophases and transition temperatures of the tetrafluorinated compounds **F2356n** with the nonfluorinated analogs **Hn**. [3]

Figure 8.5 Textures of M_H phase for (a,b) **F2356 8** and (c) **F2356 10**; d) model of the mesh phase.

Table 8.2 Structural data of the 3D mesophases of the investigated tetrafluorinated compounds. [4]

Comp.	m	n	X	Y	Phase	$T/$ °C	a/nm	$V_{cell}/$ nm³	$V_{mol}/$ nm³	$n_{cel}l$	d_{net}	L_{net}	n_{raft}	$\Phi/°$
F$_{2356}$6	6	6	F	H	$Ia3d$	140	8.94	715	1.282	498	3.87	75.86	2.95	10.02
F$_{2356}$8	6	8	F	H	$I23$	145	13.32	2363	1.331	1585	-	275.46	2.59	10.48
F$_{2356}$10	6	12	F	H	$I23$	120	13.53	2477	1.381	1602	-	279.80	2.58	10.32
F$_{2356}$14	6	14	F	H	$I23$	125	14.03	2762	1.480	1666	-	290.14	2.58	9.95
F$_{2356}$18	6	18	F	H	$I23$	110	14.66	3151	1.579	1782	-	303.17	2.64	9.53
F'$_{2356}$6	10	6	F	H	$I23$	120	14.73	3196	1.579	1807	-	304.62	2.67	9.48
F'$_{2356}$10	10	10	F	Br	$I23$	108	14.76	3216	1.731	1659	-	305.24	2.45	9.46
BB9	6	9	H	Br	$I23$	170	14.72	3190	1.385	2057	-	304.41	3.04	9.49
BB11	6	11	H	Br	$I23$	210	14.69	3170	1.434	1974	-	303.79	2.92	9.51

8.2 Effects of substitution at the tapered end

Increasing the length of the alkyl chains at the tapered end from $m = 6$ to $m = 10$ (compounds **F'$_{2356}$$n$**) removes the $Ia3d$, M- and Iso$_1$[*] phases and replaces them by the Cub$_{bi}$[*]/$I23$ phase. The LC phases are destabilized by chain elongation and therefore only for one of the investigated compounds with m = 10 the $I23$ phase can be observed (Table 8.3). Additional 2,6-dibromination of the tetrafluorinated compound at the tapered end (Comp. **BBF'$_{2356}$$n$**) further reduces the phase transition temperatures, but retains the $I23$ phase type for n = 10. The WAXS pattern of nonfluorinated (**BB9**) and the related tetrafluorinated compound (**BBF'$_{2356}$10**) show two diffuse maxima, at 0.46 nm and 0.35 nm for **BB9** and at 0.44 and 0.34 nm for **BBF'$_{2356}$10** (Fig. 8.6) This indicates face-to-face $\pi-\pi$ stacking in both cases. However, the intensity of the second maxima for **BBF'$_{2356}$10** is much smaller than for **BB9**. It appears that core fluorination reduces the contribution of $\pi-\pi$ stacking (Fig. 8.6).

Table 8.3 Phase transitions of the fluorinated and non-fluorinated polycatenars depending on 2,6-bromination at the tapered end.
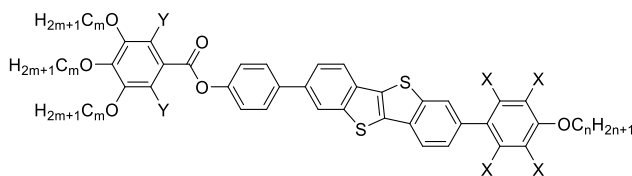
Compd.	m	n	X	Y	Phase transitions $T/$ °C [ΔH/kJ mol^{-1}]	$a_{cub}/$ nm
F'$_{2356}$6	10	6	F	H	heating: Cr 101[14.0] Cub$_{bi}^{[*]}/I23$ 132 [1.3] Iso cooling: Iso 117[1.1] Cub$_{bi}^{[*]}/I23$ 74 [14.8] Cr	14.73
F'$_{2356}$18	10	18	F	H	heating: Cr 59 [3.9] Cr$_2$ 101 [0.9] Cr$_3$ 114 [11.1] Iso cooling: Iso 101 [13.3] Cr	-
BBF'$_{2356}$6	10	6	F	Br	heating: Cr 127 [29.2] Iso cooling: Iso 117 [26.6] Cr	**-**
BBF'$_{2356}$10	10	10	F	Br	heating: Cr 106 [3.0] Cub$_{bi}^{[*]}/I23$ 111 [1.3] Iso cooling: Iso 103 [1.1] Col$_{hex}$→Cub$_{bi}/I23$ <20 Cr	14.76
BB10	6	10	H	Br	heating: Cr 115 [9.4] Cub$_{bi}^{[*]}/I23$ 229 [2.1] Iso cooling: Iso 217 [1.8] Col$_{hex}$ 205 [0.5] Cub$_{bi}^{[*]}/I23$ <20 Cr	-

The 2,6-difluorinated compound **BBF$_{26}$8** has the same N-SmC$_s$ phase sequence as found for the related nonbrominated compound **F$_{26}$8**, but at about 60 K lower temperatures (Tab. 8.3). Even the chiral domain texture in the homeotropic aligned SmC$_s$ phase is observed (Fig. 7.6), confirming that the 2,6-difluorination pattern at the apex supports the helical twist in the SmC$_s$ phases. There is an unusually high tilt of the molecules of 45° in the N$_{cybC}$ phase of **BBF$_{26}$8** and even 55° in the SmC$_s$ phase, determined by X-ray scattering with magnetically aligned samples. This high tilt leads to much smaller d-value of the SAXS compared to **F$_{26}$8**. In contrast to the cubic phases of the 2,6-dibrominated compounds **BBn**, only one broad WAXS with a maximum at $d =$ 0.43 nm can be found in the N and SmC$_s$ phases of **BBF$_{26}$8.** Interestingly, an achiral cubic phase develops slowly in the SmC$_s$ range of compound **BBF$_{26}$8** as thermodynamically stable phase. However, the transition to the cubic phase is very slow. Remarkably, on heating the Cub$_{bi}$ phase of **BBF$_{26}$8** is retained throughout the SmC-N phase transition up to 90 °C even coexisting with the nematic phase in a certain temperature range (see Tab. 8.4).
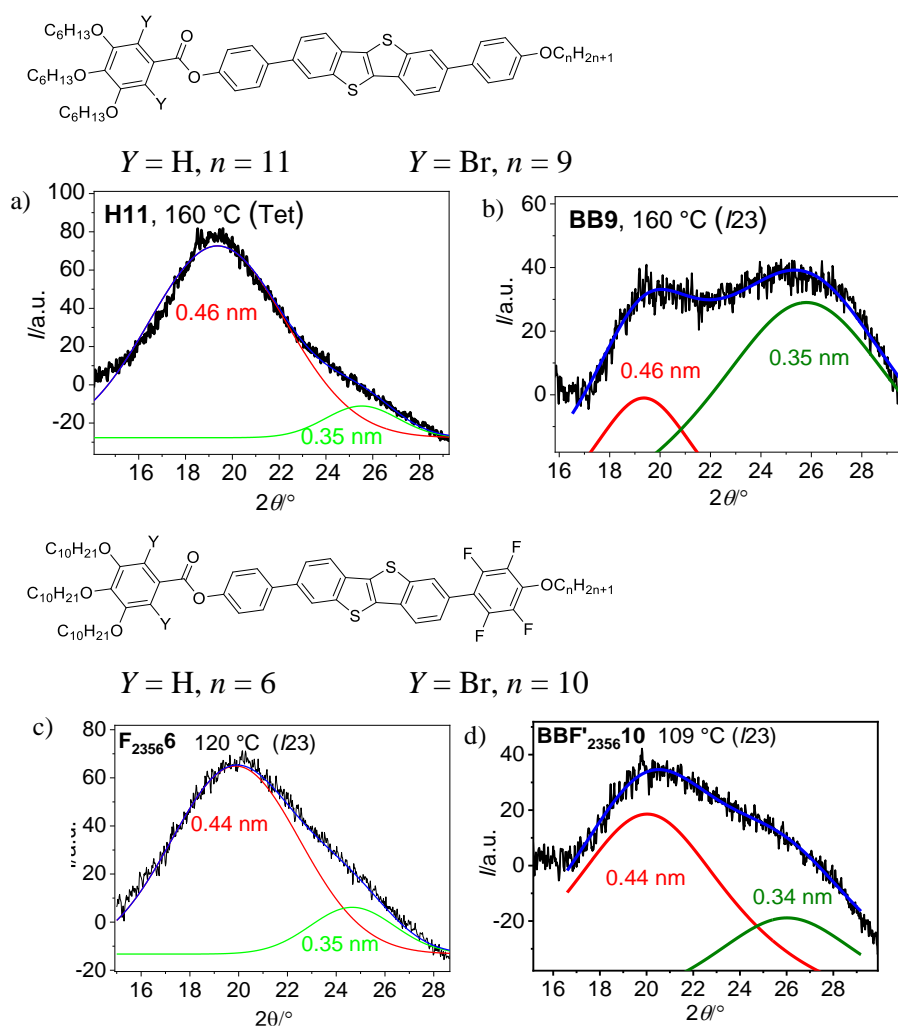
Figure 8.6 Effects of core fluorination at the apex and core bromination at the tapered end on the shape of the WAXS patterns.

The inside directed 2,6-difluorination of the apex ($F_{26}8$) is the only substitution pattern which removes the network phases and leads to compounds with highly tilted nematic and smectic phases, whereas additional 2,6-dibromination of the fluorinated polycatenars at the opposite tapered end (2,6-dibromo-3,4,5-trialkoxybenzoates) ($BBF_{26}8$) retains the cubic network phases and shifts the phase transitions to lower temperatures (Tab. 8.4).

Table 8.4 Phase transitions of the difluorinated polycatenars depending on 2,6-bromination at the tapered end.

Comp.	Y	Phase transitions (T/°C, ΔH/kJ mol⁻¹)	d_{SmC}/nm tilt_{exp} /°	d_N/nm tilt /°	L/nm tilt_{calc}/°
F₂₆8	H	H: Cr₁ 106 [28.2] Cr₂ 116 [17.7] SmC_s 143 [0.2] N 192 [0.6] Iso C: Iso 190 [-0.9] N 140 [-0.2] SmC_s 68 [-21.6] Cr	4.4 30-40	4.1 n.d.	5.2 32
BBF₂₆8	Br	H: Cr 88 [12.2] (SmC_s 86 [0.6]) Cub_{bi}/Ia3d 90 [-] N 134 [0.2] Iso C: Iso 132 [-0.2] N 85 [-0.6] SmC_s >20 Cr	3.3 55	3.6 45	5.9 56

8.3 Charge carrier mobility

The charge carrier mobility in the Cub_{bi}[*]/I23 phases was measured using the time of flight (TOF) method for the dibrominated compound **BB9** and the tetrafluorinated compound **F₂₃₅₆14** and is compare with the previously investigated monobrominated and non-fluorinated compound **B12** (Fig. 8.7). The hole mobility of **BB9** is almost two times lower than measured for the monobrominated compound **B12**. Moreover, the fluorinated compound **F₂₃₅₆14** appears to have an even more reduced mobility of holes than the dibrominated derivative. This is a bit surprising as the face-to-face packing of the aromatics proposed for the dibrominated compound [3] should be favorable for charge mobility. But as deduced from the WAXS pattern the scattering attributed to the π-stacking organization is diffuse (Fig. 8.6d), meaning that there is still significant disorder and the face-to-face stacking is only short range. Moreover, the bulky bromines might sterically distort the core packing; a similar effect of the four fluorines could be responsible for the reduced charge mobility of **F₂₃₅₆14**. Another explanation could be a preferred arrangement of the polyhalogenated molecules with the π-faces parallel to the network direction, which reduces the capability of charge transportation along the networks. The relatively small number of only two to three molecules organized in each raft of the networks could support this explanation. Another

source of distortion might result from the increased helical twist provided by these polyhalogenated compounds if compared to the non- and mono-halogenated. Thus, further work is required to understand and improve the charge carrier mobility in the soft helical network phases.
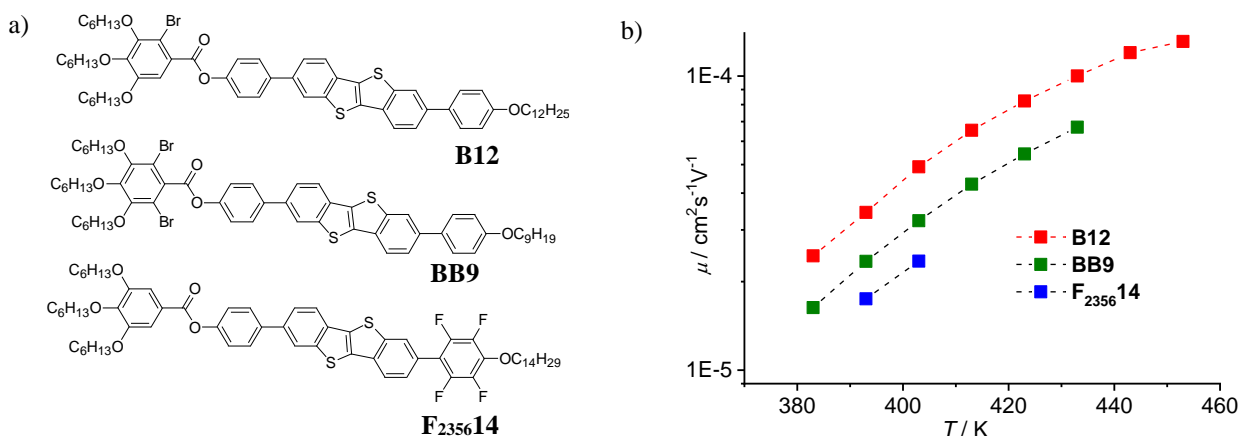
Figure 8.7 a) Molecular struecutres of **B12**[5], **BB9**[3] and **F$_{2356}$14;** b) dependence of the charge carrier mobility on temperature as measured on cooling for the Cub$_{bi}$[*]/$I$23 phases of compounds **B12**, **BB9** and **F$_{2356}$14**.

Furthermore, since **BBF'$_{2356}$10** forms both Col$_{hex}$ and Cub$_{bi}$[*]/$I$23 phase at the same temperature depending on the cooling rate, the charge carrier mobility of the two LC phase can be compared. For the measurement of the Col$_{hex}$ phase, the cooling rate was higher than 20K/min, and heating and cooling were repeated for each measurement to induce only Col$_{hex}$ phase. For the measurement of Cub$_{bi}$[*]/$I$23 phase, cooling rate was lower than 5K/min to induce only the Cub$_{bi}$[*]/$I$23 phase. As expected, the charge carrier mobility of columnar phase is 2-3 times higher than the Cub$_{bi}$[*]/$I$23 phase. It is because the pathway for the electrons for columnar phase is significant shorter than for the network phase. As the Fig. 8.8 shows, time of flight of holes for the Cub$_{bi}$[*]/$I$23 phase is longer and the dissipation of electrons is less than in the columnar phase. However the dissipation in the Cub$_{bi}$[*]/$I$23 phase is not as good as recorded for compound **B12**.[5]
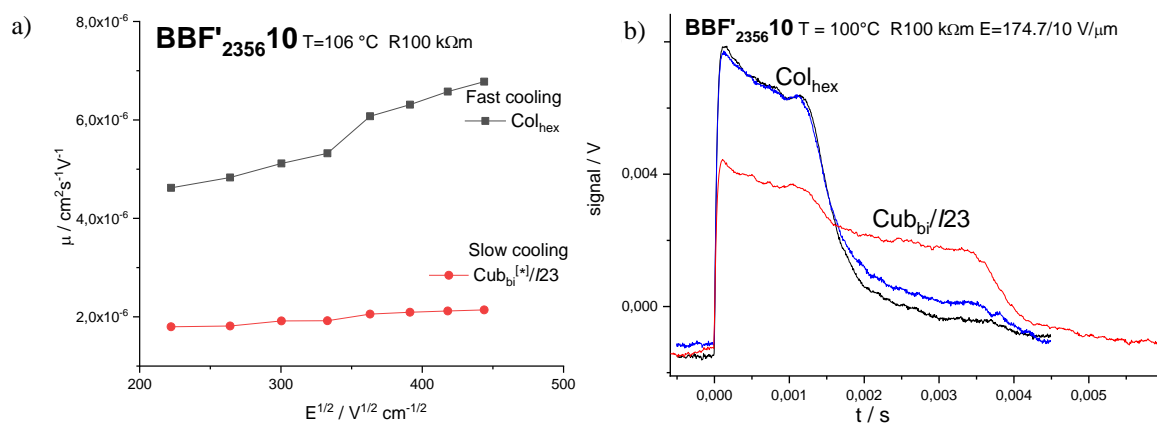
Figure 8.8 a) Field dependence of the charge carrier mobility on LC phases; $Cub_{bi}^{[*]}/I23$ (slow cooling) and Col_{hex} phase (fast cooling); and b) ToF transients of holes of $Cub_{bi}^{[*]}/I23$ and Col_{hex} phase for **BBF'$_{2356}$10**.

8.4. Summary and conclusion

The tetrafluorinated compounds have a significantly lower mesophase stability than the related non-fluorinated compounds. They have a strong tendency to form the mirror symmetry broken $I23$ phase and the highly birefringent mesophase M_H instead of the double gyroid $Ia3d$ phase. Combination of apex tetrafluorination with bromination at the tapered end retains the $I23$ phase as long as the melting and crystallization temperatures are sufficiently low. There is a strong effect of bromination on the orientation of the faces of the π-conjugated rods for both cases, the tetrafluorinated as well as the non-fluorinated compounds. However, this π-stacking is obviously only short range and does not increase the charge carrier mobility. Even a reduction of the charge mobility is also observed for the investigated tetrafluorinated compound. It is speculated that a certain tendency of these polyhalogenated compounds to be preferably organized with their π-faces parallel to the network direction could be an explanation of this effect.

References

1   M. L. Tang, Z. Bao, Chem. Mater. 2011, 23, 446-455; H. Usta, A. Facchetti, T. J. Marks, *Acc. Chem. Res.* **2011**, 44, 501.

2   a) J. H. Ryu, N. K. Oh, W. C. Zin and M. Lee *J. Am. Chem. Soc.* **2004**, 126, 3551; b) N. K. Oh, W. C. Zin, J. H. Im, J. H. Ryub and M. Lee, *Chem. Commun.* **2004**, 1092.

3   O. Kwon, X. Cai, A. Saeed, F. Liu, S. Poppe and C. Tschierske, *Chem. Comm.* **2021** 10.1039/d1cc01922h.

4   F. Liu, Xi'an Jiaotong University, P. R. China 710049, unpublished results

5   O. Kwon, X. Cai, W. Qu, F. Liu, J. Szydłowska, E. Gorecka, M. J. Han, D. K. Yoon, S. Poppe and C. Tschierske, *Adv. Func. Mater.* **2021**, 202102271.

9. Short-core tetracatenars with wide ranges of the chiral liquid and frustration at the $Ia\bar{3}d - I23$ cross-over
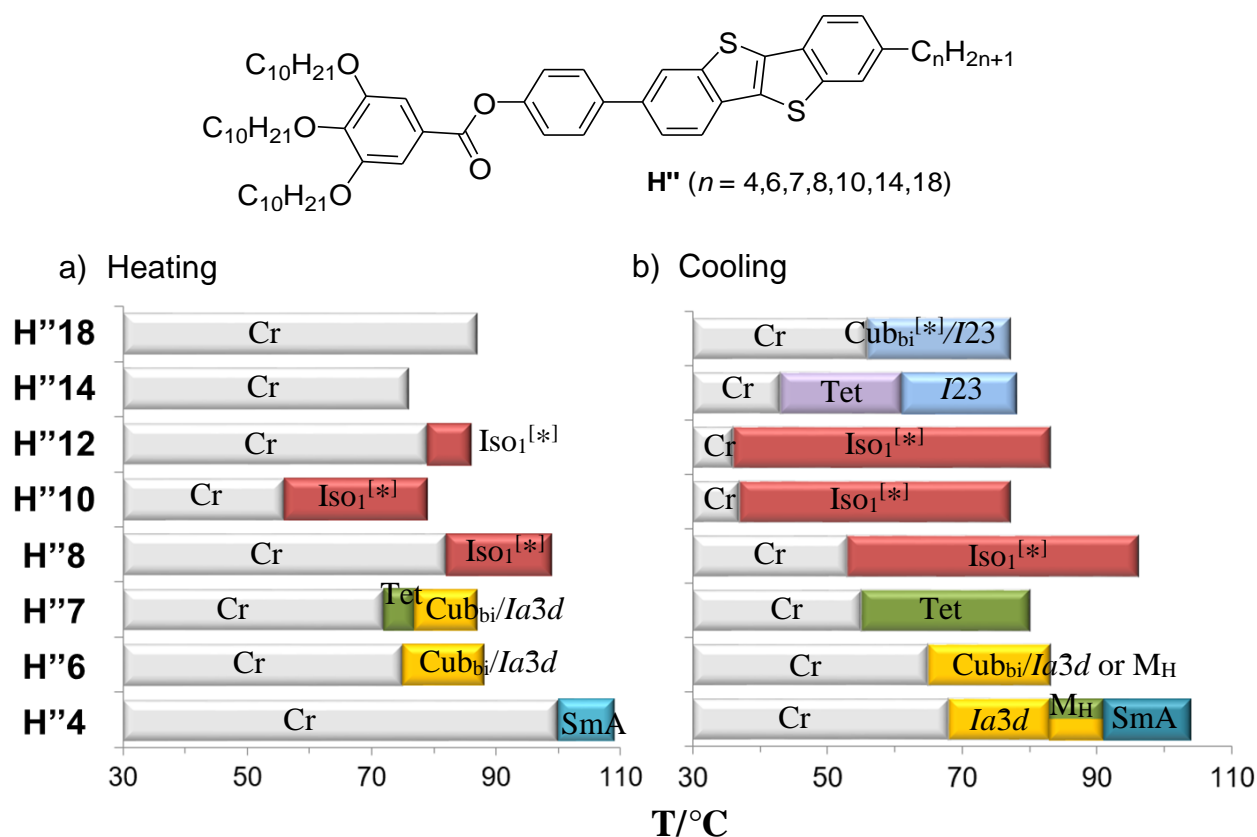
Figure 9.1 Structure and transition temperatures of the 7-alkyl-substituted BTBTs **H"n** as observed a) on first heating and b) on the following cooling (rate 10 K min^{-1}).

Two series of compounds 7-alkylsubstituted BTBTs were investigated. At first the series **H"n** with three decyloxy chains at the tapered end will be discussed and then series **H'n** with three hexyloxy chains.

Table 9.1 Phase transition temperatures (T/°C) and associated enthalpies (ΔH/kJ mol^{-1}) of compounds **H''n.**

	Phase Transitions [ΔH/kJ mol^{-1}]
H''4	H: Cr 100 [53.4] SmA 109 [0.4] Iso
	C: Iso 107 [0.4] SmA 94 [-] M_H + Cub$_{bi}$/*Ia*3*d* 86 [0.9] 83 Cub$_{bi}$/*Ia*3*d* 68 [46.4] Cr
H''6	H: Cr 75 [31.1] Cub$_{bi}$/*Ia*3*d* 88 [1.0] Iso$_2$
	C: Iso$_2$ 83 [-] Cub$_{bi}$/*Ia*3*d* or M_H 65 [30.8] Cr
H''7	H: Cr 72 [31.1] Tet/P4$_1$2$_1$2 77 [0.3] Cub$_{bi}$/*Ia*3*d* 87 [0.5] Iso$_2$
	C Iso$_2$ 80 [-] Tet/P4$_1$2$_1$2 55 [32.6] Cr
H''8	H: Cr$_1$ 69 [31.2] Cr$_2$ 82 [-] Iso$_1$[*] 99 [0.7] Iso
	C: Iso 96 [0.4] Iso$_1$[*] 53 [33.4] Cr
H''10	H: Cr 56 [29.4] Iso$_1$[*] 79 [0.17] Iso$_2$
	Cooling: Iso$_2$ 77 [0.26] Iso$_1$[*] 37 [30.1] Cr
H''12	H: Cr 79 [43.3] Iso$_1$[*] 86 [0.08] Iso$_2$
	Cooling: Iso$_2$ 83 [0.23] Iso$_1$[*] 36 [15.2] Cr
H''14	Heating: Cr 76 [60.1] Iso
	Cooling: Iso 78 [-] Cub$_{bi}$[*]/*I*23 61 [-] Tet/*P*42$_1$2 43 [12.7] Cr
H''18	Heating: Cr$_1$ 74 [21.8] Cr$_2$ 87 [41.0] Iso
	Cooling: Iso 77 [1.0] Cub$_{bi}$[*]/*I*23 56 [35.2] Cr

9.1 Compounds H''n

9.1.1 Transition from SmA to Cub_bi/*Ia3d*
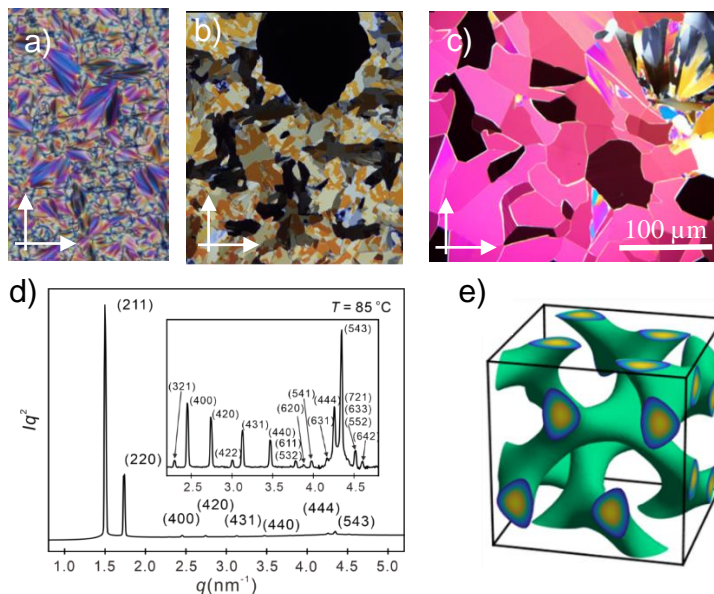
Figure 9.2 Investigation of compounds **H''4** and **H''6:** a) Textures of the SmA phase at 110 °C and b) the M_H and Cub_bi phases of **H''4** at 90 °C; c) M_H phase of **H''6** at 80°C, d) SAXS pattern and e) reconstructed ED map of the Cub/*Ia3d* phase of **H''6**. [1]

The compounds **H''n** have one benzene ring less when it is compared with the series **Hn**. Moreover, the apex chain is a *n*-alkyl chain replacing the alkoxy chain. Both structural variations lead to a significant reduction of all transition temperatures. Compound **H''4** with the shortest chain forms a lamellar phase at the transition from the isotropic liquid at 107 °C which is stable to 94 °C when it transforms to the next mesophase(s). The fan-like optical texture with dark extinctions parallel to the directions of polarizer and analyzer indicates a uniaxial smectic phase with non-tilted organization of the molecules in the layers (SmA phase), having a layer distance of $d = 4.38$ nm at 100 °C as determined by SAXS. The measured d-value is similar to the d-value of the SmA phase of compound **F_{2356}4** with a much larger core, but a bit shorter than the molecular length $L = 4.0$ nm (determined with space filling models, see Fig. 9.7), being in agreement with an antiparallel organization of the molecules with intercalation of single alkyl chain between parts of the aromatic cores. This intercalated structure allows a reduction of the interfacial curvature which supports the formation of a lamellar phase, though the degree of intercalation is reduced if compared to compound **F_{2356}4**.

Upon chain elongation or on further cooling the segregation of chains and cores sets in, which leads to an increase of the interface curvature which then gives rise to transitions to other mesophases with curved interfaces. Upon cooling compound **H''4** the SmA phase is replaced by a highly viscous and birefringent mesophase with mosaic texture, from which immediately after its formation the optically isotropic Cub_{bi} phase grows slowly. This indicates that a non-cubic 3D phase is formed first, which is then replaced by the thermodynamically more stable optically isotropic Cub_{bi} phase (dark areas in Fig. 9.2b). On heating from the cubic phase the transition to the SmA phase takes place at 100°C directly, without intermediate formation of an additional 3D phase. The SAXS pattern indicates a cubic lattice with $Ia3d$ space group and a_{cub} = 10.12 nm at 84 °C. This space group is in line with the optical inactivity of this cubic phase, appearing uniformly dark between exactly 90 ° crossed polarizers as well as after uncrossing the polarizers by a small angle in either direction. SAXS patterns of the highly birefringent mesophase (M_H) could not be recorded due to its metastability. However, it is likely that the metastable phase occurring at the Iso-Cub_{bi} transition is the same kind of AB type square mesh phase as proposed for similar compounds **F$_{2356}$n**.[2]

The next homologue **H''6** shows no smectic phase; in this case the metastable M_H phase and the Cub_{bi} phase form directly from the isotropic liquid. Fig. 9.2e shows the electron density map of the $Ia3d$ phase of **H''6** as example, indicating the double gyroid structure (yellow/green) in the continuum of the alkyl chains.

9.1.2 Transition from Cub$_{bi}$/$Ia3d$ to Iso$_1$[*] – the tetragonal $P4_12_12$ phase

The phase sequence of **H''7** is slightly different. For this compound the $Cub_{bi}Ia3d$ phase forms directly upon cooling without previous formation of the M_H phase and on further cooling the Cub_{bi} phase assumes a weakly birefringent mosaic like texture. The XRD pattern of this birefringent mesophase can be indexed to a simple tetragonal lattice with $P4_12_12$ space group and the lattice parameters a = 8.42 nm and c = 18.29 nm at 80 °C (Fig 9.3a, Tab. 9.2). Based on the positions and intensities of the diffraction peaks, an electron density map was reconstructed (Fig. 9.3c). This ED map indicates a network structure formed by 90° connected three-way junctions, very similar to that found for the $I4_122$ lattice of the SmQ phase.[3] However, in this case it is formed

only by a single network and not by two interpenetrating as in SmQ. Moreover, only the cross sectional shape of the vertical columns (along the *c*-direction) is circular, whereas it is elliptical for the horizontal (at the *a/b*-plane) (Fig. 9.3d,e). This suggest that only the vertical columns are helical, whereas the horizontal are formed by untwisted ribbons. The number of intracolumnar strata with a distance of 0.45 nm is about 18.7 along each horizontal rod connecting two junctions. The length of the vertical segments between two junctions is about 4.56 nm (*c*/4) and the number of molecular strata is again 10. Because the twist between the junctions is only 90°, the average rotation angle between the strata is about 9° similar to the values found in the cubic networks. The total number of molecules in one unit cell is calculated to be 789 (see Tab. 9.2) and therefore, each of the molecular strata consists of about 2.5 molecules (789 /(32x10)). This represents a new type of tetragonal mesophase representing networks combining helical and non-twisted columns.
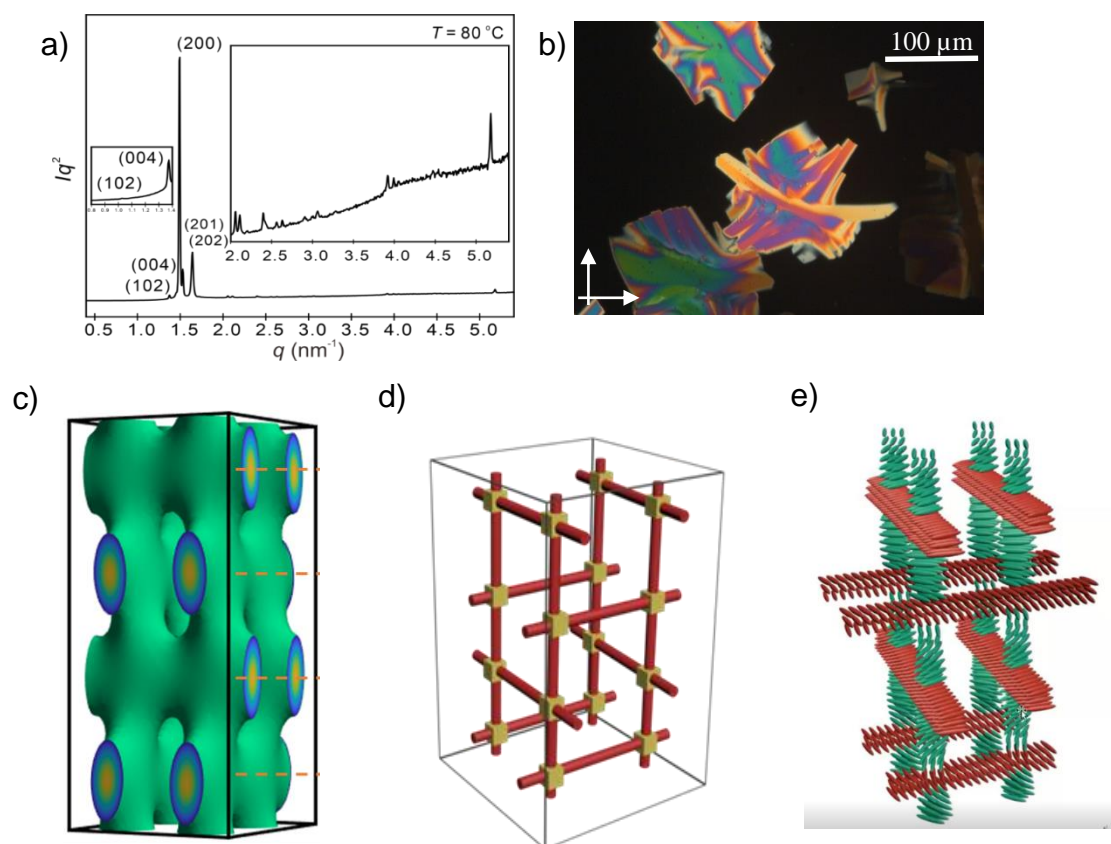
Figure 9.3 Characterization of the tetragonal phase with space group $P4_12_12$ of **H''7;** a) SAXS patterns at 80 °C; b) growing texture at 78 °C; c) reconstructed ED map and structure based on SAXS result; d,e) The optimized model of the tetragonal phase (green: vertical segments, red: horizontal layers).[1]

Table 9.2 Structural data of the 3D mesophases of compounds **H''n**.

Comp.	Phase	T/°C	a/nm	V_{cell}/ nm^3	V_{mol}/ nm^3	n_{cell}	d_{net}/ nm	L_{net}/ nm	n_{raft}	Φ/°
H''4	Cub$_{bi}$/$Ia3d$	84	10.12	1036.4	1.3939	664	4.38	85.87	3.4	8.86
H''6	Cub$_{bi}$/$Ia3d$	85	10.26	1080.0	1.4435	668	4.44	212.1	1.4	13.6
H''7	Cub$_{bi}$/$Ia3d$	85	10.27	1083.2	1.4683	659	4.45	212.3	1.4	13.6
	Tet/$P4_12_12$	80	8.42,	1296.7	1.4683	789				
H''14	Cub$_{bi}$[*]/$I2$	70	15.75	3907.0	1.6419	2125	-	325.7	2.9	8.87
	Tet/$P42_12$	56	13.23,	2358.7	1.6419	1283				
H''18	Cub$_{bi}$[*]/$I2$	80	15.8	3944.3	1.7411	2023	-	326.7	2.7	8.84

9.1.3 Iso$_1$[*] phase

Further elongation of alkyl chains leads to the complete loss of the Cub$_{bi}$ as well as the Tet phases for compounds **H''8** and **H''10**. These 3D mesophases are replaced by a relatively broad region of the mirror symmetry broken isotropic liquid phase, formed on heating as well as on cooling and showing a conglomerate of chiral domains (Iso$_1$[*]). For **H''10** the fluid Iso$_1$[*] phase is observed on cooling from 78 °C down to 37 °C (see Fig. 9.5a and Tab. 9.1) when crystallization sets in. This is the lowest temperature ever observed for an isotropic liquid, with spontaneous segregation into two enantiomorphic liquids. The DSC curve shows that the transition to the Iso$_1$[*] phase is via an achiral Iso$_1$ phase as previous found for the benzil-based polycatenars **BD** (see Fig. 1.8).[4] A broad peak is observed at the transition from Iso$_1$[*] to Iso$_1$ and from Iso$_1$ to the Iso phase. Fig. 9.5b shows two different textures of Iso$_1$[*] phases of **H''8** and **H''10**. The left one of typical fluid chiral domains (**H''8**), in contrast, the right one shows only single domain with uniform handedness (**H''10**). Here the chirality is indicated by a different color depending on the direction of the analyzer due to the wavelength dependence of optical rotation (ORD).Which type (conglomerate or uniform chirality) is formed depends on the condition and it is highly sensitive to cooling rate, thermal history and the presence of internal and external sources of chirality. It was shown that the Iso$_1$[*] phases show a huge chirality amplification power[5] and tiny traces of chirality can fix the sense of optical rotation. Chiral information can also be stored at the surfaces which can then act as seed for chiral domains. If seed formation is fast compared to their growth

the typical conglomerate texture is observed, if seed formation is slow, but their growth is fast, then chiral domains with a uniform sense of chirality can cover the complete area of view. For instance, upon cooling after staying longer time in the Iso_1 region the typical comglomerate texture of the $Iso_1^{[*]}$ phase is observed.

The $Iso - Iso_1 - Iso_1^{[*]}$ transition of compound **H''10** was investigated in more detail by SAXS and CD investigations. In the SAXS there is a single relatively broad peak. Its d-value continuously increases upon cooling from $d = 3.4$ nm at 130 °C in the Iso phase to 4.3 nm at 60 °C in the $Iso_1^{[*]}$ phase. More importantly, the line width (FWHM, see Fig. 9.5e) increases from 0.50 in the Iso phase at 130 °C to 1.56° in the $Iso_1^{[*]}$ phase at 60 °C. This indicates that there are clusters in the liquid state (Iso) which continuously grow in the Iso, Iso_1 and $Iso_1^{[*]}$ ranges. The DSC curves (Fig. 9.5a) indicate two broad features. One is in the achiral iso range (Iso – Iso_1 transition) at 83 °C and the second corresponds to the onset of mirror symmetry breaking at 77 °C upon cooling.
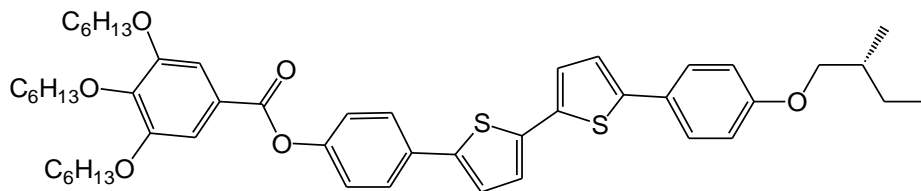
Figure 9.4 The molecular structure of the chiral dopant ((*S*)-**B6/MB**).

For CD measurement 0.1 wt% of chiral dopant ((*S*)-**B6/MB**[6], see Fig. 9.4) was mixed in **H''10** to induce uniform heix sense in the measurement. Because the beam diameter of the CD measurement is much larger than the chiral domains of $Iso_1^{[*]}$ phase of **H''10**, the CD signal is not observed without a chiral dopant. In the circular dichroism (CD) spectra there is a single maximum at 379 nm and it appear below 83 °C at the Iso → Iso_1 transition. The intensity of CD increases upon cooling and the area of the curves increases from 30 a.u. at 83 °C to 2933 a.u. at 65 °C (Fig. 9.5h) in the fully developed $Iso_1^{[*]}$ phase. Below 65 °C the area does not further increase upon cooling. The CD result confirms the presence of optical activity in the $Iso_1^{[*]}$ phases. The continuous growth of the CD signal and its reproducibility in repeated measurements indicate that the $Iso_1^{[*]}$ phase is likely to form a uniform chiral phase in this case (compare Fig. 9.5b, right). It indicates that the chirality emerges at the transition from Iso to Iso_1, though it cannot be detected optically in the Iso_1 range. It appears that chirality develops during the growth of the domains and their connection to a network in the Iso_1 range. This means that already in Iso_1 there is an induction
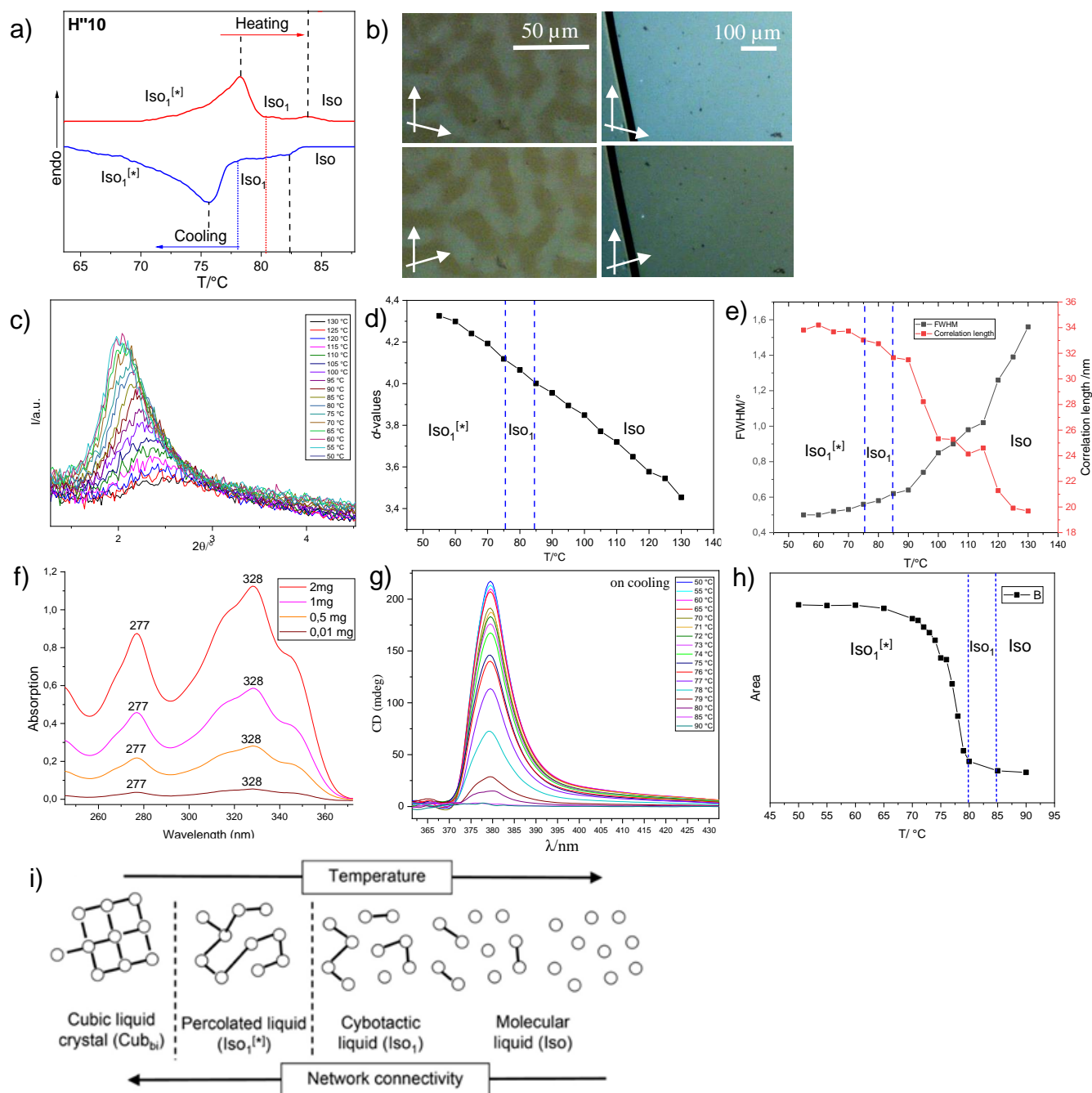
Figure 9.5 Characterization of the $Iso_1^{[*]}$ phase of **H''10;** a) DSC heating and cooling scans; b) textures of the $Iso_1^{[*]}$ phase between slightly uncrossed polarizers, showing the chiral domains from **H''8** (left) and **H''10** (right); c) T-dependent SAXS patterns; d) T-dependent d-values; e) changes of correlation length and FWMH with temperature; f) the UV spectra of **H''4** with different concentration (2, 1, 0.5 and 0.01 mg in 10ml of $CHCl_3$); g) T-dependaet CD spectra of a bulk film with 0.1 wt% of chiral dopant; h) integration of peak area from CD spectra; i) schematic sketch of transition from Iso to Cub_{bi} phase: Iso-cybotactic liquid (Iso_1)-percolated liquid ($Iso_1^{[*]}$)-Cub_{bi} by increasing connecting of the networks.

of helicity by the dopant, though no spontaneous chirality can be observed and at the transition to $Iso_1^{[*]}$ the macroscopic chirality synchronization of the bulk sample sets in, there is a jump to much higher ranges of the CD signal.

The CD can in principle result from the exciton-coupling between the twisted π-conjugated cores along the networks. But in this case a bisignated signal with a change of the sign of the CD signal at the maximum of the UV-Vis absorption wave length would be expected. However, for **H''10** only a single CD signal is formed at 379 nm, which is separated from the UV-absorption maximum of the Ph-BTBT unit at 328 nm by about 50 nm and no CD signal is associated with the UV absorption at 277 nm attributed to the carboxylate unit. The different position might be due to the different conditions, the CD was investigated in the bulk liquid state and a dilute solution was investigated by UV-vis. More surprising is the complete absence of the second half of the bisignated signal. In recent simulation work[7] it was shown that the helical organization of non-twisted ethlyene molecules give rise to the typical bisignated CD signal, whereas the bisignated CD signal is replaced by a monosignated CD signal if helically deformed ethlyenes are organized in a helical arrangement, meaning that the CD signal is in this case due to the helical twist of the π – system itself. This would mean that the CD-signal of **H''10** in the $Iso_1^{[*]}$ phase mainly results from the helical twist induced in the π – system of the individual molecules forming the helical aggregates. This supports the hypothesis of a cooperative effect allowing the synchronization of helical molecular conformations the confined geometry of the helical aggregates.[8]

9.1.4 Transition from $Iso_1^{[*]}$ to Cub/$I23$ phase – Tet $P42_12$ phase

Compounds **H''14** and **H''18** with the longest alkyl chains do not show any LC phases on heating, but they form different LC mesophases upon cooling. Both **H''14** and **H''18** forms a Cub_{bi} phase with $I23$ space group ($Cub_{bi}^{[*]}/I23$) which is chiral and forms a chiral conglomerate between 78 to 61 °C for **H''14** and 77 to 56 °C for **H''18** (Fig. 9.6a). The lattice parameter of the $Cub_{bi}^{[*]}/I23$ phase is $a_{cub} = 15.75$ nm, (Fig. 9.6c). In line with the transition from a double to a triple network structure the lattice parameter is 50 % larger than in the $Cub_{bi}/Ia3d$ phase of **H'4-H'7**. Upon further cooling, relatively low birefringent spherulites grow below 61 °C (Fig. 9.6b). The SAXS pattern changes completely at this transition and can now be indexed to a tetragonal
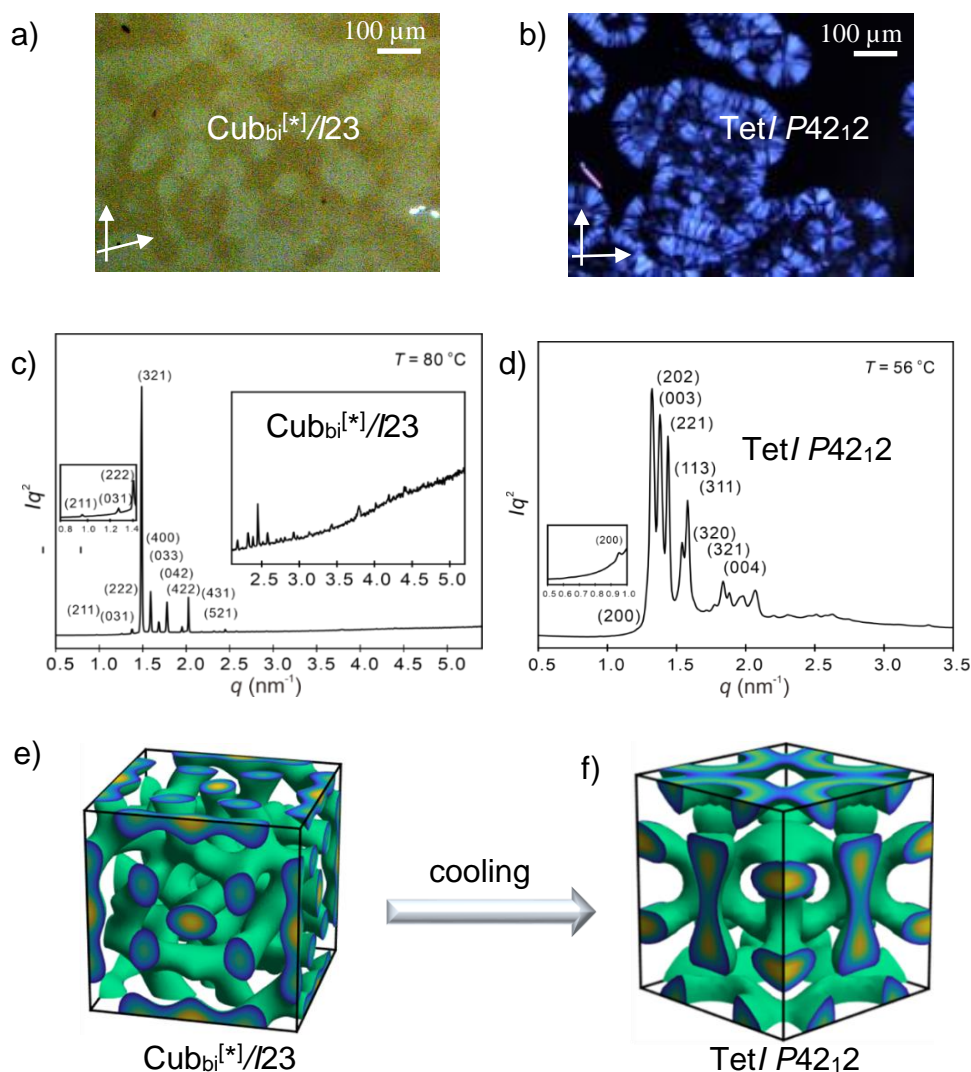
Figure 9.6 Textures of a) $Cub_{bi}^{[*]}/I23$ and b) Tet/ $P42_12$ phase c) SAXS patterns c) of the $Cub_{bi}^{[*]}/I23$ phase of **H''18,** d) of the Tet phase with $P42_12$ lattice of **H''14**; and e,f) ED maps reconstructed from these diffraction patterns. The inset in b) shows the typical texture of the Tet phase.[1]

lattice with $P42_12$ space group and the lattice parameters $a = 13.23$ nm, $c = 13.63$ nm. (Fig. 9.6d, Tab. 9.2). This tetragonal phase has two almost identical lattice parameters which are only a bit smaller than a_{cub} parameter in the adjacent $Cub_{bi}^{[*]}/I23$ phase, suggesting that this phase could possibly represent a distorted version of the $I23$ phase and that it is very different from the Tet phase of **H''7**. The large lattice parameter and the difficulty of choosing the correct phase angle which for this non-centrosymmetric lattice can assume any value between 0 and π it is difficult to

develop a model of this tetragonal phase. The very different diffraction patterns of $Cub_{bi}[*]/I23$ phase and Tet exclude an only slightly distorted version of the $I23$ phase and shows that the structure should be different. The most reasonable ED map obtained is shown in Fig. 9.6f .

Though it is likely that chirality is retained in the tetragonal phases we cannot state this with certainty, because the linear birefringence is much larger than the effects provided by optical rotation. For this reason, also homogeneous chiral Tet phases can presently not be distinguished from racemic forms composed of two enantiomorphic nets. Nevertheless, the proven chirality of the SmQ phase[3] indicates that a preferred homochiral packing between the helical column segments is in principle possible in the case of 90° junctions, whereas in the gyroid with 120° junctions it is proven to be heterochiral.

9.2 Compounds H'n

9.2.1 Transition from SmC to $Cub_{bi}/Ia\bar{3}d$ phase
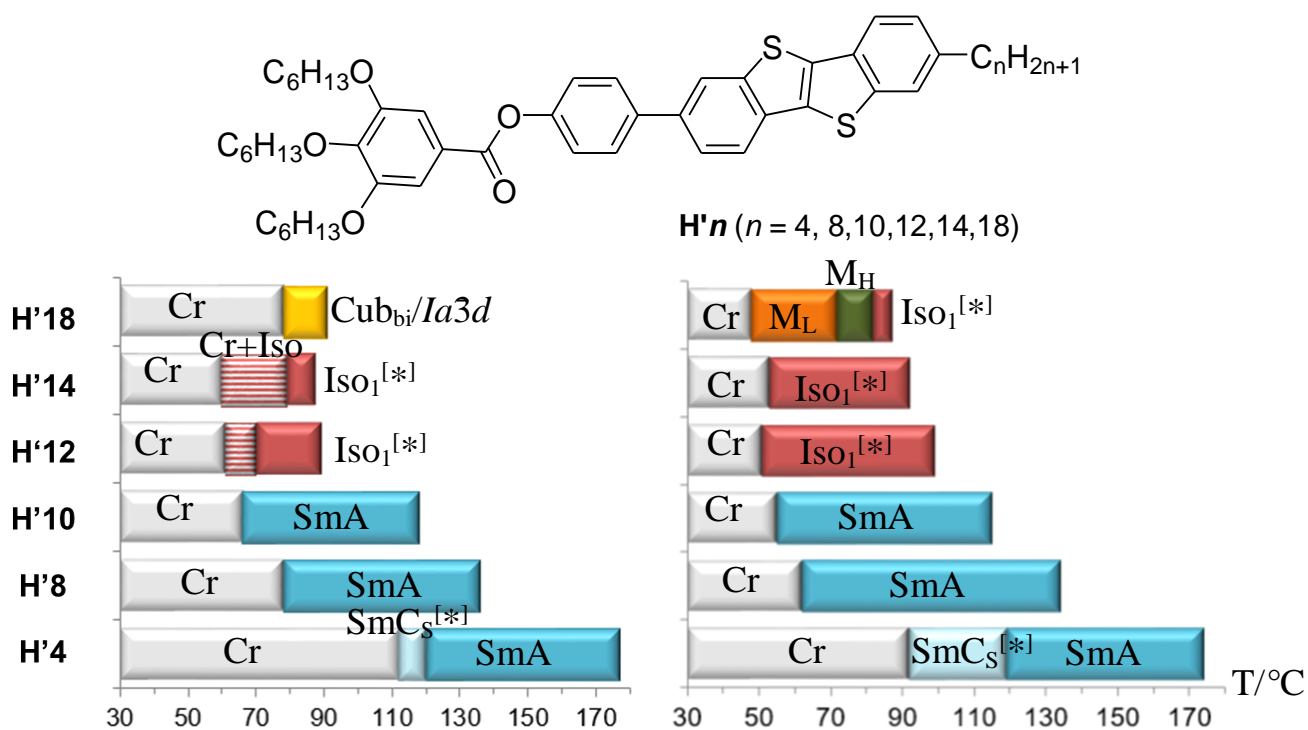
Figure 9.7 Structure and transition temperatures of compounds **H'n** as observed a) on first heating and b) on the following cooling (rate 10 K min^{-1}).

The phase transitions of compounds with shorter alkyloxy chains (trihexyloxy instead of decyloxy) (**H'4** - **H'18**) are collected in Fig. 9.7. Compound **H'4** exhibits a smectic A phase (SmA) with a layer spacing of $d = 4.22$ nm from 174 °C on cooling (Fig. 9.9a,b), which is associated with a transition enthalpy of $\Delta H = 0.7$ kJ mol^{-1}(see Table 9.3). In the textures, dark area are dominating, which represent homeotropic aligned areas where the orientation of the layer is parallel to the substrate surfaces (Fig. 9.9a,b). Upon cooling, the dark areas are converted to a schlieren texture, indicating the transition to a tilted SmC phases with chiral domains (SmC$_S$[*]) at 119 °C (Fig. 9.9c-f). The layer spacing in the SmC phase is $d = 4.08$ nm. The molecular length of **H'4** ($L_{mol} = 3.5$ nm, Fig. 9.8) is a bit smaller than the d-values of the SmA and SmC phases. Thus, a partly intercalated bilayer model can be proposed as for the SmCs phase of **F$_{26}$8** (see Fig. 8.3). The orientation of the extinction in planar alignment (Fig. 9.9c) indicates synclinic and the high birefringent texture of the homeotropic region (Fig. 9.9d) indicates synclinic as well.

Figure 9.8 CPK space filling model of compound **H'4** ($L = 3.5$ nm, for **H"4** $L = 4.0$ nm).

Elongation of the alkyl chain significantly lowers the thermal stability of the SmA phase, shifting the temperature range from between 178 to 119 °C for **H'4** to between 115 to 55 °C for **H'10** on cooling. Surprisingly, no transition to a SmC phase could be detected for **H'8** and **H'10**, though for usual rod-like molecules it is known that chain elongationg favours the SmC phase formation. Upon further chain elongation the SmA phase is replaced by the Iso$_1$[*] phase. Compounds **H'12** and **H'14** show similar behavior, the only difference is the temperature range of the LC phases. For **H'14**, Iso$_1$[*] is formed between 92 and 53 °C upon cooling (see Fig. 9.9h). Another birefringent mesophase appears upon heating when the compound is reheated from the crystalline state from 60 °C to 75 °C (see Fig. 9.9g) as weakly birefringent platelets. Upon futher heating the crystals are completely removed at 79 °C, replaced by growing chiral domains (Iso$_1$[*]).

Table 9.3 Phase transition temperatures (T/°C) and associated enthalpies (ΔH/kJ mol^{-1}) of compounds **H'n.**

	Phase Transitions
H'4	Heating: Cr 112 [17.7] SmC$_S$[*] 120 [-] SmA 177 [4.9] Iso
	Cooling: Iso 174 [4.5] SmA 119 SmC$_S$[*] 92 [15.3] Cr
H'8	Heating: Cr 78 [19.8] SmA 136 [2.5] Iso
	Cooling: Iso 134 [1.6] SmA 62 [19.8] Cr
H'10	Heating: Cr 66 [16.1] SmA 118 [0.9] Iso
	Cooling: Iso 115 [0.8] SmA 55 [18.2] Cr
H'12	Heating: Cr 61 [18.7] Cr+Iso 72 [0.5] Iso$_1$[*] 91 Iso
	Cooling: Iso$_2$ 89 Iso$_1$[*] 51 [18.4] Cr
H'14	Heating: Cr 60 [26.2] Cr+Iso 79 [0.7] Iso$_1$[*] 93 Iso
	Cooling: Iso$_2$ 92 [0.1] Iso$_1$[*] 53 [24.2] Cr
H'18	Heating: Cr 78 [52.5] Cub$_{bi}$/*Ia*3*d* 91 [1.4] Iso
	Cooling: Iso$_2$ 87 [0.1] Iso$_1$[*] 82 M$_H$ 72 M$_L$ 48 [40.5] Cr

In case of **H'18**, the Iso$_1$[*] phases is formed for a short range from 87 to 82 °C and is slowly replaced by a highly birefringent mesophase (M$_H$) (see Fig. 9.9j) and a relatively low birefringent mesophase (M$_L$) (see Fig. 9.9k) upon cooling. Both M phases have high viscosity and hence, appear to be 3D mesophase. Upon heating both M phases are replaced by an optical isotropic Cub$_{bi}$ phase without any chiral domain, which is assumed to be the Cub$_{bi}$*Ia*3*d* phase. The M phases behave very simiar to the M$_H$ and M$_{L1}$ phases of **F$_2$8** (see scheme 7.1). Likewise, the thermodynamic stability of the phases of **H'18** decreases in the order *Ia*3*d* > M$_H$ > M$_L$.
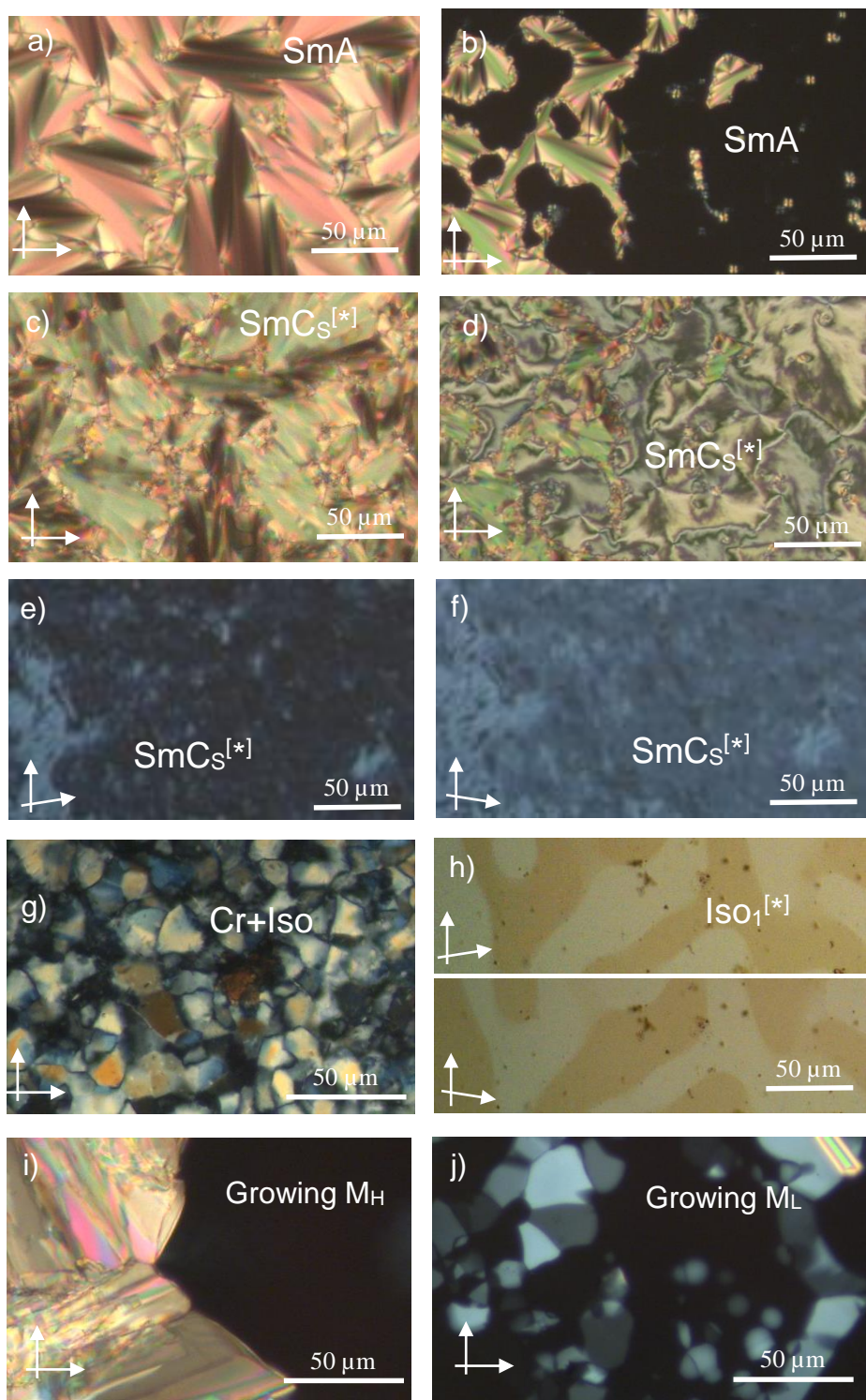
Figure 9.9 Textures of compound **H'*n***; a,b) SmA phase at 150 ℃ and c-f) SmC$_S$[*] phase at 130 ℃ upon cooling from **H'4**; g) M+Iso phase of **H'12** at 75 ℃ upon heating and h) Iso$_1$[*] phase at 80 ℃ on cooling from **H'14**; i) growing M$_H$ of **H'18** at 80 ℃ and j) M$_L$ phase **H'18** at 65 ℃ upon cooling.

9.3 Conclusions

In summary, first compounds showing chiral isotropic liquids at low temperature, close to ambient temperature, and forming them as the only mesophase, were obtained by molecular design. They appear at the transition from the achiral double gyroid to the chiral triple network $I23$ phases upon alkyl chain elongation, if this transition occurs close to the transition from layers to networks (SmA-Cub$_{bi}$-transition). It is accompanied by additional birefringent mesophases with tetragonal 3D lattice. Two of them were solved; one of them is similar to the recently solved SmQ phase, but forms a single network combining helical and non-helical segments. The other one is a more complex network structure which might represents a precursor of the triple network $I23$ phase.
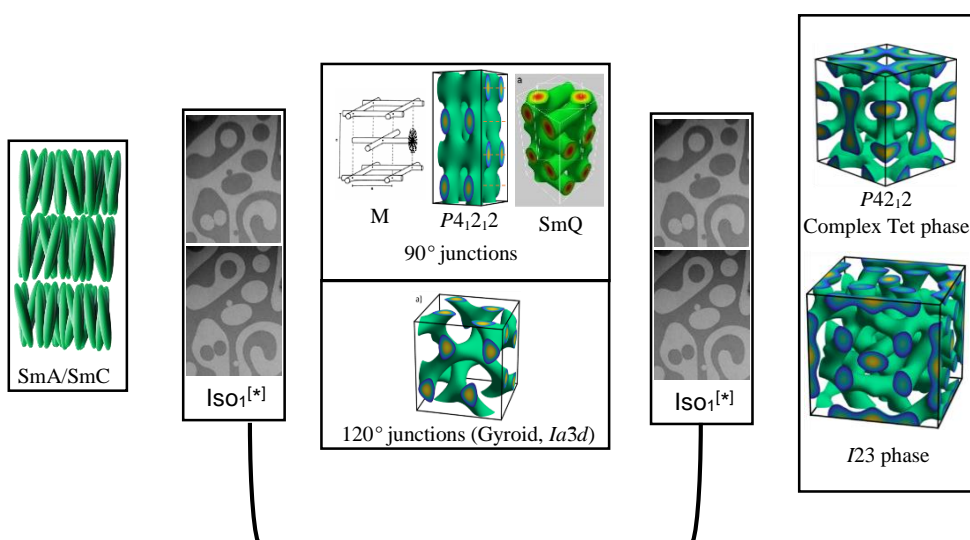
Figure 9.10 Suggested development of complex phases around the mirror-symmetry broken liquid Iso$_1$[*] phase by the development of network connectivity and chirality at the transition from lamellar to columnar self-assembly.

The development of helical networks from flat layers seems to lead to a square mesh with 90° four-way junctions in a first step (M$_H$ phase). In the next step the 90° 4-way junctions are retained, but the meshes transform into a tetragonal 3D network with $P4_12_12$ symmetry. However, these networks with 4-way junctions are in competition with the trigonal 3-way junctions in the gyroid double network with cubic $Ia3d$ lattice, which under most conditions becomes the thermodynamically more stable structure. As the twist in the networks increases by chain elongation a frustration arises between the helical pitch length along the networks and the distance between the junctions, determined by the chain volume and chain length. It appears that for a

certain twist angle range there is no solution for this geometric frustration which would allow the formation of a long-range lattice. Then a liquid with local network structure is formed where the chirality synchronization is retained though the long range periodicity is lost.

After crossing the non-resonance range other more complex network phases, such as the 3D tetragonal phase with $P42_12$ lattice and the recently solved $I23$ phase with triple network structure can be found before upon further increase of the alkyl chain volume the gyroid is formed again ($Ia3d_{(S)}$). The reason for this diversity of complicated phases with an intermediate disordered state (Iso$_1$[*]) seems to be that the polycatenar compounds tend to organize in helical aggregates. As soon as the helical aggregates fuse to networks, the helical pitch has to be in resonance with the junction distance provided by the network in the formed lattice, thus leading to resonant (Cub$_{bi}$ and Tet) and dissonant (Iso$_1$[*]) states.

References

1   F. Liu, Xi'an Jiaotong University, P. R. China 710049, unpublished results

2   a) J. H. Ryu, N. K. Oh, W. C. Zin and M. Lee *J. Am. Chem. Soc.* **2004**, 126, 3551; b) N. K. Oh, W. C. Zin, J. H. Im, J. H. Ryub and M. Lee, *Chem. Comm*. **2004**, 1092.

3   H. Lu, X. Zeng, G. Ungar, C. Dressel, C. Tschierske, *Angew. Chem. Int. Ed.* **2018**, *57,* 2835.

4   C. Tschierske and C. Dressel, *Symmetry* **2020**, 12, 1098.

5   C. Dressel, T. Reppe, M. Prehm, M. Brautzsch and C. Tschierske, *Nat. Chem.* **2014**, 6, 971.

6   T. Reppe, Master thesis, *Martin-Luther-Universitat Halle- Wittenberg*, Halle, **2015**.

7   P. Norman, M. Linares, *Chirality* **2014**, 26, 483.

8   E. Yashima, N. Ousaka, D. Taura, K. Shimomura, T. Ikai, K. Maeda, *Chem. Rev.* **2016** 116, 22, 13752.

10. Summary

$H'n$ (*m*=6)
$H''n$ (*m*=10)

Hn (m= 6, **X, Y,** = H) F_Xn (*m*= 6, **X= F, Y** = H)
Bn (*m*= 6, **X, Y$_1$** = H, **Y$_2$** = Br) F'_Xn (*m*= 10, **X= F, Y** = H)
BBn (*m*= 6, **X** = H, **Y$_1$, Y$_2$** = Br) BF_Xn (m= 6, **X= F, Y** = Br)
$B'n$ (*m*=10, **X, Y$_1$** = H, **Y$_2$** = Br) BF'_Xn (*m*=10, **X= F, Y** = Br)
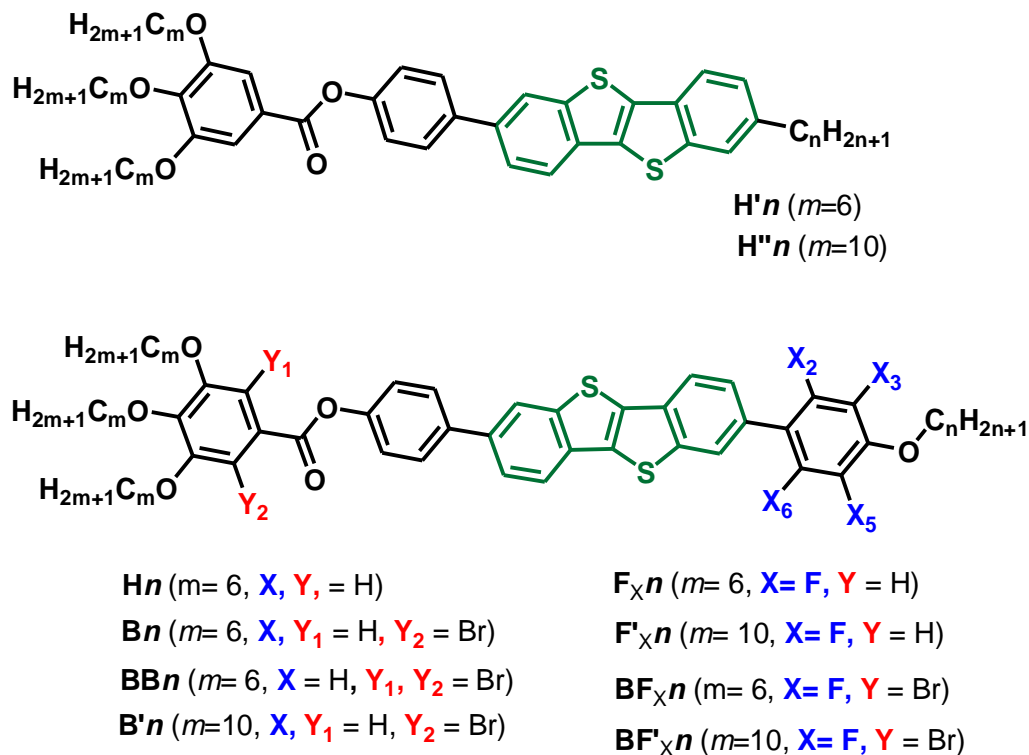
Figure 10.1 Molecular structures of the synthesized BTBT based polycatenars.

In summary, new multi-chain (polycatenar) achiral compounds based on the rod-like π-conjugated [1]benzothieno[3,2-b]benzothiophene (BTBT) unit as a new building block were designed and successfully synthesized (Fig. 10.1). The series **Hn** involving the 3,4,5-trihexyloxybenzoyl group form a variety of helical network phases, ranging from soft crystalline via Cub$_{bi}$ phase to mirror symmetry broken liquids. These compounds especially form extremely wide ranges of bicontinuous cubic network phases including ambient temperature. The Cub$_{bi}$ phase type can be controlled by adjusting the intermolecular twist along the networks by chain length modification ($Ia\bar{3}d$ or $I23$) at the triple or mono-substituted end. At the transition between the two different Cub$_{bi}$ phases a highly birefringent M$_H$ phase and a relative low birefringent tetragonal 3D phase (Tet) emerge.

The range of the tetragonal phase can be reduced and the Cub$_{bi}$-range can be expanded by bromination of the tapered benzoate end group (**Bn**, **BBn**). Bromination also decreases the melting

points and also leads to Cub_{bi} phases even at ambient temperature. The dibromination (compounds **BB***n*) can even lead to a complete removal of the Tet phases while introducing an additional hexagonal columnar phase (Col_{hex}). Further increasing bromination has a strong effect on the helical twist angle, which causes a shift of the transition from $Ia\overline{3}d$ to $I23$ to shorter chain length (**H12** → **BB9**), and moreover, it changes the mode of π–π stacking from edge-to-face to face-to-face by restricting the rotation of the molecules around their long axis.

No additional Tet phase at the transition from $Ia\overline{3}d_{(L)}$ to $I23$ was also found for compounds with three elongated chains at the tapered end. Elongation of the single end chain, leads in this case to another phase transition from $I23$ to a short pitch $Ia\overline{3}d_{(S)}$ phase with another birefringent 3D phase (Tet) appearing at this transition. The $Ia\overline{3}d_{(S)}$ phase appears only on heating because it is competing with comlumnar phases.

The effect of core fluorination at the monosubstituted end was investigated for compound **H8**. Peripheral fluorination (ortho to the alkyloxychain) primarily causes an increase of helical twist, which leads to a transition from the achiral double gyroid $Ia\overline{3}d$ phase to the mirror symmetry broken $I23$ phase and suggests that the steric effect is dominating. In contrast, the inside directed fluorination results in replacement of the cubic phases by 3D tetragonal phases and shifts the self-assembly towards the lamellar phases in line with a broadening of the core unit. The tetrafluorinated compounds **F₂₃₅₆***n*, involving both peripheral and inside directed fluorination, exhibits dominantly a highly birefringent Tet phase and the chiral $I23$ phase and has significantly lower mesophase stability than all other compounds.

Spontaneous chiral isotropic liquids appear for all of these series. The $Iso_1^{[*]}$ phase tends to broaden its temperature range when it has less bulky substituent like a bromine or a fluorine and when the compounds involve shorter chains. Interestingly, polycatenar compounds involving a shorter rigid core can show the $Iso_1^{[*]}$ phase as the only mesophase in a range close to ambient temperature. This is of significant importance, as primarily reported $Iso_1^{[*]}$ phases were always accompanied by additional LC phases and were observed at high temperature (~200 ℃) which limited their investigation and application. It appears that the $Iso_1^{[*]}$ phases can appear either at the transition from lamellar to the achiral double gyroid $Ia3d$ or from the gyroid to the chiral triple network $I23$ phases upon alkyl chain elongation At these transitions they compete with different birefringent (tetragonal) phases, among these square mesh, Tet/ $P4_12_12$ or Tet/ $P42_12$ phases. A

structure formed by 90 junctions between helical and non-helical columns was predicted for the $P4_12_12$ lattice whereas the $P42_12$ phase is more complicated.

Overall at the transition between lamellar and columnar phases numerous complicated LC phases were detected including bicontinuous cubic phases; the achiral $Ia3d$ and the chiral $I23$ phase, tetragonal phases and disordered isotropic liquid (Iso$_1$[*]) (Fig.10.2). It appears that the helical pitch induced by the collision of the bulky terminal chains and substituents have to be in resonance with the junction distance furnished by the network in the formed lattice, thus leading to resonant (Cub$_{bi}$ and Tet) and dissonant (Iso$_1$[*]) states. The dissonant state (Iso$_1$[*] phase) was found at the transiton from lamellar via $Ia3d$ to the $I23$ phase when there is no proper pitches legnth ftting the junction distance of any of the periodic network phases. If it does not fit to a Cub$_{bi}$ phase then the cubic lattice is distorted and various Tet phases could be formed or with. Among them phases related to the organization in the SmQ lattice dominated by 90° twist junctions, distorted gyroid structures or possibly also by the $I23$ phase.
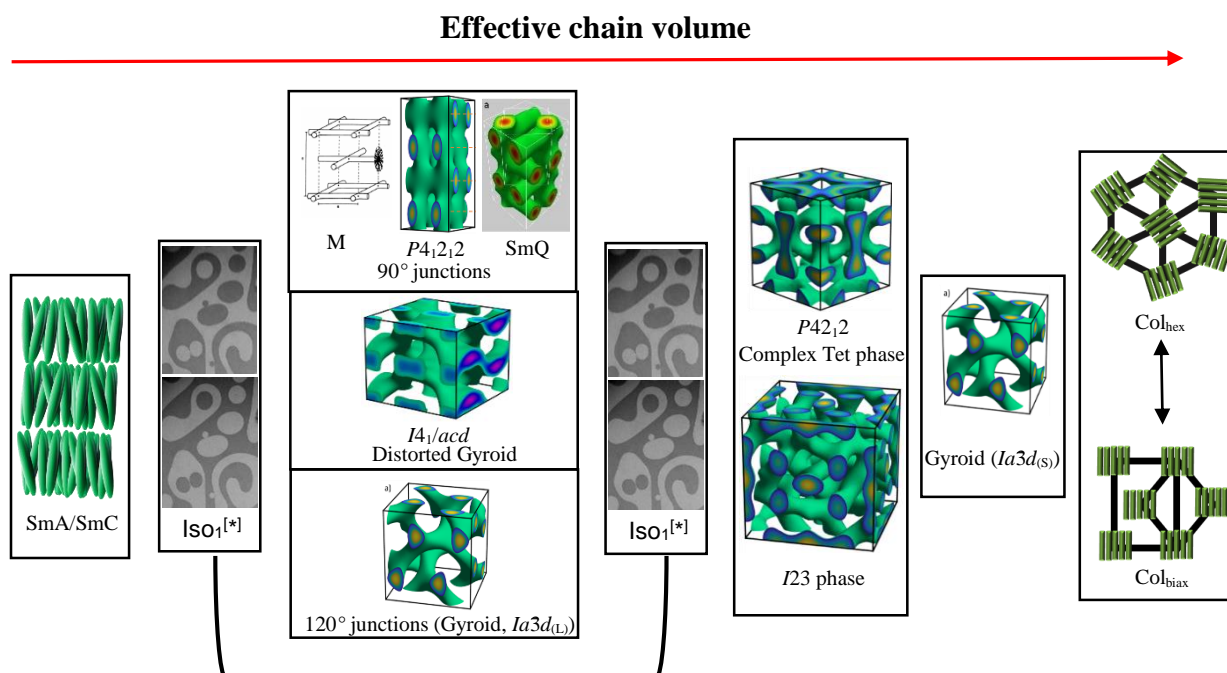
Figure 10.2 The phase transition sequence of the investigated BTBT based polycatenars from lamellar to columnar phases on increasing side chain volume. The Iso$_1$[*] phase can occur as intermediate phase at both side of the Tet and /$Ia3d$ phases.

The investigation of OFET cells and TOF experiments indicated that the capability of the Cub_{bi} phase for charge transport in all three spatial directions can be advantageous over the 1D transport in the columnar phases. The character of hole current vs. time is non-dispersive with very well-defined cut–off which are rarely observed for LC materials. This suggests a considerably lower number of defects in the structure and lower molecular mobility than in the other LC phases. It allows propagation of the charge wave through the sample without dissipation. This provides a new concept for (semi)conducting LCs, complementing the previously known 2D conducting lamellar and 1D conducting columnar systems by the new concept of 3D networks. The transition to isotropic crystalline phases leads to an increase of the charge carrier mobility and suggests that in the Cr_{Iso}[*] phase the network structure is retained.
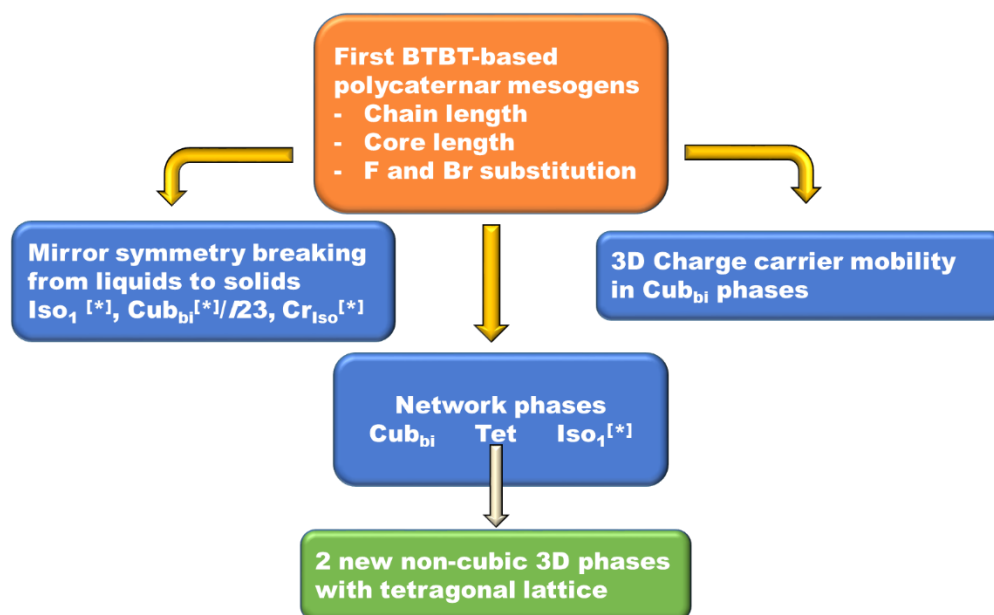
Scheme 10.1 Major achievement of this work.

Overall this work 1) contributes to the understanding of network formation for development of complex three dimensional mesophases, 2) provided first compounds with spontaneous mirror symmetry broken liquids close to ambient temperature, 3) contributes to the understanding of the $Ia3d \rightarrow I23$ transition and 4) mainly it estabilishes the concept of 3D-networks for use in organic electronic materials. 5) This work has lead to new types of LC 3D phases. Though the structure of some tetragonal phases could be solved, and there are several 3D phases which will need to be resolved in furture work.

11. Experimental

11.1 General

All starting materials were purchased from commercial sources and used without further purification. A list of purchased chemicals is provided in the following table. Column chromatography was performed with silica gel 60 (63-200 μm, Fluka). The purity of all products was checked with thin layer chromatography (silicagel 60 F_{254}, Merck). NMR spectra were recorded on Varian Gemini 2000 or Unity Inova 500 spectrometers at 27 °C. Mass spectra were taken on Finnigan LCQ (electrospray, spray-voltage 6.7 kV, sheath gas nitrogen). The measurements were performed in THF (1 mg/mL) with 0.1 mg/mL LiCl. Mass spectrometry was performed on BRUKER's HR-ESI-TOF device. Each sample was dissolved in THF (1mg/mL) and mixed with LiCl (0.1mg/mL).

Chemical	Company	Chemical	Company
n-Bromoethane	Apolda	(Dichloromethyl)benzene	abcr
n-Bromopropane	Apolda	4-Bromo-2-fluorophenol	abcr
n-Bromobutane	Apolda	4-Bromo-3-fluorophenol	abcr
n-Bromopentane	Apolda	4- Bromo-2,3-difluoro-phenol	abcr
n-Bromohexane	Apolda	4-Bromo-3,5-difluoro-phenol	abcr
n-Bromooctane	Sigma	Iodopentafluorobenzene	Sigma
n-Bromononan	Sigma	4-Hydroxyphenylboronic acid	abcr
n-Bromodecane	Sigma	1-Butanol	abcr
n-Bromoundecane	Sigma	1-Hexanol	abcr
n-Bromododecane	Sigma	1-Octanol	abcr
n-Bromotetradecane	Sigma	1-Decanol	abcr
n-Bromooctadecane	Sigma	1-Tetradecanol	abcr
n-Bromodocosane	abcr	1-Octadecanol	abcr
butyryl chloride	Sigma	decanoyl chloride	Sigma
hexanoyl chloride	Sigma	dodecanoyl chloride	Sigma
heptanoyl chloride	Sigma	myristoyl chloride	Sigma
octanoyl chloride	Sigma	stearoyl chloride	Sigma

Abbreviation: Apolda= VEB Apolda, Sigma= Sigma-Aldrich

11.2 Synthesis and analytical data of the 6-bromo-3,4,5-trihexyloxybenzoates B*n*

The synthesis was performed according to schemes 2.2-2.4.

11.2.1 Synthesis and analytical data of intermediates

[1]Benzothieno[3,2-b]benzothiophene (1).[S1]
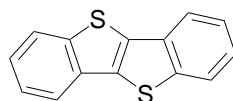
(Dichloromethyl)benzene (100 g, 0.62 mol) and sulfur 24.7 g (0.77 mol) were prepared in two-neck flask under argon atmosphere. The mixture was refluxed for 24 hours at 265 °C. After the mixture was cooled down, chloroform (300 ml) was added and refluxed to dissolve. Then, silica gel (150 g) was added and chloroform was removed under low pressure. The residue was placed on the top of the column chromatography and eluted with n-hexane. The crude product was recrystallized by toluene; yield 26.3 g (0.11 mol, 35%); light yellow solid; m.p. 216 °C (ref[S1] gives m.p. 216-218 °C); ^{1}H NMR (500 MHz, CDCl$_3$) δ 7.91 (dd, J = 16.8, 7.9 Hz, 4H), 7.46 (tt, J = 6.5, 3.2 Hz, 2H), 7.41 (tt, J = 6.5, 3.2 Hz, 2H).

2-Bromo[1]benzothieno[3,2-b]benzothiophene (2).[S2]
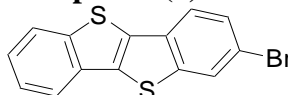
1 (5.0 g, 0.021 mol) was dissolved in DCM (300 ml). Bromine (3.6 g, 0.023 mol) was dissolved in DCM and added dropwise via dropping funnel. The mixture was stirred for 3h at RT. The reaction was quenched by adding Na$_2$S$_2$O$_3$ solution. The crude product was extracted with DCM. The organic mixture was dried with Na$_2$SO$_4$. Solvent was removed via rotary evaporator. From the residue, product was recrystallized by chloroform; yield 3.5 g (0.011 mol, 53%); colorless solid; m.p. 204 °C; ^{1}H NMR (400 MHz, CDCl$_3$) δ 8.06 (d, J = 1.7 Hz, 1H), 7.90 (dd, J = 17.6, 7.4 Hz, 2H), 7.74 (d, J = 8.4 Hz, 1H), 7.56 (dd, J = 8.4, 1.7 Hz, 1H), 7.51 – 7.38 (m, 2H).

3,4,5-Tri-n-hexyloxybenzoic acid (6a)
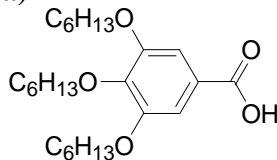
To synthesize 3,4,5-Tri-n-hexyloxybenzoic acid, Williamson ether synthesis was carried out. Ethyl gallate (10.0 g, 50.5 mmol) was dissolved in Butanone (300 ml). Subsequently, K$_2$CO$_3$ (49.8 g, 0.36 mol) and bromohexane (27.5g, 0.17 mol) were added. The solution was refluxed for 8 hours. Butanone was removed via rotary evaporator and the crude product was purified via liquid column chromatography with (Chloroform/n-hexane). To detach the ethlyl group from the compound (17.5 g, 38.8 mmol), KOH (21.7g, 0.39 mol) was used in EtOH (150 ml) and H$_2$O (75 ml). The solution was refluxed for 4 hours and cooled down to 0°C. When the solution was cooled, concentrated HCl solution was added until precipitate appeared. The product was collected and

washed with water (3 x 50 ml). Finally, it was recrystallized by MeOH; yield 14.5 g (34.3 mmol, 67.9%);[S3] colorless solid; m.p. 39 °C (ref[S4] gives m.p. 39 °C)^{1}H NMR (500 MHz, CDCl$_3$) δ 7.32 (s, 2H, Ar-H), 4.04 (dt, J = 9.7, 6.6 Hz, 6H, OCH$_2$), 1.85 – 1.79 (m, 4H), 1.78 – 1.72 (m, 2H, CH$_2$), 1.56 – 1.44 (m, 6H, CH$_2$), 1.40 – 1.23 (m, 12H, CH$_2$), 0.91 (t, J = 7.0 Hz, 6H, CH$_3$).

4-(3,4,5-Tri-n-hexyloxybenzoyloxy)phenylboronic acid pinacol ester (7a)
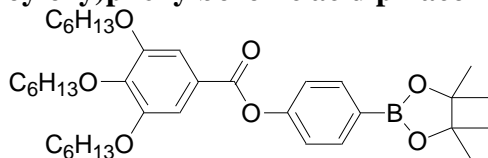
6a (4.0 g, 6.77 mmol) was dissolved in SOCl$_2$ (20ml. The solution was refluxed for 30 mins under Argon atmosphere. Then, SOCl$_2$ was removed under vacuum. Subsequently, 4-Hydroxyphenylboronic acid pinacol ester (1.5g, 6.77 mmol) with dry pyridine (10 ml) were added to the solution. The solution was stirred overnight at RT. Solvent was removed via rotary evaporator. The crude product was purified with column chromatography (Chloroform; yield 2.7 g (3.43 mmol, 50.7%), colorless liquid;[5] ^{1}H NMR (500 MHz, CDCl$_3$) δ 7.88 (d, J = 8.5 Hz, 2H, Ar-H), 7.40 (s, 2H, Ar-H), 7.20 (d, J = 8.5 Hz, 2H, Ar-H), 4.11 – 3.94 (m, 6H, OCH$_2$), 1.88 – 1.80 (m, 4H, CH$_2$), 1.80 – 1.72 (m, 2H, CH$_2$), 1.54 – 1.42 (m, 6H, CH$_2$), 1.41 – 1.26 (m, 24H, CH$_2$+CH$_3$), 0.94 – 0.88 (m, 9H, CH$_2$).

2-[4-(3,4,5-Tri-n-hexyloxybenzoyloxy)phenyl]-[1]benzothieno[3,2-b]benzothiophene (9a).
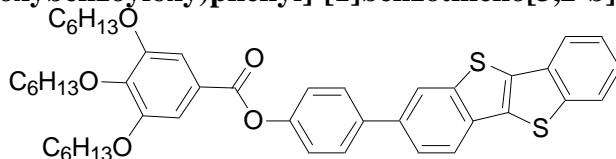
 Suzuki coupling reaction was used.[S6] In two-neck flask, **7a** (2.85 g, 4.55 mmol) **2** (1.50 g, 4.60 mmol), THF (100 ml) and saturated NaHCO$_3$ solution (50 ml) were prepared, and degassed with argon for 15 minutes. After purging, [Pd(PPh$_3$)$_4$] (0.1 g, 0.087 mmol) was added. The solution was refluxed for 6 hours. When the mixture was cooled down, the organic phase was extracted with CHCl$_3$. Then, it was dried over Na$_2$SO$_4$. After it was concentrated in vacuum, it was purified by column chromatography (eluent: CHCl$_3$/n-hexane 2/1)[5]; yield 1.7 g (2.31 mmol, 51%), colorless solid; m.p. 104 °C; ^{1}H NMR (400 MHz, CDCl$_3$) δ 8.14 (d, J = 1.1 Hz, 1H, BTBT-H), 7.97 – 7.89 (m, 3H, BTBT-H), , 7.74 (d, J = 8.7 Hz, 2H, Ar-H), 7.70 (dd, J = 8.3, 1.6 Hz, 1H, BTBT-H), 7.51 – 7.39 (m, 4H, BTBT-H+Ar-H), 7.32 (d, J = 8.7 Hz, 2H, Ar-H), 4.08 (td, J = 6.5, 3.3 Hz, 6H, OCH$_2$CH$_2$), 1.92 – 1.69 (m, 6H, OCH$_2$CH$_2$), 1.58 – 1.43 (m, 6H, CH$_2$), 1.44 – 1.28 (m, 12H, CH$_2$), 0.92 (t, J = 7.0 Hz, 9H, CH$_3$).

2-[4-(2-Bromo-3,4,5-tri-n-hexyloxybenzoyloxy)phenyl]-7-bromo-[1]benzothieno[3,2-b]benzothiophene (10a).
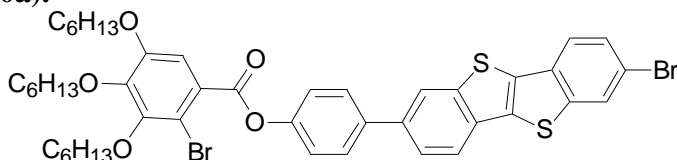
The same procedure as described for **2** was used. **9a** (1.7 g, 2.31 mmol), bromine (0.74 g, 4.61 mmol), DCM (60 ml), reaction time 14 h, RT, column chromatography (eluent: CHCl$_3$/n-hexane

2/1); yield 1.70 g (1.90 mmol, 82 %); colorless solid, m.p. 183 ℃; ^{1}H NMR (500 MHz, cdcl$_3$) δ 8.10 (dd, J = 22.0, 1.4 Hz, 2H, BTBT-H), 7.94 (tdd, J = 26.9, 8.1, 0.5 Hz, 2H, BTBT-H), 7.78 – 7.69 (m, 3H, BTBT-H + Ar-H), 7.59 (dd, J = 8.4, 1.7 Hz, 1H, BTBT-H), 7.42 – 7.38 (m, J = 9.4, 2.7 Hz, 2H, Ar-H), 7.37 (s, 1H, Ar-H), 4.18 – 3.97 (m, 6H, OCH$_2$CH$_2$), 2.01 – 1.72 (m, 6H, OCH$_2$CH$_2$), 1.60 – 1.46 (m, 6H, CH$_2$), 1.43 – 1.29 (m, 12H, CH$_2$), 0.94 (t, J = 5.9 Hz, 9H, CH$_3$).

2-[4-(2-Bromo-3,4,5-tri-n-hexyloxybenzoyloxy)phenyl]-7-(4-hydroxyphenyl)-[1]benzothieno[3,2-b]benzothiophene (11a).
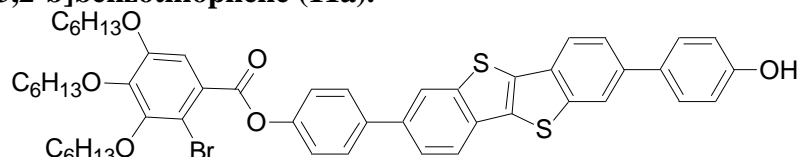
The same procedure for the synthesis of **9a** was used. **10a** (1.7 g, 1.90 mmol), 4-hydroxyphenylboronic acid pinacol ester (0.42 g, 1.90 mmol), THF (100 ml) and saturated NaHCO$_3$ solution (50 ml), column chromatography (eluent: CHCl$_3$/MeOH 19/1); yield 0.85 g (0.94 mmol, 49 %); colorless solid, heating: Cr 175 SmA 238, cooling: Iso 238 SmA 158 Cr; Iso; ^{1}H NMR (400 MHz, CDCl$_3$) δ 8.04 (dd, J = 34.3, 1.1 Hz, 2H, BTBT-H), 7.88 (dd, J = 15.4, 8.2 Hz, 2H, BTBT-H), 7.73 (d, J = 8.6 Hz, 2H, Ar-H), 7.70 – 7.57 (m, 2H, BTBT-H), 7.54 (d, J = 8.5 Hz, 2H, Ar-H), 7.38 (s, 1H, Ar-H), 7.37 (d, J = 8.5 Hz, 2H, Ar-H), 6.90 (d, J = 8.5 Hz, 2H, Ar-H), 5.08 (s, 1H, Ar-OH), 4.20 – 3.94 (m, 6H, OCH$_2$CH$_2$), 1.97 – 1.70 (m, 6H, OCH$_2$CH$_2$), 1.61 – 1.45 (m, 6H, CH$_2$), 1.41 – 1.28 (m, 12H, CH$_2$), 0.92 (t, J = 6.8 Hz, 9H, CH$_3$).

11.2.2 Synthesis and analytical data of compounds B6 – B22
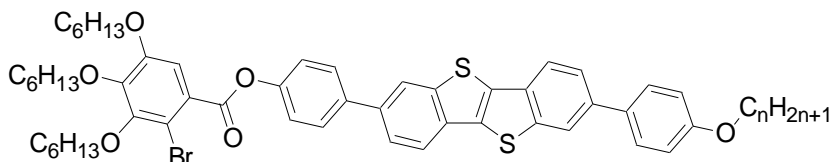
Williamson ether synthesis was used for the final step. **11a** (120 mg, 0.13 mmol), K$_2$CO$_3$ (200 mg, 1.45 mmol), TBAI (20 mg, 0.054 mmol), 1-bromoalkane (0.4 mmol) were dissolved/suspended in butanone (50 ml). The solution is refluxed for 5 hours. Butanone was removed via rotary evaporator and the crude product was purified via liquid column chromatography with (chloroform/n-hexane 2/1). Then, recrystallization from THF/EtOH is repeated. All compounds are colorless solids with transition temperatures collated in Table S1.

2-[4-(2-Bromo-3,4,5-tri-n-hexyloxybenzoyloxy)phenyl]-7-(4-hexyloxyphenyl)-[1]benzothieno[3,2-b]benzothiophene (B6)

Synthesized by dissolving **11a** (120 mg, 0.13 mmol) and 1-bromohexane (65 mg, 0.4 mmol) in butanone (50 ml) with K$_2$CO$_3$ (200 mg, 1.45 mmol) and TBAI (20 mg, 0.054 mmol); yield 52 mg (0.052 mmol, 40%); ^{1}H NMR (500 MHz, CDCl$_3$) δ 8.11 (dd, J = 18.0, 1.4 Hz, 2H, BTBT-H), 7.94 (dd, J = 11.0, 9.1 Hz, 2H, BTBT-H), 7.75 (d, J = 8.5 Hz, 2H, Ar-H), 7.69 (ddd, J = 11.6, 8.6, 1.4 Hz, 2H, BTBT-H), 7.62 (d, J = 8.5 Hz, 2H, Ar-H), 7.38 (d, J = 8.4 Hz, 2H, Ar-H), 7.36 (s, 1H, Ar-H), 7.02 (d, J = 8.6 Hz, 2H, Ar-H), 4.11 – 4.01 (m, 8H, OCH$_2$CH$_2$), 1.90 – 1.75 (m, 8H, OCH$_2$CH$_2$), 1.58 – 1.45 (m, 8H, CH$_2$), 1.41 – 1.32 (m, 16H, CH$_2$), 0.97 – 0.85 (m, 12H, CH$_3$).^{13}C NMR (126 MHz, CDCl$_3$) δ 158.97 (C=O), 152.67, 152.29, 138.25, 138.23, 128.39, 128.30, 124.49, 124.23,

122.33, 122.10, 121.75, 121.72, 114.98, 111.35, 110.39, 110.28 (BTBT-C + Ar-C), 74.20, 74.14, 69.24, 68.17 (OCH$_2$), 32.00, 31.66, 31.60, 31.52, 30.78, 30.24, 30.16, 29.27, 29.17, 25.73, 22.64 (CH$_2$), 14.05, 14.04, 13.99 (CH$_3$); HRMS (m/z): [M]+Li$^+$ calcd. for C$_{57}$H$_{67}$BrO$_6$S$_2$Li, 997.372; found 997.374

2-[4-(2-Bromo-3,4,5-tri-n-hexyloxybenzoyloxy)phenyl]-7-(4-octyloxyphenyl)-[1]benzothieno[3,2-b]benzothiophene (B8)

Synthesized by dissolving **11a** (120 mg, 0.13 mmol) and 1-bromooctane (80 mg, 0.4 mmol) in butanone (50 ml) with K$_2$CO$_3$ (200 mg, 1.45 mmol) and TBAI (20 mg, 0.054 mmol); yield 44 mg (0.043 mmol, 33%); ^{1}H NMR (400 MHz, CDCl$_3$) δ 8.11 (dd, J = 14.5, 1.5 Hz, 2H, BTBT-H), 7.94 (dd, J = 9.0, 8.5 Hz, 2H, BTBT-H), 7.75 (d, J = 8.6 Hz, 1H, Ar-H), 7.69 (ddd, J = 10.0, 5.1, 1.0 Hz, 2H, BTBT-H), 7.62 (d, J = 8.7 Hz, 2H, Ar-H), 7.38 (d, J = 8.6 Hz, 2H, Ar-H), 7.36 (s, 1H, Ar-H), 7.02 (d, J = 8.7 Hz, 2H, Ar-H), 4.11 – 4.00 (m, 8H, OCH$_2$CH$_2$), 1.90 – 1.74 (m, 8H, OCH$_2$CH$_2$), 1.56 – 1.45 (m, 8H, CH$_2$), 1.42 – 1.24 (m, 20H, CH$_2$), 0.95 – 0.88 (m, 12H, CH$_3$). 13C NMR (101 MHz, CDCl$_3$) δ 164.70, 158.95 (C=O), 152.27, 143.21, 143.10, 142.31, 138.71, 138.24, 137.38, 136.38, 133.68, 131.64, 128.38, 128.29, 126.23, 124.47, 124.22, 122.32, 122.09, 121.74, 121.70, 114.96, 110.38 (BTBT-C + Ar-C), 74.18, 74.12, 69.23, 69.22, 68.16 (OCH$_2$), 54.05, 36.54, 31.81, 31.65, 31.50, 30.23, 30.14, 29.36, 29.29, 29.23, 29.15, 26.06, 25.71, 25.69, 25.66, 22.68, 22.63, 22.57 (CH$_2$), 14.08, 14.04, 14.03, 13.98 (CH$_2$); HRMS (m/z): [M]+Li$^+$ calcd. for C$_{59}$H$_{71}$BrO$_6$S$_2$Li, 1025.403; found 1025.408.

2-[4-(2-Bromo-3,4,5-tri-n-hexyloxybenzoyloxy)phenyl]-7-(4-nonyloxyphenyl)-[1]benzothieno[3,2-b]benzothiophene (B9)

Synthesized by dissolving **11a** (120 mg, 0.13 mmol), 1-bromononane (85 mg, 0.4 mmol) in butanone (50 ml) with K$_2$CO$_3$ (200 mg, 1.45 mmol) and TBAI (20 mg, 0.054 mmol); yield 35 mg (0.034 mmol, 26%); ^{1}H NMR (500 MHz, CDCl$_3$) δ 8.11 (dd, J = 18.2, 1.5 Hz, 2H, BTBT-H), 7.94 (dd, J = 11.3, 8.3 Hz, 2H, BTBT-H), 7.75 (d, J = 8.6 Hz, 2H, Ar-H), 7.69 (ddd, J = 11.7, 8.2, 1.6 Hz, 2H, BTBT-H), 7.62 (d, J = 8.7 Hz, 2H, Ar-H), 7.38 (d, J = 8.6 Hz, 2H, Ar-H), 7.36 (s, 1H, Ar-H), 7.02 (d, J = 8.7 Hz, 2H, Ar-H), 4.12 – 4.01 (m, 8H, OCH$_2$CH$_2$), 1.89 – 1.75 (m, 8H, OCH$_2$CH$_2$), 1.56 – 1.45 (m, 8H, CH$_2$), 1.41 – 1.25 (m, 22H, CH$_2$), 0.96 – 0.88 (m, 12H, CH$_3$); ^{13}C NMR (126 MHz, CDCl$_3$) δ 164.69, 158.96 (C=O), 152.27, 151.48, 150.37, 146.36, 143.22, 138.71, 138.24, 137.38, 133.68, 133.09, 132.92, 132.36, 131.64, 128.37, 128.28, 124.47, 124.21, 122.31, 122.08, 121.73, 121.70, 114.97, 111.35, 110.37 (BTBT-C + Ar-C), 74.19, 74.12, 69.23, 68.17 (OCH$_2$), 31.86, 31.65, 31.50, 30.23, 30.14, 29.53, 29.40, 29.29, 29.25, 29.16, 26.05, 25.71, 25.69, 25.65, 22.65, 22.62, 22.56 (CH$_2$) 14.08, 14.03, 14.02, 13.97 (CH$_3$); HRMS (m/z): [M]+Li$^+$ calcd. for C$_{60}$H$_{73}$BrO$_6$S$_2$Li, 1039.419; found 1039.425.

2-[4-(2-Bromo-3,4,5-tri-n-hexyloxybenzoyloxy)phenyl]-7-(4-decyloxyphenyl)-[1]benzothieno[3,2-b]benzothiophene (B10)

Synthesized by dissolving **11a** (120 mg, 0.13 mmol), 1-bromodecane (90 mg, 0.4 mmol) in butanone (50 ml) with K$_2$CO$_3$ (200 mg, 1.45 mmol) and TBAI (20 mg, 0.054 mmol); yield 44 mg (0.042 mmol, 32%); ^{1}H NMR (400 MHz, CDCl$_3$) δ 8.11 (dd, J = 14.5, 2.3 Hz, 2H, BTBT-H), 7.94 (dd, J = 9.0, 8.4 Hz, 2H, BTBT-H), 7.75 (d, J = 8.6 Hz, 2H, Ar-H), 7.69 (ddd, J = 9.8, 8.4, 1.6 Hz, 2H, BTBT-H), 7.62 (d, J = 8.7 Hz, 2H, Ar-H), 7.38 (d, J = 8.7 Hz, 2H, Ar-H), 7.36 (s, 1H, Ar-H), 7.02 (d, J = 8.8 Hz, 2H, Ar-H), 4.11 – 4.01 (m, 8H, OCH$_2$CH$_2$), 1.90 – 1.74 (m, 8H, OCH$_2$CH$_2$), 1.57 – 1.45 (m, 8H, CH$_2$), 1.41 – 1.26 (m, 24H, CH$_2$), 0.95 – 0.87 (m, 12H, CH$_3$); ^{13}C NMR (101

MHz, CDCl$_3$) δ 158.96, 151.48 (C=O), 150.36, 143.21, 143.10, 138.71, 137.38, 133.68, 132.92, 131.19, 128.38, 128.29, 124.47, 124.22, 122.92, 122.32, 122.09, 121.74, 121.71, 114.97 (BTBT-C + Ar-C), 74.19, 74.13, 69.22, 68.16 (OCH$_2$), 31.88, 31.65, 31.50, 30.23, 30.14, 29.58, 29.55, 29.40, 29.31, 29.29, 29.16, 26.05, 25.71, 25.69, 25.66, 22.66, 22.63, 22.57 (CH$_2$), 14.09, 14.04, 14.03, 13.98 (CH$_3$); HRMS (m/z): [M]+Li$^+$ calcd. for C$_{61}$H$_{75}$BrO$_6$S$_2$Li, 1053.434; found 1053.439.

2-[4-(2-Bromo-3,4,5-tri-n-hexyloxybenzoyloxy)phenyl]-7-(4-undecyloxyphenyl)-[1]benzothieno[3,2-b]benzothiophene (B11)

Synthesized by dissolving **11a** (120 mg, 0.13 mmol), 1-bromoundecane (95 mg, 0.4 mmol) in butanone (50 ml) with K$_2$CO$_3$ (200 mg, 1.45 mmol) and TBAI (20 mg, 0.054 mmol); yield 25 mg (0.024 mmol, 18%); ^{1}H NMR (500 MHz, CDCl$_3$) δ 8.11 (dd, *J* = 18.2, 1.5 Hz, 2H, BTBT-H), 7.94 (dd, *J* = 11.4, 8.3 Hz, 2H, BTBT-H), 7.75 (d, *J* = 8.6 Hz, 2H, Ar-H), 7.69 (ddd, J = 11.8, 8.3, 1.6 Hz, 2H, BTBT-H), 7.62 (d, *J* = 8.7 Hz, 2H, Ar-H), 7.38 (d, *J* = 8.7 Hz, 2H, Ar-H), 7.36 (s, 1H, Ar-H), 7.02 (d, *J* = 8.8 Hz, 2H, Ar-H), 4.11 – 4.01 (m, 8H, OCH$_2$CH$_2$), 1.90 – 1.74 (m, 8H, OCH$_2$CH$_2$), 1.56 – 1.43 (m, 8H, CH$_2$), 1.41 – 1.24 (m, 26H, CH$_2$), 0.96 – 0.86 (m, 12H, CH$_3$). ^{13}C NMR (126 MHz, CDCl$_3$) δ 164.69, 158.96 (C=O), 152.27, 151.48, 150.37, 146.36, 143.22, 143.10, 138.71, 138.24, 137.38, 133.68, 133.09, 132.92, 132.36, 131.64, 128.37, 128.28, 126.24, 124.47, 124.21, 122.31, 122.08, 121.73, 121.70, 114.97, 111.35, 110.38 (BTBT-C + Ar-C), 74.18, 74.12, 69.23, 68.17 (OCH$_2$), 31.89, 31.65, 31.50, 30.23, 30.14, 29.60, 29.57, 29.40, 29.32, 29.29, 29.16, 26.05, 25.71, 25.69, 25.65, 22.67, 22.62, 22.56 (CH$_2$), 14.09, 14.04, 14.02, 13.97 (CH$_3$); HRMS (m/z): [M]+Li$^+$ calcd. for C$_{62}$H$_{77}$BrO$_6$S$_2$Li, 1067.450; found 1067.453.

2-[4-(2-Bromo-3,4,5-tri-n-hexyloxybenzoyloxy)phenyl]-7-(4-dodecyloxyphenyl)-[1]benzothieno[3,2-b]benzothiophene (B12)

Synthesized by dissolving **11a** (120 mg, 0.13 mmol), 1-bromododecane (100 mg, 0.4 mmol) in butanone (50 ml) with K$_2$CO$_3$ (200 mg, 1.45 mmol) and TBAI (20 mg, 0.054 mmol); yield 35 mg (0.033 mmol, 25%); ^{1}H NMR (500 MHz, CDCl$_3$) δ 8.11 (dd, J = 18.3, 1.0 Hz, 2H, BTBT-H), 7.94 (dd, J = 11.4, 8.2 Hz, 2H, BTBT-H), 7.75 (d, J = 8.8 Hz, 2H, Ar-H), 7.69 (ddd, J = 11.8, 8.3, 1.6 Hz, 2H, BTBT-H), 7.62 (d, J = 8.8 Hz, 2H, Ar-H), 7.38 (d, J = 8.7 Hz, 2H, Ar-H), 7.36 (s, 1H, Ar-H), 7.02 (d, J = 8.8 Hz, 2H, Ar-H), 4.11 – 4.01 (m, 8H, OCH$_2$CH$_2$), 1.90 – 1.75 (m, 8H, OCH$_2$CH$_2$), 1.57 – 1.45 (m, 8H, CH$_2$), 1.41 – 1.23 (m, 28H, CH$_2$), 0.96 – 0.86 (m, 12H, CH$_3$). ^{13}C NMR (126 MHz, CDCl$_3$) δ 164.71, 158.97 (C=O), 152.29, 151.49, 150.38, 146.37, 143.23, 143.12, 138.72, 138.26, 137.40, 133.69, 133.11, 132.94, 132.37, 131.65, 128.39, 128.29, 126.25, 124.48, 124.22, 122.33, 122.10, 121.75, 121.71, 114.98, 111.36, 110.39 (BTBT-C + Ar-C), 74.20, 74.13, 69.24, 68.18 (OCH$_2$), 31.91, 31.66, 31.51, 30.24, 30.15, 29.63, 29.60, 29.41, 29.34, 29.30, 29.17, 26.06, 25.72, 25.70, 25.67, 22.68, 22.63, 22.58 (CH$_2$), 14.10, 14.05, 14.03, 13.99 (CH$_3$); HRMS (m/z): [M]+Li$^+$ calcd. for C$_{63}$H$_{79}$BrO$_6$S$_2$Li, 1081.466; found 1081.471.

2-[4-(2-Bromo-3,4,5-tri-n-hexyloxybenzoyloxy)phenyl]-7-(4-tetradecyloxyphenyl)-[1]benzothieno[3,2-b]benzothiophene (B14)

Synthesized by dissolving **11a** (120 mg, 0.13 mmol), 1-bromotetradecane (110 mg, 0.4 mmol) in butanone (50 ml) with K$_2$CO$_3$ (200 mg, 1.45 mmol) and TBAI (20 mg, 0.054 mmol); yield 60 mg (0.054 mmol, 41%); ^{1}H NMR (400 MHz, CDCl$_3$) δ 8.11 (dd, J = 14.6, 1.7 Hz, 2H, BTBT-H), 7.94 (dd, J = 9.1, 8.5 Hz, 2H, BTBT-H), 7.75 (d, J = 8.6 Hz, 2H, Ar-H), 7.69 (ddd, J = 9.6, 8.2, 1.5 Hz, 2H, BTBT-H), 7.62 (d, J = 8.6 Hz, 2H, Ar-H), 7.38 (d, J = 8.7 Hz, 2H, Ar-H), 7.36 (s, 1H, Ar-H),

7.02 (d, J = 8.8 Hz, 2H, Ar-H), 4.11 – 4.01 (m, 8H, OCH$_2$CH$_2$), 1.90 – 1.74 (m, 8H, OCH$_2$CH$_2$), 1.57 – 1.45 (m, 8H, CH$_2$), 1.41 – 1.23 (m, 32H, CH$_2$), 0.95 – 0.86 (m, 12H, CH$_3$). ^{13}C NMR (101 MHz, CDCl$_3$) δ 164.70 (C=O), 145.80, 145.80, 143.70, 143.37, 142.66, 137.38, 133.10, 128.38, 128.29, 124.22, 122.79, 122.32, 122.09, 121.99, 121.74, 121.71, 119.27, 114.97, 111.37 (BTBT-C + Ar-C), 74.13, 69.22, 68.17 (OCH$_2$), 31.91, 31.65, 31.63, 30.23, 30.14, 29.67, 29.66, 29.65, 29.64, 29.59, 29.57, 29.40, 29.34, 29.28, 29.15, 26.06, 26.05, 25.71, 25.69, 25.68, 25.66, 22.67, 22.62, 22.57 (CH$_2$), 14.09, 14.04, 13.98 (CH$_3$); HRMS (m/z): [M]+Li$^+$ calcd. for C$_{65}$H$_{83}$BrO$_6$S$_2$Li, 1109.497; found 1109.502.

2-[4-(2-Bromo-3,4,5-tri-n-hexyloxybenzoyloxy)phenyl]-7-(4-octadecyloxyphenyl)-[1]benzothieno[3,2-b]benzothiophene (B18)

Synthesized by dissolving **11a** (120 mg, 0.13 mmol), 1-bromooctadecane (135 mg, 0.4 mmol) in butanone (50 ml) with K$_2$CO$_3$ (200 mg, 1.45 mmol) and TBAI (20 mg, 0.054 mmol); yield 55 mg (0.047 mmol, 36%); ^{1}H NMR (400 MHz, CDCl$_3$) δ 8.11 (dd, J = 14.6, 1.1 Hz, 2H, BTBT-H), 7.94 (dd, J = 9.1, 8.4 Hz, 2H, BTBT-H), 7.75 (d, J = 8.7 Hz, 2H, Ar-H), 7.69 (ddd, J = 9.6, 8.4, 1.6 Hz, 2H, BTBT-H), 7.62 (d, J = 8.7 Hz, 2H, Ar-H), 7.38 (d, J = 8.6 Hz, 2H, Ar-H), 7.36 (s, 1H, Ar-H), 7.02 (d, J = 8.8 Hz, 2H, Ar-H), 4.12 – 3.99 (m, 8H, OCH$_2$CH$_2$), 1.90 – 1.74 (m, 8H, OCH$_2$CH$_2$), 1.58 – 1.44 (m, 8H, CH$_2$), 1.42 – 1.21 (m, 40H, CH$_2$), 0.96 – 0.83 (m, 12H, CH$_3$). ^{13}C NMR (101 MHz, CDCl$_3$) δ 164.70, 158.95(C=O), 152.27, 151.48, 150.36, 146.35, 143.21, 143.10, 138.24, 137.38, 133.68, 128.38, 128.28, 126.23, 124.47, 124.21, 122.32, 122.09, 121.74, 121.70, 114.96, 111.34 (BTBT-C + Ar-C), 74.19, 74.12, 69.22, 68.16 (OCH$_2$), 31.91, 31.65, 31.50, 30.23, 30.14, 29.68, 29.64, 29.59, 29.57, 29.40, 29.34, 29.29, 29.15, 26.05, 25.71, 25.66, 22.67, 22.63, 22.57 (CH$_2$), 14.09, 14.04, 14.03, 13.98 (CH$_3$); HRMS (m/z): [M]+Li$^+$ calcd. for C$_{69}$H$_{91}$BrO$_6$S$_2$Li, 1165.560; found 1165.562.

2-[4-(2-Bromo-3,4,5-tri-n-hexyloxybenzoyloxy)phenyl]-7-(4-docosyloxyphenyl)-[1]benzothieno[3,2-b]benzothiophene (B22)

Synthesized by dissolving **11a** (120 mg, 0.13 mmol), 1-bromodocosane (155 mg, 0.4 mmol) in butanone (50 ml) with K$_2$CO$_3$ (200 mg, 1.45 mmol) and TBAI (20 mg, 0.054 mmol); yield 45 mg (0.037 mmol, 28%); ^{1}H NMR (400 MHz, CDCl$_3$) δ 8.11 (dd, J = 14.7, 1.1 Hz, 2H, BTBT-H), 7.94 (dd, J = 9.2, 8.4 Hz, 2H, BTBT-H), 7.75 (d, J = 8.7 Hz, 2H, Ar-H), 7.69 (ddd, J = 9.6, 8.4, 1.6 Hz, 2H, BTBT-H), 7.62 (d, J = 8.8 Hz, 2H, Ar-H), 7.38 (d, J = 8.6 Hz, 2H, Ar-H), 7.36 (s, 1H, Ar-H), 7.02 (d, J = 8.8 Hz, 2H, Ar-H), 4.12 – 4.00 (m, 8H, OCH$_2$CH$_2$), 1.90 – 1.74 (m, 8H, OCH$_2$CH$_2$), 1.58 – 1.45 (m, 8H, CH$_2$), 1.42 – 1.23 (m, 48H, CH$_2$), 0.95 – 0.85 (m, 12H, CH$_3$). ^{13}C NMR (101 MHz, CDCl$_3$) δ 158.96 (C=O), 152.27, 151.48, 138.69, 138.24, 131.64, 130.04, 128.38, 128.29, 124.47, 124.21, 122.32, 122.09, 121.74, 121.70, 114.97, 110.37 (BTBT-C + Ar-C), 74.19, 74.12, 69.22, 68.16 (OCH$_2$), 31.90, 31.65, 31.50, 30.23, 29.68, 29.59, 29.57, 29.34, 29.28, 26.05, 25.71, 25.69, 25.66, 22.67, 22.57 (CH$_2$), 14.09, 14.04, 14.03, 13.98 (CH$_3$); HRMS (m/z): [M]+Li$^+$ calcd. for C$_{73}$H$_{99}$BrO$_6$S$_2$Li, 1221.622; found 1221.628.

11.2.3 Representative NMR and HRMS spectra
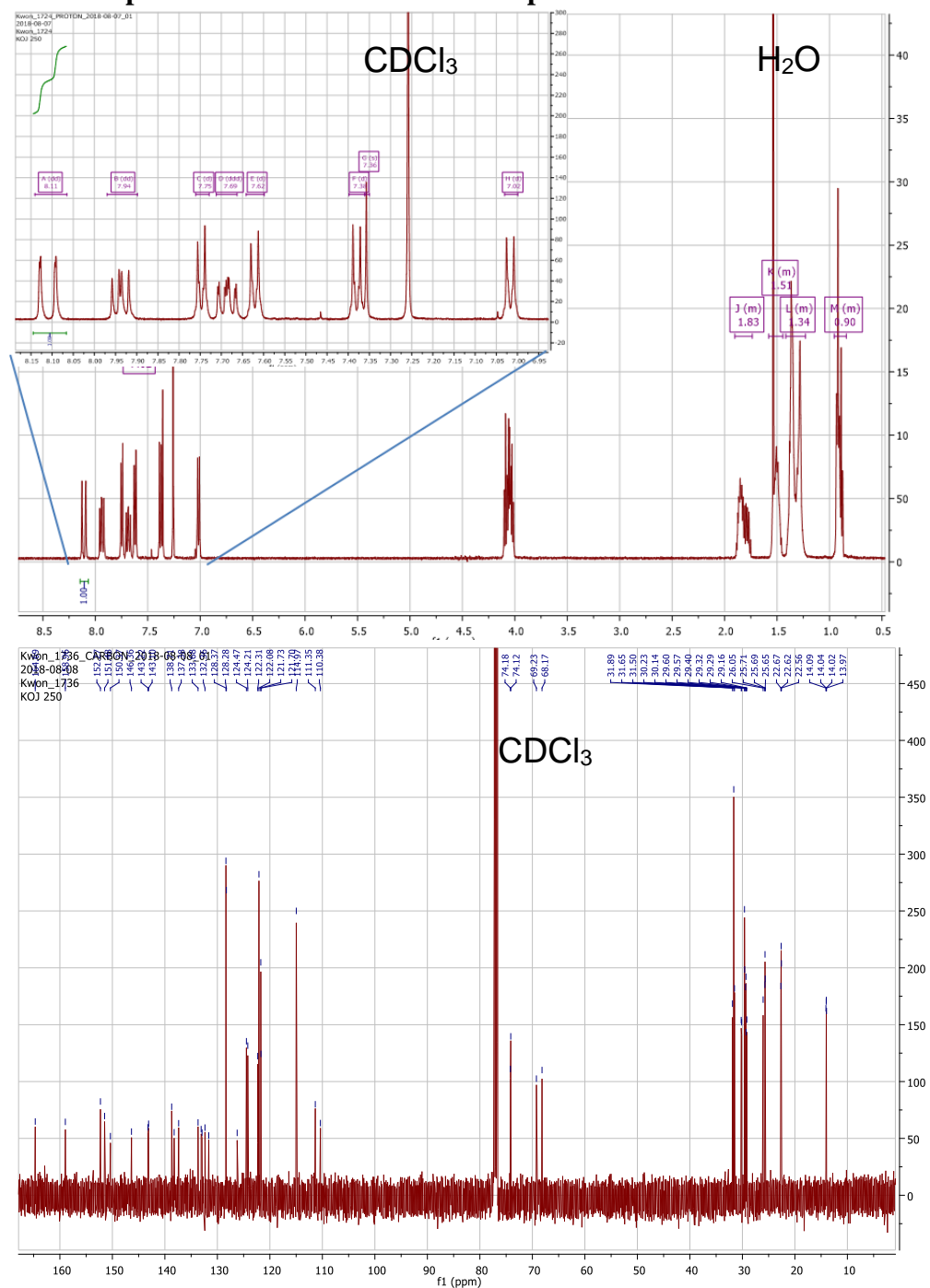
Figure 11.1 ^{1}H- and ^{13}C-NMR of compound **B11**. The spectra were measured at 27 °C, with the frequencies 500 MHz (^{1}H) and 126 MHz (^{13}C) in CDCl$_3$ as solvent
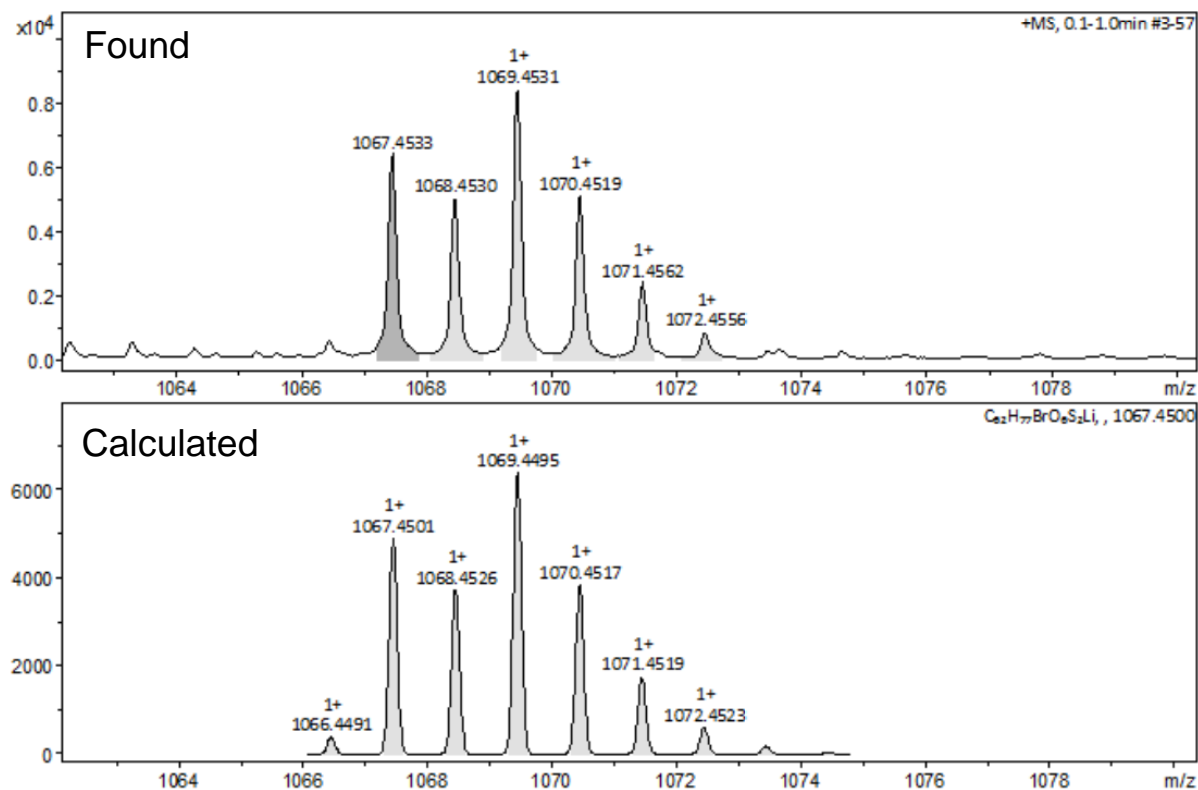
Figure 11.2 HRMS spectra for **B11**.

11.3 Synthesis and analytical data of the 3,4,5-trihexyloxybenzoates H*n* and the 2,6-dibromo-3,4,5-trihexyloxybenzoates BB*n*

The synthesis was performed according to schemes 2.2-2.4.

11.3.1 Synthesis and analytical data of intermediates

2,7- Dibromo [1]Benzothieno[3,2-b]benzothiophene (3)
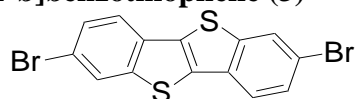
1 (5.00 g, 0.021 mol) was dissolved in DCM (300 ml). Bromine (7.20 g, 0.045 mol) with DCM was prepared in a dropping funnel and added dropwise to the solution. The mixture was stirred for 48h at RT. The reaction was quenched by adding $Na_2S_2O_3$ solution. The crude product was filtered and washed with H_2O. Then, it was purified by extraction in a Soxhlet apparatus using DCM as solvent. The final product was recrystallized in the cold DCM; [S7] yield 4.1 g (0.0095 mol, 46%); colorless solid; m.p. 299 °C; ^{1}H NMR (400 MHz, $CDCl_3$) δ 8.06 (d, J = 1.7 Hz, 2H), 7.73 (d, J = 8.5 Hz, 2H), 7.58 (dd, J = 8.5, 1.7 Hz, 2H).

2-[4-(3,4,5-Tri-n-hexyloxybenzoyloxy)phenyl]-7-bromo-[1]benzothieno[3,2-b]benzothiophene (10a)
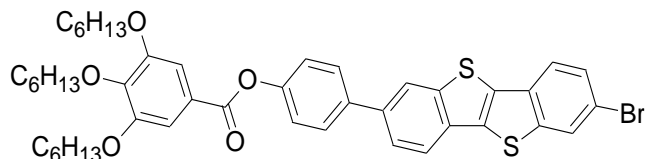
Suzuki coupling reaction was used.[S6] In two-neck flask, **7a** (2.19 g, 3.50 mmol) **3** (1.59 g, 4.00 mmol), THF (50 ml), toluene (100 ml) and saturated NaHCO$_3$ solution (70 ml) were prepared, and degassed with argon for 15 minutes. After purging, [Pd(PPh$_3$)$_4$] (0.1 g, 0.0865 mmol) was added. The solution was refluxed for 6 hours. When the mixture was cooled down, the organic phase was extracted with Toluene. Then, it was dried over Na$_2$SO$_4$. After it was concentrated in vacuum, it was purified by column chromatography (eluent: CHCl$_3$/n-hexane 2/1); yield 1.20 g (1.47 mmol, 42 %) colorless solid; heating: Cr 128 SmA 150 Iso (°C); cooling: Iso 141 SmA 88 Cr (°C); ^{1}H NMR (500 MHz, CDCl$_3$) δ 8.10 (dd, *J* = 26.4, 1.2 Hz, 2H, BTBT-H), 7.94 (tdd, *J* = 28.3, 8.1, 0.6 Hz, 2H, BTBT-H), 7.77 – 7.69 (m, 3H, BTBT-H + Ar-H), 7.58 (dd, *J* = 8.4, 1.7 Hz, 1H, BTBT-H), 7.44 (s, 2H, Ar-H), 7.34 – 7.31 (m, 2H, Ar-H), 4.12 – 4.05 (m, 6H, OCH$_2$CH$_2$), 1.89 – 1.75 (m, 6H, OCH$_2$CH$_2$), 1.56 – 1.48 (m, 6H, CH$_2$), 1.41 – 1.32 (m, 12H, CH$_2$), 0.95 – 0.89 (m, 9H, CH$_3$).

2-[4-(3,4,5-Tri-n-hexyloxybenzoyloxy)phenyl]-7-(4-hydroxyphenyl)-[1]benzothieno[3,2-b]benzothiophene (11a)
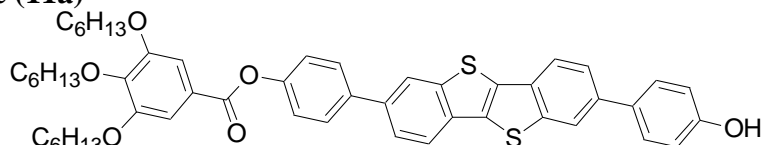
The same procedure for **10a** was used. **10a** (1.20 g, 1.47 mmol), 4-hydroxyphenylboronic acid pinacol ester (0.33 g, 1.50 mmol), THF (100 ml) and saturated NaHCO$_3$ solution (50 ml), column chromatography (eluent: CHCl$_3$/MeOH 19/1); yield 0.65 g (0.785 mmol, 53 %); colorless solid; heating: Cr 215 SmA 238 Iso (°C); cooling: Iso 236 SmA 179 Cr (°C); ^{1}H NMR (400 MHz, CDCl$_3$) δ 8.04 (dd, *J* = 38.3, 0.4 Hz, 2H, BTBT-H), 7.96 – 7.84 (m, 2H, BTBT-H), 7.73 (d, *J* = 8.6 Hz, 2H, Ar-H), 7.70 – 7.58 (m, 2H, BTBT-H), 7.51 (d, *J* = 10.0 Hz, 1H, BTBT-H), 7.46 (s, 2H, Ar-H), 7.32 (d, *J* = 8.6 Hz, 2H, Ar-H), 6.89 (d, *J* = 8.4 Hz, 2H, Ar-H), 5.14 (s, 1H, Ar-OH), 4.14 – 4.01 (m, 6H, OCH$_2$CH$_2$), 1.91 – 1.73 (m, 6H, OCH$_2$CH$_2$), 1.63 – 1.44 (m, 6H, CH$_2$), 1.43 – 1.29 (m, 12H, CH$_2$), 0.97 – 0.87 (m, 9H, CH$_3$).

2-[4-(2,6-Dibromo-3,4,5-tri-n-hexyloxybenzoyloxy)phenyl]-7-bromo-[1]benzothieno[3,2-b]benzothiophene (10c)
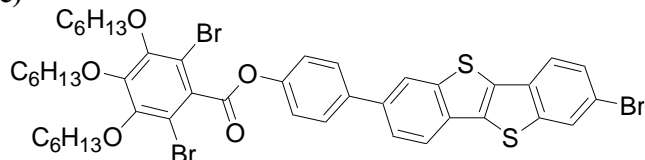
The same procedure for **BTBT-Br** was used. **2** (1.20 g, 1.63 mmol), bromine (0.910 g, 5.71 mmol), DCM (60 ml), reaction time 72 h, RT, column chromatography (eluent: CHCl$_3$/n-hexane 2/1); yield 1.00 g (1.027 mmol, 63 %); colorless gel; ^{1}H NMR (500 MHz, CDCl$_3$) δ 8.08 (dd, *J* = 17.3, 1.6 Hz, 2H, BTBT-H), 8.04 (d, *J* = 1.4 Hz, 1H, BTBT-H), 7.86 (d, *J* = 1.4 Hz, 1H, BTBT-H), 7.74 – 7.70 (m, 3H, BTBT-H + Ar-H), 7.60 – 7.57 (m, 1H, BTBT-H), 7.46 (d, *J* = 8.7 Hz, 2H, Ar-H),

4.10 – 4.04 (m, 6H, OCH$_2$CH$_2$), 1.87 – 1.75 (m, 6H, OCH$_2$CH$_2$), 1.58 – 1.45 (m, 6H, CH$_2$), 1.41 – 1.20 (m, 12H, CH$_2$), 0.97 – 0.85 (m, 9H, CH$_3$).

2-[4-(2,6-Dibromo-3,4,5-tri-n-hexyloxybenzoyloxy)phenyl]-7-(4-hydroxyphenyl)-[1]benzothieno[3,2-b]benzothiophene (11c)
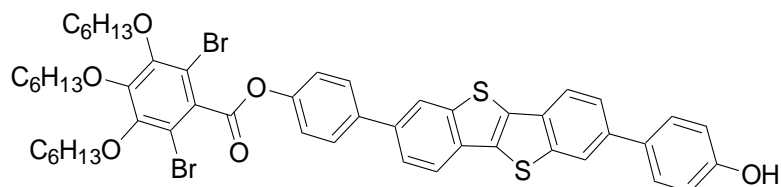
The same procedure for **10a** was used. **10c** (1.00 g, 1.03 mmol), 4-hydroxyphenylboronic acid pinacol ester (0.24 g, 1.10 mmol), THF (100 ml) and saturated NaHCO$_3$ solution (50 ml), column chromatography (eluent: CHCl$_3$/MeOH 19/1); yield 0.67 g (0.679 mmol, 66 %); colorless solid; heating: Cr 210 Iso (°C); cooling: Iso 205 SmA 190 Cr (°C); 1H NMR (400 MHz, CDCl3) δ 8.09 (dd, J = 20.1, 1.1 Hz, 2H, BTBT-H), 7.93 (dd, J = 10.4, 8.2 Hz, 2H, BTBT-H), 7.75 (d, J = 8.7 Hz, 2H, Ar-H), 7.67 (ddd, J = 16.0, 8.3, 1.6 Hz, 2H, BTBT-H), 7.58 (d, J = 8.7 Hz, 2H, Ar-H), 7.46 (d, J = 8.7 Hz, 2H, Ar-H), 6.94 (d, J = 8.7 Hz, 2H, Ar-H), 4.84 (s, 1H, Ar-OH), 4.07 (t, J = 6.6 Hz, 6H, OCH2CH2), 1.88 – 1.74 (m, 6H, OCH2CH2), 1.57 – 1.45 (m, 6H, CH2), 1.41 – 1.33 (m, 12H, CH2), 0.93 (t, J = 7.0 Hz, 9H, CH3).

11.3.2 Synthesis and analytical data of the compounds (H8 – H12)
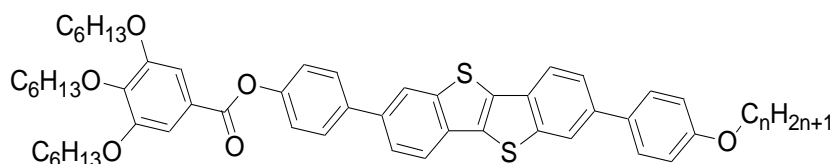
Williamson ether synthesis was used for the final step. **11a** (120 mg, 0.145 mmol), K$_2$CO$_3$ (200 mg, 1.45 mmol), TBAI (20 mg, 0.062 mmol), 1-bromoalkane (0.43 mmol) are prepared in butanone (50 ml). The solution is refluxed for 5 hours. Butanone was removed via rotary evaporator and the crude product was puri2ied via liquid column chromatography with (chloroform/n-hexane 2/1). Then, recrystallization from THF/EtOH is repeated.

2-[4-(3,4,5-Tri-n-hexyloxybenzoyloxy)phenyl]-7-(4-octyloxyphenyl)-[1]benzothieno[3,2-b]benzothiophene (H8)

11a (100 mg, 0.12 mmol), K$_2$CO$_3$ (200 mg, 1.45 mmol), TBAI (20 mg, 0.054 mmol), 1-bromooctane (70 mg, 0.36 mmol) and butanone (50 ml); yield 30 mg (0.032 mmol, 26%); colorless solid; M = 941.33 g mol^{-1}; ^{1}H NMR (500 MHz, CDCl$_3$) δ 8.12 (dd, J = 22.5, 0.9 Hz, 2H, BTBT-H), 7.94 (dd, J = 12.0, 8.2 Hz, 2H, BTBT-H), 7.75 (d, J = 8.6 Hz, 2H, Ar-H), 7.69 (ddd, J = 16.7, 8.3, 1.4 Hz, 2H, BTBT-H), 7.62 (d, J = 8.7 Hz, 2H, Ar-H), 7.45 (s, 2H, Ar-H), 7.33 (d, J = 8.6 Hz, 2H, Ar-H), 7.02 (d, J = 8.7 Hz, 2H, Ar-H), 4.11 – 4.01 (m, 8H, OCH$_2$CH$_2$), 1.89 – 1.74 (m, 8H, OCH$_2$CH$_2$), 1.58 – 1.44 (m, 8H, CH$_2$), 1.42 – 1.25 (m, 20H, CH$_2$), 0.94 – 0.87 (m, 12H, CH$_3$); ^{13}C NMR (126 MHz, CDCl$_3$) δ 165.05, 158.95 (C=O), 152.98, 150.64, 143.21, 143.10, 138.44, 138.23, 137.43, 133.65, 133.10, 132.92, 132.33, 131.64, 128.34, 128.28, 124.46, 124.21, 123.81, 122.30, 122.23, 121.72, 121.69, 114.97, 108.64 (BTBT-C + Ar-C), 73.58, 69.30, 68.16 (OCH$_2$), 31.81, 31.71, 31.54, 30.28, 29.36, 29.29, 29.26, 29.23, 26.06, 25.73, 25.69, 22.66, 22.65, 22.59 (CH$_2$),

14.08, 14.06, 14.00 (CH$_3$); HRMS (m/z): [M]+Li$^+$ calcd. for C$_{59}$H$_{72}$O$_6$S$_2$Li, 947.493; found 947.501.

2-[4-(3,4,5-Tri-n-hexyloxybenzoyloxy)phenyl]-7-(4-nonyloxyphenyl)-[1]benzothieno[3,2-b]benzothiophene (H9)

11a (100 mg, 0.12 mmol), K$_2$CO$_3$ (200 mg, 1.45 mmol), TBAI (20 mg, 0.054 mmol), 1-bromononane (75 mg, 0.36 mmol) and butanone (50 ml); yield 40 mg (0.042 mmol, 35%); colorless solid; M = 955.36 g mol^{-1}; ^{1}H NMR (500 MHz, CDCl$_3$) δ 8.11 (dd, *J* = 22.7, 1.1 Hz, 2H, BTBT-H), 7.94 (dd, *J* = 12.1, 8.3 Hz, 2H, BTBT-H), 7.75 (d, *J* = 8.7 Hz, 2H, Ar-H), 7.69 (ddd, *J* = 16.7, 8.3, 1.6 Hz, 2H, BTBT-H), 7.62 (d, *J* = 8.8 Hz, 2H, Ar-H), 7.45 (s, 2H, Ar-H), 7.33 (d, *J* = 8.7 Hz, 2H, Ar-H), 7.02 (d, *J* = 8.8 Hz, 2H, Ar-H), 4.10 – 4.01 (m, 8H, OCH$_2$CH$_2$), 1.89 – 1.74 (m, 8H, OCH$_2$CH$_2$), 1.56 – 1.45 (m, 8H, CH$_2$), 1.40 – 1.27 (m, 22H, CH$_2$), 0.94 – 0.88 (m, 12H, CH$_3$); ^{13}C NMR (126 MHz, CDCl$_3$) δ 165.06, 158.96 (C=O), 152.98, 150.65, 143.22, 143.11, 138.45, 138.23, 137.43, 133.66, 133.11, 132.33, 131.65, 128.35, 128.29, 124.46, 124.22, 123.82, 122.31, 122.24, 121.74, 121.70, 114.97, 108.65 (BTBT-C + Ar-C), 73.59, 69.31, 68.17 (OCH$_2$), 31.87, 31.72, 31.54, 30.29, 29.54, 29.41, 29.30, 29.26, 26.06, 25.74, 25.69, 22.66, 22.60 (CH$_2$), 14.09, 14.06, 14.00 (CH$_3$); HRMS (m/z): [M]+Li$^+$ calcd. for C$_{60}$H$_{74}$O$_6$S$_2$Li, 961.508; found 961.513.

2-[4-(3,4,5-Tri-n-hexyloxybenzoyloxy)phenyl]-7-(4-decyloxyphenyl)-[1]benzothieno[3,2-b]benzothiophene (H10)

11a (100 mg, 0.12 mmol), K$_2$CO$_3$ (200 mg, 1.45 mmol), TBAI (20 mg, 0.054 mmol), 1-bromodecane (80 mg, 0.36 mmol) and butanone (50 ml); yield 33 mg (0.034 mmol, 28%); colorless solid; M = 969.38 g mol^{-1}; ^{1}H NMR (500 MHz, CDCl$_3$) δ 8.11 (dd, *J* = 22.7, 0.9 Hz, 2H, BTBT-H), 7.93 (dd, *J* = 12.0, 8.2 Hz, 2H, BTBT-H), 7.75 (d, *J* = 8.6 Hz, 2H, Ar-H), 7.69 (ddd, *J* = 16.7, 8.3, 1.5 Hz, 2H, BTBT-H), 7.62 (d, *J* = 8.7 Hz, 2H, Ar-H), 7.45 (s, 2H, Ar-H), 7.33 (d, *J* = 8.6 Hz, 2H, Ar-H), 7.02 (d, *J* = 8.7 Hz, 2H, Ar-H), 4.11 – 4.00 (m, 8H, OCH$_2$CH$_2$), 1.89 – 1.75 (m, 8H, OCH$_2$CH$_2$), 1.57 – 1.45 (m, 8H, CH$_2$), 1.41 – 1.23 (m, 24H, CH$_2$), 0.95 – 0.87 (m, 12H, CH$_3$); ^{13}C NMR (126 MHz, CDCl$_3$) δ 165.05, 158.95 (C=O), 152.98, 150.64, 143.21, 143.10, 138.44, 138.22, 137.42, 133.65, 133.10, 132.92, 132.32, 131.64, 128.34, 128.28, 124.45, 124.21, 123.81, 122.30, 122.23, 121.73, 121.69, 114.97, 108.64 (BTBT-C + Ar-C), 73.58, 69.30, 68.16 (OCH$_2$), 31.89, 31.71, 31.54, 30.28, 29.58, 29.55, 29.40, 29.31, 29.29, 29.26, 26.06, 25.74, 25.69, 22.66, 22.60 (CH$_2$), 14.09, 14.06, 14.00 (CH$_3$); HRMS (m/z): [M]+Li$^+$ calcd. for C$_{61}$H$_{76}$O$_6$S$_2$Li, 975.524; found 975.531.

2-[4-(3,4,5-Tri-n-hexyloxybenzoyloxy)phenyl]-7-(4-undecyloxyphenyl)-[1]benzothieno[3,2-b]benzothiophene (H11)

11a (100 mg, 0.12 mmol), K$_2$CO$_3$ (200 mg, 1.45 mmol), TBAI (20 mg, 0.054 mmol), 1-bromoundecane (85 mg, 0.36 mmol) and butanone (50 ml); yield 45 mg (0.046 mmol, 38%); colorless solid; M = 983.41 g mol^{-1} ^{1}H NMR (400 MHz, CDCl$_3$) δ 8.12 (dd, *J* = 18.1, 1.2 Hz, 2H, BTBT-H), 7.94 (dd, *J* = 9.4, 8.6 Hz, 2H, BTBT-H), 7.75 (d, *J* = 8.6 Hz, 2H, Ar-H), 7.69 (ddd, *J* = 13.3, 8.3, 1.6 Hz, 2H, BTBT-H), 7.62 (d, *J* = 8.7 Hz, 2H, Ar-H), 7.45 (s, 2H, Ar-H), 7.33 (d, *J* = 8.6 Hz, 2H, Ar-H), 7.02 (d, *J* = 8.7 Hz, 2H, Ar-H), 4.10 – 4.00 (m, 8H, OCH$_2$CH$_2$), 1.89 – 1.74 (m, 8H, OCH$_2$CH$_2$), 1.59 – 1.44 (m, 8H, CH$_2$), 1.41 – 1.24 (m, 26H, CH$_2$), 0.96 – 0.85 (m, 12H, CH$_3$); ^{13}C NMR (101 MHz, CDCl$_3$) δ 165.05, 158.96 (C=O), 152.98, 150.64, 143.21, 143.10,

138.23, 137.43, 133.66, 133.10, 132.92, 131.64, 128.34, 128.28, 124.46, 124.21, 123.81, 122.30, 122.23, 121.74, 121.73, 121.70, 114.97, 108.64 (BTBT-C + Ar-C), 73.58, 69.30, 68.16 (OCH$_2$), 31.90, 31.71, 31.54, 30.28, 29.61, 29.60, 29.57, 29.40, 29.32, 29.29, 29.26, 26.05, 25.74, 25.69, 22.67, 22.60 (CH$_2$), 14.09, 14.06, 14.00 (CH$_3$); HRMS (m/z): [M]+Li$^+$ calcd. for C$_{62}$H$_{78}$O$_6$S$_2$Li, 989.540; found 989.542.

2-[4-(3,4,5-Tri-n-hexyloxybenzoyloxy)phenyl]-7-(4-dodecyloxyphenyl)-[1]benzothieno[3,2-b]benzothiophene (H12)

H-OH (100 mg, 0.12 mmol), K$_2$CO$_3$ (200 mg, 1.45 mmol), TBAI (20 mg, 0.054 mmol), 1-bromododecane (90 mg, 0.36 mmol) and butanone (50 ml); yield 38 mg (0.038 mmol, 31%); colorless solid; M = 997.44 g mol^{-1}; ^{1}H NMR (500 MHz, CDCl$_3$) δ 8.12 (dd, J = 22.7, 1.4 Hz, 2H, BTBT-H), 7.94 (dd, J = 12.1, 8.3 Hz, 2H, BTBT-H), 7.75 (d, J = 8.6 Hz, 2H, Ar-H), 7.69 (ddd, J = 16.7, 8.2, 1.5 Hz, 2H, BTBT-H), 7.62 (d, J = 8.6 Hz, 2H, Ar-H), 7.45 (s, 2H, Ar-H), 7.33 (d, J = 8.5 Hz, 2H, Ar-H), 7.02 (d, J = 8.7 Hz, 2H, Ar-H), 4.10 – 4.01 (m, 8H, OCH$_2$CH$_2$), 1.88 – 1.75 (m, 8H, OCH$_2$CH$_2$), 1.54 – 1.46 (m, 8H, CH$_2$), 1.40 – 1.25 (m, 28H, CH$_2$), 0.94 – 0.87 (m, 12H, CH$_3$); ^{13}C NMR (101 MHz, CDCl$_3$) δ 165.05, 158.96 (C=O), 152.98, 150.65, 143.21, 143.11, 143.10, 138.45, 138.23, 137.90, 137.85, 137.43, 133.66, 133.25, 132.92, 132.48, 132.33, 132.09, 129.56, 128.34, 128.29, 124.52, 124.46, 124.21, 123.81, 122.31, 122.24, 121.74, 121.72, 121.70, 114.97, 108.64 (BTBT-C + Ar-C), 73.58, 69.30, 68.17 (OCH$_2$), 31.91, 31.71, 31.54, 30.28, 29.65, 29.62, 29.59, 29.40, 29.33, 29.29, 29.26, 26.06, 25.74, 25.69, 22.66, 22.60 (CH$_2$), 14.10, 14.06, 14.00 (CH$_3$); HRMS (m/z): [M]+Li$^+$ calcd. for C$_{63}$H$_{80}$O$_6$S$_2$Li, 1003.555; found 1003.565.

11.3.3 The synthesis and analytical data of the compounds (BB7, BB9 – BB12)

The same procedure for **H8**-**H12** was used.

2-[4-(2,6-dibromo-3,4,5-tri-n-hexyloxybenzoyloxy)phenyl]-7-(4-heptyloxyphenyl)-[1]benzothieno[3,2-b]benzothiophene (BB7)

BB-OH (120 mg, 0.12 mmol), K$_2$CO$_3$ (200 mg, 1.45 mmol), TBAI (20 mg, 0.054 mmol), 1-bromoheptane (65 mg, 0.37 mmol) and butanone (50 ml); yield 72 mg (0.066 mmol, 55%); colorless solid; M =1085.09 g mol^{-1}; ^{1}H NMR (400 MHz, CDCl$_3$) δ 8.11 (dd, J = 11.8, 1.2 Hz, 2H, BTBT-H), 7.94 (dd, J = 9.0, 8.5 Hz, 2H, BTBT-H), 7.76 (d, J = 8.7 Hz, 2H, Ar-H), 7.68 (ddd, J = 8.4, 6.8, 1.6 Hz, 2H, BTBT-H), 7.62 (d, J = 8.8 Hz, 2H, Ar-H), 7.46 (d, J = 8.6 Hz, 2H, Ar-H), 7.02 (d, J = 8.8 Hz, 2H, Ar-H), 4.10 – 4.01 (m, 8H, OCH$_2$CH$_2$), 1.88 – 1.74 (m, 8H, OCH$_2$CH$_2$), 1.56 – 1.43 (m, 8H, CH$_2$), 1.42 – 1.30 (m, 18H, CH$_2$), 0.96 – 0.88 (m, 12H, CH$_3$); ^{13}C NMR (101 MHz, CDCl$_3$) δ 164.41, 158.95 (C=O), 150.96, 148.57, 143.22, 143.10, 139.18, 138.24, 133.71, 132.92, 132.40, 132.37, 131.63, 128.50, 128.29, 124.51, 124.21, 122.36, 121.94, 121.74, 121.71, 114.97, 109.96 (BTBT-C + Ar-C), 74.62, 74.45, 68.16 (OCH$_2$), 31.78, 31.61, 30.14, 29.29, 29.07, 26.02, 25.64, 25.63, 22.60 (CH$_2$), 14.07, 14.03, 14.00 (CH$_3$); HRMS (m/z): [M]+Li$^+$ calcd. for C$_{58}$H$_{68}$Br$_2$O$_6$S$_2$Li, 1089.298; found 1089.309.

2-[4-(2,6-Dibromo-3,4,5-tri-n-hexyloxybenzoyloxy)phenyl]-7-(4-nonyloxyphenyl)-[1]benzothieno[3,2-b]benzothiophene (BB9)

BB-OH (120 mg, 0.12 mmol), K_2CO_3 (200 mg, 1.45 mmol), TBAI (20 mg, 0.054 mmol), 1-bromononane (75 mg, 0.37 mmol) and butanone (50 ml); yield 48 mg (0.043 mmol, 35%); colorless solid; M = 1113.15 g mol^{-1};^{1}H NMR (400 MHz, CDCl$_3$) δ 8.11 (dd, J = 11.8, 1.4 Hz, 2H, BTBT-H), 7.94 (dd, J = 9.0, 8.6 Hz, 2H, BTBT-H), 7.76 (d, J = 8.6 Hz, 2H, Ar-H), 7.68 (ddd, J = 8.4, 7.0, 1.5 Hz, 2H, BTBT-H), 7.62 (d, J = 8.6 Hz, 2H, Ar-H), 7.46 (d, J = 8.6 Hz, 2H, Ar-H), 7.02 (d, J = 8.7 Hz, 2H, Ar-H), 4.10 – 4.01 (m, 8H, OCH$_2$CH$_2$), 1.88 – 1.74 (m, 8H, OCH$_2$CH$_2$), 1.56 – 1.44 (m, 8H, CH$_2$), 1.41 – 1.26 (m, 22H, CH$_2$), 0.96 – 0.87 (m, 12H, CH$_3$);^{13}C NMR (101 MHz, CDCl$_3$) δ 164.42, 159.95 (C=O), 150.96, 150.96, 150.07, 148.57, 143.10, 139.18, 138.25, 137.35, 133.09, 132.92, 132.40, 131.63, 128.50, 128.29, 124.51, 124.22, 122.36, 121.94, 121.75, 121.71, 121.70, 114.97, 109.96 (BTBT-C + Ar-C), 74.61, 74.45, 68.16 (OCH$_2$), 31.87, 31.61, 30.14, 29.53, 29.40, 29.29, 29.25, 26.05, 25.64, 25.63, 22.66, 22.60 (CH$_2$), 14.09, 14.03, 14.00 (CH$_3$); HRMS (m/z): [M]+Li$^+$ calcd. for C$_{60}$H$_{72}$Br$_2$O$_6$S$_2$Li, 1117.329; found 1117.325.

2-[4-(2,6-Dibromo-3,4,5-tri-n-hexyloxybenzoyloxy)phenyl]-7-(4-decyloxyphenyl)-[1]benzothieno[3,2-b]benzothiophene (BB10)

BB-OH (120 mg, 0.12 mmol), K_2CO_3 (200 mg, 1.45 mmol), TBAI (20 mg, 0.054 mmol), 1-bromodecane (80 mg, 0.37 mmol) and butanone (50 ml); yield 35 mg (0.031 mmol, 26%); colorless solid; M = 1127.17 g mol^{-1}; ^{1}H NMR (400 MHz, CDCl$_3$) δ 8.11 (dd, J = 11.8, 1.1 Hz, 2H, BTBT-H), 7.94 (dd, J = 9.0, 8.5 Hz, 2H, BTBT-H), 7.76 (d, J = 8.7 Hz, 2H, Ar-H), 7.68 (ddd, J = 8.4, 6.9, 1.6 Hz, 2H, BTBT-H), 7.62 (d, J = 8.8 Hz, 2H, Ar-H), 7.46 (d, J = 8.6 Hz, 2H, Ar-H), 7.02 (d, J = 8.8 Hz, 2H, Ar-H), 4.09 – 4.00 (m, 8H, OCH$_2$CH$_2$), 1.88 – 1.74 (m, 8H, OCH$_2$CH$_2$), 1.57 – 1.44 (m, 8H, CH$_2$), 1.42 – 1.24 (m, 24H, CH$_2$), 0.96 – 0.87 (m, 12H, CH$_3$); ^{13}C NMR (126 MHz, CDCl$_3$) δ 164.41, 158.95 (C=O), 150.96, 150.07, 148.57, 143.22, 143.10, 139.18, 138.24, 137.35, 133.71, 133.09, 132.92, 132.40, 132.37, 131.63, 128.50, 128.29, 124.51, 124.21, 122.36, 121.94, 121.75, 121.71, 114.97, 109.96 (BTBT-C + Ar-C), 74.62, 74.45, 68.16 (OCH$_2$), 31.88, 31.61, 30.14, 29.58, 29.55, 29.40, 29.31, 29.29, 26.05, 25.64, 25.63, 22.66, 22.60 (CH$_2$), 14.09, 14.03, 14.00 (CH$_3$); HRMS (m/z): [M]+Li$^+$ calcd. for C$_{61}$H$_{74}$Br$_2$O$_6$S$_2$Li, 1131.345; found 1131.352.

2-[4-(2,6-dibromo-3,4,5-tri-n-hexyloxybenzoyloxy)phenyl]-7-(4-undecyloxyphenyl)-[1]benzothieno[3,2-b]benzothiophene (BB11)

BB-OH (120 mg, 0.12 mmol), K_2CO_3 (200 mg, 1.447 mmol), TBAI (20 mg, 0.054 mmol), 1-bromoundecane (85 mg, 0.37 mmol) and butanone (50 ml); yield 55 mg (0.048 mmol, 40%); colorless solid; M = 1141.20 g mol^{-1}; ^{1}H NMR (400 MHz, CDCl$_3$) δ 8.11 (dd, J = 11.8, 1.1 Hz, 2H, BTBT-H), 7.94 (dd, J = 9.1, 8.5 Hz, 2H, BTBT-H), 7.76 (d, J = 8.5 Hz, 2H, Ar-H), 7.69 (ddd, J = 8.3, 6.9, 1.3 Hz, 2H, BTBT-H), 7.62 (d, J = 8.7 Hz, 2H, Ar-H), 7.46 (d, J = 8.5 Hz, 2H, Ar-H), 7.02 (d, J = 8.7 Hz, 2H, Ar-H), 4.09 – 4.01 (m, 8H, OCH$_2$CH$_2$), 1.88 – 1.74 (m, 8H, OCH$_2$CH$_2$), 1.56 – 1.45 (m, 8H, CH$_2$), 1.41 – 1.25 (m, 26H, CH$_2$), 0.95 – 0.87 (m, 12H, CH$_3$); ^{13}C NMR (101 MHz, CDCl$_3$) δ 158.95 (C=O), 150.96, 148.57, 139.18, 137.48, 136.58, 128.50, 128.29, 125.88, 124.51, 124.22, 122.37, 121.94, 121.75, 121.71, 114.97 (BTBT-C + Ar-C), 74.62, 74.45, 68.16 (OCH$_2$), 31.89, 31.60, 30.14, 29.60, 29.59, 29.57, 29.40, 29.32, 26.05, 25.64, 25.63, 24.72, 22.67, 22.60 (CH$_2$), 14.09, 14.02, 14.00 (CH$_3$); HRMS (m/z): [M]+Li$^+$ calcd. for C$_{62}$H$_{76}$Br$_2$O$_6$S$_2$Li, 1145.361; found 1145.367.

4-(2,6-dibromo-3,4,5-tri-n-hexyloxybenzoyloxy)phenylboronic acid pinacol ester (8b)
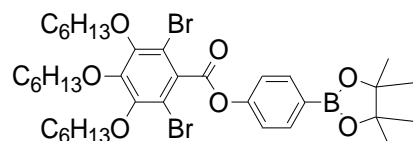
The same procedure for **BTBTBr** was used. **1** (1.0 g, 1.60 mmol), bromine 2.2 eq. (0.56 g, 3.52 mmol), DCM (60 ml), reaction time 72 h, RT, column chromatography (n-hexane/CHCl$_3$); yield: 0.62 g (0.79 mmol, 49%); colorless liquid; ^{1}H NMR (500 MHz, CDCl$_3$) δ 7.89 (d, J = 8.5 Hz, 2H, Ar-H), 7.32 (d, J = 8.5 Hz, 2H, Ar-H), 4.07 – 4.02 (m, 6H, OCH$_2$CH$_2$), 1.86 – 1.73 (m, 6H, OCH$_2$CH$_2$), 1.53 – 1.42 (m, 6H, CH$_2$), 1.39 – 1.31 (m, 24H, CH$_2$ + CH$_3$), 0.92 (t, J = 7.1 Hz, 9H, CH$_3$).

4-octyloxyphenylboronic acid pinacol ester (12)

The same procedure for **H8**-**H12** was used.4-Hydroxyphenylboronic acid pinacol ester (3.00 g, 13.63 mmol), K$_2$CO$_3$ (5.65 g, 40.89 mmol), TBAI (50 mg, 0.14 mmol), 1-bromooctane (2.90 g, 14.99 mmol), butanone (100 ml); yield: 2.1 g (6.32 mmol, 46%); colorless liquid; ^{1}H NMR (500 MHz, CDCl$_3$) δ 7.73 (d, J = 8.7 Hz, 2H, Ar-H), 6.88 (d, J = 8.7 Hz, 2H, Ar-H), 3.97 (t, J = 6.6 Hz, 2H, OCH$_2$CH$_2$), 1.81 – 1.74 (m, 2H, OCH$_2$CH$_2$), 1.48 – 1.40 (m, 2H, CH$_2$), 1.36 – 1.25 (m, 20H, CH$_2$ + CH$_3$), 0.89 (t, J = 7.0 Hz, 3H, CH$_3$).

2-Bromo-7-(4-octyloxyphenyl)-[1]benzothieno[3,2-b]benzothiophene (13)

The same procedure for **2** was used. **12** (1.0 g, 3.01 mmol), **3** (1.59 g, 4.00 mmol), THF (50 ml), toluene (100 ml), saturated NaHCO$_3$ solution (70 ml), [Pd(PPh$_3$)$_4$] (0.1 g, 0.087 mmol) yield: 0.54 g (1.03 mmol, 34 %); colorless solid; heating: Cr 105 SmA 210 Iso (℃), cooling: Iso 208 SmA 88 Cr (℃); ^{1}H NMR (400 MHz, CDCl$_3$) δ 8.11 – 8.04 (m, 2H, 2H, BTBT-H), 7.96 – 7.81 (m, 2H, BTBT-H), 7.75 – 7.46 (m, 4H, Ar-H + BTBT-H), 7.03 – 6.98 (m, 2H, Ar-H), 4.08 (t, J = 6.5 Hz, 2H, OCH$_2$CH$_2$), 1.85 (qd, J = 14.0, 6.6 Hz, 2H, OCH$_2$CH$_2$), 1.56 – 1.43 (m, 2H, CH$_2$), 1.43 – 1.25 (m, 8H, CH$_2$), 0.90 (t, J = 6.7 Hz, 3H, CH$_3$).

2-[4-(2,6-dibromo-3,4,5-Tri-n-hexyloxybenzoyloxy)phenyl]-7-(4-octyloxyphenyl)-[1]benzothieno[3,2-b]benzothiophene (BB8)

The same procedure for **10** was used: **8a** (0.55 g, 0.70 mmol), **13** (0.54 g, 1.03 mmol), THF (50 ml), saturated NaHCO$_3$ solution (30 ml), [Pd(PPh$_3$)$_4$] (0.03 g, 0.026 mmol) yield: 75 mg (0.068 mmol, 10 %); colorless solid; M = 1099.12 g mol^{-1}; ^{1}H NMR (500 MHz, CDCl$_3$) δ 8.11 (dd, J = 14.7, 0.8 Hz, 2H, BTBT-H), 7.94 (dd, J = 11.5, 8.4 Hz, 2H, BTBT-H), 7.76 (d, J = 8.6 Hz, 2H, Ar-H), 7.69 (ddd, J = 9.2, 8.2, 1.2 Hz, 2H, BTBT-H), 7.62 (d, J = 8.5 Hz, 2H, Ar-H), 7.46 (d, J = 8.5 Hz, 2H, Ar-H), 7.02 (d, J = 8.7 Hz, 2H, Ar-H), 4.10 – 4.00 (m, 8H, OCH$_2$CH$_2$), 1.88 – 1.74 (m, 8H, OCH$_2$CH$_2$), 1.61 – 1.45 (s, 8H, CH$_2$), 1.41 – 1.23 (m, 20H, CH$_2$), 0.95 – 0.86 (m, 12H, CH$_3$); ^{13}C NMR (126 MHz, CDCl$_3$) δ 158.95 (C=O), 150.96, 150.07, 148.57, 143.10, 139.18, 138.25, 137.36, 128.50, 128.29, 122.37, 121.94, 121.75, 121.72, 114.97 (BTBT-C + Ar-C), 74.62, 74.45 (OCH$_2$), 31.81, 31.60, 30.92, 30.14, 29.67, 29.36, 29.29, 29.23, 26.06, 25.64, 25.63, 22.65, 22.60 (CH$_2$), 14.08, 14.02, 14.00 (CH$_3$); HRMS (m/z): [M]+Li$^+$ calcd. for C$_{59}$H$_{70}$Br$_2$O$_6$S$_2$Li, 1103.314; found 1103.317.

11.3.4 Representative NMR and HRMS spectra
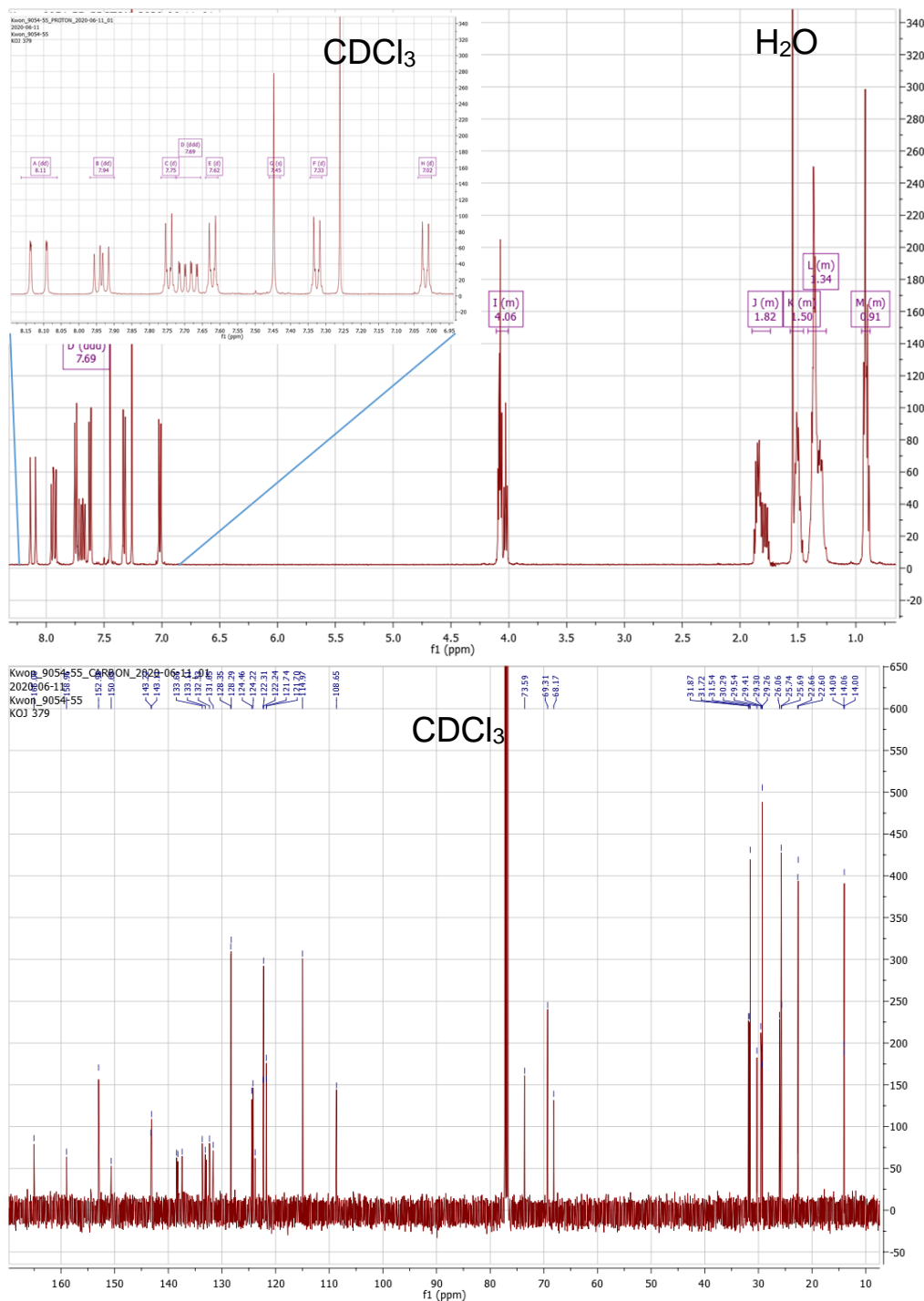
Figure 11.3 ^{1}H- and ^{13}C-NMR of compound **H9**. The spectra were measured at 27 °C, with the frequencies 500 MHz (^{1}H) and 126 MHz (^{13}C) in CDCl$_3$ as solvent.

Figure 11.4 HRMS spectra for **H9.**

Figure 11.5 HRMS spectra for **BB10.**

Figure 11.5 ^{1}H- and ^{13}C-NMR of compound **BB10**. The spectra were measured at 27 °C, with the frequencies 400 MHz (^{1}H) and 126 MHz (^{13}C) in CDCl$_3$ as solvent.
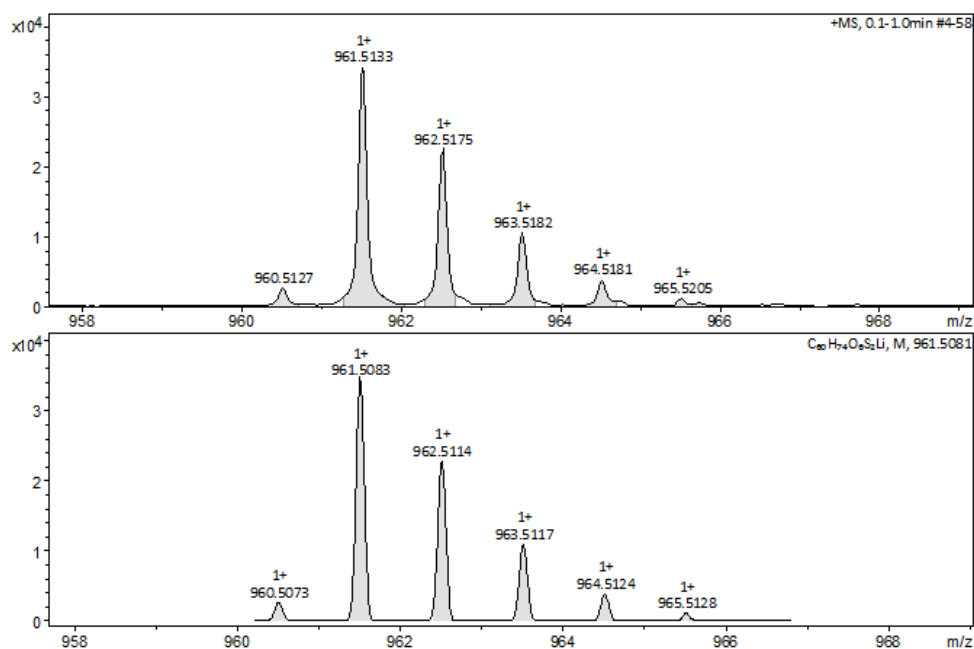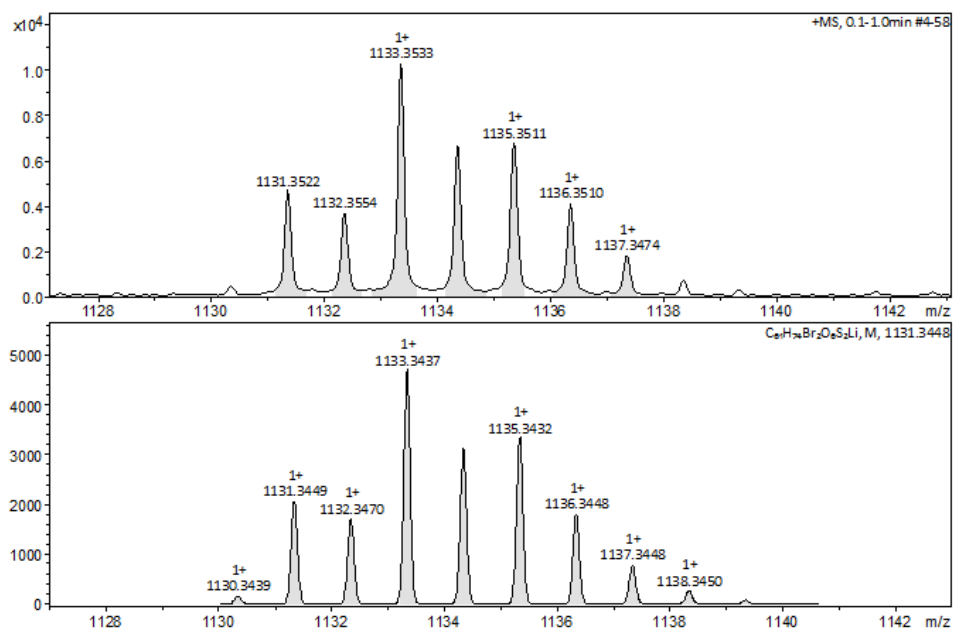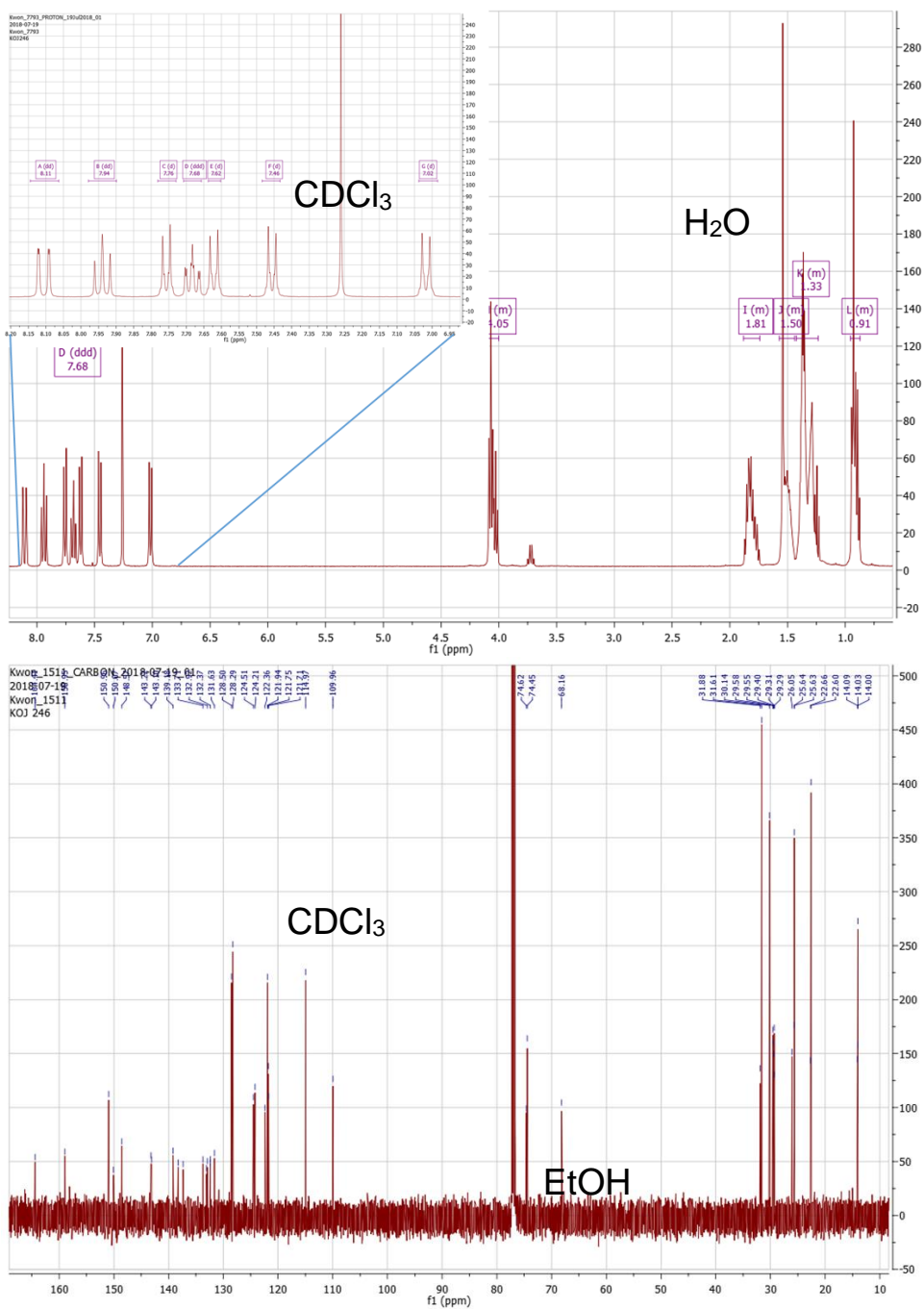
11.4 Synthesis and analytical data of the 6-bromo-3,4,5-tridecyloxybenzoates B'*n*

The synthesis was performed according to schemes 2.4.

11.4.1 Synthesis and analytical data of intermediates

All of the compounds were synthesized by same procedure as reported (chapter 4). The difference is only the alkyl chain length.

### 4-(3,4,5-Tri-n-decyloxybenzoyloxy)phenylboronic acid pinacol ester (7b)

The same procedure for synthesis of **7a** was used. 3,4,5-Tri-n-decyloxybenzoic acid (4.0 g, 6.77 mmol), $SOCl_2$ (20ml), 4-hydroxyphenylboronic acid pinacol ester (1.5g, 6.77 mmol), dry pyridine (10 ml); yield 2.7 g (3.43 mmol, 50.7%), colorless liquid; ^{1}H NMR (500 MHz, $CDCl_3$) δ 7.88 (d, J = 8.5 Hz, 2H, Ar-H), 7.40 (s, 2H, Ar-H), 7.20 (d, J = 8.5 Hz, 2H, Ar-H), 4.11 – 3.94 (m, 6H, OCH_2), 1.88 – 1.80 (m, 4H, CH_2), 1.80 – 1.72 (m, 2H, CH_2), 1.54 – 1.42 (m, 6H, CH_2), 1.41 – 1.26 (m, 48H, CH_2+CH_3), 0.94 – 0.88 (m, 9H, CH_3).

2-[4-(3,4,5-Tri-n-decyloxybenzoyloxy)phenyl]-[1]benzothieno[3,2-b]benzothiophene (9b)
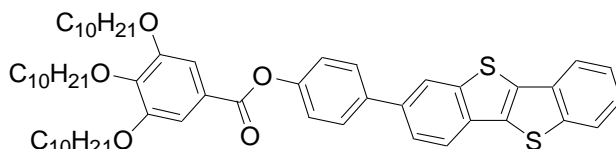

8b (2.3 g, 2.90 mmol) **2** (0.96 g, 3.0 mmol), THF (100 ml) and saturated $NaHCO_3$ solution (50 ml), [Pd(PPh$_3$)$_4$] (0.1 g, 0.1 mmol); yield 1.8 g (1.96 mmol, 85%); Mol. Wt.: 905.34 g/mol; colorless solid; m.p. 84 ℃; C57H76O5S2; ^{1}H NMR (400 MHz, $CDCl_3$) δ 8.14 (d, J = 1.4 Hz, 1H, BTBT-H), 7.97 – 7.89 (m, 3H, BTBT-H), 7.77 – 7.69 (m, 3H, Ar-H + BTBT-H) 7.50 – 7.39 (m, 4H, BTBT-H+Ar-H), 7.32 (d, J = 8.6 Hz, 2H, Ar-H), 4.07 (td, J = 6.5, 3.5 Hz, 6H, OCH_2CH_2), 1.91 – 1.71 (m, 6H, OCH_2CH_2), 1.56 – 1.43 (m, 6H, CH_2), 1.42 – 1.21 (m, 36H, CH_2), 0.89 (td, J = 6.8, 2.8 Hz, 9H, CH_3).

2-[4-(2-bromo-3,4,5-tri-n-decyloxybenzoyloxy)phenyl]-7-bromo-[1]benzothieno[3,2-b]benzothiophene (10d)
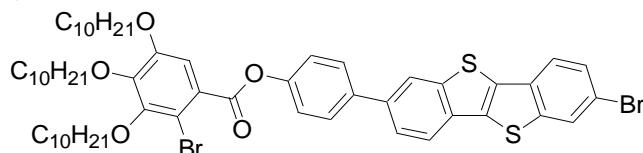
9b (1.8 g, 1.96 mmol), bromine (0.7 g, 4.00 mmol), DCM (60 ml); yield 1.6 g (1.50 mmol, 76 %); Mol. Wt.: 1063.13 g/mol; m.p. 101 ℃; ^{1}H NMR (500 MHz, $CDCl_3$) δ 8.10 (dd, J = 21.2, 1.2 Hz, 2H, BTBT-H), 7.94 (tdd, J = 28.7, 8.1, 0.6 Hz, 2H, BTBT-H), 7.78 – 7.69 (m, 3H, BTBT-H + Ar-H), 7.58 (dd, J = 8.4, 1.7 Hz, 1H, BTBT-H), 7.40 – 7.35 (m, J = 9.4, 2.7 Hz, 2H, Ar-H), 7.37 (s, 1H, Ar-H), 4.11 – 4.01 (m, 6H, OCH_2CH_2), 1.91 – 1.73 (m, 6H, OCH_2CH_2), 1.57 – 1.44 (m, 6H, CH_2), 1.41 – 1.23 (m, 36H, CH_2), 0.89 (dt, J = 7.0, 2.6 Hz, 9H, CH_3).

2-[4-(2-bromo-3,4,5-tri-n-decyloxybenzoyloxy)phenyl]-7-(4-hydroxyphenyl)-[1]benzothieno[3,2-b]benzothiophene (11d)
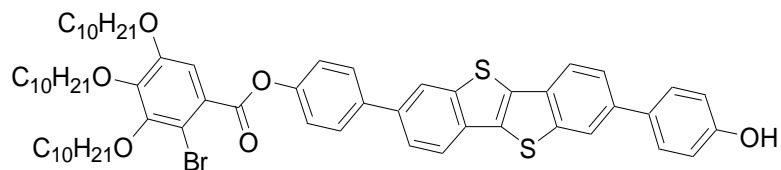
10d (1.6 g, 1.50 mmol), 4-hydroxyphenylboronic acid pinacol ester (0.33 g, 1.50 mmol), THF (100 ml), saturated NaHCO$_3$ solution (50 ml); yield 0.90 g (0.84 mmol, 56 %); Mol. Wt.: 1076.33 g/mol; heating: Cr 198 Cub 245 Iso, cooling: Iso 240 Cub 155 Cr; Iso; ^{1}H NMR (400 MHz, CDCl$_3$) δ 8.09 (d, J = 1.0 Hz, 1H, BTBT-H), 8.02 (d, J = 0.6 Hz, 1H, BTBT-H), 7.89 (dd, J = 14.7, 8.3 Hz, 2H, BTBT-H), 7.74 (d, J = 8.6 Hz, 2H, Ar-H), 7.65 (ddd, J = 26.0, 8.3, 1.5 Hz, 2H, BTBT-H) 7.55 (d, J = 8.6 Hz, 2H, Ar-H), 7.37 (s, 1H, Ar-H), 7.37 (d, J = 8.6 Hz, 2H, Ar-H), 6.91 (d, J = 8.6 Hz, 2H, Ar-H), 5.00 (s, 1H, Ar-OH), 4.07 (dt, J = 6.7, 5.5 Hz, 6H, OCH$_2$CH$_2$), 1.91 − 1.74 (m, 6H, OCH$_2$CH$_2$), 1.57 − 1.45 (m, 6H, CH$_2$), 1.42 − 1.22 (m, 36H, CH$_2$), 0.89 (dt, J = 5.6 Hz, 9H, CH$_3$).

11.4.2 The synthesis and analytical data of the compounds (B'2 – B'22)
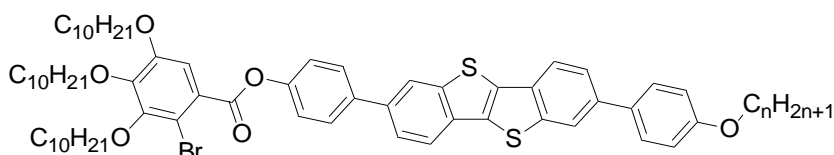
2-[4-(2-bromo-3,4,5-tri-n-decyloxybenzoyloxy)phenyl]-7-(4-ethyloxyphenyl)-[1]benzothieno[3,2-b]benzothiophene (B'2)

11d (130 mg, 0.12 mmol), K$_2$CO$_3$ (200 mg, 1.45 mmol), TBAI (20 mg, 0.062 mmol), 1-bromoethane (40 mg, 0.36 mmol) and butanone (50 ml); yield 45 mg (0.041 mmol, 34%); ^{1}H NMR (400 MHz, CDCl$_3$) δ 8.11 (dd, J = 13.9, 1.0 Hz, 2H, BTBT-H), 7.94 (dd, J = 9.1, 7.8 Hz, 2H, BTBT-H), 7.75 (d, J = 8.7 Hz, 2H, Ar-H), 7.71 − 7.66 (m, 2H, BTBT-H), 7.63 (d, J = 8.8 Hz, 2H, Ar-H), 7.38 (d, J = 8.6 Hz, 2H, Ar-H), 7.36 (s, 1H, Ar-H), 7.02 (d, J = 8.8 Hz, 2H, Ar-H), 4.15 − 4.02 (m, 8H, OCH$_2$CH$_2$), 1.90 − 1.74 (m, 6H, OCH$_2$CH$_2$), 1.56 − 1.43 (m, 9H, CH$_2$ + OCH$_2$CH$_3$), 1.42 − 1.22 (m, 36H, CH$_2$), 0.93 − 0.85 (m, 9H, CH$_3$). ^{13}C NMR (101 MHz, CDCl$_3$) δ 164.70 (C=O), 152.27, 151.48, 151.42, 150.36, 146.36, 143.21, 140.42, 138.70, 138.20, 137.38, 133.10, 132.36, 128.37, 128.31, 126.21, 124.47, 124.21, 122.31, 122.09, 121.75, 121.71, 114.94, 111.34, 110.38, 109.55 (BTBT-C + Ar-C), 74.18, 74.13, 69.22, 68.24 , 63.57, (OCH$_2$+OCH$_2$CH$_3$) 31.91, 30.29, 30.19, 29.68, 29.64, 29.63, 29.60, 29.59, 29.56, 29.50, 29.47, 29.36, 29.33, 29.32, 29.20, 26.06, 26.05, 26.02, 22.68, 22.66 (CH$_2$), 14.85, 14.09 (CH$_3$); HRMS (m/z): [M]+Li$^+$ calcd. for C$_{65}$H$_{83}$BrO$_6$S$_2$Li, 1109.497; found 1109.506.

2-[4-(2-bromo-3,4,5-tri-n-decyloxybenzoyloxy)phenyl]-7-(4-propylloxyphenyl)-[1]benzothieno[3,2-b]benzothiophene (B'3)

11d (130 mg, 0.12 mmol), K$_2$CO$_3$ (200 mg, 1.45 mmol), TBAI (20 mg, 0.062 mmol), 1-bromopropane (45 mg, 0.36 mmol) and butanone (50 ml); yield 52 mg (0.046 mmol, 38%); ^{1}H NMR (500 MHz, CDCl$_3$) δ 8.11 (dd, J = 17.5, 1.1 Hz, 2H, BTBT-H), 7.94 (dd, J = 11.0, 8.4 Hz, 2H, BTBT-H), 7.75 (d, J = 8.7 Hz, 2H, Ar-H), 7.72 − 7.66 (m, 2H, BTBT-H), 7.63 (d, J = 8.7 Hz,

2H, Ar-H), 7.38 (d, J = 8.7 Hz, 2H, Ar-H), 7.36 (s, 1H, Ar-H), 7.02 (d, J = 8.8 Hz, 2H, Ar-H), 4.11 – 3.98 (m, 8H, OCH$_2$CH$_2$), 1.90 – 1.75 (m, 8H, OCH$_2$CH$_2$), 1.55 – 1.46 (m, 6H, CH$_2$), 1.42 – 1.23 (m, 36H, CH$_2$), 1.08 (t, J = 7.4 Hz, 3H, CH$_3$), 0.92 – 0.86 (m, m, 9H, CH$_3$). ^{13}C NMR (101 MHz, CDCl$_3$) δ 164.69, 158.94 (C=O), 152.27, 151.48, 150.37, 146.36, 143.22, 143.10, 138.70, 138.23, 137.38, 133.68, 133.10, 132.94, 132.36, 131.64, 128.37, 128.29, 126.22, 124.47, 124.21, 122.31, 122.09, 121.74, 121.70, 114.97, 111.34, 110.38, (BTBT-C + Ar-C) 74.18, 74.13, 69.65, 69.22 (OCH$_2$), 31.91, 31.90, 31.89, 30.29, 30.19, 29.68, 29.64, 29.63, 29.60, 29.59, 29.55, 29.50, 29.47, 29.36, 29.33, 29.32, 29.20, 26.06, 26.05, 26.02, 22.68, 22.66, 22.61 (CH$_2$), 14.09, 10.52 (CH$_3$); HRMS (m/z): [M]+Li$^+$ calcd. for C$_{66}$H$_{85}$BrO$_6$S$_2$Li, 1123.513; found 1123.517.

2-[4-(2-bromo-3,4,5-tri-n-decyloxybenzoyloxy)phenyl]-7-(4-butyloxyphenyl)-[1]benzothieno[3,2-b]benzothiophene (B'4)

11d (130 mg, 0.12 mmol), K$_2$CO$_3$ (200 mg, 1.45 mmol), TBAI (20 mg, 0.062 mmol), 1-bromobutane (50 mg, 0.36 mmol) and butanone (50 ml); yield 65 mg (0.057 mmol, 48%); ^{1}H NMR (400 MHz, CDCl$_3$) δ 8.11 (dd, J = 14.4, 1.6 Hz, 2H, BTBT-H), 7.94 (dd, J = 9.1, 8.2 Hz, 2H, BTBT-H), 7.75 (d, J = 8.6 Hz, 2H, Ar-H), 7.71 – 7.66 (m, 2H, BTBT-H), 7.62 (d, J = 8.7 Hz, 2H, Ar-H), 7.38 (d, J = 8.6 Hz, 2H, Ar-H), 7.36 (s, 1H, Ar-H), 7.02 (d, J = 8.8 Hz, 2H, Ar-H), 4.13 – 3.99 (m, 8H, OCH$_2$CH$_2$), 1.91 – 1.73 (m, 8H, OCH$_2$CH$_2$), 1.59 – 1.44 (m, 8H, CH$_2$), 1.42 – 1.20 (m, 36H, CH$_2$), 1.01 (t, J = 7.4 Hz, 3H, CH$_3$), 0.94 – 0.82 (m, 9H, CH$_3$).^{13}C NMR (101 MHz, CDCl$_3$) δ 164.70, 158.95 (C=O), 152.27, 151.48, 150.36, 146.36, 143.21, 143.10, 138.71, 138.23, 137.38, 132.93, 132.36, 131.64, 128.37, 128.29, 126.21, 124.47, 124.22, 122.33, 122.32, 122.09, 121.74, 121.70, 114.96, 110.38 (BTBT-C + Ar-C), 74.18, 74.13, 69.22, 67.83 (OCH$_2$), 31.91, 31.34, 30.29, 30.19, 29.68, 29.63, 29.62, 29.60, 29.59, 29.55, 29.50, 29.47, 29.36, 29.33, 29.32, 29.20, 26.06, 26.02, 22.67 (CH$_2$), 19.26, 14.09, 13.85 (CH$_3$); HRMS (m/z): [M]+Li$^+$ calcd. for C$_{67}$H$_{87}$BrO$_6$S$_2$Li, 1137.528; found 1123.531.

2-[4-(2-bromo-3,4,5-tri-n-decyloxybenzoyloxy)phenyl]-7-(4-pentyloxyphenyl)-[1]benzothieno[3,2-b]benzothiophene (B'5)

11d (130 mg, 0.12 mmol), K$_2$CO$_3$ (200 mg, 1.45 mmol), TBAI (20 mg, 0.062 mmol), 1-bromopentane (55 mg, 0.36 mmol) and butanone (50 ml); yield 45 mg (0.039 mmol, 32%); ^{1}H NMR (400 MHz, CDCl$_3$) δ 8.11 (dd, J = 14.3, 1.3 Hz, 2H, BTBT-H), 7.93 (dd, J = 8.9, 8.3 Hz, 2H, BTBT-H), 7.74 (d, J = 8.7 Hz, 2H, Ar-H), 7.71 – 7.65 (m, 2H, BTBT-H), 7.62 (d, J = 8.7 Hz, 2H, Ar-H), 7.38 (d, J = 8.6 Hz, 2H, Ar-H), 7.36 (s, 1H, Ar-H), 7.02 (d, J = 8.8 Hz, 2H, Ar-H), 4.12 – 3.99 (m, 8H, OCH$_2$CH$_2$), 1.90 – 1.74 (m, 8H, OCH$_2$CH$_2$), 1.56 – 1.44 (m, 8H, CH$_2$), 1.44 – 1.23 (m, 38H, CH$_2$), 0.96 (t, J = 7.1 Hz, 3H, CH$_3$), 0.92 – 0.86 (m, 9H, CH$_3$); ^{13}C NMR (101 MHz, CDCl$_3$) δ 164.69, 158.95 (C=O), 152.27, 151.48, 150.36, 146.36, 143.21, 143.10, 138.70, 138.22, 137.36, 133.68, 133.09, 132.92, 132.35, 131.63, 128.37, 128.28, 126.22, 124.46, 124.20, 122.30, 122.09, 121.73, 121.70, 114.96, 111.34, 110.39 (BTBT-C + Ar-C), 74.18, 74.13, 69.22, 68.14 (OCH$_2$), 31.92, 31.90, 31.89, 30.29, 30.20, 29.68, 29.64, 29.63, 29.60, 29.56, 29.50, 29.48, 29.36, 29.34, 29.32, 29.20, 28.99, 28.22, 26.06, 26.03, 22.68, 22.66, 22.47 (CH$_2$), 14.09, 14.02 (CH$_3$); HRMS (m/z): [M]+Li$^+$ calcd. for C$_{68}$H$_{89}$BrO$_6$S$_2$Li, 1151.544; found 1151.551.

2-[4-(2-bromo-3,4,5-tri-n-decyloxybenzoyloxy)phenyl]-7-(4-hexyloxyphenyl)-[1]benzothieno[3,2-b]benzothiophene (B'6)

11d (130 mg, 0.12 mmol), K$_2$CO$_3$ (200 mg, 1.45 mmol), TBAI (20 mg, 0.062 mmol), 1-bromohexane (60 mg, 0.36 mmol) and butanone (50 ml); yield 73 mg (0.063 mmol, 52%); ^{1}H

NMR (500 MHz, CDCl$_3$) δ 8.11 (dd, J = 17.9, 1.3 Hz, 2H, BTBT-H), 7.94 (dd, J = 11.3, 8.3 Hz, 2H, BTBT-H), 7.75 (d, J = 8.6 Hz, 2H, Ar-H), 7.71 – 7.66 (m, 2H, BTBT-H), 7.62 (d, J = 8.7 Hz, 2H, Ar-H), 7.38 (d, J = 8.6 Hz, 2H, Ar-H), 7.36 (s, 1H, Ar-H), 7.02 (d, J = 8.7 Hz, 2H, Ar-H), 4.11 – 4.01 (m, 8H, OCH$_2$CH$_2$), 1.90 – 1.75 (m, 8H, OCH$_2$CH$_2$), 1.55 – 1.45 (m, 8H, CH$_2$), 1.41 – 1.23 (m, 40H, CH$_2$), 0.95 – 0.86 (m, 12H, CH$_3$); ^{13}C NMR (126 MHz, CDCl$_3$) δ 164.71, 158.97 (C=O), 152.28, 146.37, 143.12, 138.72, 135.26, 133.69, 133.10, 132.94, 128.39, 128.39, 128.30, 124.48, 124.23, 122.33, 122.10, 121.75, 121.72, 114.98, 111.35 (BTBT-C + Ar-C), 74.19, 74.14, 69.23, 68.17 (OCH$_2$), 31.92, 31.91, 31.90, 31.60, 30.30, 30.20, 29.69, 29.64, 29.63, 29.61, 29.60, 29.56, 29.51, 29.48, 29.37, 29.34, 29.33, 29.27, 29.21, 26.07, 25.74, 22.69, 22.67, 22.61 (CH$_2$), 14.10, 14.03 (CH$_3$); HRMS (m/z): [M]+Li$^+$ calcd. for C$_{69}$H$_{91}$BrO$_6$S$_2$Li, 1165.560; found 1165.565.

2-[4-(2-bromo-3,4,5-tri-n-decyloxybenzoyloxy)phenyl]-7-(4-octyloxyphenyl)-[1]benzothieno[3,2-b]benzothiophene (B'8)

11d (130 mg, 0.121 mmol), K$_2$CO$_3$ (200 mg, 1.45 mmol), TBAI (20 mg, 0.062 mmol), 1-bromooctane (70 mg, 0.36 mmol) and butanone (50 ml); yield 53 mg (0.045 mmol, 37%); ^{1}H NMR (400 MHz, CDCl$_3$) δ 8.11 (dd, J = 14.3, 1.2 Hz, 2H, BTBT-H), 7.94 (dd, J = 8.9, 8.4 Hz, 2H, BTBT-H), 7.75 (d, J = 8.7 Hz, 2H, Ar-H), 7.72 – 7.66 (m, 2H, BTBT-H), 7.62 (d, J = 8.8 Hz, 2H, Ar-H), 7.38 (d, J = 8.7 Hz, 2H, Ar-H), 7.36 (s, 1H, Ar-H), 7.02 (d, J = 8.7 Hz, 2H, Ar-H), 4.11 – 4.01 (m, 8H, OCH$_2$CH$_2$), 1.90 – 1.74 (m, 8H, OCH$_2$CH$_2$), 1.56 – 1.45 (m, 8H, CH$_2$), 1.42 – 1.23 (m, 44H, CH$_2$), 0.93 – 0.86 (m, 12H, CH$_3$); ^{13}C NMR (101 MHz, CDCl$_3$) δ 164.70, 158.96 (C=O), 152.27, 151.48, 150.36, 143.21, 143.10, 133.09, 128.37, 128.29, 124.47, 124.22, 122.32, 122.09, 121.74, 121.70, 114.97 (BTBT-C + Ar-C), 74.18, 74.13, 69.22, 68.16 (OCH$_2$), 31.91, 31.90, 31.89, 31.81, 30.29, 30.19, 30.18, 29.68, 29.63, 29.62, 29.60, 29.59, 29.55, 29.50, 29.47, 29.36, 29.33, 29.32, 29.29, 29.23, 29.20, 26.06, 26.05, 26.02, 22.67, 22.66, 22.65 (CH$_2$), 14.09, 14.08 (CH$_3$); HRMS (m/z): [M]+Li$^+$ calcd. for C$_{71}$H$_{95}$BrO$_6$S$_2$Li, 1193.591; found 1193.597.

2-[4-(2-bromo-3,4,5-tri-n-decyloxybenzoyloxy)phenyl]-7-(4-decyloxyphenyl)-[1]benzothieno[3,2-b]benzothiophene (B'10)

11d (130 mg, 0.12 mmol), K$_2$CO$_3$ (200 mg, 1.45 mmol), TBAI (20 mg, 0.062 mmol), 1-bromodecane (80 mg, 0.36 mmol) and butanone (50 ml); yield 35 mg (0.029 mmol, 24%); ^{1}H NMR (400 MHz, CDCl$_3$) δ 8.11 (dd, J = 14.4, 1.1 Hz, 2H, BTBT-H), 7.94 (dd, J = 8.9, 8.4 Hz, 2H, BTBT-H), 7.75 (d, J = 8.7 Hz, 2H, Ar-H), 7.72 – 7.66 (m, 2H, BTBT-H), 7.62 (d, J = 8.8 Hz, 2H, Ar-H), 7.38 (d, J = 8.7 Hz, 2H, Ar-H), 7.36 (s, 1H, Ar-H), 7.02 (d, J = 8.8 Hz, 2H, Ar-H), 4.11 – 4.00 (m, 8H, OCH$_2$CH$_2$), 1.90 – 1.74 (m, 8H, OCH$_2$CH$_2$), 1.57 – 1.44 (m, 8H, CH$_2$), 1.42 – 1.23 (m, 48H, CH$_2$), 0.92 – 0.85 (m, 12H, CH$_3$); ^{13}C NMR (101 MHz, CDCl$_3$) δ 158.95 (C=O), 152.27, 150.36, 149.85, 138.24, 133.93, 133.09, 132.36, 131.63, 128.38, 128.29, 124.85, 124.47, 124.22, 122.32, 122.09, 121.74, 121.70, 114.97 (BTBT-C + Ar-C), 74.18, 74.13, 69.21, 68.17 (OCH$_2$), 62.19, 31.92, 31.91, 31.90, 31.89, 30.29, 30.19, 29.68, 29.63, 29.62, 29.59, 29.57, 29.55, 29.50, 29.47, 29.40, 29.35, 29.33, 29.32, 29.31, 29.29, 29.20, 26.06, 26.02, 22.67, 22.66 (CH$_2$), 14.09, 14.08 (CH$_3$); HRMS (m/z): [M]+Li$^+$ calcd. for C$_{73}$H$_{99}$BrO$_6$S$_2$Li, 1221.622; found 1221.624.

2-[4-(2-bromo-3,4,5-tri-n-decyloxybenzoyloxy)phenyl]-7-(4-dodecyloxyphenyl)-[1]benzothieno[3,2-b]benzothiophene (B'12)

11d (130 mg, 0.12 mmol), K$_2$CO$_3$ (200 mg, 1.45 mmol), TBAI (20 mg, 0.062 mmol), 1-bromododecane (90 mg, 0.36 mmol) and butanone (50 ml); yield 23 mg (0.019 mmol, 15%); ^{1}H

NMR (500 MHz, CDCl$_3$) δ 8.11 (dd, *J* = 18.1, 1.0 Hz, 2H, BTBT-H), 7.94 (dd, *J* = 11.4, 8.2 Hz, 2H, BTBT-H), 7.75 (d, *J* = 8.7 Hz, 2H, Ar-H), 7.71 – 7.66 (m, 2H, BTBT-H), 7.62 (d, *J* = 8.8 Hz, 2H, Ar-H), 7.38 (d, *J* = 8.7 Hz, 2H, Ar-H), 7.36 (s, 1H, Ar-H), 7.02 (d, *J* = 8.8 Hz, 2H, Ar-H), 4.11 – 4.01 (m, 8H, OCH$_2$CH$_2$), 1.90 – 1.75 (m, 8H, OCH$_2$CH$_2$), 1.57 – 1.45 (m, 8H, CH$_2$), 1.41 – 1.22 (m, 52H, CH$_2$), 0.92 – 0.85 (m, 12H, CH$_3$); ^{13}C NMR (126 MHz, CDCl$_3$) δ 164.71, 158.97 (C=O), 152.28, 151.49, 146.37, 143.23, 143.12, 143.12, 138.72, 138.25, 137.39, 134.19, 133.69, 133.10, 132.93, 132.37, 131.65, 128.39, 128.39, 128.30, 128.30, 124.48, 124.23, 122.33, 122.10, 121.75, 121.72, 114.98, 111.35, 110.39 (BTBT-C + Ar-C), 74.19, 74.14, 69.23, 68.18 (OCH$_2$), 31.92, 31.91, 31.90, 30.30, 30.20, 29.69, 29.66, 29.64, 29.63, 29.60, 29.59, 29.56, 29.51, 29.48, 29.41, 29.37, 29.37, 29.34, 29.33, 29.30, 29.21, 26.07, 26.03, 22.68, 22.67 (CH$_2$), 14.10, 14.09 (CH$_3$); HRMS (m/z): [M]+Li$^+$ calcd. for C$_{75}$H$_{103}$BrO$_6$S$_2$Li, 1249.654; found 1249.657.

2-[4-(2-bromo-3,4,5-tri-n-decyloxybenzoyloxy)phenyl]-7-(4-tetradecyloxyphenyl)-[1]benzothieno[3,2-b]benzothiophene (B'14)

11d (130 mg, 0.12 mmol), K$_2$CO$_3$ (200 mg, 1.45 mmol), TBAI (20 mg, 0.062 mmol), 1-bromotetradecane (100 mg, 0.36 mmol) and butanone (50 ml); yield 77 mg (0.061 mmol, 50%); ^{1}H NMR (500 MHz, CDCl$_3$) δ 8.11 (dd, *J* = 18.1, 1.0 Hz, 2H, BTBT-H), 7.94 (dd, *J* = 11.4, 8.2 Hz, 2H, BTBT-H), 7.75 (d, *J* = 8.7 Hz, 2H, Ar-H), 7.71 – 7.66 (m, 2H, BTBT-H), 7.62 (d, *J* = 8.8 Hz, 2H, Ar-H), 7.38 (d, *J* = 8.6 Hz, 2H, Ar-H), 7.36 (s, 1H, Ar-H), 7.02 (d, *J* = 8.8 Hz, 2H, Ar-H), 4.13 – 3.99 (m, 8H, OCH$_2$CH$_2$), 1.89 – 1.74 (m, 8H, OCH$_2$CH$_2$), 1.58 – 1.44 (m, 8H, CH$_2$), 1.41 – 1.21 (m, 56H, CH$_2$), 0.93 – 0.81 (m, 12H, CH$_3$); ^{13}C NMR (126 MHz, CDCl$_3$) δ 164.71, 158.97 (C=O), 151.49, 151.19, 143.84, 143.23, 138.25, 135.27, 133.69, 133.11, 131.65, 128.39, 128.30, 124.49, 124.23, 122.33, 122.10, 121.75, 121.72, 114.98 (BTBT-C + Ar-C), 74.14, 69.23, 68.18 (OCH$_2$), 31.92, 31.90, 30.30, 30.20, 29.69, 29.68, 29.66, 29.65, 29.64, 29.60, 29.58, 29.56, 29.51, 29.48, 29.41, 29.37, 29.35, 29.35, 29.33, 29.30, 29.21, 26.07, 26.03, 22.68, 22.67 (CH$_2$), 14.10, 14.09 (CH$_3$); HRMS (m/z): [M]+Li$^+$ calcd. for C$_{77}$H$_{107}$BrO$_6$S$_2$Li, 1277.685; found 1277.690.

2-[4-(2-bromo-3,4,5-tri-n-decyloxybenzoyloxy)phenyl]-7-(4-hexadecyloxyphenyl)-[1]benzothieno[3,2-b]benzothiophene (B'16)

11d (130 mg, 0.12 mmol), K$_2$CO$_3$ (200 mg, 1.45 mmol), TBAI (20 mg, 0.062 mmol), 1-bromohexadecane (110 mg, 0.36 mmol) and butanone (50 ml); yield 55 mg (0.042 mmol, 35%); ^{1}H NMR (400 MHz, CDCl$_3$) δ 8.11 (dd, *J* = 14.6, 1.3 Hz, 2H, BTBT-H), 7.94 (dd, *J* = 8.9, 8.5 Hz, 2H, BTBT-H), 7.75 (d, *J* = 8.7 Hz, 2H, Ar-H), 7.72 – 7.66 (m, 2H, BTBT-H), 7.62 (d, *J* = 8.7 Hz, 2H, Ar-H), 7.38 (d, *J* = 8.6 Hz, 2H, Ar-H), 7.36 (s, 1H, Ar-H), 7.02 (d, *J* = 8.7 Hz, 2H, Ar-H), 4.11 – 4.00 (m, 8H, OCH$_2$CH$_2$), 1.90 – 1.74 (m, 8H, OCH$_2$CH$_2$), 1.56 – 1.44 (m, 8H, CH$_2$), 1.43 – 1.21 (m, 60H, CH$_2$), 0.94 – 0.84 (m, 12H, CH$_3$); ^{13}C NMR (101 MHz, CDCl$_3$) δ 164.69 (C=O) 152.27, 151.48, 143.47, 137.64, 136.68, 133.92, 132.92, 130.43, 128.38, 128.36, 128.29, 124.22, 122.32, 122.09, 121.74, 121.70, 118.14, 116.55, 114.97, 111.33, 110.38 (BTBT-C + Ar-C), 74.18, 69.22, 68.17 (OCH$_2$), 31.91, 30.19, 29.68, 29.65, 29.64, 29.62, 29.59, 29.57, 29.55, 29.50, 29.47, 29.40, 29.36, 29.34, 29.33, 29.32, 29.29, 29.20, 26.05, 26.02, 22.67 (CH$_2$), 14.09, 14.08 (CH$_3$); HRMS (m/z): [M]+Li$^+$ calcd. for C$_{79}$H$_{111}$BrO$_6$S$_2$Li, 1305.716; found 1305.724.

2-[4-(2-bromo-3,4,5-tri-n-decyloxybenzoyloxy)phenyl]-7-(4-octadecyloxyphenyl)-[1]benzothieno[3,2-b]benzothiophene (B'18)
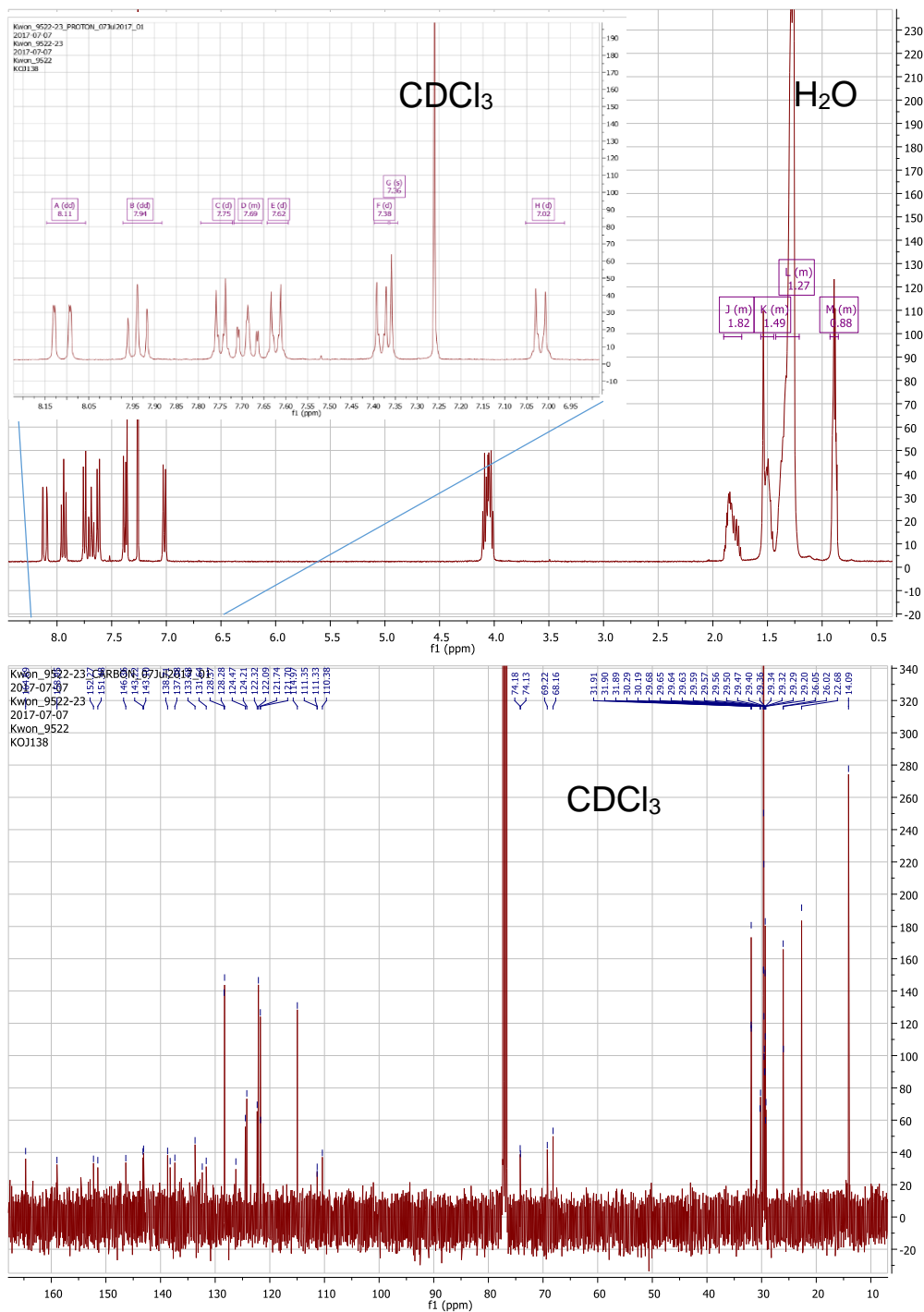
11d (130 mg, 0.12 mmol), K$_2$CO$_3$ (200 mg, 1.45 mmol), TBAI (20 mg, 0.062 mmol), 1-bromooctadecane (120 mg, 0.36 mmol) and butanone (50 ml); yield 60 mg (0.045 mmol, 37%);

^{1}H NMR (500 MHz, CDCl$_3$) δ 8.11 (dd, J = 18.2, 1.3 Hz, 2H, BTBT-H), 7.94 (dd, J = 11.6, 8.2 Hz, 2H, BTBT-H), 7.75 (d, J = 8.7 Hz, 2H, Ar-H), 7.71 – 7.66 (m, 2H, BTBT-H), 7.62 (d, J = 8.9 Hz, 2H, Ar-H), 7.38 (d, J = 8.5 Hz, 2H, Ar-H), 7.36 (s, 1H, Ar-H), 7.02 (d, J = 8.7 Hz, 2H, Ar-H), 4.15 – 3.99 (m, 8H, OCH$_2$CH$_2$), 1.91 – 1.72 (m, 8H, OCH$_2$CH$_2$), 1.57 – 1.45 (m, 8H, CH$_2$), 1.41 – 1.20 (m, 60H, CH$_2$), 0.94 – 0.84 (m, 12H, CH$_3$); ^{13}C NMR (126 MHz, CDCl$_3$) δ 164.71, 158.97 (C=O), 151.49, 145.57, 143.12, 141.94, 138.72, 138.24, 137.39, 135.97, 134.93, 133.11, 132.93, 132.38, 131.65, 128.39, 128.30, 128.08, 124.49, 124.23, 122.33, 122.10, 121.94, 121.75, 121.72, 114.98 (BTBT-C + Ar-C), 74.20, 74.14, 68.18 (OCH$_2$), 31.91, 30.30, 30.20, 29.69, 29.65, 29.63, 29.60, 29.58, 29.56, 29.51, 29.48, 29.40, 29.37, 29.35, 29.35, 29.33, 29.30, 26.06, 26.03, 22.68, 22.67 (CH$_2$), 14.10 (CH$_3$); HRMS (m/z): [M]+Li$^+$ calcd. for C$_{81}$H$_{115}$BrO$_6$S$_2$Li, 1333.748; found 1333.776.

2-[4-(2-bromo-3,4,5-tri-n-decyloxybenzoyloxy)phenyl]-7-(4-docosyloxyphenyl)-[1]benzothieno[3,2-b]benzothiophene (B'22)

11d (130 mg, 0.12 mmol), K$_2$CO$_3$ (200 mg, 1.45 mmol), TBAI (20 mg, 0.062 mmol), 1-bromodocosane (141 mg, 0.36 mmol) and butanone (50 ml); yield 72 mg (0.052 mmol, 43%); ^{1}H NMR (400 MHz, CDCl$_3$) δ 8.11 (dd, J = 14.5, 1.5 Hz, 2H, BTBT-H), 7.94 (dd, J = 8.9, 8.5 Hz, 2H, BTBT-H), 7.75 (d, J = 8.6 Hz, 2H, Ar-H), 7.72 – 7.65 (m, 2H, BTBT-H), 7.62 (d, J = 8.7 Hz, 2H, Ar-H), 7.38 (d, J = 8.6 Hz, 2H, Ar-H), 7.36 (s, 1H, Ar-H), 7.02 (d, J = 8.8 Hz, 2H, Ar-H), 4.11 – 4.00 (m, 8H, OCH$_2$CH$_2$), 1.90 – 1.74 (m, 8H, OCH$_2$CH$_2$), 1.56 – 1.44 (m, 8H, CH$_2$), 1.42 – 1.21 (m, 72H, CH$_2$), 0.93 – 0.85 (m, 12H, CH$_3$); ^{13}C NMR (101 MHz, CDCl$_3$) δ 164.69, 158.95 (C=O), 152.27, 151.48, 146.36, 143.22, 143.10, 138.71, 138.24, 137.38, 133.68, 132.36, 131.64, 128.37, 128.28, 126.21, 124.47, 124.21, 122.32, 122.09, 121.74, 121.70, 114.97, 111.35, 111.33, 110.38 (BTBT-C + Ar-C), 74.18, 74.13, 69.22, 68.16 (OCH$_2$), 31.91, 31.90, 31.89, 30.29, 30.19, 29.68, 29.65, 29.64, 29.63, 29.59, 29.57, 29.56, 29.50, 29.47, 29.40, 29.36, 29.34, 29.32, 29.29, 29.20, 26.05, 26.02, 22.68 (CH$_2$), 14.09 (CH$_3$); HRMS (m/z): [M]+Li$^+$ calcd. for C$_{85}$H$_{123}$BrO$_6$S$_2$Li, 1389.810; found 1389.823.

11.4.3 Representative NMR and HRMS spectra

Figure 11.7 ¹H- and ¹³C-NMR of compound **B'22**. The spectra were measured at 27 °C, with the frequencies 500 MHz (¹H) and 126 MHz (¹³C) in CDCl₃ as solvent.
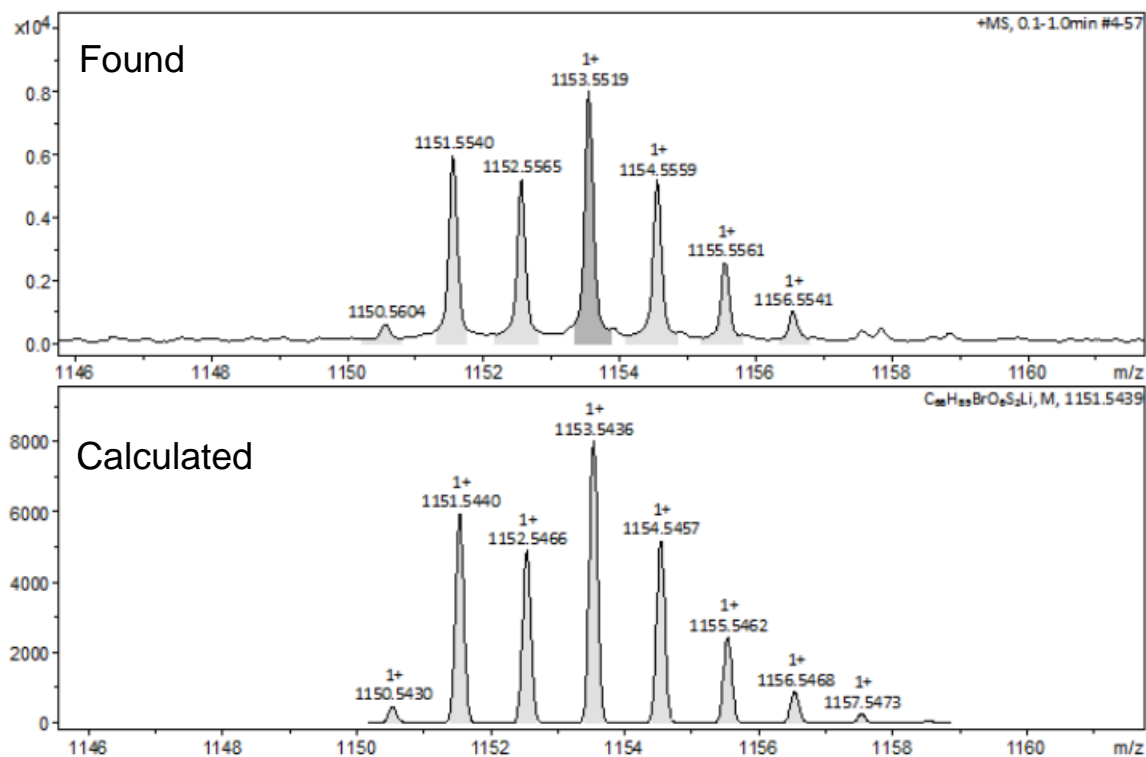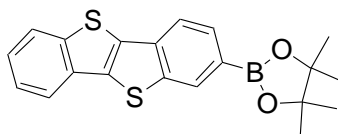
Figure 11.8 HRMS spectra for **B'5.**

11.5 Synthesis and analytical data of the 3,4,5-trihexyloxybenzoates with fluorinated octyloxybenzene F$_X$8

The synthesis was performed according to schemes 2.3 and 2.6.

11.5.1 Synthesis and analytical data of intermediates

2-(4,4,5,5-tetramethyl-1,3,2-dioxaborolan-2-yl)- [1]benzothieno[3,2-*b*][1]benzothiophene (4)

Miyaura Borylation was used. [8] In two-neck flask, BTBT-Br (1.50 g, 4.60 mmol), Bis(pinacolato)diboron (3.5 g, 13.8 mmol), Potassium acetate (1.35 g, 13.8 mmol) and DMSO (150 ml) were prepared, and degassed with argon for 15 minutes. After purging, Pd(dppf)Cl$_2$ (0.1 g, 0.138 mmol) was added. The solution was stirred at 90 °C for 20 hours. Water (100 ml) was added to the solution. When the mixture was cooled down, the organic phase was extracted with CHCl$_3$. Then, it was dried over Na$_2$SO$_4$. After it was concentrated in vacuum, it was purified by column chromatography (eluent: CHCl$_3$); yield 0.73 g (1.99 mmol, 43%); colorless solid; m.p: 163 °C; ^{1}H NMR (400 MHz, cdcl$_3$) δ 8.40 (s, 1H, Ar-H), 7.95 – 7.86 (m, 4H, Ar-H), 7.44 (dtd, *J* = 16.5, 7.3, 1.2 Hz, 2H, Ar-H), 1.39 (s, 12H, CH$_3$).
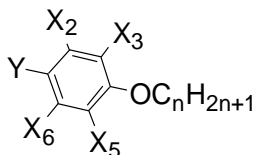
Synthesis of 17F$_x$$n$

Williamson ether synthesis was used. 4-Bromo-X-fluorophenol, 1-bromooctane, K$_2$CO$_3$, TBAI, were dissolved/suspended in butanone. The solution is refluxed for 5 hours. Butanone was removed via rotary evaporator and the crude product was purified via liquid column chromatography with n-hexane.

4-Bromo-2-fluoro-1-octyloxy-benzene (17F$_3$8)

4-Bromo-2-fluorophenol (5.0 g, 0.026 mol) K$_2$CO$_3$ (7.2 g, 0.052 mol), TBAI (20 mg, 0.062 mmol), 1-bromooctane (5.6 g, 0.029 mol), butanone (100 ml); yield 5.8 g (0.019 mol, 73%); transparent liquid; ^{1}H NMR (500 MHz, CDCl$_3$) δ 7.22 (dd, J = 10.6, 2.4 Hz, 1H, Ar-H), 7.16 (ddd, J = 8.7, 2.3, 1.6 Hz, 1H, Ar-H), 6.83 (t, J = 8.8 Hz, 1H, Ar-H), 3.99 (t, J = 6.6 Hz, 2H, OCH$_2$CH$_2$), 1.83 – 1.77 (m, 2H, OCH$_2$CH$_2$), 1.50 – 1.38 (m, 2H, CH$_2$), 1.38 – 1.22 (m, 8H, CH$_2$), 0.89 (t, J = 7.0 Hz, 3H, CH$_3$); ^{19}F NMR (470 MHz, CDCl$_3$) δ -131.32 (t, J = 9.7 Hz).

1-Bromo-2-fluoro-4-octyloxy-benzene (17F$_2$8)

4-Bromo-3-fluorophenol (5.0 g, 0.026 mol), K$_2$CO$_3$ (7.2 g, 0.052), TBAI (20 mg, 0.062 mmol), 1-bromooctane (5.6 g, 0.029 mol), butanone (100 ml); yield 6.0 g (0.020 mol, 76%); transparent liquid; ^{1}H NMR (400 MHz, CDCl$_3$) δ 7.38 (dd, J = 8.8, 8.1 Hz, 1H, Ar-H), 6.68 (dd, J = 10.5, 2.8 Hz, 1H, Ar-H), 6.59 (ddd, J = 8.9, 2.8, 1.0 Hz, 1H, Ar-H), 3.91 (t, J = 6.6 Hz, 2H, OCH$_2$CH$_2$), 1.81 – 1.71 (m, 2H, OCH$_2$CH$_2$), 1.49 – 1.39 (m, 2H, CH$_2$), 1.39 – 1.24 (m, 8H, CH$_2$), 0.89 (t, J = 6.9 Hz, 3H, CH$_3$); ^{19}F NMR (376 MHz, CDCl$_3$) δ -105.59 (dd, J = 10.4, 8.2 Hz).

1-Bromo-2,3-difluoro-4-octyloxy-benzene (17F$_{23}$8)

4-Bromo-2,3-difluoro-phenol (5.0 g, 0.024 mol), K$_2$CO$_3$ (6.6 g, 0.048 mol), TBAI (20 mg, 0.062 mmol), 1-bromooctane (5.1 g, 0.026 mol), butanone (100 ml); yield 5.5 g (0.017 mol, 72%); transparent liquid; ^{1}H NMR (500 MHz, CDCl$_3$) δ 7.19 (ddd, J = 9.2, 7.2, 2.5 Hz, 1H, Ar-H), 6.68 – 6.62 (m, 1H), 4.02 (t, J = 6.6 Hz, 2H, OCH$_2$CH$_2$), 1.84 – 1.77 (m, 2H, OCH$_2$CH$_2$), 1.49 – 1.42 (m, 2H, CH$_2$), 1.38 – 1.23 (m, 8H, CH$_2$), 0.89 (t, J = 7.0 Hz, 3H, CH$_3$); ^{19}F NMR (470 MHz, CDCl$_3$) δ -129.20 (ddd, J = 20.2, 7.1, 2.0 Hz), -154.81 (ddd, J = 20.2, 7.6, 2.3 Hz).

5-Bromo-1,3-difluoro-2-octyloxy-benzene (17F$_{35}$8)

4-Bromo-2,6-difluoro-phenol (5.0 g, 0.024 mol), K$_2$CO$_3$ (6.6 g, 0.048 mol), TBAI (20 mg, 0.062 mmol), 1-bromooctane (5.1 g, 0.026 mol), butanone (100 ml); yield 6.1 g (0.019 mol, 79%); transparent liquid; ^{1}H NMR (400 MHz, CDCl$_3$) δ 7.11 – 7.02 (m, 2H, Ar-H), 4.10 (t, J = 6.6 Hz, 2H, OCH$_2$CH$_2$), 1.79 – 1.69 (m, 2H, OCH$_2$CH$_2$), 1.49 – 1.38 (m, 2H), 1.37 – 1.23 (m, 8H), 0.89 (t, J = 6.9 Hz, 3H); ^{19}F NMR (376 MHz, CDCl$_3$) δ -125.97 – -126.05 (m).

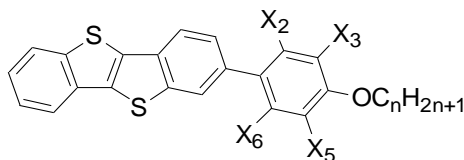### 2-Bromo-1,3-difluoro-5-octyloxy-benzene (17F$_{26}$8)

4-Bromo-3,5-difluoro-phenol (5.0 g, 0.024 mol), K$_2$CO$_3$ (6.6 g, 0.048 mol), TBAI (20 mg, 0.062 mmol), 1-bromooctane (5.1 g, 0.026 mol), butanone (100 ml); yield 5.8 g (0.018 mol, 76%);

transparent liquid; ^{1}H NMR (400 MHz, CDCl$_3$) δ 6.55 – 6.49 (m, 2H, Ar-H), 3.90 (t, J = 6.5 Hz, 2H, OCH$_2$CH$_2$), 1.81 – 1.72 (m, 2H, OCH$_2$CH$_2$), 1.48 – 1.38 (m, 2H, CH$_2$), 1.39 – 1.23 (m, 8H, CH$_2$), 0.89 (t, J = 6.9 Hz, 3H, CH$_3$); ^{19}F NMR (376 MHz, CDCl$_3$) δ -105.22 – -105.28 (m).

1,2,4,5-Tetrafluoro-3-iodo-6-octyloxy-benzene (17F$_{2356}$8)

Iodopentafluorobenzene (5.0 g, 0.017 mol), 1-octanol (4.4 g, 0.034 mol), K$_2$CO$_3$ (7.1 g, 0.051 mol), DMF (50 ml) were dissolved/suspended in DMF. The solution is stirred at 80 ℃ for 24 hours and then water (50ml) was added to the solution. The organic mixture was extracted with chloroform. It was washed with water three times. After the solvent was removed via rotary evaporator, the crude product was purified via liquid column chromatography with n-hexane; yield 2.8g (6.93 mmol, 41%); transparent liquid; ^{1}H NMR (400 MHz, CDCl$_3$) δ 4.23 (t, J = 6.6 Hz, 2H, OCH$_2$CH$_2$), 1.81 – 1.73 (m, 2H, OCH$_2$CH$_2$), 1.51 – 1.40 (m, 2H, CH$_2$), 1.39 – 1.22 (m, 8H, CH$_2$), 0.89 (t, J = 6.9 Hz, 3H, CH$_3$); ^{19}F NMR (376 MHz, CDCl$_3$) δ -121.66 (td, J = 10.1, 5.1 Hz), -154.47 (td, J = 10.0, 5.0 Hz).

Synthesis of 18F$_X$n

Suzuki coupling reaction was used.[S6] In two-neck flask, **17F$_X$n** (2.73 mmol), **4** (0.5 g, 1.37 mmol), THF (100 ml) and saturated NaHCO$_3$ solution (50 ml) were prepared, and degassed with argon for 15 minutes. After purging, [Pd(PPh$_3$)$_4$] (0.1 g, 0.1 mmol) was added. The solution was refluxed for 6 hours. When the mixture was cooled down, the organic phase was extracted with CHCl$_3$. Then, it was dried over Na$_2$SO$_4$. After it was concentrated in vacuum, it was purified by column chromatography (eluent: CHCl$_3$/n-hexane 1/2)

2-(3-Fluoro-4-octyloxyphenyl)-[1]benzothieno[3,2-b]benzothiophene (18F$_3$8)

17F$_3$8 (0.88 g, 2.73 mmol), **4** (0.5 g, 1.37 mmol), THF (100 ml), saturated NaHCO$_3$ solution (50 ml), Pd(PPh$_3$)$_4$ (0.1 g, 0.1 mmol); yield 280 mg (0.61 mmol, 44 %); colorless solid; H: Cr 179 SmA 218 Iso; C: Iso 214 SmA 154 Cr; ^{1}H NMR (500 MHz, CDCl$_3$) δ 8.06 (d, J = 1.3 Hz, 1H, BTBT-H), 7.92 (dd, J = 17.2, 9.0 Hz, 3H, BTBT-H), 7.63 (dd, J = 8.3, 1.6 Hz, 1H, BTBT-H), 7.50 – 7.36 (m, 4H, BTBT-H + Ar-H), 7.06 (t, J = 8.6 Hz, 1H, Ar-H), 4.09 (t, J = 6.6 Hz, 2H, OCH$_2$CH$_2$), 1.92 – 1.80 (m, 2H, OCH$_2$CH$_2$), 1.57 – 1.44 (m, 2H, CH$_2$), 1.42 – 1.24 (m, 8H, CH$_2$), 0.90 (t, J = 6.9 Hz, 3H, CH$_3$); ^{19}F NMR (470 MHz, CDCl$_3$) δ -133.98 (dd, J = 12.2, 8.9 Hz).

2-(2-Fluoro-4-octyloxyphenyl)-[1]benzothieno[3,2-b]benzothiophene (18F$_2$8)

17F$_2$8 (0.88 g, 2.73 mmol), **4** (0.5 g, 1.37 mmol), THF (100 ml), saturated NaHCO$_3$ solution (50 ml) and Pd(PPh$_3$)$_4$ (0.1 g, 0.1 mmol); yield 230 mg (0.50 mmol, 36 %); colorless solid; H: Cr 128 N 165 Iso; C: Iso 162 N 115 Cr; ^{1}H NMR (400 MHz, CDCl$_3$) δ 8.06 (s, 1H, BTBT-H), 7.95 – 7.88 (m, 3H, BTBT-H), 7.62 (dt, J = 8.3, 1.5 Hz, 1H, BTBT-H), 7.50 – 7.36 (m, 3H, BTBT-H + Ar-H), 6.78 (ddd, J = 15.1, 10.6, 2.5 Hz, 2H, Ar-H), 4.00 (t, J = 6.6 Hz, 2H, OCH$_2$CH$_2$), 1.87 – 1.76 (m, 2H, OCH$_2$CH$_2$), 1.54 – 1.40 (m, 2H, CH$_2$), 1.42 – 1.24 (m, 8H, CH$_2$), 0.90 (t, J = 6.8 Hz, 3H, CH$_3$); ^{19}F NMR (376 MHz, CDCl$_3$) δ -115.50 (dd, J = 11.6, 10.1 Hz).

2-(2,3-Difluoro-4-octyloxyphenyl)-[1]benzothieno[3,2-b]benzothiophene (18F$_{23}$8)

17F$_{23}$8 (0.88 g, 2.73 mmol), **4** (0.5 g, 1.37 mmol), THF (100 ml), saturated NaHCO$_3$ solution (50 ml), Pd(PPh$_3$)$_4$ (0.1 g, 0.1 mmol); yield 270 mg (0.56 mmol, 41 %); colorless solid; H: Cr 170 N 194 Iso; C: Iso 192 N 157 Cr; ^{1}H NMR (500 MHz, CDCl$_3$) δ 8.05 (s, 1H, BTBT-H), 7.96 – 7.88 (m, 3H, BTBT-H), 7.61 (dt, J = 8.3, 1.6 Hz, 1H, BTBT-H), 7.50 – 7.40 (m, 2H, BTBT-H), 7.19 (td, J = 8.7, 2.3 Hz, 1H), 6.84 (ddd, J = 9.1, 7.7, 1.8 Hz, 1H), 4.10 (t, J = 6.6 Hz, 2H, Ar-H, OCH$_2$CH$_2$), 1.91 – 1.82 (m, 2H, OCH$_2$CH$_2$), 1.55 – 1.43 (m, 2H, CH$_2$), 1.43 – 1.25 (m, 8H, CH$_2$), 0.90 (t, J = 6.9 Hz, 3H, CH$_3$); ^{19}F NMR (470 MHz, CDCl$_3$) δ -141.55 (dd, J = 19.6, 7.5 Hz), -158.43 (ddd, J = 19.8, 7.4, 1.9 Hz).

2-(3,5-Difluoro-4-octyloxyphenyl)-[1]benzothieno[3,2-b]benzothiophene (18F$_{35}$8)

17F$_{35}$8 (0.88 g, 2.73 mmol), **4** (0.5 g, 1.37 mmol), THF (100 ml), saturated NaHCO$_3$ solution (50 ml), Pd(PPh$_3$)$_4$ (0.1 g, 0.1 mmol); yield 280 mg (0.58 mmol, 43 %); colorless solid; H: Cr 135 SmA 233 Iso; C: Iso 232 SmA 127 Cr; ^{1}H NMR (400 MHz, CDCl$_3$) δ 8.05 (d, J = 1.4 Hz, 1H, BTBT-H), 7.96 – 7.89 (m, 3H, BTBT-H), 7.61 (dd, J = 8.3, 1.6 Hz, 1H, BTBT-H), 7.53 – 7.40 (m, 2H, BTBT-H), 7.23 (d, J = 9.4 Hz, 2H, Ar-H), 4.19 (t, J = 6.6 Hz, 2H, OCH$_2$CH$_2$), 1.84 – 1.75 (m, 2H, OCH$_2$CH$_2$), 1.57 – 1.44 (m, 2H, CH$_2$), 1.42 – 1.24 (m, 8H, CH$_2$), 0.90 (t, J = 6.8 Hz, 3H, CH$_3$); ^{19}F NMR (376 MHz, CDCl$_3$) δ -127.50 (d, J = 9.1 Hz).

2-(2,6-Difluoro-4-octyloxyphenyl)-[1]benzothieno[3,2-b]benzothiophene (18F$_{26}$8)

17F$_{26}$8 (0.83 g, 2.73 mmol), **4** (0.5 g, 1.37 mmol), THF (100 ml), saturated NaHCO$_3$ solution (50 ml), Pd(PPh$_3$)$_4$ (0.1 g, 0.1 mmol); yield 240 mg (0.50 mmol, 37 %); colorless solid; m.p.138 ℃; ^{1}H NMR (400 MHz, CDCl$_3$) δ 7.99 (s, 1H, BTBT-H), 7.94 (d, J = 8.3 Hz, 2H, BTBT-H), 7.90 (d, J = 7.5 Hz, 1H, BTBT-H), 7.53 (dd, J = 8.2, 1.4 Hz, 1H, BTBT-H), 7.50 – 7.39 (m, 2H, BTBT-H), 6.58 (d, J = 9.8 Hz, 2H, Ar-H), 3.98 (t, J = 6.5 Hz, 2H, OCH$_2$CH$_2$), 1.86 – 1.77 (m, 2H, OCH$_2$CH$_2$), 1.52 – 1.41 (m, 2H, CH$_2$), 1.43 – 1.26 (m, 8H, CH$_2$), 0.90 (t, J = 6.9 Hz, 3H, CH$_3$); ^{19}F NMR (376 MHz, CDCl$_3$) δ -113.70 (d, J = 9.6 Hz).

2-(2,3,5,6-Tetrafluoro-4-octyloxyphenyl)-[1]benzothieno[3,2-b]benzothiophene (18F$_{2356}$8)

17F$_{2356}$8 0.83 g (2.73 mmol), **4** (0.5 g, 1.37 mmol), THF (100 ml), saturated NaHCO$_3$ solution (50 ml), Pd(PPh$_3$)$_4$ (0.1 g, 0.1 mmol); yield 270 mg (0.52 mmol, 38%); colorless solid; m.p. 220 ℃; ^{1}H NMR (400 MHz, CDCl$_3$) δ 8.00 (d, J = 0.7 Hz, 1H, BTBT-H), 7.98 (d, J = 8.3 Hz, 1H, BTBT-H), 7.93 (dd, J = 11.1, 7.4 Hz, 2H, BTBT-H), 7.53 (dd, J = 8.3, 1.4 Hz, 1H, BTBT-H), 7.46 (dtd, J = 16.5, 7.3, 1.3 Hz, 2H, BTBT-H), 4.29 (t, J = 6.6 Hz, 2H, OCH$_2$CH$_2$), 1.87 – 1.78 (m, 2H, OCH$_2$CH$_2$), 1.56 – 1.46 (m, 2H, CH$_2$), 1.42 – 1.25 (m, 8H, CH$_2$), 0.90 (t, J = 6.8 Hz, 3H, CH$_3$); ^{19}F NMR (376 MHz, CDCl$_3$) δ -145.11 (dd, J = 22.3, 8.8 Hz), -157.24 (dd, J = 22.2, 8.6 Hz).

Synthesis of 19F$_X$$n$
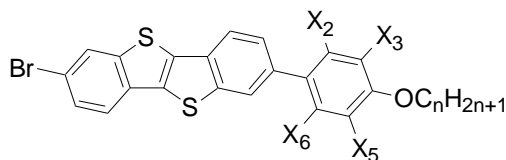
18Fx*n* was dissolved in DCM. Bromine with DCM was prepared in a dropping funnel and added dropwise to the solution. The mixture was stirred for 20h at RT. The reaction was quenched by adding $Na_2S_2O_3$ solution. The crude product was extracted with DCM. The organic mixture was dried with Na_2SO_4. Solvent was removed via rotary evaporator. The residue was purified by column chromatography (eluent: Toluene)

2-Bromo-7-(3-fluoro-4-octyloxyphenyl)-[1]benzothieno[3,2-b]benzothiophene (19F₃8)

18F₃8 (280 mg, 0.61 mmol), Br_2 (110 mg, 0.67 mmol) and DCM (60 ml); yield 250 mg (0.46 mmol, 76%); colorless solid; m.p.138 °C; ^{1}H NMR (500 MHz, CDCl₃) δ 8.06 (dd, J = 6.6, 1.2 Hz, 2H, BTBT-H), 7.90 (dd, J = 8.3, 0.5 Hz, 1H, BTBT-H), 7.76 – 7.72 (m, 1H, BTBT-H), 7.64 (dd, J = 8.3, 1.6 Hz, 1H, BTBT-H), 7.57 (dd, J = 8.4, 1.7 Hz, 1H, BTBT-H), 7.42 (dd, J = 12.4, 2.2 Hz, 1H, Ar-H), 7.38 (ddd, J = 8.5, 2.2, 1.0 Hz, 1H, Ar-H), 7.06 (t, J = 8.6 Hz, 1H, Ar-H), 4.09 (t, J = 6.6 Hz, 2H, OCH₂CH₂), 1.89 – 1.81 (m, 2H, OCH₂CH₂), 1.55 – 1.45 (m, 2H, CH₂), 1.40 – 1.24 (m, 8H, CH₂), 0.90 (t, J = 7.0 Hz, 3H, CH₃); ^{19}F NMR (470 MHz, CDCl₃) δ -133.90 (dd, J = 12.1, 9.0 Hz).
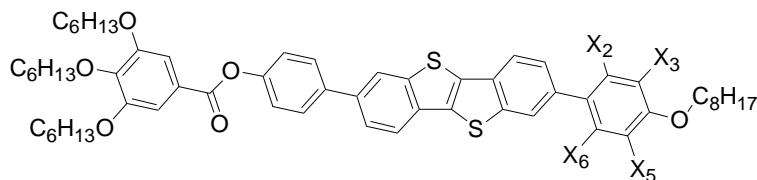
2-Bromo-7-(2-fluoro-4-octyloxyphenyl)-[1]benzothieno[3,2-b]benzothiophene (19F₂8)

18F₂8 (230 mg, 0.50 mmol), Br_2 (90 mg, 0.55 mmol) and DCM (60 ml); yield 230 mg (0.42 mmol, 85%); colorless solid; H: Cr 135 SmA 217 Iso; C: Iso 213 SmA 102 Cr; ^{1}H NMR (400 MHz, CDCl₃) δ 8.07 (d, J = 1.6 Hz, 1H, BTBT-H), 8.04 (s, 1H, BTBT-H), 7.91 (d, J = 8.3 Hz, 1H, BTBT-H), 7.73 (dd, J = 13.4, 8.4 Hz, 2H, BTBT-H), 7.64 – 7.55 (m, 3H, BTBT-H + Ar-H), 6.76 (d, J = 12.2 Hz, 1H, Ar-H), 4.06 (t, J = 6.5 Hz, 2H, OCH₂CH₂), 1.93 – 1.82 (m, 2H, OCH₂CH₂), 1.57 – 1.43 (m, 2H, CH₂), 1.43 – 1.28 (m, 8H, CH₂), 0.90 (t, J = 6.8 Hz, 3H, CH₃); ^{19}F NMR (376 MHz, CDCl₃) δ -115.81 (dd, J = 12.2, 8.2 Hz).

2-Bromo-7-(2,3-difluoro-4-octyloxyphenyl)-[1]benzothieno[3,2-b]benzothiophene (19F₂₃8)

18F₂₃8 (270 mg, 0.56 mmol), Br_2 (100 mg, 0.63 mmol) and DCM (60 ml); yield 260 mg (0.46 mmol, 83%); colorless solid; H: Cr 150 SmA 288 Iso; C: Iso 285 SmA 127 Cr; ^{1}H NMR (500 MHz, CDCl₃) δ 8.08 – 8.02 (m, 2H, BTBT-H), 7.91 (d, J = 8.3 Hz, 1H, BTBT-H), 7.74 (d, J = 8.4 Hz, 1H, BTBT-H), 7.64 – 7.55 (m, 2H, BTBT-H), 7.21 – 7.15 (m, 1H, Ar-H), 6.86 – 6.81 (m, 1H, Ar-H), 4.10 (t, J = 6.6 Hz, 2H, OCH₂CH₂), 1.92 – 1.81 (m, 2H, OCH₂CH₂), 1.56 – 1.43 (m, 2H, CH₂), 1.43 – 1.24 (m, 8H, CH₂), 0.90 (t, J = 6.9 Hz, 3H, CH₃); ^{19}F NMR (470 MHz, CDCl₃) δ -141.53 (dd, J = 19.5, 7.1 Hz), -158.37 (ddd, J = 19.7, 7.6, 1.9 Hz).

2-Bromo-7-(3,5-difluoro-4-octyloxyphenyl)-[1]benzothieno[3,2-b]benzothiophene (19F₃₅8)

18F₃₅8 (280 mg, 0.58 mmol), Br_2 (100 mg, 0.63 mmol) and DCM (60 ml); yield 250 mg (0.45 mmol, 77%); colorless solid; H: Cr 128 SmA 273 Iso; C: Iso 270 SmA 101 Cr; ^{1}H NMR (400 MHz, cdcl₃) δ 8.04 (dd, J = 12.3, 1.4 Hz, 2H, BTBT-H), 7.90 (d, J = 8.3 Hz, 1H, BTBT-H), 7.73 (d, J = 8.5 Hz, 1H, BTBT-H), 7.58 (ddd, J = 12.0, 8.4, 1.7 Hz, 2H, BTBT-H), 7.22 (d, J = 9.4 Hz, 2H, Ar-H), 4.19 (t, J = 6.6 Hz, 2H, OCH₂CH₂), 1.84 – 1.75 (m, 2H, OCH₂CH₂), 1.54 – 1.44 (m, 2H, CH₂), 1.40 – 1.24 (m, 8H, CH₂), 0.90 (t, J = 6.9 Hz, 8H, CH₃); ^{19}F NMR (376 MHz, cdcl₃) δ -127.40 (d, J = 9.0 Hz).

2-Bromo-7-(2,6-difluoro-4-octyloxyphenyl)-[1]benzothieno[3,2-b]benzothiophene (19F₂₆8)

18F$_{26}$8 (240 mg, 0.50 mmol), Br$_2$ (90 mg, 0.55 mmol) and DCM (60 ml); yield 220 mg (0.39 mmol, 79%); colorless solid; H: Cr 140 N 201 Iso; C: Iso 197 N 124 Cr; ^{1}H NMR (400 MHz, cdcl$_3$) δ 8.07 (d, J = 1.6 Hz, 1H, BTBT-H), 7.98 (s, 1H, BTBT-H), 7.92 (d, J = 8.3 Hz, 1H, BTBT-H), 7.75 (d, J = 8.5 Hz, 1H, BTBT-H), 7.57 (dd, J = 8.5, 1.7 Hz, 1H, BTBT-H), 7.54 (dd, J = 8.2, 1.4 Hz, 1H, BTBT-H), 6.58 (d, J = 9.8 Hz, 2H, Ar-H), 3.98 (t, J = 6.5 Hz, 2H, OCH$_2$CH$_2$), 1.86 – 1.76 (m, 2H, OCH$_2$CH$_2$), 1.52 – 1.42 (m, 2H, CH$_2$), 1.41 – 1.24 (m, 8H, CH$_2$), 0.90 (t, J = 6.8 Hz, 3H, CH$_3$); ^{19}F NMR (376 MHz, cdcl$_3$) δ -113.72 (d, J = 9.8 Hz).

2-Bromo-7-(2,3,5,6-tetrafluoro-4-octyloxyphenyl)-[1]benzothieno[3,2-b]benzothiophene (19F$_{2356}$8)

18F$_{23}$8 (270 mg, 0.52 mmol), Br$_2$ (95 mg, 0.58 mmol), DCM (60 ml); yield 260 mg (0.43 mmol, 84%); colorless solid; H: Cr 188 SmA 220 Iso; C: Iso 218 SmA 175 Cr; ^{1}H NMR (400 MHz, CDCl$_3$) δ 8.08 (d, J = 1.7 Hz, 1H, BTBT-H), 8.00 (d, J = 1.1 Hz, 1H, BTBT-H), 7.97 (d, J = 8.4 Hz, 1H, BTBT-H), 7.77 (d, J = 8.5 Hz, 1H, BTBT-H), 7.59 (dd, J = 8.5, 1.7 Hz, 1H, BTBT-H), 7.54 (dd, J = 8.3, 1.5 Hz, 1H, BTBT-H), 4.29 (t, J = 6.6 Hz, 2H, OCH$_2$CH$_2$), 1.86 – 1.78 (m, 2H, OCH$_2$CH$_2$), 1.57 – 1.45 (m, 2H, CH$_2$), 1.41 – 1.26 (m, 8H, CH$_2$), 0.90 (t, J = 6.9 Hz, 3H, CH$_3$); ^{19}F NMR (376 MHz, CDCl$_3$) δ -145.11 (dd, J = 21.8, 8.2 Hz), -157.17 (dd, J = 21.9, 8.3 Hz).

11.5.2 Synthesis and analytical data of the compounds (F$_X$8)

Suzuki coupling reaction was used. The same procedure for the synthesis of **18F$_X$n** was used.

2-[4-(3,4,5-Tri-n-hexyloxybenzoyloxy)phenyl]-7-(3-fluoro-4-octyloxyphenyl)-[1]benzothieno[3,2-b]benzothiophene (F$_3$8)

19F$_3$8 (120 mg, 0.22 mmol), **7** (140 mg, 0.22 mmol), THF (50 ml), saturated NaHCO$_3$ solution (25 ml) and Pd(PPh$_3$)$_4$ (20 mg, 0.02 mmol); yield 62 mg (0.065 mmol, 29 %); colorless solid; ^{1}H NMR (400 MHz, CDCl$_3$) δ 8.11 (dd, J = 26.2, 1.5 Hz, 2H, BTBT-H), 7.94 (dd, J = 9.3, 8.6 Hz, 2H, BTBT-H), 7.75 (d, J = 8.6 Hz, 2H, Ar-H), 7.71 (dd, J = 8.3, 1.6 Hz, 1H, BTBT-H), 7.65 (dd, J = 8.3, 1.6 Hz, 1H, BTBT-H), 7.45 (s, 2H, Ar-H), 7.46 – 7.37 (m, 2H), 7.33 (d, J = 8.6 Hz, 2H, Ar-H), 7.07 (t, J = 8.6 Hz, 1H, Ar-H), 4.12 – 4.05 (m, 8H, OCH$_2$CH$_2$), 1.90 – 1.73 (m, 8H, OCH$_2$CH$_2$), 1.55 – 1.46 (m, 8H, CH$_2$), 1.42 – 1.25 (m, 20H, CH$_2$), 0.95 – 0.88 (m, 12H, CH$_3$); ^{19}F NMR (376 MHz, CDCl$_3$) δ -133.95 (dd, J = 12.1, 8.7 Hz); ^{13}C NMR (126 MHz, CDCl$_3$) δ 165.06 (C=O), 152.99, 150.68, 143.24, 143.17, 143.13, 142.46, 142.10, 138.41, 137.58, 133.58, 133.46, 132.26, 132.07, 128.36, 128.36, 124.52, 124.10, 123.81, 122.80, 122.77, 122.33, 122.26, 121.84, 121.81, 121.80, 115.21, 115.19, 115.07, 114.92, 112.70, 108.66 (BTBT-C + Ar-C), 73.60, 69.65, 69.31 (OCH$_2$), 31.81, 31.72, 31.55, 30.30, 29.33, 29.27, 29.24, 29.22, 25.94, 25.75, 25.70, 22.67, 22.65, 22.61 (CH$_2$), 14.09, 14.07, 14.01 (CH$_3$); HRMS (m/z): [M]+Li$^+$ calcd. for C$_{59}$H$_{71}$FO$_6$S$_2$Li, 965.483; found 965.479.

2-[4-(3,4,5-Tri-n-hexyloxybenzoyloxy)phenyl]-7-(2-fluoro-4-octyloxyphenyl)-[1]benzothieno[3,2-b]benzothiophene (F$_2$8)

19F$_2$8 (120 mg, 0.22 mmol), **7** (140mg, 0.22 mmol), THF (50 ml), saturated NaHCO$_3$ solution (25 ml) and Pd(PPh$_3$)$_4$ (20 mg, 0.02 mmol); yield 75 mg (0.078 mmol, 35 %); colorless solid; ^{1}H NMR (400 MHz, CDCl$_3$) δ 8.14 (d, J = 1.1 Hz, 1H, BTBT-H), 8.07 (s, 1H, BTBT-H), 7.95 (t, J = 8.7 Hz, 2H, BTBT-H), 7.75 (d, J = 8.6 Hz, 2H, Ar-H), 7.71 (dd, J = 8.3, 1.5 Hz, 1H, BTBT-H), 7.63 (dt, J = 8.7, 1.4 Hz, 1H, BTBT-H), 7.45 (s, 2H, Ar-H), 7.47 – 7.41 (m, 1H, Ar-H), 7.33 (d, J = 8.6 Hz, 2H, Ar-H), 6.81 (dd, J = 8.5, 2.5 Hz, 1H, Ar-H), 6.76 (dd, J = 12.5, 2.5 Hz, 1H, Ar-H), 4.11 – 4.05 (m, 6H, OCH$_2$CH$_2$), 4.01 (t, J = 6.6 Hz, 2H, OCH$_2$CH$_2$), 1.89 – 1.73 (m, 8H, OCH$_2$CH$_2$), 1.58 – 1.46 (m, 8H, CH$_2$), 1.40 – 1.28 (m, 20H, CH$_2$), 0.96 – 0.88 (m, 12H, CH$_3$); ^{19}F NMR (376 MHz, CDCl$_3$) δ -115.48 (dd, J = 11.3, 10.2 Hz); ^{13}C NMR (101 MHz, CDCl$_3$) δ 165.05, 161.59, 160.08 (C=O), 152.98, 150.66, 145.37, 143.18, 143.11, 142.72, 138.42, 137.50, 133.62, 133.46, 132.95, 132.27, 131.92, 131.08, 131.03, 128.35, 126.02, 125.99, 124.46, 123.99, 123.96, 123.82, 122.30, 122.24, 121.78, 121.35, 120.53, 111.04, 108.64, 102.76, 102.50 (BTBT-C + Ar-C), 73.59, 69.30, 68.51 (OCH$_2$), 31.80, 31.72, 31.54, 30.29, 29.33, 29.26, 29.22, 29.13, 26.00, 25.74, 25.69, 22.66, 22.65, 22.60 (CH$_2$), 14.08, 14.06, 14.00 (CH$_3$); HRMS (m/z): [M]+Li$^+$ calcd. for C$_{59}$H$_{71}$FO$_6$S$_2$Li, 965.483; found 965.482.

2-[4-(3,4,5-Tri-n-hexyloxybenzoyloxy)phenyl]-7-(2,3-difluoro-4-octyloxyphenyl)-[1]benzothieno[3,2-b]benzothiophene (F$_{23}$8)

19F$_{23}$8 (120 mg, 0.21 mmol), **7** (140 mg, 0.22 mmol), THF (50 ml), saturated NaHCO$_3$ solution (25 ml) and Pd(PPh$_3$)$_4$ (20 mg, 0.02 mmol); yield 55 mg (0.056 mmol, 26 %); colorless solid; ^{1}H NMR (500 MHz, CDCl$_3$) δ 8.14 (d, J = 1.0 Hz, 1H, BTBT-H), 8.07 (s, 1H, BTBT-H), 7.96 (dd, J = 7.9, 7.4 Hz, 2H, BTBT-H), 7.75 (d, J = 8.7 Hz, 2H, Ar-H), 7.72 (dd, J = 8.3, 1.6 Hz, 1H, BTBT-H), 7.62 (dt, J = 8.2, 1.5 Hz, 1H, BTBT-H), 7.45 (s, 2H, Ar-H), 7.33 (d, J = 8.7 Hz, 2H, Ar-H), 7.20 (td, J = 8.5, 2.3 Hz, 1H, Ar-H), 6.85 (ddd, J = 9.0, 7.4, 1.7 Hz, 1H, Ar-H), 4.14 – 4.03 (m, 8H, OCH$_2$CH$_2$), 1.91 – 1.74 (m, 8H, OCH$_2$CH$_2$), 1.56 – 1.46 (m, 8H, CH$_2$), 1.41 – 1.25 (m, 20H, CH$_2$), 0.94 – 0.88 (m, 12H, CH$_3$); ^{19}F NMR (470 MHz, CDCl$_3$) δ -141.52 (dd, J = 19.7, 7.8 Hz), -158.40 (dd, J = 19.8, 6.4 Hz); ^{13}C NMR (126 MHz, CDCl$_3$) δ 165.06 (C=O), 152.99, 150.70, 143.25, 143.13, 142.77, 138.40, 137.68, 133.80, 133.56, 132.35, 132.21, 131.99, 131.96, 128.37, 125.90, 125.88, 124.53, 124.04, 124.01, 123.81, 123.78, 123.75, 123.72, 122.52, 122.43, 122.34, 122.26, 121.87, 121.50, 109.73, 108.66 (BTBT-C + Ar-C),73.60, 69.98, 69.31 (OCH$_2$), 31.80, 31.72, 31.55, 30.30, 29.30, 29.27, 29.20, 29.17, 25.89, 25.75, 25.70, 22.67, 22.65, 22.61 (CH$_2$), 14.08, 14.07, 14.01 (CH$_3$); HRMS (m/z): [M]+Li$^+$ calcd. for C$_{59}$H$_{70}$F$_2$O$_6$S$_2$Li, 983.474; found 983.471.

2-[4-(3,4,5-Tri-n-hexyloxybenzoyloxy)phenyl]-7-(3,5-difluoro-4-octyloxyphenyl)-[1]benzothieno[3,2-b]benzothiophene (F$_{35}$8)

19F$_{35}$8 (120 mg, 0.21 mmol), **7** (140 mg, 0.22 mmol), THF (50 ml), saturated NaHCO$_3$ solution (25 ml) and Pd(PPh$_3$)$_4$ (20 mg, 0.02 mmol); yield 65 mg (0.067 mmol, 31 %); colorless solid; ^{1}H NMR (500 MHz, CDCl$_3$) δ 8.14 (d, J = 0.9 Hz, 1H, BTBT-H), 8.06 (d, J = 1.0 Hz, 1H, BTBT-H), 7.95 (dd, J = 9.5, 8.5 Hz, 2H, BTBT-H), 7.75 (d, J = 8.6 Hz, 2H, Ar-H), 7.72 (dd, J = 8.3, 1.5 Hz, 1H, BTBT-H), 7.62 (dd, J = 8.3, 1.6 Hz, 1H, BTBT-H), 7.45 (s, 2H, Ar-H), 7.33 (d, J = 8.6 Hz, 2H, Ar-H), 7.24 (d, J = 9.0 Hz, 2H, Ar-H), 4.20 (t, J = 6.6 Hz, 2H, OCH$_2$CH$_2$), 4.10 – 4.05 (m, 6H, OCH$_2$CH$_2$), 1.88 – 1.74 (m, 8H, OCH$_2$CH$_2$), 1.56 – 1.46 (m, 8H, CH$_2$), 1.39 – 1.28 (m, 20H,

CH$_2$), 0.94 – 0.87 (m, 12H, CH$_3$); ^{19}F NMR (470 MHz, CDCl$_3$) δ -127.46 (d, J = 8.8 Hz); ^{13}C NMR (126 MHz, CDCl$_3$) δ 165.05, 157.28, 155.30 (C=O), 152.99, 150.71, 143.25, 143.23, 143.14, 138.34, 137.75, 135.86, 135.62, 135.22, 135.11, 133.93, 133.46, 132.65, 132.14, 128.36, 124.56, 124.33, 123.97, 123.79, 122.33, 122.27, 122.01, 121.92, 121.88, 110.88, 108.65 (BTBT-C + Ar-C),74.93, 73.59, 69.31(OCH$_2$), 31.79, 31.72, 31.54, 30.29, 29.98, 29.28, 29.26, 29.21, 25.74, 25.69, 25.66, 22.66, 22.64, 22.60 (CH$_2$), 14.08, 14.06, 14.00 (CH$_3$); HRMS (m/z): [M]+Li$^+$ calcd. for C$_{59}$H$_{70}$F$_2$O$_6$S$_2$Li, 983.474; found 983.471.

2-[4-(3,4,5-Tri-n-hexyloxybenzoyloxy)phenyl]-7-(2,6-difluoro-4-octyloxyphenyl)-[1]benzothieno[3,2-b]benzothiophene (F$_{26}$8)

19F$_{26}$8 (120 mg, 0.21 mmol), **7** (140 mg, 0.22 mmol), THF (50 ml), saturated NaHCO$_3$ solution (25 ml) and Pd(PPh$_3$)$_4$ (20 mg, 0.02 mmol); yield 80 mg (0.082 mmol, 38 %); colorless solid; ^{1}H NMR (400 MHz, CDCl$_3$) δ 8.14 (d, J = 1.1 Hz, 1H, BTBT-H), 8.00 (s, 1H, BTBT-H), 7.96 (dd, J = 8.2, 5.1 Hz, 2H, BTBT-H), 7.75 (d, J = 8.6 Hz, 2H, Ar-H), 7.71 (dd, J = 8.3, 1.5 Hz, 1H, BTBT-H), 7.55 (dd, J = 8.2, 1.2 Hz, 1H, BTBT-H), 7.45 (s, 2H, Ar-H), 7.33 (d, J = 8.6 Hz, 2H, Ar-H), 6.59 (d, J = 9.7 Hz, 2H, Ar-H), 4.10 – 4.05 (m, 6H, OCH$_2$CH$_2$), 3.99 (t, J = 6.5 Hz, 2H, OCH$_2$CH$_2$), 1.89 – 1.73 (m, 8H, OCH$_2$CH$_2$), 1.58 – 1.44 (m, 8H, CH$_2$), 1.42 – 1.24 (m, 20H, CH$_2$), 0.94 – 0.89 (m, 12H, CH$_3$).^{19}F NMR (376 MHz, CDCl$_3$) δ -113.68 (d, J = 9.3 Hz); ^{13}C NMR (101 MHz, CDCl$_3$) δ 165.05, 161.84, 159.49 (C=O), 152.98, 150.67, 143.24, 143.11, 142.35, 138.42, 137.62, 133.80, 133.64, 132.40, 132.22, 128.36, 127.35, 126.34, 125.71, 124.48, 123.82, 122.33, 122.24, 121.86, 121.14, 108.64, 98.86, 98.56 (BTBT-C + Ar-C), 73.59, 69.30, 68.77 (OCH$_2$), 31.79, 31.72, 31.54, 30.29, 29.28, 29.26, 29.20, 28.97, 25.94, 25.74, 25.69, 22.66, 22.64, 22.60 (CH$_2$), 14.08, 14.06, 14.00 (CH$_3$); HRMS (m/z): [M]+Li$^+$ calcd. for C$_{59}$H$_{70}$F$_2$O$_6$S$_2$Li, 983.474; found 983.470.

2-[4-(3,4,5-Tri-n-hexyloxybenzoyloxy)phenyl]-7-(2,3,5,6-tetrafluoro-4-octyloxyphenyl)-[1]benzothieno[3,2-b]benzothiophene (F$_{2356}$8)

19F$_{2356}$8 (120 mg, 0.20 mmol), **7** (130 mg, 0.20 mmol), THF (50 ml), saturated NaHCO$_3$ solution (25 ml) and Pd(PPh$_3$)$_4$ (20 mg, 0.02 mmol); yield 42 mg (0.041 mmol, 21 %); colorless solid; ^{1}H NMR (500 MHz, CDCl$_3$) δ 8.15 (d, J = 1.0 Hz, 1H, BTBT-H), 8.03 – 7.97 (m, 3H, BTBT-H), 7.76 – 7.71 (m, 3H, BTBT-H + Ar-H), 7.55 (dd, J = 8.3, 1.2 Hz, 1H, BTBT-H), 7.45 (s, 2H, Ar-H), 7.33 (d, J = 8.6 Hz, 2H, Ar-H), 4.30 (t, J = 6.6 Hz, 2H, OCH$_2$CH$_2$), 4.08 (td, J = 6.5, 3.6 Hz, 6H, OCH$_2$CH$_2$), 1.88 – 1.75 (m, 8H, OCH$_2$CH$_2$), 1.57 – 1.47 (m, 8H, CH$_2$), 1.41 – 1.26 (m, 20H, CH$_2$), 0.95 – 0.87 (m, 12H, CH$_3$); ^{19}F NMR (470 MHz, CDCl$_3$) δ -145.10 (dd, J = 22.4, 8.6 Hz), -157.22 (dd, J = 22.4, 8.5 Hz); ^{13}C NMR (126 MHz, CDCl$_3$) δ 165.05 (C=O), 152.98, 150.73, 143.13, 142.49, 137.93, 134.47, 133.49, 133.24, 132.05, 128.38, 126.99, 124.60, 123.79, 122.37, 122.27, 121.99, 121.52, 108.65 (BTBT-C + Ar-C), 75.44, 73.59, 69.30 (OCH$_2$), 31.76, 31.71, 31.54, 30.28, 29.92, 29.26, 29.21, 29.17, 25.74, 25.69, 25.55, 22.66, 22.62, 22.59 (CH$_2$), 14.06, 14.06, 14.00 (CH$_3$); HRMS (m/z): [M]+Li$^+$ calcd. for C$_{59}$H$_{68}$F$_4$O$_6$S$_2$Li, 1019.455; found 1019.454.

11.5.3 Representative NMR and HRMS spectra
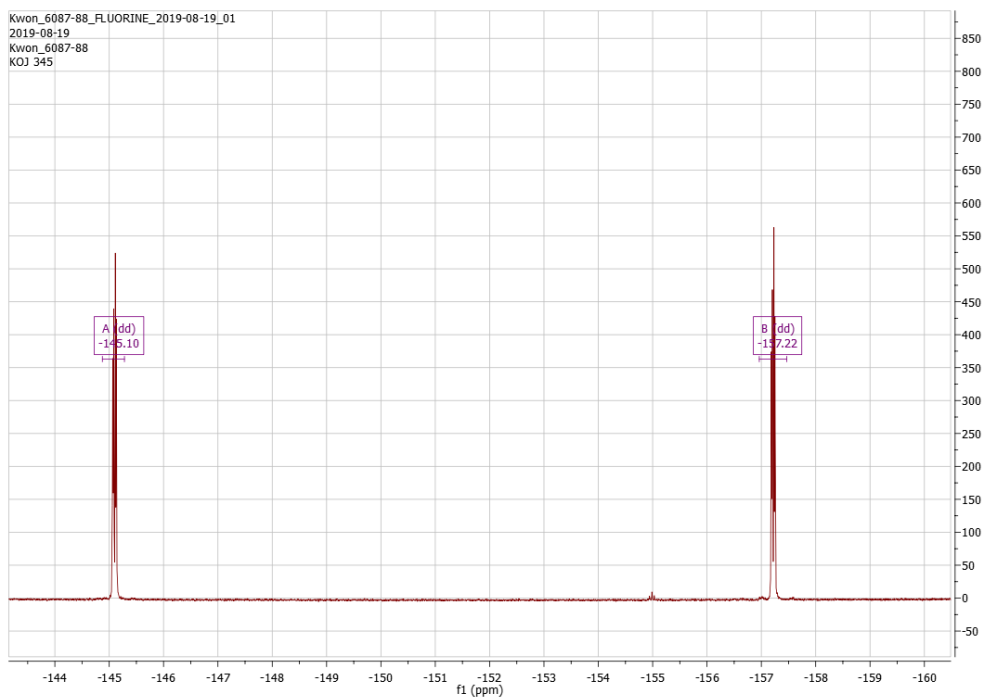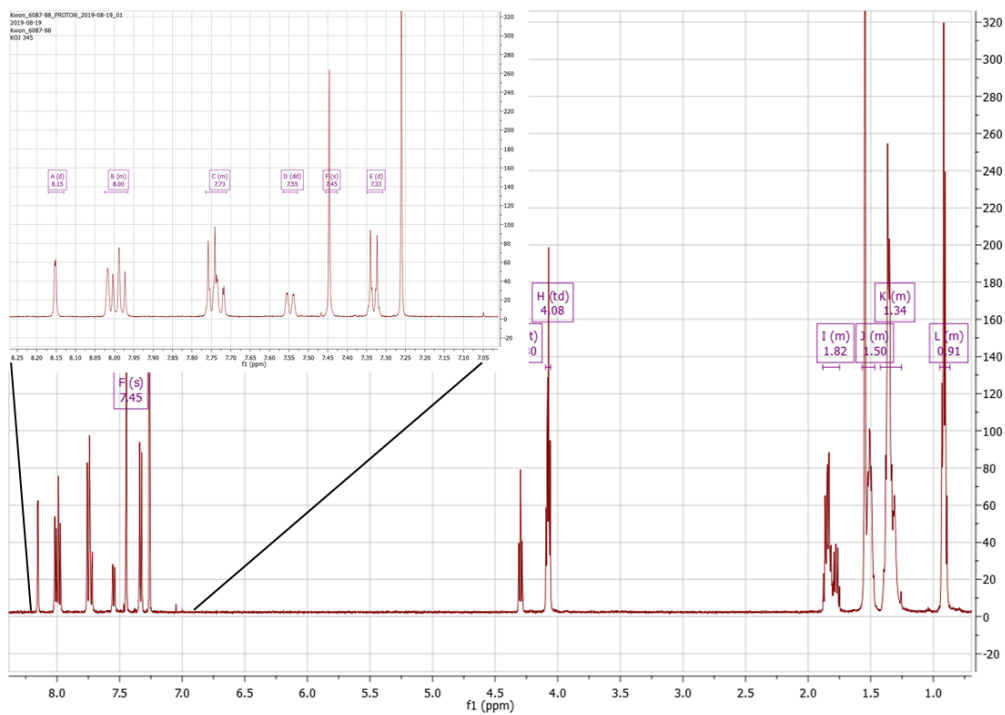
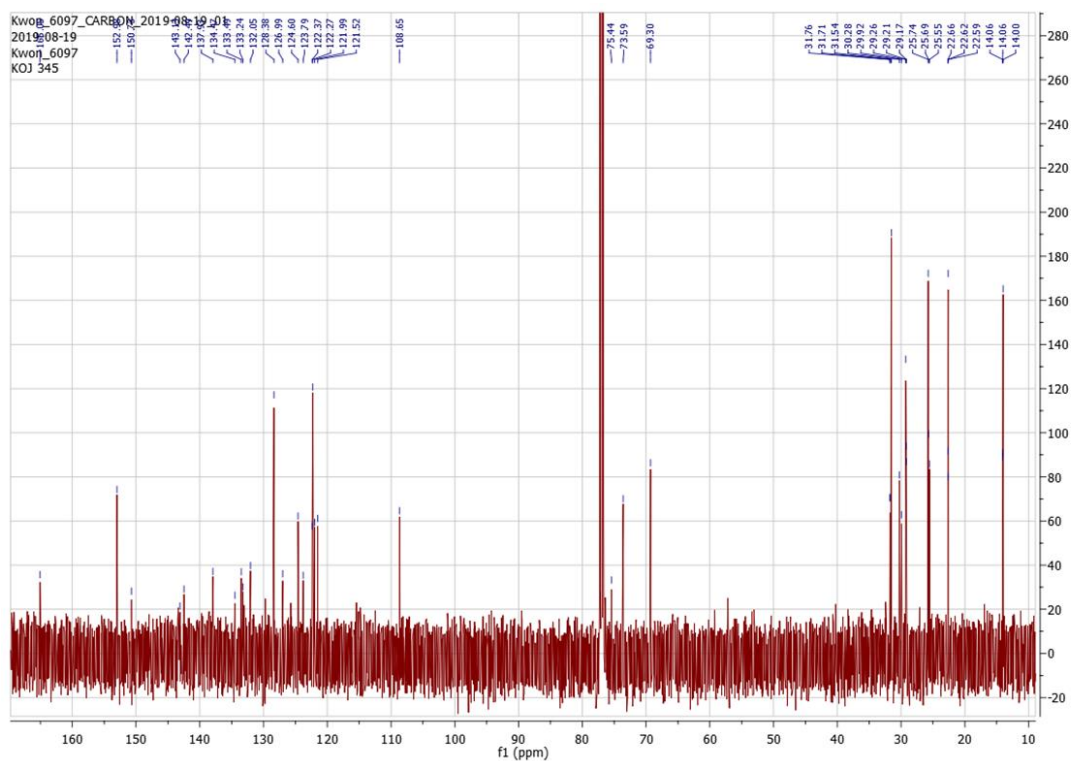**Figure S11.9** ^{1}H-, ^{19}F- and ^{13}C-NMR of compound **F$_{2356}$8**. The spectra were measured at 27 °C, with the frequencies 500 MHz (^{1}H), 470 MHz (^{19}F) and 126 MHz (^{13}C) in CDCl$_3$ as solvent.
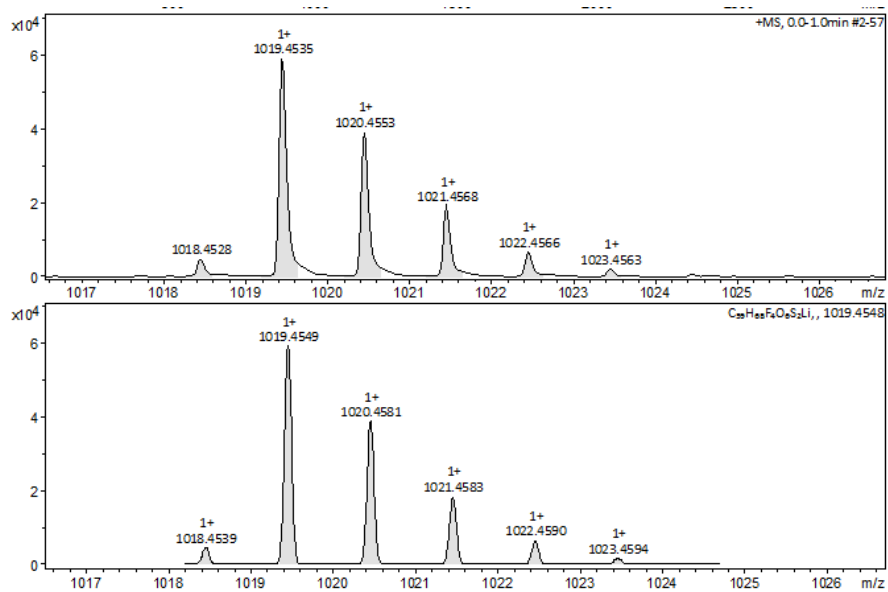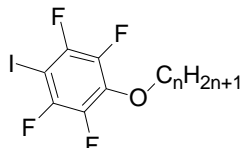

Figure S11.10 HRMS spectra for **F$_{2356}$8.**

11.6 Synthesis and analytical data of the 3,4,5-trihexyloxybenzoates, 3,4,5-tridecyloxybenzoates, 2,6-dibromo-3,4,5-tridecyloxybenzoates with tetrafluorinated benzene $F_X n$, $F'_X n$, $BBF'_X n$

The synthesis was performed according to schemes 2.6.

11.6.1 Synthesis and analytical data of intermediates
Synthesis of $17F_{2356}n$

1,2,4,5-Tetrafluoro-3-iodo-6-butyloxy-benzene ($17F_{2356}4$)

Iodopentafluorobenzene 5.0 g (1.70 mmol), 1-butanol 2.5 g (0.034 mmol), K_2CO_3 7.1 g (0.051 mol), DMF (50 ml); yield 3.6g (0.0103 mol, 61%); transparent liquid; ^{1}H NMR (500 MHz, CDCl$_3$) δ 4.24 (t, J = 6.5 Hz, 2H, OCH$_2$CH$_2$), 1.80 – 1.71 (m, 2H, OCH$_2$CH$_2$), 1.54 – 1.45 (m, 2H, CH$_2$), 0.97 (t, J = 7.4 Hz, 3H, CH$_3$); ^{19}F NMR (470 MHz, CDCl$_3$) δ -121.65 (dt, J = 24.8, 4.8 Hz), -154.51 (td, J = 8.6, 4.7 Hz).

1,2,4,5-Tetrafluoro-3-iodo-6-hexyloxy-benzene ($17F_{2356}6$)

Iodopentafluorobenzene 5.0 g (1.70 mmol), 1-hexanol 3.5 g (0.034 mol), K_2CO_3 7.1 g (0.051 mol), DMF (50 ml); yield 3.5g (9.31 mmol, 55%); transparent liquid; ^{1}H NMR (400 MHz, CDCl$_3$) δ 4.23 (t, J = 6.6 Hz, 2H, OCH$_2$CH$_2$), 1.81 – 1.72 (m, 2H, OCH$_2$CH$_2$), 1.52 – 1.40 (m, 2H, CH$_2$), 1.39 – 1.28 (m, 4H, CH$_2$), 0.90 (t, J = 7.0 Hz, 3H, CH$_3$); ^{19}F NMR (376 MHz, CDCl$_3$) δ -121.65 (td, J = 11.0, 6.0 Hz), -154.48 (td, J = 10.1, 5.0 Hz).

1,2,4,5-Tetrafluoro-3-iodo-6-decyloxy-benzene ($17F_{2356}10$)

Iodopentafluorobenzene 5.0 g (0.017 mol), 1-decanol 5.4 g (0.034 mol), K_2CO_3 7.1 g (0.051 mol), DMF (50 ml); yield 4.2 g (9.72 mmol, 57%); transparent liquid; ^{1}H NMR (400 MHz, CDCl$_3$) δ 4.23 (t, J = 6.4 Hz, 2H, OCH$_2$CH$_2$), 1.82 – 1.72 (m, 2H, OCH$_2$CH$_2$), 1.51 – 1.39 (m, 2H, CH$_2$), 1.38 – 1.20 (m, 12H, CH$_2$), 0.88 (t, J = 6.7 Hz, 3H, CH$_3$); ^{19}F NMR (376 MHz, CDCl$_3$) δ -121.66 (td, J = 10.0, 5.0 Hz), -154.47 (td, J = 10.0, 5.0 Hz).

1,2,4,5-Tetrafluoro-3-iodo-6-tetradecyloxy-benzene ($17F_{2356}14$)

Iodopentafluorobenzene 5.0 g (0.017 mol), 1-tetradecanol 7.3 g (0.034 mol), K_2CO_3 7.1 g (0.051 mol), DMF (50 ml); yield 4.4g (9.01 mmol, 53%); transparent liquid; ^{1}H NMR (500 MHz, CDCl$_3$) δ 4.23 (t, J = 6.6 Hz, 2H, OCH$_2$CH$_2$), 1.81 – 1.74 (m, 2H, OCH$_2$CH$_2$), 1.50 – 1.42 (m, 2H, CH$_2$), 1.40 – 1.22 (m, 20H, CH$_2$), 0.88 (t, J = 6.9 Hz, 3H, CH$_3$); ^{19}F NMR (470 MHz, CDCl$_3$) δ -121.64 (td, J = 9.7, 4.8 Hz), -154.46 (td, J = 9.9, 5.0 Hz).

1,2,4,5-Tetrafluoro-3-iodo-6-octadecyloxy-benzene ($17F_{2356}18$)

Iodopentafluorobenzene 5.0 g (0.017 mol), 1-octadecanol 9.2 g (0.034 mol), K_2CO_3 7.1 g (0.051 mmol), DMF (50 ml); yield 4.0 g (7.35 mmol, 43%); transparent liquid; ^1H NMR (400 MHz, $CDCl_3$) δ 4.23 (t, J = 6.6 Hz, 2H, OCH_2CH_2), 1.82 – 1.72 (m, 2H, OCH_2CH_2), 1.49 – 1.40 (m, 2H, CH_2), 1.37 – 1.21 (m, 28H, CH_2), 0.88 (t, J = 6.9 Hz, 3H, CH_3); ^{19}F NMR (376 MHz, $CDCl_3$) δ -121.65 (td, J = 10.0, 5.0 Hz), -154.46 (td, J = 9.8, 4.9 Hz).

Synthesis of 18F$_{2356}n$
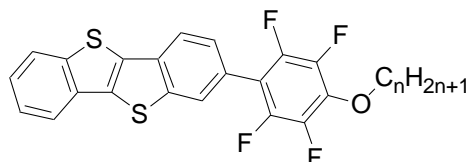
2-(2,3,5,6-Tetrafluoro-4-butyloxyphenyl)-[1]benzothieno[3,2-b]benzothiophene (18F$_{2356}$4)

4 0.7 g (1.91 mmol), **17F$_{2356}$4** 2.0 g (5.74 mmol), THF (100 ml) and saturated $NaHCO_3$ solution (50 ml), [Pd(PPh$_3$)$_4$] (30 mg, 0.026 mmol); yield 250 mg (0.54 mmol, 28%); transparent solid; m.p. 233 °C; ^1H NMR (400 MHz, $CDCl_3$) δ 8.00 (d, J = 0.4 Hz, 1H, BTBT-H)), 7.98 (d, J = 8.3 Hz, 1H, BTBT-H)), 7.93 (dd, J = 11.3, 7.4 Hz, 2H, BTBT-H)), 7.53 (dd, J = 8.3, 1.4 Hz, 1H, BTBT-H)), 7.46 (dtd, J = 16.5, 7.3, 1.2 Hz, 2H, BTBT-H)), 4.31 (t, J = 6.5 Hz, 2H, OCH_2CH_2), 1.86 – 1.77 (m, 2H, OCH_2CH_2), 1.59 – 1.48 (m, 2H, CH_2), 1.01 (t, J = 7.4 Hz, 3H, CH_3); ^{19}F NMR (376 MHz, $CDCl_3$) δ -145.10 (dd, J = 22.4, 8.8 Hz), -157.28 (dd, J = 22.1, 8.6 Hz).

2-(2,3,5,6-Tetrafluoro-4-hexyloxyphenyl)-[1]benzothieno[3,2-b]benzothiophene (18F$_{2356}$6)

4 0.7 g (1.91 mmol), **17F$_{2356}$6** 2.2 g (5.74 mmol), THF (100 ml) and saturated $NaHCO_3$ solution (50 ml), [Pd(PPh$_3$)$_4$] (30 mg, 0.026 mmol); yield 230 mg (0.47 mmol, 25%); transparent solid; m.p. 221 °C; ^1H NMR (400 MHz, $CDCl_3$) δ 8.00 (d, J = 0.8 Hz, 1H, BTBT-H), 7.98 (d, J = 8.3 Hz, 1H, BTBT-H), 7.93 (dd, J = 11.1, 7.4 Hz, 2H, BTBT-H), 7.53 (dd, J = 8.3, 1.5 Hz, 1H, BTBT-H), 7.46 (dtd, J = 16.4, 7.3, 1.2 Hz, 2H, BTBT-H), 4.29 (t, J = 6.5 Hz, 2H, OCH_2CH_2), 1.87 – 1.78 (m, 2H, OCH_2CH_2), 1.57 – 1.45 (m, 2H, CH_2), 1.41 – 1.31 (m, 4H, CH_2), 0.93 (t, J = 7.0 Hz, 3H, CH_3); ^{19}F NMR (376 MHz, $CDCl_3$) δ -145.11 (dd, J = 22.3, 8.8 Hz), -157.25 (dd, J = 22.1, 8.6 Hz).

2-(2,3,5,6-Tetrafluoro-4-decyloxyphenyl)-[1]benzothieno[3,2-b]benzothiophene (18F$_{2356}$10)

4 0.7 g (1.91 mmol), **17F$_{2356}$10** 2.5 g (5.74 mmol), THF (100 ml) and saturated $NaHCO_3$ solution (50 ml), [Pd(PPh$_3$)$_4$] (30 mg, 0.026 mmol); yield 180 mg (0.33 mmol, 17%); transparent solid; m.p. 219 °C; ^1H NMR (500 MHz, $CDCl_3$) δ 8.00 (d, J = 1.7 Hz, 1H, BTBT-H), 7.98 (d, J = 9.2 Hz, 1H , BTBT-H), 7.93 (dd, J = 13.1, 8.0 Hz, 2H, BTBT-H), 7.53 (dd, J = 8.6, 0.8 Hz, 1H, BTBT-H), 7.46 (dtd, J = 24.1, 7.6, 0.8 Hz, 2H, BTBT-H), 4.29 (t, J = 6.5 Hz, 2H, OCH_2CH_2), 1.87 – 1.79 (m, 2H, OCH_2CH_2), 1.55 – 1.46 (m, 2H, CH_2), 1.41 – 1.23 (m, 12H, CH_2), 0.89 (t, J = 6.6 Hz, 3H, CH_3); ^{19}F NMR (470 MHz, $CDCl_3$) δ -145.11 (dd, J = 22.3, 8.7 Hz), -157.24 (dd, J = 22.2, 8.6 Hz).

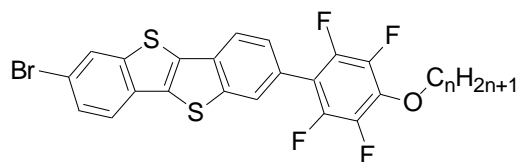## 2-(2,3,5,6-Tetrafluoro-4-tetradecyloxyphenyl)-[1]benzothieno[3,2-b]benzothiophene (18F$_{2356}$14)

4 0.7 g (1.91 mmol), **17F$_{2356}$14** 2.8 g (5.74 mmol), THF (100 ml) and saturated $NaHCO_3$ solution (50 ml), [Pd(PPh$_3$)$_4$] (30 mg, 0.026 mmol); yield 250 mg (0.42 mmol, 22 %); transparent solid;

m.p. 185 ℃; ^{1}H NMR (400 MHz, CDCl$_3$) δ 8.00 (d, J = 1.1 Hz, 1H, BTBT-H), 7.98 (d, J = 8.3 Hz, 1H, BTBT-H), 7.93 (dd, J = 10.4, 8.3 Hz, 2H, BTBT-H), 7.53 (dd, J = 8.3, 0.6 Hz, 1H, BTBT-H), 7.46 (dtd, J = 19.2, 7.2, 0.9 Hz, 2H, BTBT-H), 4.29 (t, J = 6.5 Hz, 2H, OCH$_2$CH$_2$), 1.86 – 1.78 (m, 2H, OCH$_2$CH$_2$), 1.56 – 1.46 (m, 2H, CH$_2$), 1.42 – 1.22 (m, 20H, CH$_2$), 0.88 (t, J = 6.6 Hz, 3H, CH$_3$); ^{19}F NMR (376 MHz, CDCl$_3$) δ -145.11 (dd, J = 22.3, 8.7 Hz), -157.24 (dd, J = 22.2, 8.6 Hz).

2-(2,3,5,6-Tetrafluoro-4-octadecyloxyphenyl)-[1]benzothieno[3,2-b]benzothiophene (18F$_{2356}$18)

4 0.7 g (1.91 mmol), **17F$_{2356}$18** 3.1 g (5.74 mmol), THF (100 ml) and saturated NaHCO$_3$ solution (50 ml), [Pd(PPh$_3$)$_4$] (30 mg, 0.026 mmol); yield 230 mg (0.35 mmol, 19 %); transparent solid; m.p. 189 ℃; ^{1}H NMR (500 MHz, CDCl$_3$) δ 8.00 (d, J = 0.8 Hz, 1H, BTBT-H), 7.98 (d, J = 8.3 Hz, 1H, BTBT-H), 7.93 (dd, J = 13.7, 7.8 Hz, 2H, BTBT-H), 7.53 (dd, J = 8.2, 1.4 Hz, 1H, BTBT-H), 7.46 (dtd, J = 15.1, 7.3, 1.2 Hz, 2H, BTBT-H), 4.29 (t, J = 6.5 Hz, 2H, OCH$_2$CH$_2$), 1.86 – 1.77 (m, 2H, OCH$_2$CH$_2$), 1.53 – 1.43 (m, 2H, OCH$_2$CH$_2$), 1.39 – 1.23 (m, 28H, CH$_2$), 0.88 (t, J = 6.9 Hz, 3H, CH$_3$); ^{19}F NMR (470 MHz, CDCl$_3$) δ -145.10 (dd, J = 22.3, 8.7 Hz), -157.23 (dd, J = 22.3, 8.6 Hz).

Synthesis of 19F$_{2356}$*n*

2-Bromo-7-(2,3,5,6-tetrafluoro-4-butyloxyphenyl)-[1]benzothieno[3,2-b]benzothiophene (19F$_{2356}$4)

18F$_{2356}$4 (250 mg, 0.54 mmol), bromine (100 mg, 0.63 mmol), DCM (50 ml); yield 210 mg (0.39 mmol, 72%); transparent solid; m.p. 230 ℃; ^{1}H NMR (500 MHz, CDCl$_3$) δ 8.08 (d, J = 1.5 Hz, 1H), 8.00 (d, J = 0.9 Hz, 1H), 7.97 (d, J = 8.2 Hz, 1H), 7.77 (d, J = 8.5 Hz, 1H), 7.59 (dd, J = 8.4, 1.7 Hz, 1H), 7.54 (dd, J = 8.3, 1.4 Hz, 2H), 4.31 (t, J = 6.5 Hz, 4H), 1.85 – 1.78 (m, 3H), 1.58 – 1.51 (m, 11H), 1.01 (t, J = 7.4 Hz, 5H); ^{19}F NMR (470 MHz, CDCl$_3$) δ -145.11 (dd, J = 22.0, 8.5 Hz), -157.21 (dd, J = 22.4, 8.8 Hz).

2-Bromo-7-(2,3,5,6-tetrafluoro-4-hexyloxyphenyl)-[1]benzothieno[3,2-b]benzothiophene (19F$_{2356}$6)

18F$_{2356}$6 (230 mg, 0.47 mmol), bromine (90 mg, 0.56 mmol), DCM (50 ml); yield 200 mg (0.35 mmol, 75%); transparent solid; H: Cr 192 SmA 221 Iso; C: Iso 221 SmA 180 Cr; ^{1}H NMR (400 MHz, CDCl$_3$) δ 8.08 (d, J = 1.7 Hz, 1H, BTBT-H), 8.00 (d, J = 1.1 Hz, 1H, BTBT-H), 7.97 (d, J = 8.3 Hz, 1H, BTBT-H), 7.77 (d, J = 8.4 Hz, 1H, BTBT-H), 7.59 (dd, J = 8.5, 1.7 Hz, 1H, BTBT-H), 7.54 (dd, J = 8.2, 1.4 Hz, 1H, BTBT-H), 4.30 (t, J = 6.6 Hz, 2H, OCH$_2$CH$_2$), 1.86 – 1.78 (m, 2H, OCH$_2$CH$_2$), 1.56 – 1.47 (m, 2H, CH$_2$), 1.41 – 1.32 (m, 4H, CH$_2$), 0.93 (t, J = 7.0 Hz, 3H, CH$_3$); ^{19}F NMR (376 MHz, CDCl$_3$) δ -145.11 (dd, J = 22.3, 8.9 Hz), -157.18 (dd, J = 21.9, 8.3 Hz).
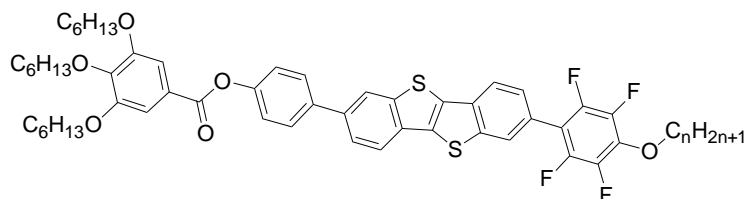
2-Bromo-7-(2,3,5,6-tetrafluoro-4-decyloxyphenyl)-[1]benzothieno[3,2-b]benzothiophene (19F$_{2356}$10)

18F₂₃₅₆10 (180 mg, 0.33 mmol), bromine (60 mg, 0.38 mmol), DCM (50 ml); yield 170 mg (0.27 mmol, 82%); transparent solid; m.p. 95°C'; ^{1}H NMR (400 MHz, CDCl$_3$) δ 8.08 (d, J = 1.7 Hz, 1H, BTBT-H), 8.00 (d, J = 1.3 Hz, 1H, BTBT-H), 7.97 (d, J = 8.4 Hz, 1H, BTBT-H), 7.77 (d, J = 8.5 Hz, 1H, BTBT-H), 7.59 (dd, J = 8.4, 1.7 Hz, 1H, BTBT-H), 7.54 (dd, J = 8.2, 1.4 Hz, 1H, BTBT-H), 4.29 (t, J = 6.5 Hz, 2H, OCH$_2$CH$_2$), 1.86 – 1.78 (m, 2H, OCH$_2$CH$_2$), 1.56 – 1.46 (m, 2H, CH$_2$), 1.40 – 1.24 (m, 12H, CH$_2$), 0.89 (t, J = 6.8 Hz, 3H, CH$_3$); ^{19}F NMR (376 MHz, CDCl$_3$) δ -145.12 (dd, J = 22.1, 8.7 Hz), -157.17 (dd, J = 21.9, 8.3 Hz).

2-Bromo-7-(2,3,5,6-tetrafluoro-4-tetradecyloxyphenyl)-[1]benzothieno[3,2-b]benzothiophene (19F₂₃₅₆14)

18F₂₃₅₆14 (250 mg, 0.41 mmol), bromine (80 mg, 0.50 mmol), DCM (50 ml); yield 230 mg (0.34 mmol, 81%); transparent solid; H: Cr 176 SmA 180 Iso; C: Iso 178 SmA 165 Cr; ^{1}H NMR (500 MHz, CDCl$_3$) δ 8.08 (d, J = 1.4 Hz, 1H, BTBT-H), 8.00 (d, J = 0.9 Hz, 1H, BTBT-H), 7.97 (d, J = 8.3 Hz, 1H, BTBT-H), 7.77 (d, J = 8.5 Hz, 1H, BTBT-H), 7.59 (dd, J = 8.4, 1.7 Hz, 1H, BTBT-H), 7.54 (dd, J = 8.2, 1.6 Hz, 1H, BTBT-H), 4.29 (t, J = 6.5 Hz, 2H, OCH$_2$CH$_2$), 1.86 – 1.79 (m, 2H, OCH$_2$CH$_2$), 1.55 – 1.46 (m, 2H, CH$_2$), 1.40 – 1.23 (m, 20H, CH$_2$), 0.88 (t, J = 6.9 Hz, 3H, CH$_3$); ^{19}F NMR (470 MHz, cdcl$_3$) δ -145.11 (dd, J = 22.8, 6.1 Hz), -157.16 (dd, J = 22.5, 9.0 Hz).

2-Bromo-7-(2,3,5,6-tetrafluoro-4-octadecyloxyphenyl)-[1]benzothieno[3,2-b]benzothiophene (19F₂₃₅₆18)

18F₂₃₅₆18 (230 mg, 0.35 mmol), bromine (70 mg, 0.44 mmol), DCM (50 ml); yield 200 mg (0.27 mmol, 78%); transparent solid; m.p 160°C; ^{1}H NMR (500 MHz, CDCl$_3$) δ 8.08 (d, J = 1.6 Hz, 1H, BTBT-H), 8.00 (d, J = 0.9 Hz, 1H, BTBT-H), 7.97 (d, J = 8.3 Hz, 1H, BTBT-H), 7.76 (d, J = 8.5 Hz, 1H, BTBT-H), 7.59 (dd, J = 8.5, 1.7 Hz, 1H, BTBT-H), 7.54 (dd, J = 8.2, 0.9 Hz, 1H, BTBT-H), 4.29 (t, J = 6.6 Hz, 2H, OCH$_2$CH$_2$), 1.86 – 1.78 (m, 2H, OCH$_2$CH$_2$), 1.55 – 1.46 (m, 2H, CH$_2$), 1.40 – 1.21 (m, 28H, CH$_2$), 0.88 (t, J = 6.9 Hz, 3H, CH$_3$); ^{19}F NMR (470 MHz, CDCl$_3$) δ -145.11 (dd, J = 22.2, 8.5 Hz), -157.16 (dd, J = 22.3, 8.7 Hz).

11.6.2 Synthesis and analytical data of compounds F₂₃₅₆n

2-[4-(3,4,5-Tri-n-hexyloxybenzoyloxy)phenyl]-7-(2,3,5,6-tetrafluoro-4-butyloxyphenyl)-[1]benzothieno[3,2-b]benzothiophene (F₂₃₅₆4)

19F₂₃₅₆4 (120 mg, 0.22 mmol), **7a** (140 mg, 0.22 mmol), THF (50 ml), saturated NaHCO$_3$ solution (25 ml) and Pd(PPh$_3$)$_4$ (20 mg, 0.02 mmol); yield 52 mg (0.054 mmol, 24 %); transparent solid; ^{1}H NMR (400 MHz, CDCl$_3$) δ 8.15 (d, J = 1.3 Hz, 1H, BTBT-H), 8.03 – 7.96 (m, 3H, BTBT-H), 7.77 – 7.71 (m, 3H, BTBT-H + Ar-H), 7.55 (dd, J = 8.3, 1.4 Hz, 1H, BTBT-H), 7.45 (s, 2H, Ar-H), 7.33 (d, J = 8.6 Hz, 2H, Ar-H), 4.31 (t, J = 6.5 Hz, 2H, OCH$_2$CH$_2$), 4.08 (td, J = 6.5, 3.3 Hz, 6H, OCH$_2$CH$_2$), 1.89 – 1.74 (m, 8H, OCH$_2$CH$_2$), 1.59 – 1.47 (m, 8H, CH$_2$), 1.41 – 1.32 (m, 12H, CH$_2$), 1.01 (t, J = 7.4 Hz, 3H, CH$_2$), 0.92 (t, J = 6.6 Hz, 9H, CH$_3$); ^{19}F NMR (376 MHz, CDCl$_3$) δ -145.09 (dd, J = 22.5, 8.7 Hz), -157.25 (dd, J = 22.3, 8.6 Hz); ^{13}C NMR (126 MHz, CDCl$_3$) δ

165.04 (C=O), 152.99, 150.73, 143.37, 143.13, 142.49, 138.32, 137.92, 134.47, 133.49, 133.24, 132.05, 128.38, 126.98, 125.72, 124.59, 123.79, 122.36, 122.27, 121.99, 121.51, 108.65 (BTBT-C + Ar-C), 75.12, 73.59, 69.31 (OCH$_2$), 31.94, 31.72, 31.54, 30.29, 29.26, 25.74, 25.69, 22.66, 22.60, (CH$_2$) 18.81, 14.06, 14.00, 13.70 (CH$_3$); HRMS (m/z): [M]+Li$^+$ calcd. for C$_{55}$H$_{60}$F$_4$O$_6$S$_2$Li, 963.392; found 963.391.

2-[4-(3,4,5-Tri-n-hexyloxybenzoyloxy)phenyl]-7-(2,3,5,6-tetrafluoro-4-hexyloxyphenyl)-[1]benzothieno[3,2-b]benzothiophene (F$_{2356}$6)

19F$_{2356}$6 (120 mg, 0.21 mmol), **7a** (140 mg, 0.22 mmol), THF (50 ml), saturated NaHCO$_3$ solution (25 ml) and Pd(PPh$_3$)$_4$ (20 mg, 0.02 mmol); yield 40 mg (0.041 mmol, 19 %); transparent solid; ^{1}H NMR (400 MHz, CDCl$_3$) δ 8.15 (d, *J* = 1.2 Hz, 1H, BTBT-H), 8.03 – 7.96 (m, 3H, BTBT-H), 7.77 – 7.71 (m, 3H, BTBT-H + Ar-H), 7.55 (dd, *J* = 8.3, 1.4 Hz, 1H, BTBT-H), 7.45 (s, 2H, Ar-H), 7.33 (d, *J* = 8.6 Hz, 2H, Ar-H), 4.30 (t, *J* = 6.6 Hz, 2H, OCH$_2$CH$_2$), 4.08 (td, *J* = 6.5, 2.8 Hz, 6H, OCH$_2$CH$_2$), 1.89 – 1.74 (m, 8H, OCH$_2$CH$_2$), 1.57 – 1.46 (m, 8H, CH$_2$), 1.40 – 1.32 (m, 16H, CH$_2$), 0.95 – 0.90 (m, 12H, CH$_3$); ^{19}F NMR (376 MHz, CDCl$_3$) δ -145.10 (dd, *J* = 22.4, 8.6 Hz), -157.22 (dd, *J* = 22.3, 8.5 Hz); ^{13}C NMR (101 MHz, CDCl$_3$) δ 165.05 (C=O), 152.98, 150.73, 143.37, 142.49, 138.33, 137.93, 133.49, 133.24, 132.05, 128.38, 126.99, 124.60, 122.37, 122.28, 121.99, 121.52, 108.64 (BTBT-C + Ar-C), 73.59, 69.30 (OCH$_2$), 31.71, 31.54, 31.43, 30.28, 29.88, 29.26, 29.26, 25.74, 25.69, 25.22, 25.22, 22.66, 22.60, 22.54 (CH$_2$), 14.06, 14.00, 13.98 (CH$_3$).;HRMS (m/z): [M]+Li$^+$ calcd. for C$_{57}$H$_{64}$F$_4$O$_6$S$_2$Li, 991.424; found 991.425.

2-[4-(3,4,5-Tri-n-hexyloxybenzoyloxy)phenyl]-7-(2,3,5,6-tetrafluoro-4-decyloxyphenyl)-[1]benzothieno[3,2-b]benzothiophene (F$_{2356}$10)

19F$_{2356}$10 (120 mg, 0.19 mmol), **7a** (130 mg, 0.20 mmol), THF (50 ml), saturated NaHCO$_3$ solution (25 ml) and Pd(PPh$_3$)$_4$ (20 mg, 0.02 mmol); yield 53 mg (0.051 mmol, 24 %); transparent solid; ^{1}H NMR (500 MHz, CDCl$_3$) δ 8.15 (d, *J* = 1.2 Hz, 1H, BTBT-H), 8.03 – 7.97 (m, 3H, BTBT-H), 7.76 – 7.71 (m, 3H, BTBT-H + Ar-H), 7.57 – 7.52 (m, 1H, BTBT-H), 7.45 (s, 2H, Ar-H), 7.33 (d, *J* = 8.6 Hz, 2H, Ar-H), 4.30 (t, *J* = 6.6 Hz, 2H, OCH$_2$CH$_2$), 4.08 (td, *J* = 6.5, 3.6 Hz, 6H, OCH$_2$CH$_2$), 1.88 – 1.74 (m, 8H, OCH$_2$CH$_2$), 1.56 – 1.47 (m, 8H, CH$_2$), 1.40 – 1.25 (m, 24H, CH$_2$), 0.94 – 0.86 (m, 12H, CH$_3$).^{19}F NMR (470 MHz, CDCl$_3$) δ -145.10 (dd, *J* = 22.4, 8.6 Hz), -157.21 (dd, *J* = 22.4, 8.5 Hz); ^{13}C NMR (101 MHz, CDCl$_3$) δ 165.04 (C=O),, 152.98, 143.37, 137.93, 133.24, 128.38, 126.99, 124.59, 124.04, 122.37, 122.27, 121.99, 121.51, 108.65 (BTBT-C + Ar-C), 73.58, 69.30 (OCH$_2$), 31.87, 31.71, 31.54, 30.28, 29.92, 29.51, 29.28, 29.25, 25.73, 25.69, 25.55, 22.66, 22.59 (CH$_2$), 14.08, 14.06, 14.00 (CH$_3$); HRMS (m/z): [M]+Li$^+$ calcd. for C$_{61}$H$_{72}$F$_4$O$_6$S$_2$Li, 1019.455; found 1019.454.

2-[4-(3,4,5-Tri-n-hexyloxybenzoyloxy)phenyl]-7-(2,3,5,6-tetrafluoro-4-tetradecyloxyphenyl)-[1]benzothieno[3,2-b]benzothiophene (F$_{2356}$14)
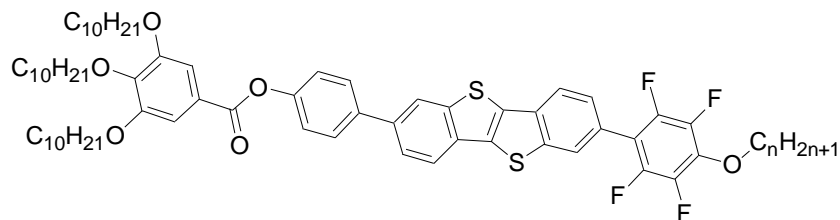
19F$_{2356}$14 (120 mg, 0.18 mmol), **7a** (120 mg, 0.19 mmol), THF (50 ml), saturated NaHCO$_3$ solution (25 ml) and Pd(PPh$_3$)$_4$ (20 mg, 0.02 mmol); yield 62 mg (0.057 mmol, 32 %); transparent solid; ^{1}H NMR (500 MHz, CDCl$_3$) δ 8.15 (d, *J* = 1.1 Hz, 1H, BTBT-H), 8.02 – 7.97 (m, 3H, BTBT-H), 7.77 – 7.71 (m, 3H, BTBT-H + Ar-H), 7.55 (d, *J* = 8.2 Hz, 1H, BTBT-H), 7.45 (s, 2H, Ar-H), 7.33 (d, *J* = 8.6 Hz, 2H, Ar-H), 4.30 (t, *J* = 6.5 Hz, 2H, OCH$_2$CH$_2$), 4.08 (td, *J* = 6.5, 3.9 Hz, 6H, OCH$_2$CH$_2$), 1.89 – 1.74 (m, 8H, OCH$_2$CH$_2$), 1.54 – 1.47 (m, 8H, CH$_2$), 1.41 – 1.23 (m, 32H, CH$_2$), 0.95 – 0.86 (m, 12H, CH$_3$); ^{19}F NMR (470 MHz, CDCl$_3$) δ -145.09 (dd, *J* = 22.4, 8.6

Hz), -157.21 (dd, J = 22.4, 8.5 Hz); ^{13}C NMR (126 MHz, CDCl$_3$) δ 165.04 (C=O), 152.99, 150.73, 143.37, 143.13, 142.49, 138.33, 137.93, 134.47, 133.49, 133.24, 132.05, 128.38, 126.99, 125.72, 124.59, 123.79, 122.37, 122.27, 121.99, 121.51, 108.65 (BTBT-C + Ar-C), 75.44, 73.59, 69.31 (OCH$_2$), 31.91, 31.71, 31.54, 30.29, 29.92, 29.68, 29.66, 29.63, 29.55, 29.52, 29.34, 29.26, 29.25, 25.74, 25.69, 25.55, 22.67, 22.66, 22.60 (CH$_2$), 14.09, 14.06, 14.00 (CH$_3$); HRMS (m/z): [M]+Li$^+$ calcd. for C$_{65}$H$_{80}$F$_4$O$_6$S$_2$Li, 1103.549; found 1103.546.

2-[4-(3,4,5-Tri-n-hexyloxybenzoyloxy)phenyl]-7-(2,3,5,6-tetrafluoro-4-octadecyloxyphenyl)-[1]benzothieno[3,2-b]benzothiophene (F$_{2356}$18)

19F$_{2356}$18 (120 mg, 0.16 mmol), **7a** (110 mg, 0.18 mmol), THF (50 ml), saturated NaHCO$_3$ solution (25 ml) and Pd(PPh$_3$)$_4$ (20 mg, 0.02 mmol); yield 55 mg (0.048 mmol, 29 %); transparent solid; ^{1}H NMR (400 MHz, CDCl$_3$) δ 8.15 (d, J = 1.1 Hz, 1H, BTBT-H), 8.03 – 7.96 (m, 3H, BTBT-H), 7.77 – 7.71 (m, 3H, BTBT-H + Ar-H), 7.55 (dd, J = 8.3, 1.4 Hz, 1H, BTBT-H), 7.45 (s, 2H, Ar-H), 7.33 (d, J = 8.7 Hz, 2H, Ar-H), 4.30 (t, J = 6.5 Hz, 2H, OCH$_2$CH$_2$), 4.08 (td, J = 6.5, 2.9 Hz, 6H, OCH$_2$CH$_2$), 1.89 – 1.74 (m, 8H, OCH$_2$CH$_2$), 1.56 – 1.46 (m, 8H, CH$_2$), 1.41 – 1.22 (m, 40H, CH$_2$), 0.96 – 0.84 (m, 12H, CH$_3$); ^{19}F NMR (376 MHz, CDCl$_3$) δ -145.10 (dd, J = 22.4, 8.7 Hz), -157.21 (dd, J = 22.3, 8.5 Hz); ^{13}C NMR (101 MHz, CDCl$_3$) δ 165.05 (C=O), 152.98, 150.73, 143.37, 143.12, 142.48, 138.33, 137.93, 134.47, 133.49, 133.24, 132.05, 128.38, 127.00, 125.72, 124.59, 123.79, 122.37, 122.27, 121.99, 121.51, 108.64 (BTBT-C + Ar-C), 75.47, 73.59, 69.30 (OCH$_2$), 31.90, 31.71, 31.54, 30.28, 29.92, 29.68, 29.63, 29.55, 29.51, 29.34, 29.25, 25.73, 25.69, 25.55, 22.67, 22.66, 22.59 (CH$_2$), 14.09, 14.06, 14.00 (CH$_3$); HRMS (m/z): [M]+Li$^+$ calcd. for C$_{69}$H$_{88}$F$_4$O$_6$S$_2$Li, 1159.611; found 1159.611.

11.6.3 Synthesis and analytical data of compounds F'$_{2356}$$n$

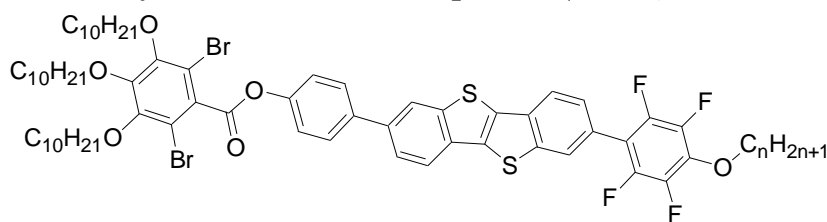### 2-[4-(3,4,5-Tri-n-decyloxybenzoyloxy)phenyl]-7-(2,3,5,6-tetrafluoro-4-hexyloxyphenyl)-[1]benzothieno[3,2-b]benzothiophene (F'$_{2356}$6)

19F$_{2356}$6 (120 mg, 0.18 mmol), **7b** (150 mg, 0.19 mmol), THF (50 ml), saturated NaHCO$_3$ solution (25 ml) and Pd(PPh$_3$)$_4$ (20 mg, 0.02 mmol); yield 55 mg (0.048 mmol, 27 %); transparent solid; ^{1}H NMR (500 MHz, CDCl$_3$) δ 8.15 (d, J = 1.1 Hz, 1H, BTBT-H), 8.00 (dd, J = 15.0, 6.9 Hz, 3H, BTBT-H), 7.76 – 7.70 (m, 3H, BTBT-H + Ar-H), 7.55 (dd, J = 8.2, 1.4 Hz, 1H, BTBT-H), 7.44 (s, 2H, Ar-H), 7.33 (d, J = 8.7 Hz, 2H, Ar-H), 4.30 (t, J = 6.5 Hz, 2H, OCH$_2$CH$_2$), 4.08 (dt, J = 10.3, 5.1 Hz, 6H, OCH$_2$CH$_2$), 1.89 – 1.73 (m, 8H, OCH$_2$CH$_2$), 1.57 – 1.46 (m, 8H, CH$_2$), 1.41 – 1.21 (m, 40H, CH$_2$), 0.96 – 0.85 (m, 12H, CH$_3$); ^{19}F NMR (470 MHz, CDCl$_3$) δ -145.10 (dd, J = 22.5, 8.6 Hz), -157.22 (dd, J = 22.4, 8.6 Hz); ^{13}C NMR (126 MHz, CDCl$_3$) δ 165.02 (C=O), 152.97, 150.72, 143.36, 143.13, 142.47, 138.30, 137.91, 134.45, 133.47, 133.22, 132.03, 128.36, 126.97, 125.71, 124.57, 123.76, 122.35, 122.25, 121.97, 121.49, 108.64 (BTBT-C + Ar-C), 75.42, 73.58, 69.29 (OCH$_2$), 31.91, 31.88, 31.42, 30.33, 29.87, 29.70, 29.64, 29.60, 29.55, 29.37, 29.32, 29.29, 26.06, 26.04, 25.20, 22.65, 22.52 (CH$_2$), 14.07, 13.96 (CH$_3$); HRMS (m/z): [M]+Li$^+$ calcd. for C$_{69}$H$_{88}$F$_4$O$_6$S$_2$Li, 1159.611; found 1159.610.

2-[4-(3,4,5-Tri-n-decyloxybenzoyloxy)phenyl]-7-(2,3,5,6-tetrafluoro-4-octadecyloxyphenyl)-[1]benzothieno[3,2-b]benzothiophene (F'$_{2356}$8)

19F$_{2356}$8 (120 mg, 0.16 mmol), **7b** (150 mg, 0.19 mmol), THF (50 ml), saturated NaHCO$_3$ solution (25 ml) and Pd(PPh$_3$)$_4$ (20 mg, 0.02 mmol); yield 48 mg (0.042 mmol, 26 %); transparent solid; ^{1}H NMR (500 MHz, CDCl$_3$) δ 8.15 (d, *J* = 1.0 Hz, 1H, BTBT-H), 8.00 (dd, *J* = 14.8, 6.6 Hz, 3H, BTBT-H), 7.77 – 7.69 (m, 3H, BTBT-H + Ar-H), 7.55 (dd, *J* = 8.2, 1.4 Hz, 1H, BTBT-H), 7.44 (s, 2H, Ar-H), 7.33 (d, *J* = 8.6 Hz, 2H, Ar-H), 4.30 (t, *J* = 6.4 Hz, 2H, OCH$_2$CH$_2$), 4.08 (dt, *J* = 10.4, 5.2 Hz, 6H, OCH$_2$CH$_2$), 1.90 – 1.72 (m, 8H, OCH$_2$CH$_2$), 1.59 – 1.44 (m, 8H, CH$_2$), 1.42 – 1.17 (m, 64H, CH$_2$), 0.93 – 0.85 (m, 12H, CH$_3$); ^{19}F NMR (470 MHz, CDCl$_3$) δ -145.10 (dd, *J* = 22.5, 8.5 Hz), -157.21 (dd, *J* = 22.4, 8.6 Hz); ^{13}C NMR (126 MHz, CDCl$_3$) δ 152.98, 150.85, 144.86, 143.37, 142.49, 134.46, 132.05, 128.38, 122.37, 122.27, 121.99, 121.52, 108.65 (BTBT-C + Ar-C), 73.59, 69.31(OCH$_2$), 31.92, 31.90, 31.89, 30.34, 29.92, 29.71, 29.68, 29.66, 29.63, 29.62, 29.57, 29.55, 29.51, 29.38, 29.34, 29.33, 29.30, 29.24, 26.08, 26.05, 22.68, 22.66(CH$_2$), 14.08 (CH$_3$); HRMS (m/z): [M]+Li$^+$ calcd. for C$_{81}$H$_{112}$F$_4$O$_6$S$_2$Li, 1327.799; found 1327.799.

### 11.6.4 Synthesis and analytical data of final compounds (BF'$_{X}$*n*)

2-[4-(2,6-dibromo-3,4,5-tri-n-decyloxybenzoyloxy)phenyl]-7-(2,3,5,6-tetrafluoro-4-hexyloxyphenyl)-[1]benzothieno[3,2-b]benzothiophene (BF'$_{2356}$6)

19F$_{2356}$6 (120 mg, 0.18 mmol), **8b** (150 mg, 0.19 mmol), THF (50 ml), saturated NaHCO$_3$ solution (25 ml) and Pd(PPh$_3$)$_4$ (20 mg, 0.02 mmol); yield 63 mg (0.048 mmol, 27 %); transparent solid; ^{1}H NMR (400 MHz, CDCl$_3$) δ 8.13 (d, *J* = 1.0 Hz, 1H, BTBT-H), 8.03 – 7.96 (m, 3H, BTBT-H), 7.76 (d, *J* = 8.7 Hz, 2H, BTBT-H), 7.71 (dd, *J* = 8.3, 1.6 Hz, 1H, BTBT-H), 7.55 (dd, *J* = 8.3, 1.3 Hz, 1H, BTBT-H), 7.46 (d, *J* = 8.7 Hz, 2H, Ar-H), 4.30 (t, *J* = 6.6 Hz, 2H, OCH$_2$CH$_2$), 4.06 (t, *J* = 6.6 Hz, 6H, OCH$_2$CH$_2$), 1.88 – 1.74 (m, 8H, OCH$_2$CH$_2$), 1.56 – 1.43 (m, 8H, CH$_2$), 1.42 – 1.23 (m, 40H), 0.95 – 0.86 (m, 12H, CH$_3$); ^{19}F NMR (376 MHz, CDCl$_3$) δ -145.09 (dd, *J* = 22.5, 8.7 Hz), -157.22 (dd, *J* = 22.3, 8.6 Hz); ^{13}C NMR (126 MHz, CDCl$_3$) δ 164.37 (C=O), 150.94, 150.13, 148.55, 143.34, 142.47, 139.03, 137.82, 134.43, 133.51, 133.20, 132.33, 132.10, 128.50, 126.96, 125.69, 124.62, 122.40, 121.99, 121.95, 121.50, 109.93 (BTBT-C + Ar-C), 75.41, 74.59, 74.42, 74.42, 31.87, 31.40, 30.16, 29.86, 29.57, 29.41, 29.31, 25.96, 25.19, 22.64, 22.51 (CH$_2$), 14.06, 13.95 (CH$_3$); HRMS (m/z): [M]+Li$^+$ calcd. for C$_{69}$H$_{86}$Br$_2$F$_4$O$_6$S$_2$Li, 1315.433; found 1315.434.

2-[4-(2,6-dibromo-3,4,5-tri-n-decyloxybenzoyloxy)phenyl]-7-(2,3,5,6-tetrafluoro-4-decyloxyphenyl)-[1]benzothieno[3,2-b]benzothiophene (BF'$_{2356}$10)

19F$_{2356}$10 (120 mg, 0.19 mmol), **8b** (160 mg, 0.20 mmol), THF (50 ml), saturated NaHCO$_3$ solution (25 ml) and Pd(PPh$_3$)$_4$ (20 mg, 0.02 mmol); yield 43 mg (0.031 mmol, 16 %); transparent solid; ^{1}H NMR (400 MHz, CDCl$_3$) δ 8.14 (d, *J* = 1.4 Hz, 1H, BTBT-H), 8.03 – 7.96 (m, 3H, BTBT-H), 7.76 (d, *J* = 8.6 Hz, 2H, BTBT-H), 7.71 (dd, *J* = 8.3, 1.6 Hz, 1H, BTBT-H), 7.55 (dd, *J* = 8.3, 1.3 Hz, 1H, BTBT-H), 7.46 (d, *J* = 8.6 Hz, 2H, , Ar-H), 4.30 (t, *J* = 6.6 Hz, 2H, OCH$_2$CH$_2$), 4.06

(t, J = 6.6 Hz, 6H, OCH$_2$CH$_2$), 1.88 – 1.73 (m, 8H, OCH$_2$CH$_2$), 1.60 – 1.42 (m, 8H, CH$_2$), 1.41 – 1.22 (m, 48H), 0.93 – 0.85 (m, 12H, CH$_3$); ^{19}F NMR (376 MHz, CDCl$_3$) δ -145.09 (dd, J = 22.5, 8.7 Hz), -157.21 (dd, J = 22.3, 8.5 Hz); ^{13}C NMR (126 MHz, CDCl$_3$) δ 164.42 (C=O), 150.98, 150.17, 148.59, 143.38, 142.51, 139.08, 137.87, 134.47, 133.56, 133.25, 132.35, 132.14, 128.55, 127.01, 125.74, 124.66, 122.45, 122.03, 122.00, 121.55, 109.96 (BTBT-C + Ar-C), 74.63, 74.46, 31.91, 31.89, 30.20, 29.93, 29.65, 29.62, 29.59, 29.52, 29.47, 29.45, 29.35, 29.34, 29.30, 29.26, 26.00, 25.56, 22.68 (CH$_2$), 14.10 (CH$_3$); HRMS (m/z): [M]+Li$^+$ calcd. for C$_{73}$H$_{94}$Br$_2$F$_4$O$_6$S$_2$Li, 1371.495; found 1371.492.

11.6.5 Synthesis and analytical data of compound BBF$_{26}$8

2-[4-(2,6-dibromo-3,4,5-tri-n-hexyloxybenzoyloxy)phenyl]-7-(2,6-difluoro-4-octyloxyphenyl)-[1]benzothieno[3,2-b]benzothiophene (BBF$_{26}$8)
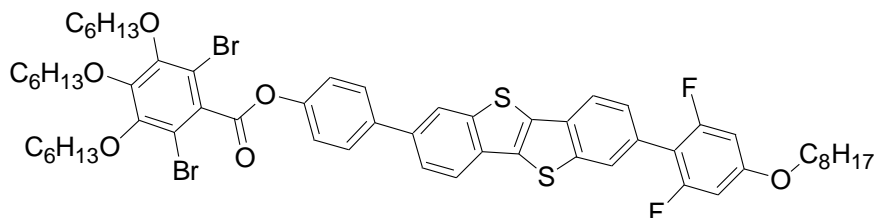
19F$_{23}$8 (120 mg, 0.21 mmol), **8a** (170 mg, 0.22 mmol), THF (50 ml), saturated NaHCO$_3$ solution (25 ml) and Pd(PPh$_3$)$_4$ (20 mg, 0.02 mmol); yield 55 mg (0.049 mmol, 23 %); transparent solid; ^{1}H NMR (400 MHz, CDCl$_3$) δ 8.13 (d, J = 1.3 Hz, 1H, BTBT-H), 8.02 – 7.94 (m, 3H, BTBT-H), 7.76 (d, J = 8.6 Hz, 2H, BTBT-H), 7.70 (dd, J = 8.3, 1.5 Hz, 1H, BTBT-H), 7.55 (dd, J = 8.2, 1.2 Hz, 1H, BTBT-H), 7.46 (d, J = 8.6 Hz, 2H, Ar-H), 6.59 (d, J = 9.7 Hz, 2H, Ar-H), 4.07 (t, J = 6.6 Hz, 6H, OCH$_2$CH$_2$), 3.99 (t, J = 6.5 Hz, 2H, OCH$_2$CH$_2$), 1.89 – 1.74 (m, 8H, OCH$_2$CH$_2$), 1.59 – 1.44 (m, 8H, CH$_2$), 1.42 – 1.25 (m, 20H, CH$_2$), 0.95 – 0.88 (m, 12H, CH$_3$); ^{19}F NMR (376 MHz, CDCl$_3$) δ -113.67 (d, J = 9.4 Hz); ^{13}C NMR (101 MHz, CDCl$_3$) δ 164.41 (C=O), 150.97, 150.09, 148.57, 143.24, 142.36, 139.16, 137.56, 133.79, 133.69, 132.37, 132.30, 128.52, 127.36, 125.71, 124.54, 122.40, 121.95, 121.17, 109.96 (BTBT-C + Ar-C), 74.62, 74.45, 68.77, 31.78, 31.61, 30.14, 29.28, 29.19, 28.97, 25.94, 25.65, 22.64, 22.60 (CH$_2$), 14.07, 14.03, 14.00 (CH$_3$); HRMS (m/z): [M]+Li$^+$ calcd. 1139.295 for C$_{59}$H$_{68}$Br$_2$F$_2$O$_6$S$_2$Li; found 1139.290.

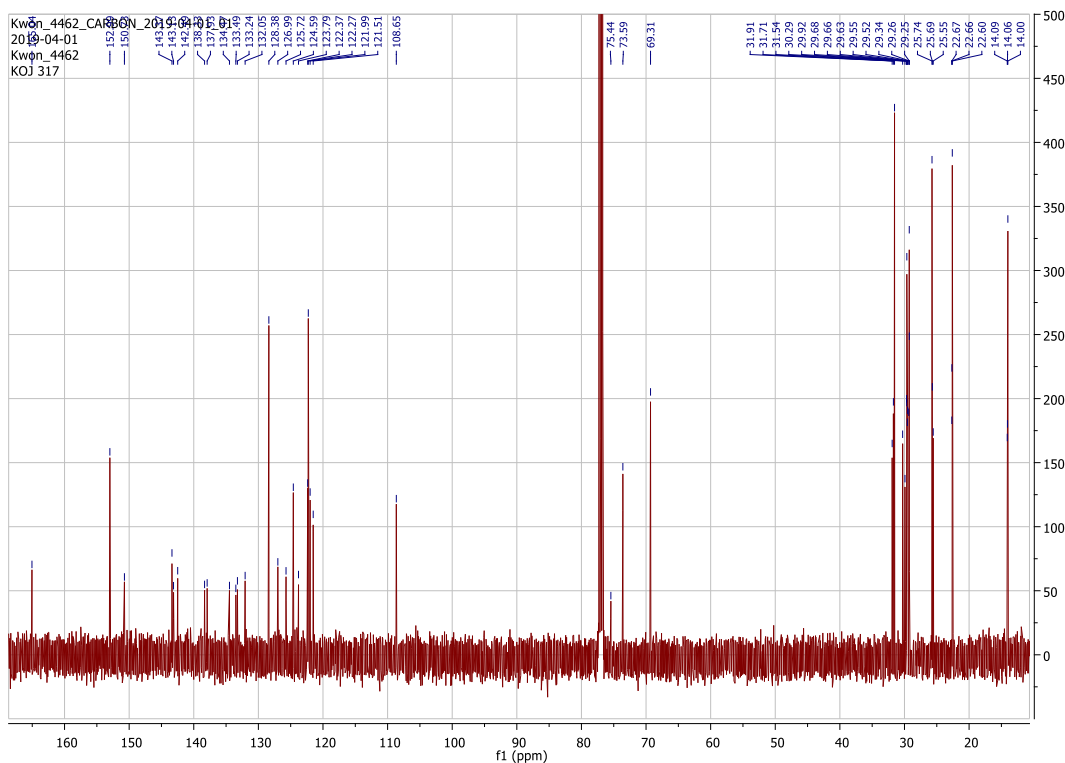## 11.6.6 Representative NMR and HRMS spectra
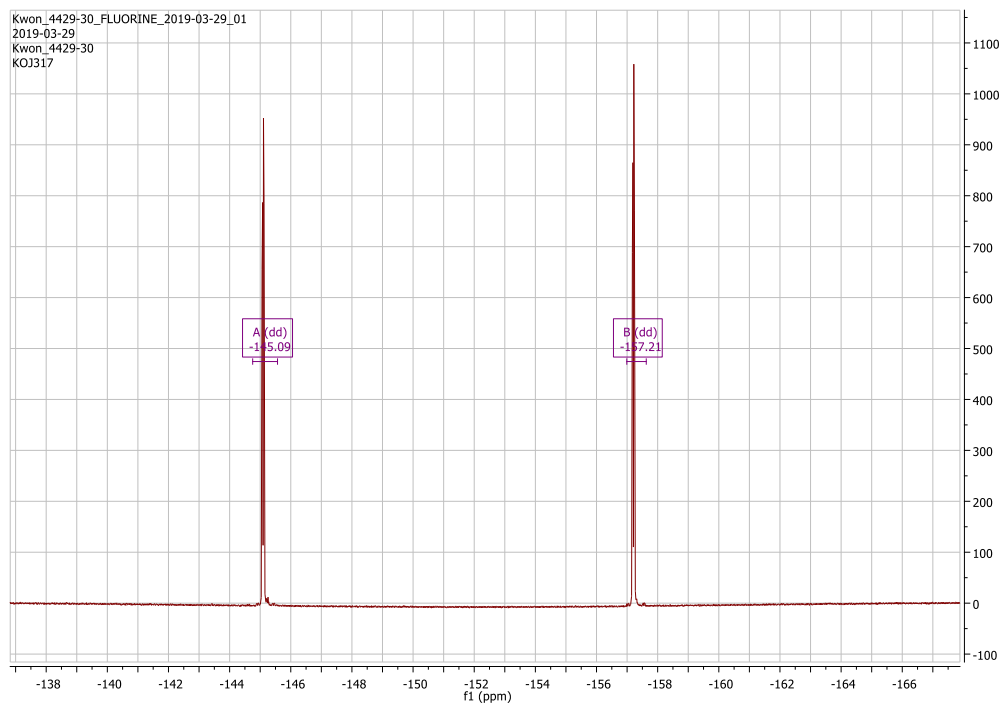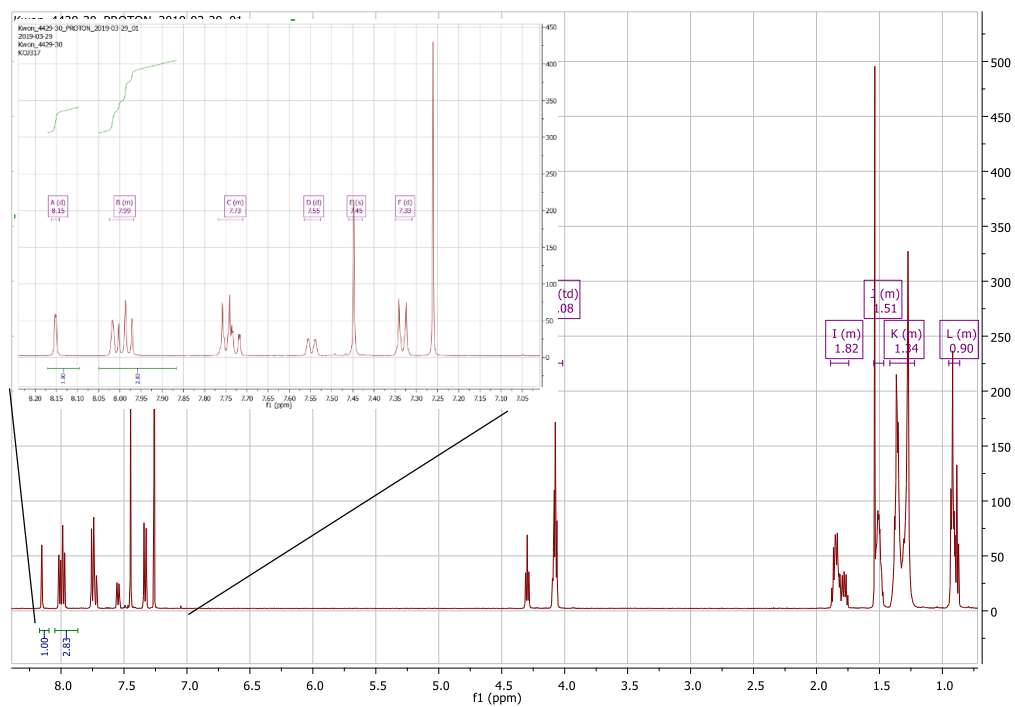
Figure S11.11 ^{1}H-, ^{19}F- and ^{13}C-NMR of compound **F$_{2356}$14**. The spectra were measured at 27 °C, with the frequencies 500 MHz (^{1}H), 470 MHz (^{19}F) and 126 MHz (^{13}C) in CDCl$_3$ as solvent.
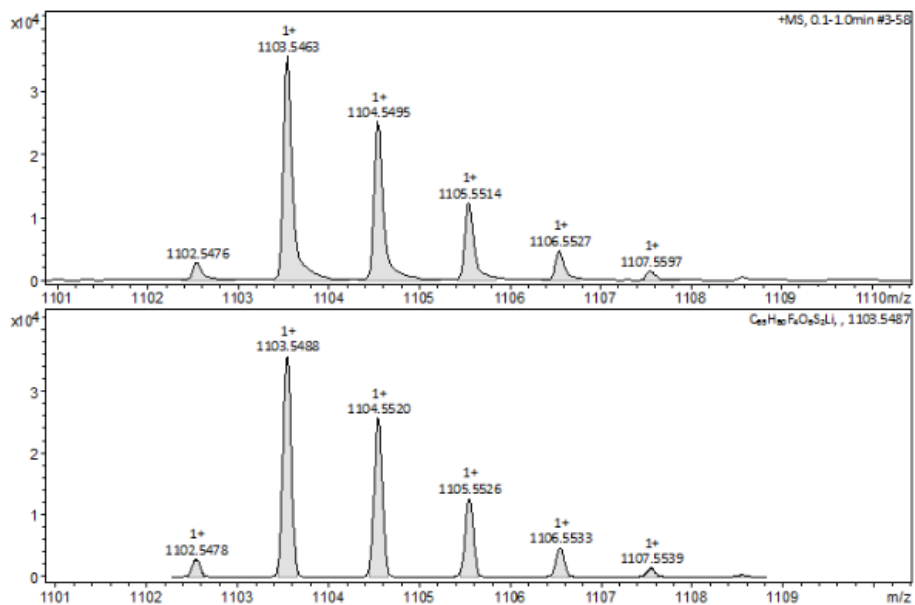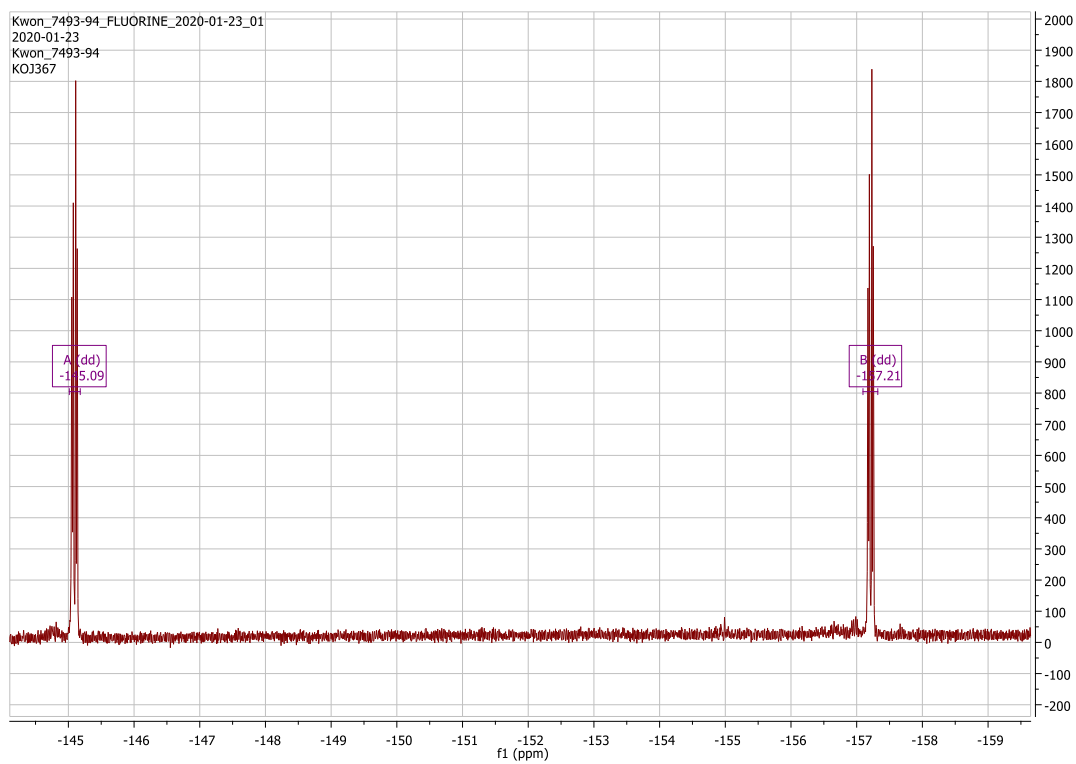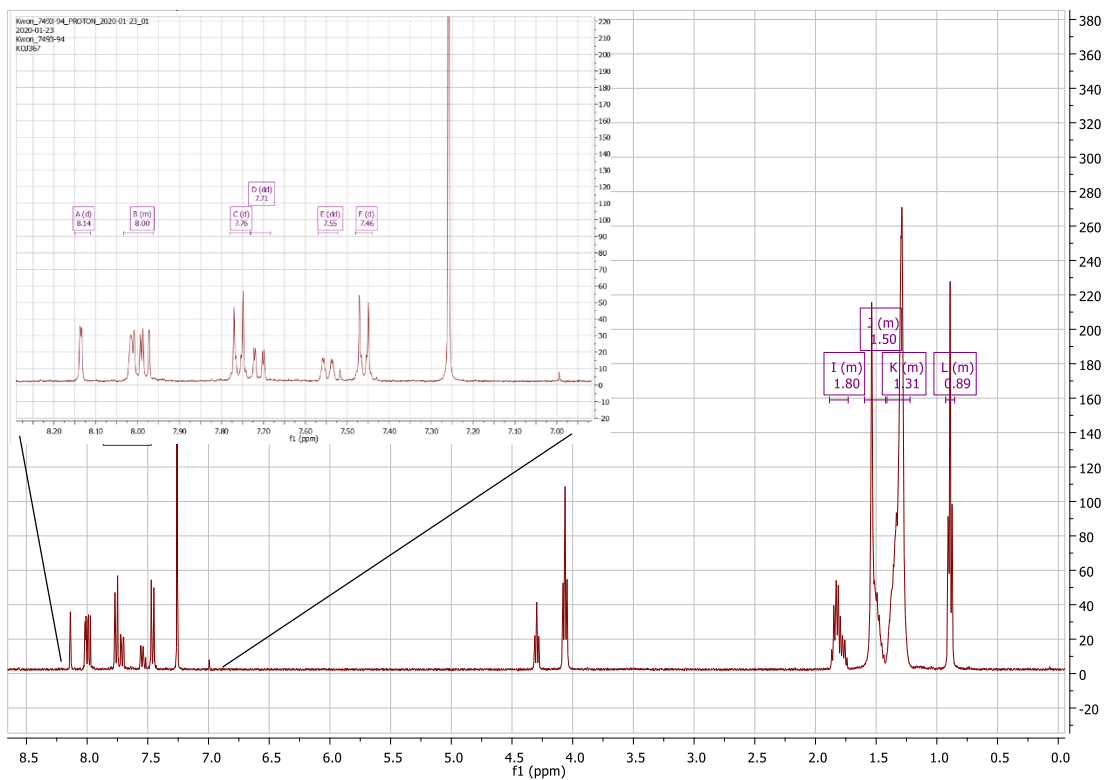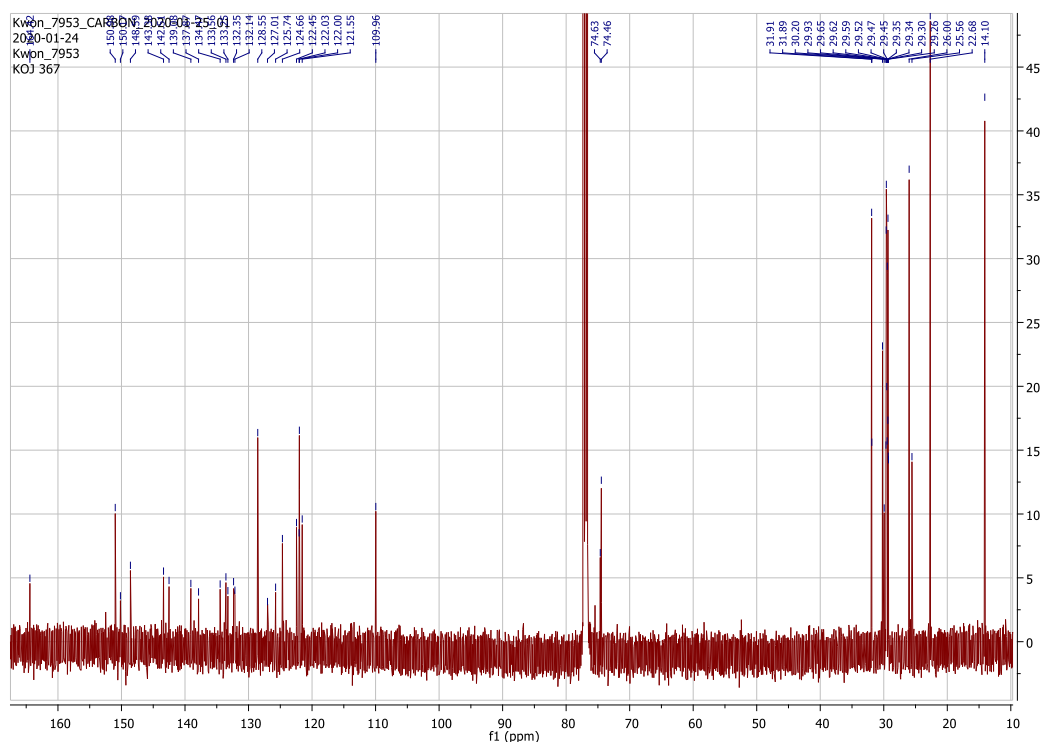

Figure S11.12 HRMS spectra for **F14**.

Figure S11.13 ^{1}H-, ^{19}F- and ^{13}C-NMR of compound **BF'$_{2356}$10**. The spectra were measured at 27 °C, with the frequencies 500 MHz (^{1}H), 470 MHz (^{19}F) and 126 MHz (^{13}C) in CDCl$_3$ as solvent.
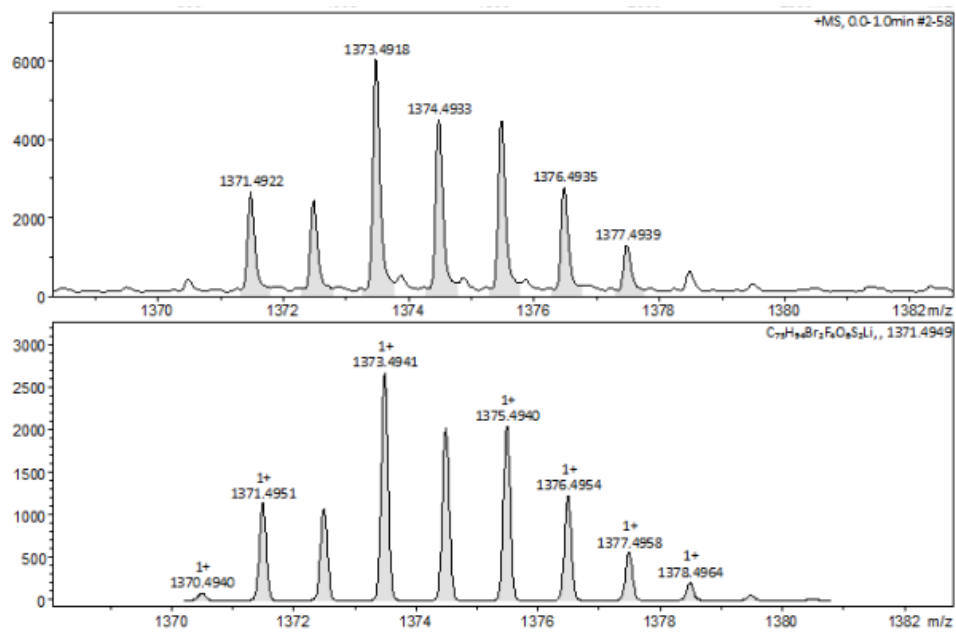

Figure S11.14 HRMS spectra for **BF$_{2356}$10**.

11.7 Synthesis and analytical data of the short core 3,4,5-trihexyloxybenzoates and 3,4,5-tridecyloxybenzoates H'*n*, H''*n*

The synthesis was performed according to scheme 2.5.

11.7.1 Synthesis and analytical data of intermediates

Synthesis of ([1]Benzothieno[3,2-b][1]benzothien-2-yl)-alkyl-1-one (14(*n*))[S9]

BTBT was dissolved in dry DCM under argon. After the solution was cooled down to -20 °C, $AlCl_3$ was added into it. The mixture was stirred for 1 hour at the given temperature. Then, proper n-alkyloyl chloride was added dropwise to the mixture. After one hour stirring at -20 °C, water (100 mL) was added. The organic mixture was extracted with DCM. The organic mixture was washed with water three times and dried with Na_2SO_4. Solvent was removed via rotary evaporator. The crude product was purified via liquid column chromatography with toluene

([1]Benzothieno[3,2-b][1]benzothien-2-yl)-butan-1-one (14(4))

BTBT 1.3 g (5.41 mmol), butyryl chloride 1.0 g (9.66 mmol), $AlCl_3$ 1.3 g (9.75 mmol), DCM 170 ml; yield 1.0 g (3.22 mmol, 60 %); colorless solid; m.p. 199 °C; ^1H NMR (400 MHz, $CDCl_3$) δ 8.55 (d, J = 0.9 Hz, 1H, BTBT-H), 8.06 (dd, J = 8.4, 1.4 Hz, 1H, BTBT-H), 7.96 – 7.91 (m, 3H, BTBT-H), 7.52 – 7.43 (m, 2H, BTBT-H), 3.06 (t, J = 7.3 Hz, 2H, BTBT-COCH$_2$), 1.89 – 1.79 (m, 2H, CH$_2$), 1.06 (t, J = 7.4 Hz, 3H, CH$_3$).

([1]Benzothieno[3,2-b][1]benzothien-2-yl)-hexan-1-one (14(6))

BTBT 1.3 g (5.41 mmol), hexanoyl chlorid 1.3 g (9.66 mmol), $AlCl_3$ 1.3 g (9.75 mmol), DCM 170 ml; yield 1.0 g (2.95 mmol, 55 %); colorless solid; m.p. 188 °C; ^1H NMR (500 MHz, $CDCl_3$) δ 8.55 (d, J = 0.9 Hz, 1H, BTBT-H), 8.06 (dd, J = 8.3, 1.5 Hz, 1H, BTBT-H), 7.96 – 7.91 (m, 3H, BTBT-H), 7.51 – 7.44 (m, 2H, BTBT-H), 3.07 (t, J = 7.4 Hz, 2H, BTBT-COCH$_2$), 1.84 – 1.77 (m, 2H, CH$_2$), 1.44 – 1.37 (m, 4H, CH$_2$), 0.94 (t, J = 6.9 Hz, 3H, CH$_3$).

([1]Benzothieno[3,2-b][1]benzothien-2-yl)-heptan-1-one (14(7))

BTBT 1.3 g (5.41 mmol), heptanoyl chloride 1.4 g (9.66 mmol), $AlCl_3$ 1.3 g (9.75 mmol), DCM 170 ml; yield 1.1 g (3.12 mmol, 58 %); colorless solid; m.p. 183 °C; ^1H NMR (400 MHz, cdcl$_3$) δ 8.55 (d, J = 1.0 Hz, 1H, BTBT-H), 8.06 (dd, J = 8.4, 1.5 Hz, 1H, BTBT-H), 7.96 – 7.91 (m, 3H, BTBT-H), 7.52 – 7.43 (m, 2H, BTBT-H), 3.07 (t, J = 7.4 Hz, 2H, BTBT-COCH$_2$), 1.84 – 1.75 (m, 2H, CH$_2$), 1.48 – 1.30 (m, 6H, CH$_2$), 0.91 (t, J = 6.8 Hz, 3H, CH$_3$).

([1]Benzothieno[3,2-b][1]benzothien-2-yl)-octan-1-one (14(8))

BTBT 1.3 g (5.41 mmol), octanoyl chloride 1.6 g (9.66 mmol), $AlCl_3$ 1.3 g (9.75 mmol), DCM 170 ml; yield 1.0 g (2.73 mmol, 50 %); colorless solid; m.p. 179 °C; ^1H NMR (400 MHz, $CDCl_3$) δ 8.55 (d, J = 1.0 Hz, 1H, BTBT-H), 8.06 (dd, J = 8.4, 1.4 Hz, 1H, BTBT-H), 7.96 – 7.91 (m, 3H, BTBT-H), 7.52 – 7.43 (m, 2H, BTBT-H), 3.07 (t, J = 7.4 Hz, 2H, BTBT-COCH$_2$), 1.84 – 1.75 (m, 2H, CH$_2$), 1.46 – 1.26 (m, 8H, CH$_2$), 0.90 (t, J = 6.6 Hz, 3H, CH$_3$).

([1]Benzothieno[3,2-b][1]benzothien-2-yl)-decan-1-one (14(10))

BTBT 1.3 g (5.41 mmol), decanoyl chloride 1.8 g (9.66 mmol), AlCl$_3$ 1.3 g (9.75 mmol), DCM 170 ml; yield 1.4 g (3.55 mmol, 66 %); colorless solid; m.p. 172 °C; ^{1}H NMR (500 MHz, CDCl$_3$) δ 8.55 (d, J = 1.2 Hz, 1H, BTBT-H), 8.06 (dd, J = 8.3, 1.5 Hz, 1H, BTBT-H), 7.96 – 7.90 (m, 3H, BTBT-H), 7.51 – 7.44 (m, 2H, BTBT-H), 3.06 (t, J = 7.4 Hz, 2H, BTBT-COCH$_2$), 1.83 – 1.76 (m, 2H, CH$_2$), 1.45 – 1.24 (m, 12H, CH$_2$), 0.89 (t, J = 6.7 Hz, 3H, CH$_3$).

([1]Benzothieno[3,2-b][1]benzothien-2-yl)-dodecan-1-one (14(12))
BTBT 1.3 g (5.41 mmol), dodecanoyl chloride 2.1 g (9.66 mmol), AlCl$_3$ 1.3 g (9.75 mmol), DCM 170 ml; yield 1.3 g (3.08 mmol, 57 %); colorless solid; m.p. 165 °C; ^{1}H NMR (500 MHz, CDCl$_3$) δ 8.55 (d, J = 0.9 Hz, 1H, BTBT-H), 8.06 (dd, J = 8.3, 1.4 Hz, 1H, BTBT-H), 7.96 – 7.91 (m, 3H, BTBT-H), 7.51 – 7.44 (m, 2H, BTBT-H), 3.07 (t, J = 7.4 Hz, 2H, BTBT-COCH$_2$), 1.83 – 1.73 (m, 2H, CH$_2$), 1.45 – 1.20 (m, 16H, CH$_2$), 0.88 (t, J = 6.7 Hz, 3H, CH$_3$).

([1]Benzothieno[3,2-b][1]benzothien-2-yl)-tetradecan-1-one (14(14))
BTBT 1.3 g (5.41 mmol), myristoyl chloride 2.4 g (9.66 mmol), AlCl$_3$ 1.3 g (9.75 mmol), DCM 170 ml; yield 1.3 g (2.88 mmol, 53 %); colorless solid; m.p. 148 °C; ^{1}H NMR (500 MHz, CDCl$_3$) δ 8.55 (d, J = 0.9 Hz, 1H, BTBT-H), 8.06 (dd, J = 8.3, 1.4 Hz, 1H, BTBT-H), 7.96 – 7.91 (m, 3H, BTBT-H), 7.51 – 7.44 (m, 2H, BTBT-H), 3.07 (t, J = 7.4 Hz, 2H, BTBT-COCH$_2$), 1.86 – 1.73 (m, 2H, CH$_2$), 1.46 – 1.20 (m, 20H, CH$_2$), 0.88 (t, J = 6.7 Hz, 3H, CH$_3$).

([1]Benzothieno[3,2-b][1]benzothien-2-yl)-octadecan-1-one (14(18))
BTBT 1.3 g (5.41 mmol), stearoyl chloride 2.9 g (9.66 mmol), AlCl$_3$ 1.3 g (9.75 mmol), DCM 170 ml; yield 1.4 g (2.76 mmol, 51 %); colorless solid; m.p. 143 °C; ^{1}H NMR (500 MHz, CDCl$_3$) δ 8.56 (d, J = 0.9 Hz, 1H, BTBT-H), 8.06 (dd, J = 8.4, 1.5 Hz, 1H, BTBT-H), 7.97 – 7.92 (m, 3H, BTBT-H), 7.52 – 7.44 (m, 2H, BTBT-H), 3.07 (t, J = 7.3 Hz, 2H, BTBT-COCH$_2$), 1.84 – 1.76 (m, 2H, CH$_2$), 1.46 – 1.18 (m, 28H, CH$_2$), 0.88 (t, J = 6.5 Hz, 3H, CH$_3$).

Synthesis of 2-alkyl-[1]benzothieno[3,2-*b*][1]benzothiophene (15(*n*))[S9]

14(*n*), sodium borohydride, aluminum chloride, were dissolved/suspended in dry THF under argon atmosphere. was dissolved in dry DCM under argon. The mixture was refluxed for 4 hours. After it is cooled down, water was added to quench. The organic mixture was extracted with DCM. The organic mixture was washed with water three times and dried with Na$_2$SO$_4$. Solvent was removed via rotary evaporator. The crude product was purified via liquid column chromatography with toluene.

2-Butyl-[1]benzothieno[3,2-*b*][1]benzothiophene (15(4))
14(4) (1.0 g, 3.22 mmol), NaBH$_4$ (0.61 g, 16.1 mmol), AlCl$_3$ (1.07 g, 8.05 mmol), THF (50 ml); yield 0.53 g (1.79 mmol, 56%); colorless solid; m.p. 133 °C; ^{1}H NMR (400 MHz, CDCl$_3$) δ 7.91 (d, J = 7.9 Hz, 1H, BTBT-H), 7.86 (d, J = 7.7 Hz, 1H, BTBT-H), 7.79 (d, J = 8.1 Hz, 1H, BTBT-H), 7.72 (s, 1H, BTBT-H), 7.48 – 7.36 (m, 2H, BTBT-H), 7.29 (dd, J = 8.1, 1.3 Hz, 1H, BTBT-H), 2.77 (t, J = 7.7 Hz, 2H, BTBT-CH$_2$), 1.74 – 1.65 (m, 2H, CH$_2$), 1.46 – 1.35 (m, 2H, CH$_2$), 0.96 (t, J = 7.3 Hz, 3H, CH$_3$).

2-Hexyl-[1]benzothieno[3,2-*b*][1]benzothiophene (15(6))
14(6) (1.0 g, 2.95 mmol), NaBH$_4$ (0.56 g, 14.75 mmol), AlCl$_3$ (0.98 g, 7.38 mmol), THF (50 ml); yield 0.48 g (1.48 mmol, 50%); colorless solid; m.p. 128 °C; ^{1}H NMR (400 MHz, CDCl$_3$) δ 7.91 (d, J = 7.9 Hz, 1H, BTBT-H), 7.86 (d, J = 7.8 Hz, 1H, BTBT-H), 7.79 (d, J = 8.1 Hz, 1H, BTBT-

H), 7.72 (s, 1H, BTBT-H), 7.48 – 7.36 (m, 2H, BTBT-H), 7.28 (dd, J = 8.1, 1.1 Hz, 1H, BTBT-H), 2.77 (t, J = 7.7 Hz, 2H, BTBT-CH$_2$), 1.75 – 1.64 (m, 2H, CH$_2$), 1.44 – 1.24 (m, 6H, CH$_2$), 0.90 (t, J = 6.6 Hz, 3H, CH$_3$).

2-Heptyl-[1]benzothieno[3,2-*b*][1]benzothiophene (15(7))

14(7) (1.1 g, 3.12 mmol), NaBH$_4$ (0.59 g, 15.6 mmol), AlCl$_3$ (1.04 g, 7.8 mmol), THF (50 ml); yield 0.60 g (1.77 mmol, 57%); colorless solid; m.p. 118 °C; ^{1}H NMR (500 MHz, CDCl$_3$) δ 7.91 (d, J = 8.0 Hz, 1H, BTBT-H), 7.86 (d, J = 7.9 Hz, 1H, BTBT-H), 7.79 (d, J = 8.2 Hz, 1H, BTBT-H), 7.72 (s, 1H, BTBT-H), 7.49 – 7.37 (m, 2H, BTBT-H), 7.28 (dd, J = 8.2, 1.2 Hz, 1H, BTBT-H), 2.76 (t, J = 7.7 Hz, 2H, BTBT-CH$_2$), 1.74 – 1.65 (m, 2H, CH$_2$), 1.42 – 1.21 (m, 8H, CH$_2$), 0.89 (t, J = 6.9 Hz, 3H, CH$_3$).

2-Octyl-[1]benzothieno[3,2-*b*][1]benzothiophene (15(8))

14(8) (1.0 g, 2.73 mmol), NaBH$_4$ (0.52 g, 13.65 mmol), AlCl$_3$ (0.91 g, 6.83 mmol), THF (50 ml); yield 0.64 g (1.84 mmol, 67%); colorless solid; m.p. 115 °C; ^{1}H NMR (500 MHz, CDCl$_3$) δ 7.91 (d, J = 8.0 Hz, 1H, BTBT-H), 7.87 (d, J = 7.8 Hz, 1H, BTBT-H), 7.79 (d, J = 8.1 Hz, 1H, BTBT-H), 7.72 (s, 1H, BTBT-H), 7.47 – 7.37 (m, 2H, BTBT-H), 7.28 (dd, J = 8.1, 1.2 Hz, 1H, BTBT-H), 2.76 (t, J = 7.7 Hz, 2H, BTBT-CH$_2$), 1.74 – 1.67 (m, 2H, CH$_2$), 1.40 – 1.23 (m, 10H, CH$_2$), 0.88 (t, J = 6.6 Hz, 3H, CH$_3$).

2-Decyl-[1]benzothieno[3,2-*b*][1]benzothiophene (15(10))

14(10) (1.4 g, 3.55 mmol), NaBH$_4$ (0.67 g, 17.75 mmol), AlCl$_3$ (1.18 g, 8.88 mmol), THF (50 ml); yield 1.2 g (3.15 mmol, 88%); colorless solid; m.p. 113 °C; ^{1}H NMR (400 MHz, CDCl$_3$) δ 7.91 (d, J = 8.0 Hz, 1H, BTBT-H), 7.86 (d, J = 7.8 Hz, 1H, BTBT-H), 7.79 (d, J = 8.1 Hz, 1H, BTBT-H), 7.72 (s, 1H, BTBT-H), 7.48 – 7.36 (m, 2H, BTBT-H), 7.28 (dd, J = 8.1, 1.3 Hz, 1H, BTBT-H), 2.76 (t, J = 7.7 Hz, 2H, BTBT-CH$_2$), 1.74 – 1.66 (m, 2H, CH$_2$), 1.40 – 1.21 (m, 14H, CH$_2$), 0.88 (t, J = 6.7 Hz, 3H, CH$_3$).

2-Dodecyl-[1]benzothieno[3,2-*b*][1]benzothiophene (15(12))

14(12) (1.3 g, 3.08 mmol), NaBH$_4$ (0.54 g, 14.40 mmol), AlCl$_3$ (0.96 g, 7.20 mmol), THF (50 ml); yield 0.50 g (1.22 mmol, 42%); colorless solid; m.p. 118 °C; ^{1}H NMR (500 MHz, CDCl$_3$) δ 7.91 (d, J = 8.0 Hz, 1H, BTBT-H), 7.86 (d, J = 7.5 Hz, 1H, BTBT-H), 7.79 (d, J = 8.1 Hz, 1H, BTBT-H), 7.72 (s, 1H, BTBT-H), 7.47 – 7.37 (m, 2H, BTBT-H), 7.28 (dd, J = 8.1, 1.3 Hz, 1H, BTBT-H), 2.76 (t, J = 7.7 Hz, 2H, BTBT-CH$_2$), 1.74 – 1.66 (m, 2H, CH$_2$), 1.41 – 1.20 (m, 18H, CH$_2$), 0.88 (t, J = 6.8 Hz, 3H, CH$_3$).

2-Tetradecyl-[1]benzothieno[3,2-*b*][1]benzothiophene (15(14))

14(14) (1.3 g, 2.88 mmol), NaBH$_4$ (0.54 g, 14.40 mmol), AlCl$_3$ (0.96 g, 7.20 mmol), THF (50 ml); yield 0.88 g (2.02 mmol, 70%); colorless solid; m.p. 110 °C; ^{1}H NMR (500 MHz, CDCl$_3$) δ 7.91 (d, J = 8.0 Hz, 1H, BTBT-H), 7.86 (d, J = 7.5 Hz, 1H, BTBT-H), 7.79 (d, J = 8.1 Hz, 1H, BTBT-H), 7.72 (s, 1H, BTBT-H), 7.47 – 7.37 (m, 2H, BTBT-H), 7.28 (dd, J = 8.1, 1.3 Hz, 1H, BTBT-H), 2.76 (t, J = 7.7 Hz, 2H, BTBT-CH$_2$), 1.74 – 1.66 (m, 2H, CH$_2$), 1.41 – 1.20 (m, 22H, CH$_2$), 0.88 (t, J = 6.8 Hz, 3H, CH$_3$).

2-Octadecyl-[1]benzothieno[3,2-*b*][1]benzothiophene (15(18))

14(18) (1.4 g, 2.76 mmol), NaBH$_4$ (0.52 g, 13.8 mmol), AlCl$_3$ (0.92 g, 6.90 mmol), THF (50 ml); yield 0.90 g (1.83 mmol, 66%); colorless solid; m.p. 108 °C; ^{1}H NMR (400 MHz, CDCl$_3$) δ 7.91 (d, *J* = 7.9 Hz, 1H, BTBT-H), 7.86 (d, *J* = 7.5 Hz, 1H, BTBT-H), 7.79 (d, *J* = 8.1 Hz, 1H, BTBT-H), 7.72 (s, 1H, BTBT-H), 7.47 – 7.36 (m, 2H, BTBT-H), 7.28 (dd, *J* = 8.1, 1.2 Hz, 1H, BTBT-H), 2.76 (t, *J* = 7.6 Hz, 2H, BTBT-CH$_2$), 1.75 – 1.65 (m, 2H, CH$_2$), 1.43 – 1.17 (m, 30H, CH$_2$), 0.88 (t, *J* = 6.6 Hz, 3H, CH$_3$).

Synthesis of 2-Bromo-7-alkyl-[1]benzothieno[3,2-*b*][1]benzothiophene (16(*n*))

15(*n*) was dissolved in DCM. Bromine with DCM was prepared in a dropping funnel and added dropwise to the solution. The mixture was stirred for 20h at RT. The reaction was quenched by adding Na$_2$S$_2$O$_3$ solution. The crude product was extracted with DCM. The organic mixture was dried with Na$_2$SO$_4$. Solvent was removed via rotary evaporator. The residue was purified by column chromatography (eluent: Toluene)

2-Bromo-7-butyl-[1]benzothieno[3,2-*b*][1]benzothiophene (16(4))

15(4) 0.53 g (1.79 mmol), Br$_2$ 0.31 g (1.97 mmol), DCM 50 ml; yield 0.46 g (1.23 mmol, 69%); colorless solid; m.p. 182 °C; ^{1}H NMR (500 MHz, CDCl$_3$) δ 8.04 (d, *J* = 1.4 Hz, 1H, BTBT-H), 7.77 (d, *J* = 8.2 Hz, 1H, BTBT-H), 7.72 – 7.70 (m, 2H, BTBT-H), 7.55 (dd, *J* = 8.4, 1.8 Hz, 1H, BTBT-H), 7.29 (dd, *J* = 8.1, 1.5 Hz, 1H, BTBT-H), 2.77 (t, *J* = 7.6 Hz, 2H, BTBT-CH$_2$), 1.72 – 1.65 (m, 2H, CH$_2$), 1.44 – 1.36 (m, 2H, CH$_2$), 0.96 (t, *J* = 7.3 Hz, 3H, CH$_3$).

2-Bromo-7-hexyl-[1]benzothieno[3,2-*b*][1]benzothiophene (16(6))

15(6) 0.48 g (1.48 mmol), Br$_2$ 0.26 g (1.63 mmol), DCM 50 ml; yield 0.40 g (0.99 mmol, 67%); colorless solid; m.p. 165 °C; ^{1}H NMR (500 MHz, CDCl$_3$) δ 8.04 (d, *J* = 1.5 Hz, 1H, BTBT-H), 7.77 (d, *J* = 8.1 Hz, 1H, BTBT-H), 7.72 – 7.70 (m, 2H, BTBT-H), 7.55 (dd, *J* = 8.4, 1.7 Hz, 1H, BTBT-H), 7.29 (dd, *J* = 8.1, 1.4 Hz, 1H, BTBT-H), 2.76 (t, *J* = 7.6 Hz, 2H, BTBT-CH$_2$), 1.73 – 1.65 (m, 2H, CH$_2$), 1.41 – 1.28 (m, 6H, CH$_2$), 0.89 (t, *J* = 7.0 Hz, 3H, CH$_3$).

2-Bromo-7-heptyl-[1]benzothieno[3,2-*b*][1]benzothiophene (16(7))

15(7) 0.60 g (1.77 mmol), Br$_2$ 0.31 g (1.95 mmol), DCM 50 ml; yield 0.43 g (1.03 mmol, 58%); colorless solid; m.p. 173 °C; ^{1}H NMR (400 MHz, CDCl$_3$) δ 8.04 (d, *J* = 1.6 Hz, 1H, BTBT-H), 7.76 (d, *J* = 8.1 Hz, 1H, BTBT-H), 7.72 – 7.68 (m, 2H, BTBT-H), 7.55 (dd, *J* = 8.4, 1.7 Hz, 1H, BTBT-H), 7.28 (dd, *J* = 8.1, 1.4 Hz, 1H, BTBT-H), 2.75 (t, *J* = 7.6 Hz, 2H, BTBT-CH$_2$), 1.79 – 1.61 (m, 2H, CH$_2$), 1.45 – 1.20 (m, 8H, CH$_2$), 0.89 (t, *J* = 6.5 Hz, 3H, CH$_3$).

2-Bromo-7-octyl-[1]benzothieno[3,2-*b*][1]benzothiophene (16(8))

15(8) 0.64 g (1.84 mmol), Br$_2$ 0.32 g (2.02 mmol), DCM 50 ml; yield 0.60 g (1.39 mmol, 76%); colorless solid; m.p. 172 °C; ^{1}H NMR (400 MHz, CDCl$_3$) δ 8.04 (d, *J* = 1.6 Hz, 1H, BTBT-H), 7.77 (d, *J* = 8.1 Hz, 1H, BTBT-H), 7.72 – 7.69 (m, 2H, BTBT-H), 7.55 (dd, *J* = 8.5, 1.7 Hz, 1H, BTBT-H), 7.29 (dd, *J* = 8.1, 1.3 Hz, 1H, BTBT-H), 2.76 (t, *J* = 7.5 Hz, 2H, BTBT-CH$_2$), 1.74 – 1.64 (m, 2H, CH$_2$), 1.40 – 1.22 (m, 10H, CH$_2$), 0.88 (t, *J* = 6.3 Hz, 3H, CH$_3$).

2-Bromo-7-decyl-[1]benzothieno[3,2-*b*][1]benzothiophene (16(10))

15(10) 1.2 g (3.15 mmol), Br$_2$ 0.55 g (3.47 mmol), DCM 50 ml; yield 0.86 g (1.87 mmol, 59%); colorless solid; m.p. 170 °C; ^{1}H NMR (500 MHz, CDCl$_3$) δ 8.04 (d, *J* = 1.6 Hz, 1H, BTBT-H), 7.78 (d, *J* = 8.2 Hz, 1H, BTBT-H), 7.73 – 7.70 (m, 2H, BTBT-H), 7.55 (dd, *J* = 8.4, 1.7 Hz, 1H,

BTBT-H), 7.29 (dd, J = 8.5, 1.0 Hz, 1H, BTBT-H), 2.76 (t, J = 7.6 Hz, 2H, BTBT-CH$_2$), 1.73 – 1.65 (m, 2H, CH$_2$), 1.40 – 1.22 (m, 14H, CH$_2$), 0.88 (t, J = 6.6 Hz, 3H, CH$_3$).

2-Bromo-7-dodecyl-[1]benzothieno[3,2-*b*][1]benzothiophene (16(12))

15(12) 0.50 g (1.22 mmol), Br$_2$ 0.20 g (1.33 mmol), DCM 50 ml; yield 0.48 g (0.98 mmol, 80%); colorless solid; m.p. 168 °C; ^{1}H NMR (400 MHz, CDCl$_3$) δ 8.04 (d, J = 1.6 Hz, 1H, BTBT-H), 7.77 (d, J = 8.1 Hz, 1H, BTBT-H), 7.73 – 7.70 (m, 2H, BTBT-H), 7.55 (dd, J = 8.4, 1.7 Hz, 1H, BTBT-H), 7.29 (dd, J = 8.1, 1.4 Hz, 1H, BTBT-H), 2.76 (t, J = 7.5 Hz, 2H, BTBT-CH$_2$), 1.74 – 1.65 (m, 2H, CH$_2$), 1.41 – 1.21 (m, 18H, CH$_2$), 0.88 (t, J = 6.8 Hz, 3H, CH$_3$).

2-Bromo-7-tetradecyl-[1]benzothieno[3,2-*b*][1]benzothiophene (16(14))

15(14) 0.88 g (2.02 mmol), Br$_2$ 0.36 g (2.22 mmol), DCM 50 ml; yield 0.60 g (1.16 mmol, 57%); colorless solid; m.p. 169 °C; ^{1}H NMR (400 MHz, CDCl$_3$) δ 8.04 (d, J = 1.6 Hz, 1H, BTBT-H), 7.77 (d, J = 8.1 Hz, 1H, BTBT-H), 7.73 – 7.70 (m, 2H, BTBT-H), 7.55 (dd, J = 8.4, 1.7 Hz, 1H, BTBT-H), 7.29 (dd, J = 8.1, 1.4 Hz, 1H, BTBT-H), 2.76 (t, J = 7.5 Hz, 2H, BTBT-CH$_2$), 1.74 – 1.65 (m, 2H, CH$_2$), 1.41 – 1.21 (m, 22H, CH$_2$), 0.88 (t, J = 6.8 Hz, 3H, CH$_3$).

2-Bromo-7-octadecyl-[1]benzothieno[3,2-*b*][1]benzothiophene (16(18))

15(18) 0.90 g (1.83 mmol), Br$_2$ 0.32 g (2.01 mmol), DCM 50 ml; yield 0.82 g (1.43 mmol, 78%); colorless solid; m.p. 103 °C; ^{1}H NMR (500 MHz, CDCl$_3$) δ 8.04 (d, J = 1.6 Hz, 1H, BTBT-H), 7.77 (d, J = 8.1 Hz, 1H, BTBT-H), 7.72 – 7.70 (m, 2H, BTBT-H), 7.55 (dd, J = 8.4, 1.7 Hz, 1H, BTBT-H), 7.29 (dd, J = 8.3, 1.3 Hz, 1H, BTBT-H), 2.76 (t, J = 7.6 Hz, 2H, BTBT-CH$_2$), 1.74 – 1.66 (m, 2H, CH$_2$), 1.40 – 1.23 (m, 30H, CH$_2$), 0.88 (t, J = 7.0 Hz, 3H, CH$_3$).

11.7.2 Synthesis of compounds H'*n* and H''*n*

Suzuki coupling reaction was used.[S6] IIn two-neck flask, **7**, **16(*n*)**, THF and saturated NaHCO$_3$ solution were prepared, and degassed with argon for 15 minutes. After purging, Pd(PPh$_3$)$_4$ was added. The solution was refluxed for 6 hours. When the mixture was cooled down, the organic phase was extracted with CHCl$_3$. Then, it was dried over Na$_2$SO$_4$. After it was concentrated in vacuum, it was purified by column chromatography eluent: CHCl$_3$/n-hexane 3/2) Then, recrystallization from THF/EtOH or n-hexane is repeated.

2-[4-(3,4,5-Tri-n-decyloxybenzoyloxy)phenyl]-7-butyl-[1]benzothieno[3,2-b]benzothiophene (H''4)

7b 260 mg (0.33 mmol), **16(4)** 120 mg (0.32 mmol), THF 50 ml, NaHCO$_3$ solution 25 ml, Pd(PPh$_3$)$_4$ 20 mg (0.017 mmol); yield 76 mg (0.079 mmol, 25%); colorless solid; ^{1}H NMR (500 MHz, CDCl$_3$) δ 8.12 (d, J = 1.1 Hz, 1H, BTBT-H), 7.93 (d, J = 8.2 Hz, 1H, BTBT-H), 7.80 (d, J = 8.1 Hz, 1H, BTBT-H), 7.75 – 7.72 (m, 3H, BTBT-H + Ar-H), 7.69 (dd, J = 8.3, 1.6 Hz, 1H, BTBT-H), 7.44 (s, 2H, Ar-H), 7.33 – 7.29 (m, 3H, BTBT-H + Ar-H), 4.07 (td, J = 6.5, 4.2 Hz, 6H, OCH$_2$CH$_2$), 2.78 (t, J = 7.6 Hz, 2H, BTBT-CH$_2$), 1.88 – 1.66 (m, 8H, OCH$_2$CH$_{2 +}$ CH$_2$), 1.56 – 1.46 (m, 6H, CH$_2$), 1.43 – 1.22 (m, 38H, CH$_2$), 0.97 (t, J = 7.4 Hz, 3H, CH$_3$), 0.91 – 0.85 (m, 9H, CH$_3$); ^{13}C NMR (126 MHz, CDCl$_3$) δ 165.05 (C=O), 152.97, 150.60, 142.91, 142.67, 140.43, 138.50, 137.23, 133.78, 132.41, 132.33, 131.02, 128.32, 125.97, 124.37, 123.81, 123.37, 122.28, 122.21, 121.60, 121.25, 108.64 (BTBT-C + Ar-C), 73.59, 69.30 (OCH$_2$), 35.81, 33.80, 31.92, 31.89, 30.34, 29.71, 29.65, 29.61, 29.56, 29.55, 29.38, 29.33, 29.30, 26.07, 26.05, 22.68, 22.66,

22.33 (CH$_2$), 14.08, 13.94 (CH$_3$); HRMS (m/z): [M]+Li$^+$ calcd. for C$_{61}$H$_{84}$O$_5$S$_2$Li, 967.592; found 967.598.

2-[4-(3,4,5-Tri-n-decyloxybenzoyloxy)phenyl]-7-hexyl-[1]benzothieno[3,2-b]benzothiophene (H''6)

7b 240 mg (0.30 mmol), **16(6)** 120 mg (0.30 mmol), THF 50 ml, NaHCO$_3$ solution 25 ml, Pd(PPh$_3$)$_4$ 20 mg (0.017 mmol); yield 70 mg (0.071 mmol, 24%); colorless solid; ^{1}H NMR (400 MHz, CDCl$_3$) δ 8.12 (d, J = 1.3 Hz, 1H, BTBT-H), 7.93 (d, J = 8.3 Hz, 1H, BTBT-H), 7.80 (d, J = 8.1 Hz, 1H, BTBT-H), 7.75 – 7.72 (m, 3H, BTBT-H + Ar-H), 7.69 (dd, J = 8.3, 1.6 Hz, 1H, BTBT-H), 7.44 (s, 2H, Ar-H), 7.33 – 7.28 (m, 3H, BTBT-H + Ar-H), 4.07 (td, J = 6.5, 3.1 Hz, 6H, OCH$_2$CH$_2$), 2.78 (t, J = 7.7 Hz, 2H, BTBT-CH$_2$), 1.89 – 1.67 (m, 8H, OCH$_2$CH$_2$ + CH$_2$), 1.56 – 1.45 (m, 6H, CH$_2$), 1.42 – 1.23 (m, 42H), 0.93 – 0.86 (m, 12H, CH$_3$); ^{13}C NMR (101 MHz, CDCl$_3$) δ 165.05 (C=O), 152.97, 152.97, 150.60, 140.48, 138.50, 137.23, 128.32, 125.96, 124.37, 123.36, 122.28, 122.21, 121.60, 121.25, 108.64 (BTBT-C + Ar-C), 73.58, 69.30 (OCH$_2$), 36.13, 31.92, 31.89, 31.71, 31.64, 30.34, 29.71, 29.65, 29.61, 29.57, 29.55, 29.38, 29.33, 29.30, 28.96, 26.07, 26.05, 22.68, 22.66, 22.59 (CH$_2$), 14.08, 14.07 (CH3); HRMS (m/z): [M]+Li$^+$ calcd. for C$_{63}$H$_{88}$O$_5$S$_2$Li, 995.623; found 995.621.

2-[4-(3,4,5-Tri-n-decyloxybenzoyloxy)phenyl]-7-heptyl-[1]benzothieno[3,2-b]benzothiophene (H''7)

7b 230 mg (0.29 mmol), **16(7)** 120 mg (0.29 mmol), THF 50 ml, NaHCO$_3$ solution 25 ml, Pd(PPh$_3$)$_4$ 20 mg (0.017 mmol); yield 81 mg (0.081 mmol, 28%); colorless solid;
^{1}H NMR (500 MHz, CDCl$_3$) δ 8.12 (d, J = 1.0 Hz, 1H, BTBT-H), 7.93 (d, J = 8.3 Hz, 1H, BTBT-H), 7.80 (d, J = 8.2 Hz, 1H, BTBT-H), 7.75 – 7.72 (m, 3H, BTBT-H + Ar-H), 7.69 (dd, J = 8.3, 1.6 Hz, 1H, BTBT-H), 7.44 (s, 2H, Ar-H), 7.33 – 7.29 (m, 3H, BTBT-H + Ar-H), 4.07 (td, J = 6.5, 4.1 Hz, 6H, OCH$_2$CH$_2$), 2.77 (t, J = 7.5 Hz, 2H, BTBT-CH$_2$), 1.88 – 1.68 (m, 8H, OCH$_2$CH$_2$ + CH$_2$), 1.55 – 1.46 (m, 6H, CH$_2$), 1.40 – 1.23 (m, 44H, CH$_2$), 0.91 – 0.87 (m, 12H, CH$_3$); ^{13}C NMR (126 MHz, CDCl$_3$) δ 165.05 (C=O), 152.97, 150.60, 142.91, 140.49, 138.50, 137.22, 133.78, 132.41, 132.32, 131.02, 128.32, 125.96, 124.37, 123.81, 123.35, 122.28, 122.21, 121.60, 121.25, 108.64 (BTBT-C + Ar-C), 73.59, 69.30 (OCH$_2$), 36.13, 31.92, 31.89, 31.79, 31.68, 30.34, 29.71, 29.65, 29.61, 29.56, 29.55, 29.38, 29.33, 29.30, 29.25, 29.17, 26.07, 26.05, 22.68, 22.66, 22.64 (CH$_2$), 14.08, 14.07 (CH$_3$); HRMS (m/z): [M]+Li$^+$ calcd. for C$_{64}$H$_{90}$O$_5$S$_2$Li, 1009.639; found 1009.635.

2-[4-(3,4,5-Tri-n-decyloxybenzoyloxy)phenyl]-7-octyl-[1]benzothieno[3,2-b]benzothiophene (H''8)

7b 230 mg (0.29 mmol), **16(8)** 120 mg (0.28 mmol), THF 50 ml, NaHCO$_3$ solution 25 ml, Pd(PPh$_3$)$_4$ 20 mg (0.017 mmol); yield 70 mg (0.069 mmol, 25%); colorless solid; ^{1}H NMR (400 MHz, CDCl$_3$) δ 8.12 (d, J = 1.2 Hz, 1H, BTBT-H), 7.93 (d, J = 8.2 Hz, 1H, BTBT-H), 7.80 (d, J = 8.1 Hz, 1H, BTBT-H), 7.76 – 7.72 (m, 3H, BTBT-H + Ar-H), 7.69 (dd, J = 8.3, 1.6 Hz, 1H, BTBT-H), 7.44 (s, 2H, Ar-H), 7.34 – 7.28 (m, 3H, BTBT-H + Ar-H), 4.07 (td, J = 6.5, 3.1 Hz, 6H, OCH$_2$CH$_2$), 2.77 (t, J = 7.6 Hz, 2H, BTBT-CH$_2$), 1.89 – 1.66 (m, 8H, OCH$_2$CH$_2$ + CH$_2$), 1.58 – 1.44 (m, 6H, CH$_2$), 1.42 – 1.21 (m, 46H, CH$_2$), 0.93 – 0.84 (m, 12H, CH$_3$); ^{13}C NMR (101 MHz, CDCl$_3$) δ 165.05 (C=O), 152.97, 150.60, 142.91, 142.67, 140.87, 137.18, 133.79, 132.41, 131.52, 128.32, 125.96, 124.37, 123.36, 122.28, 122.21, 121.60, 121.25, 108.64 (BTBT-C + Ar-C), 73.59, 69.30 (OCH$_2$), 36.13, 31.92, 31.89, 31.86, 29.71, 29.65, 29.61, 29.56, 29.47, 29.38, 29.33, 29.30,

26.07, 26.05, 22.68, 22.66, 22.65 (CH$_2$), 14.08 (CH$_3$); HRMS (m/z): [M]+Li$^+$ calcd. for C$_{65}$H$_{92}$O$_5$S$_2$Li, 1023.654; found 1023.650.

2-[4-(3,4,5-Tri-n-decyloxybenzoyloxy)phenyl]-7-decyl-[1]benzothieno[3,2-b]benzothiophene (H''10)

7b 210 mg (0.26 mmol), **16(10)** 120 mg (0.26 mmol), THF 50 ml, NaHCO$_3$ solution 25 ml, Pd(PPh$_3$)$_4$ 20 mg (0.017 mmol); yield 45 mg (0.043 mmol, 16%); colorless solid; ^{1}H NMR (400 MHz, CDCl$_3$) δ 8.12 (d, J = 1.2 Hz, 1H, BTBT-H), 7.93 (d, J = 8.3 Hz, 1H, BTBT-H), 7.80 (d, J = 8.1 Hz, 1H, BTBT-H), 7.76 – 7.72 (m, 3H, BTBT-H + Ar-H), 7.69 (dd, J = 8.3, 1.4 Hz, 1H, BTBT-H), 7.44 (s, 2H, Ar-H), 7.34 – 7.28 (m, 3H, BTBT-H + Ar-H), 4.07 (td, J = 6.5, 3.3 Hz, 6H, OCH$_2$CH$_2$), 2.77 (t, J = 7.4 Hz, 2H, BTBT-CH$_2$), 1.88 – 1.67 (m, 8H, OCH$_2$CH$_2$ $_+$ CH$_2$), 1.55 – 1.45 (m, 6H, CH$_2$), 1.42 – 1.22 (m, 50H, CH$_2$), 0.93 – 0.85 (m, 12H, CH$_3$); ^{13}C NMR (101 MHz, CDCl$_3$) δ 165.04 (C=O), 152.97, 150.60, 142.91, 142.67, 140.49, 138.50, 137.22, 133.78, 131.02, 128.32, 125.96, 124.37, 123.81, 123.36, 122.28, 122.21, 121.60, 121.25, 108.64 (BTBT-C + Ar-C), 73.58, 69.30 (OCH$_2$), 36.13, 31.92, 31.89, 31.88, 31.67, 30.34, 29.71, 29.65, 29.61, 29.60, 29.57, 29.55, 29.50, 29.38, 29.33, 29.30, 29.29, 26.07, 26.05, 22.68, 22.66 (CH$_2$), 14.08 (CH$_3$); HRMS (m/z): [M]+Li$^+$ calcd. for C$_{67}$H$_{96}$O$_5$S$_2$Li, 1051.686; found 1051.685.

2-[4-(3,4,5-Tri-n-decyloxybenzoyloxy)phenyl]-7-dodecyl-[1]benzothieno[3,2-b]benzothiophene (H''12)

7b 200 mg (0.25 mmol), **16(12)** 120 mg (0.25 mmol), THF 50 ml, NaHCO$_3$ solution 25 ml, Pd(PPh$_3$)$_4$ 20 mg (0.017 mmol); yield 60 mg (0.056 mmol, 23%); colorless solid; ^{1}H NMR (400 MHz, CDCl$_3$) δ 8.12 (d, J = 0.9 Hz, 1H, BTBT-H), 7.93 (d, J = 8.3 Hz, 1H, BTBT-H), 7.80 (d, J = 8.0 Hz, 1H, BTBT-H), 7.76 – 7.72 (m, 3H, BTBT-H + Ar-H), 7.69 (dd, J = 8.2, 1.5 Hz, 1H, BTBT-H), 7.44 (s, 2H, Ar-H), 7.34 – 7.28 (m, 3H, BTBT-H + Ar-H), 4.07 (dt, J = 9.8, 4.9 Hz, 6H, OCH$_2$CH$_2$), 2.77 (t, J = 7.5 Hz, 2H, BTBT-CH$_2$), 1.89 – 1.66 (m, 8H, OCH$_2$CH$_2$ $_+$ CH$_2$), 1.56 – 1.44 (m, 6H, CH$_2$), 1.43 – 1.20 (m, 54H, CH$_2$), 0.93 – 0.85 (m, 12H, CH$_3$); ^{13}C NMR (101 MHz, CDCl$_3$) δ 165.05 (C=O), 152.97, 150.60, 143.11, 142.91, 142.67, 140.49, 138.50, 137.22, 133.78, 132.41, 132.33, 131.02, 128.32, 125.96, 124.36, 123.81, 123.36, 122.28, 122.21, 121.60, 121.25, 108.64 (BTBT-C + Ar-C), 73.59, 69.30 (OCH$_2$), 36.13, 31.92, 31.88, 31.66, 30.34, 29.71, 29.67, 29.66, 29.62, 29.57, 29.55, 29.50, 29.38, 29.33, 29.30, 29.28, 26.08, 26.05, 22.68, 22.66 (CH$_2$), 14.09, 14.08 (CH$_3$); HRMS (m/z): [M]+Li$^+$ calcd. for C$_{71}$H$_{104}$O$_5$S$_2$Li, 1079.717; found 1079.708.

2-[4-(3,4,5-Tri-n-decyloxybenzoyloxy)phenyl]-7-tetradecyl-[1]benzothieno[3,2-b]benzothiophene (H''14)

7b 190 mg (0.24 mmol), **16(14)** 120 mg (0.23 mmol), THF 50 ml, NaHCO$_3$ solution 25 ml, Pd(PPh$_3$)$_4$ 20 mg (0.017 mmol); yield 90 mg (0.082 mmol, 35%); colorless solid; ^{1}H NMR (400 MHz, CDCl$_3$) δ 8.12 (d, J = 0.9 Hz, 1H, BTBT-H), 7.93 (d, J = 8.3 Hz, 1H, BTBT-H), 7.80 (d, J = 8.0 Hz, 1H, BTBT-H), 7.76 – 7.72 (m, 3H, BTBT-H + Ar-H), 7.69 (dd, J = 8.2, 1.5 Hz, 1H, BTBT-H), 7.44 (s, 2H, Ar-H), 7.34 – 7.28 (m, 3H, BTBT-H + Ar-H), 4.07 (dt, J = 9.8, 4.9 Hz, 6H, OCH$_2$CH$_2$), 2.77 (t, J = 7.5 Hz, 2H, BTBT-CH$_2$), 1.89 – 1.66 (m, 8H, OCH$_2$CH$_2$ $_+$ CH$_2$), 1.56 – 1.44 (m, 6H, CH$_2$), 1.43 – 1.20 (m, 58H, CH$_2$), 0.93 – 0.85 (m, 12H, CH$_3$); ^{13}C NMR (101 MHz, CDCl$_3$) δ 165.05 (C=O), 152.97, 150.60, 143.11, 142.91, 142.67, 140.49, 138.50, 137.22, 133.78, 132.41, 132.33, 131.02, 128.32, 125.96, 124.36, 123.81, 123.36, 122.28, 122.21, 121.60, 121.25, 108.64 (BTBT-C + Ar-C), 73.59, 69.30 (OCH$_2$), 36.13, 31.92, 31.89, 31.66, 30.34, 29.71, 29.67,

29.66, 29.62, 29.57, 29.55, 29.50, 29.38, 29.33, 29.30, 29.28, 26.08, 26.05, 22.68, 22.66 (CH_2), 14.09, 14.08 (CH_3); HRMS (m/z): [M]+Li^+ calcd. for $C_{71}H_{104}O_5S_2Li$, 1107.748; found 1107.747.

2-[4-(3,4,5-Tri-n-decyloxybenzoyloxy)phenyl]-7-octadecyl-[1]benzothieno[3,2-b]benzothiophene (H''18)

7b 170 mg (0.21 mmol), **16(18)** 120 mg (0.21 mmol), THF 50 ml, NaHCO$_3$ solution 25 ml, Pd(PPh$_3$)$_4$ 20 mg (0.017 mmol); yield 79 mg (0.068 mmol, 32%); colorless solid; ^{1}H NMR (400 MHz, CDCl$_3$) δ 8.12 (d, J = 1.2 Hz, 1H, BTBT-H), 7.93 (d, J = 8.3 Hz, 1H, BTBT-H), 7.80 (d, J = 8.1 Hz, 1H, BTBT-H), 7.76 – 7.72 (m, 3H, BTBT-H + Ar-H), 7.69 (dd, J = 8.3, 1.5 Hz, 1H, BTBT-H), 7.44 (s, 2H, Ar-H), 7.34 – 7.28 (m, 3H, BTBT-H + Ar-H), 4.07 (td, J = 6.5, 3.2 Hz, 6H, OCH$_2$CH$_2$), 2.77 (t, J = 7.5 Hz, 2H, BTBT-CH$_2$), 1.89 – 1.66 (m, 8H, OCH$_2$CH$_2$ + CH$_2$), 1.56 – 1.45 (m, 6H, CH$_2$), 1.43 – 1.21 (m, 66H, CH$_2$), 0.93 – 0.84 (m, 12H, CH$_3$); ^{13}C NMR (101 MHz, CDCl$_3$) δ 165.05 (C=O), 152.97, 150.60, 142.91, 142.67, 140.49, 139.99, 132.41, 132.32, 129.53, 128.32, 125.96, 124.37, 124.10, 123.81, 123.36, 122.28, 122.21, 121.60, 121.25, 108.64 (BTBT-C + Ar-C), 73.58, 69.30 (OCH$_2$), 36.13, 31.92, 31.89, 31.66, 30.34, 29.71, 29.68, 29.66, 29.64, 29.62, 29.56, 29.49, 29.38, 29.33, 29.30, 29.28, 26.07, 26.05, 22.68, 22.66 (CH$_2$), 14.09 (CH$_3$); HRMS (m/z): [M]+Li^+ calcd. for $C_{75}H_{112}O_5S_2Li$, 1163.811; found 1163.811.

2-[4-(3,4,5-Tri-n-hexyloxybenzoyloxy)phenyl]-7-butyl-[1]benzothieno[3,2-b]benzothiophene (H'4)

7a 200 mg (0.32 mmol), **16(4)** 120 mg (0.32 mmol), THF 50 ml, NaHCO$_3$ solution 25 ml, Pd(PPh$_3$)$_4$ 20 mg (0.017 mmol); yield 55 mg (0.069 mmol, 22%); colorless solid; ^{1}H NMR (400 MHz, CDCl$_3$) δ 8.12 (d, J = 1.1 Hz, 1H, BTBT-H), 7.93 (d, J = 8.3 Hz, 1H, BTBT-H), 7.80 (d, J = 8.1 Hz, 1H, BTBT-H), 7.76 – 7.71 (m, 3H, BTBT-H + Ar-H), 7.69 (dd, J = 8.3, 1.5 Hz, 1H, BTBT-H), 7.44 (s, 2H, Ar-H), 7.34 – 7.28 (m, 3H, BTBT-H + Ar-H), 4.07 (td, J = 6.5, 2.8 Hz, 6H, OCH$_2$CH$_2$), 2.78 (t, J = 7.7 Hz, 2H, BTBT-CH$_2$), 1.89 – 1.66 (m, 8H, OCH$_2$CH$_2$ + CH$_2$), 1.56 – 1.45 (m, 6H, CH$_2$), 1.44 – 1.32 (m, 14H, CH$_2$), 0.94 (dt, J = 13.1, 6.8 Hz, 12H, CH$_3$); ^{13}C NMR (126 MHz, CDCl$_3$) δ 165.05 (C=O), 152.97, 150.60, 142.91, 142.67, 140.44, 137.23, 133.78, 132.41, 131.02, 128.32, 125.97, 124.37, 123.82, 123.37, 122.28, 122.21, 121.60, 121.25, 108.64 (BTBT-C + Ar-C), 73.58, 69.30 (OCH$_2$), 35.81, 33.80, 31.71, 31.53, 30.28, 29.25, 25.73, 25.68, 22.66, 22.59, 22.33 (CH$_2$), 14.05, 13.99, 13.94 (CH$_3$); HRMS (m/z): [M]+Li^+ calcd. for $C_{49}H_{60}O_5S_2Li$, 799.404; found 799.397.

2-[4-(3,4,5-Tri-n-hexyloxybenzoyloxy)phenyl]-7-octyl-[1]benzothieno[3,2-b]benzothiophene (H'8)

7a 180 mg (0.2882 mmol), **16(8)** 120 mg (0.2781 mmol), THF 50 ml, NaHCO$_3$ solution 25 ml, Pd(PPh$_3$)$_4$ 20 mg (0.0173 mmol); yield 50 mg (0.0589 mmol, 21%); colorless solid; ^{1}H NMR (500 MHz, CDCl$_3$) δ 8.12 (d, J = 1.1 Hz, 1H, BTBT-H), 7.93 (d, J = 8.2 Hz, 1H, BTBT-H), 7.80 (d, J = 8.1 Hz, 1H, BTBT-H), 7.76 – 7.72 (m, 3H, BTBT-H + Ar-H), 7.69 (dd, J = 8.2, 1.6 Hz, 1H, BTBT-H), 7.44 (s, 2H, Ar-H), 7.33 – 7.29 (m, 3H, BTBT-H + Ar-H), 4.07 (td, J = 6.5, 3.5 Hz, 6H, OCH$_2$CH$_2$), 2.77 (t, J = 7.7 Hz, 2H, BTBT-CH$_2$), 1.88 – 1.67 (m, 8H, OCH$_2$CH$_2$ + CH$_2$), 1.59 – 1.45 (m, 6H, CH$_2$), 1.42 – 1.23 (m, 22H, CH$_2$), 0.95 – 0.86 (m, 12H, CH$_3$); ^{13}C NMR (101 MHz, CDCl$_3$) δ 165.05 (C=O), 152.97, 150.59, 149.17, 143.10, 142.67, 140.49, 138.50, 131.02, 128.32, 125.96, 124.37, 123.82, 123.36, 122.28, 122.21, 121.60, 121.25, 108.63 (BTBT-C + Ar-C), 73.58, 69.29 (OCH$_2$), 36.13, 31.86, 31.71, 31.68, 31.54, 30.28, 29.47, 29.30, 29.25, 29.24, 25.73, 25.69,

22.66, 22.65, 22.59 (CH$_2$), 14.08, 14.06, 14.00 (CH$_3$); HRMS (m/z): [M]+Li$^+$ calcd. for C$_{53}$H$_{68}$O$_5$S$_2$Li, 855.466; found 855.462.

2-[4-(3,4,5-Tri-n-hexyloxybenzoyloxy)phenyl]-7-decyl-[1]benzothieno[3,2-b]benzothiophene (H'10)

7a 170 mg (0.27 mmol), **16(10)** 120 mg (0.26 mmol), THF 50 ml, NaHCO$_3$ solution 25 ml, Pd(PPh$_3$)$_4$ 20 mg (0.017 mmol); yield 63 mg (0.072 mmol, 28%); colorless solid; ^{1}H NMR (500 MHz, CDCl$_3$) δ 8.12 (d, J = 1.0 Hz, 1H, BTBT-H), 7.92 (d, J = 8.2 Hz, 1H, BTBT-H), 7.80 (d, J = 8.1 Hz, 1H, BTBT-H), 7.76 – 7.71 (m, 3H, BTBT-H + Ar-H), 7.69 (dd, J = 8.2, 1.4 Hz, 1H, BTBT-H), 7.44 (s, 2H, Ar-H), 7.34 – 7.28 (m, 3H, BTBT-H + Ar-H), 4.07 (td, J = 6.5, 3.9 Hz, 6H, OCH$_2$CH$_2$), 2.77 (t, J = 7.6 Hz, 2H, BTBT-CH$_2$), 1.88 – 1.67 (m, 8H, OCH$_2$CH$_{2\,+}$ CH$_2$), 1.56 – 1.47 (m, 6H, CH$_2$), 1.41 – 1.22 (m, 26H, CH$_2$), 0.95 – 0.86 (m, 12H, CH$_3$); ^{13}C NMR (126 MHz, CDCl$_3$) δ 165.06 (C=O), 152.97, 150.59, 143.09, 142.91, 142.67, 140.49, 138.51, 137.22, 133.78, 132.41, 132.32, 131.01, 128.32, 125.96, 124.37, 123.82, 123.36, 122.28, 122.21, 121.60, 121.25, 108.63 (BTBT-C + Ar-C), 73.58, 69.29 (OCH$_2$), 36.13, 31.88, 31.71, 31.67, 31.54, 30.28, 29.60, 29.57, 29.50, 29.31, 29.29, 29.25, 25.73, 25.69, 22.66, 22.59 (CH$_2$), 14.09, 14.06, 14.00 (CH$_3$); HRMS (m/z): [M]+Li$^+$ calcd. for C$_{55}$H$_{72}$O$_5$S$_2$Li, 883.498; found 883.495.

2-[4-(3,4,5-Tri-n-hexyloxybenzoyloxy)phenyl]-7-dodecyl-[1]benzothieno[3,2-b]benzothiophene (H'12)

7a 160 mg (0.26 mmol), **16(12)** 120 mg (0.25 mmol), THF 50 ml, NaHCO$_3$ solution 25 ml, Pd(PPh$_3$)$_4$ 20 mg (0.017 mmol); yield 55 mg (0.061 mmol, 25%); colorless solid; ^{1}H NMR (500 MHz, CDCl$_3$) δ 8.12 (d, J = 1.1 Hz, 1H, BTBT-H), 7.92 (d, J = 8.3 Hz, 1H, BTBT-H), 7.80 (d, J = 8.1 Hz, 1H, BTBT-H), 7.75 – 7.72 (m, 3H, BTBT-H + Ar-H), 7.69 (dd, J = 8.3, 1.6 Hz, 1H, BTBT-H), 7.44 (s, 2H, Ar-H), 7.33 – 7.29 (m, 3H, BTBT-H + Ar-H), 4.08 (td, J = 6.5, 3.9 Hz, 6H, OCH$_2$CH$_2$), 2.77 (t, J = 7.4 Hz, 2H, BTBT-CH$_2$), 1.88 – 1.67 (m, 8H, OCH$_2$CH$_{2\,+}$ CH$_2$), 1.55 – 1.47 (m, 6H, CH$_2$), 1.41 – 1.23 (m, 30H, CH$_2$), 0.94 – 0.86 (m, 12H, CH$_3$); ^{13}C NMR (126 MHz, CDCl$_3$) δ 165.06 (C=O), 152.97, 150.60, 142.91, 142.67, 140.49, 138.50, 137.22, 133.78, 132.41, 132.32, 131.02, 128.32, 125.96, 124.37, 123.82, 123.36, 122.28, 122.21, 121.60, 121.24, 108.64 (BTBT-C + Ar-C), 73.58, 69.29 (OCH$_2$), 36.13, 31.90, 31.71, 31.66, 31.54, 30.28, 29.67, 29.66, 29.65, 29.64, 29.56, 29.50, 29.34, 29.28, 29.26, 25.73, 25.69, 22.67, 22.66, 22.59 (CH$_2$), 14.09, 14.06, 14.00 (CH$_3$); HRMS (m/z): [M]+Li$^+$ calcd. for C$_{59}$H$_{80}$O$_5$S$_2$Li, 911.529; found 911.524.

2-[4-(3,4,5-Tri-n-hexyloxybenzoyloxy)phenyl]-7-tetradecyl-[1]benzothieno[3,2-b]benzothiophene (H'14)

7a 150 mg (0.24 mmol), **16(14)** 120 mg (0.23 mmol), THF 50 ml, NaHCO$_3$ solution 25 ml, Pd(PPh$_3$)$_4$ 20 mg (0.017 mmol); yield 60 mg (0.064 mmol, 28%); colorless solid; ^{1}H NMR (500 MHz, CDCl$_3$) δ 8.12 (d, J = 1.1 Hz, 1H, BTBT-H), 7.92 (d, J = 8.3 Hz, 1H, BTBT-H), 7.80 (d, J = 8.1 Hz, 1H, BTBT-H), 7.75 – 7.72 (m, 3H, BTBT-H + Ar-H), 7.69 (dd, J = 8.3, 1.6 Hz, 1H, BTBT-H), 7.44 (s, 2H, Ar-H), 7.33 – 7.29 (m, 3H, BTBT-H + Ar-H), 4.08 (td, J = 6.5, 3.9 Hz, 6H, OCH$_2$CH$_2$), 2.77 (t, J = 7.4 Hz, 2H, BTBT-CH$_2$), 1.88 – 1.67 (m, 8H, OCH$_2$CH$_{2\,+}$ CH$_2$), 1.55 – 1.47 (m, 6H, CH$_2$), 1.41 – 1.23 (m, 34H, CH$_2$), 0.94 – 0.86 (m, 12H, CH$_3$); ^{13}C NMR (126 MHz, CDCl$_3$) δ 165.05 (C=O), 152.97, 150.60, 142.91, 142.67, 140.49, 138.50, 137.22, 133.78, 132.41, 132.32, 131.02, 128.32, 125.96, 124.37, 123.82, 123.36, 122.28, 122.21, 121.60, 121.24, 108.64 (BTBT-C + Ar-C), 73.58, 69.30 (OCH$_2$), 36.13, 31.90, 31.71, 31.66, 31.54, 30.28, 29.67, 29.66,

29.65, 29.64, 29.56, 29.50, 29.34, 29.28, 29.26, 25.73, 25.69, 22.67, 22.66, 22.59 (CH$_2$), 14.09, 14.06, 14.00 (CH$_3$); HRMS (m/z): [M]+Li$^+$ calcd. for C$_{59}$H$_{80}$O$_5$S$_2$Li, 939.560; found 939.560.

2-[4-(3,4,5-Tri-n-hexyloxybenzoyloxy)phenyl]-7-octadecyl-[1]benzothieno[3,2-b]benzothiophene (H'18)

7a 140 mg (0.22 mmol), **16(18)** 120 mg (0.21 mmol), THF 50 ml, NaHCO$_3$ solution 25 ml, Pd(PPh$_3$)$_4$ 20 mg (0.017 mmol); yield 45 mg (0.0455 mmol, 22%); colorless solid; ^{1}H NMR (400 MHz, CDCl$_3$) δ 8.12 (d, J = 1.0 Hz, 1H, BTBT-H), 7.93 (d, J = 8.3 Hz, 1H, BTBT-H), 7.80 (d, J = 8.1 Hz, 1H, BTBT-H), 7.76 – 7.72 (m, 3H, BTBT-H + Ar-H), 7.69 (dd, J = 8.3, 1.4 Hz, 1H, BTBT-H), 7.44 (s, 2H, Ar-H), 7.34 – 7.28 (m, 3H, BTBT-H + Ar-H), 4.08 (td, J = 6.5, 2.9 Hz, 6H, OCH$_2$CH$_2$), 2.77 (t, J = 7.4 Hz, 2H, BTBT-CH$_2$), 1.90 – 1.66 (m, 8H, OCH$_2$CH$_2$ + CH$_2$), 1.56 – 1.45 (m, 6H, CH$_2$), 1.43 – 1.22 (m, 42H, CH$_2$), 0.95 – 0.86 (m, 12H, CH$_3$); ^{13}C NMR (101 MHz, CDCl$_3$) δ 165.05 (C=O), 152.97, 150.60, 143.10, 142.67, 140.49, 138.50, 137.22, 133.78, 132.41, 132.33, 131.02, 128.32, 125.96, 124.37, 123.82, 123.36, 122.28, 122.21, 121.60, 121.24, 108.64 (BTBT-C + Ar-C), 73.58, 69.30 (OCH$_2$), 36.13, 31.90, 31.71, 31.66, 31.54, 30.28, 29.68, 29.64, 29.56, 29.49, 29.34, 29.28, 29.25, 25.73, 25.69, 22.66, 22.59 (CH$_2$), 14.09, 14.06, 14.00 (CH$_3$); HRMS (m/z): [M]+Li$^+$ calcd. for C$_{63}$H$_{80}$O$_5$S$_2$Li, 995.623; found 995.622.

11.7.3 Representative NMR and HRMS spectra
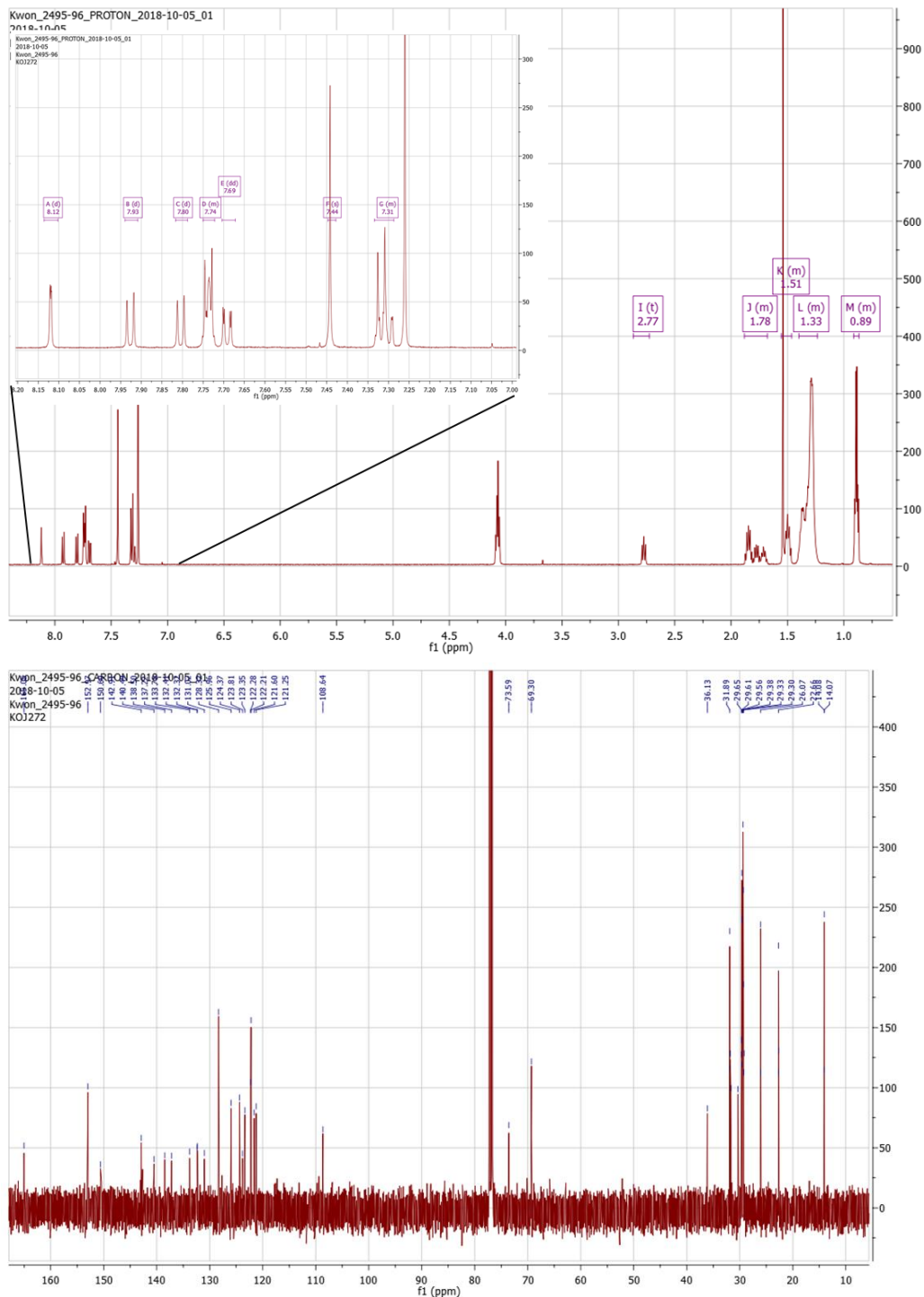
Figure 11.15 ^{1}H-, ^{13}C-NMR of compound **H''7**. The spectra were measured at 27 °C, with the frequencies 500 MHz (^{1}H), and 126 MHz (^{13}C) in CDCl$_3$ as solvent.
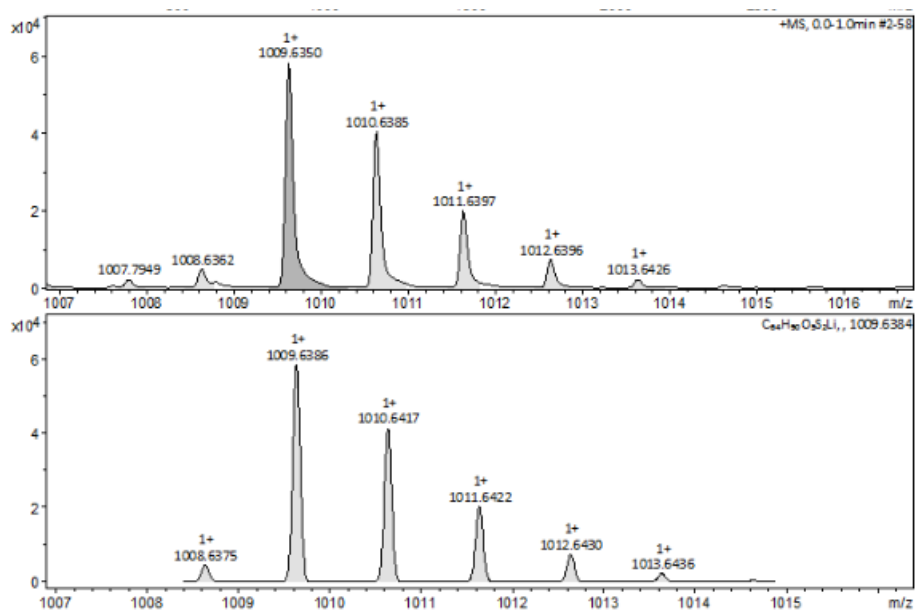
Figure S11.16 HRMS spectra for **H''7**.

References

S1   B. Košata, V. Kozmík, J. Svoboda, Coll. *Czech. Chem. Comm.* **2002**, 67, 645.

S2   S. Inoue, H. Minemawari, J. Tsutsumi, M. Chikamatsu, T. Yamada, S. Horiuchi, M. Tanaka, R. Kumai, M. Yoneya, T. Hasegawa, *Chem. Mater.* **2015**, 27, 3809.

S3   V. A. Piunova, G. M. Miyake, C. S. Daeffler, R. A. Weitekamp, R. H. Grubbs, *J. Am. Chem. Soc.* **2013**, 135, 15609.

S4   A. Schultz S. Diele S. Laschat M. Nimtz, *Adv. Funct. Mater.* **2001**, 11: 441-446

S5   C. Dressel, F. Liu, M. Prehm, X. Zeng, G. Ungar, C. Tschierske, *Angew. Chem. Int. Ed.* **2014**, 53, 13115.

S6   N. Miyaura, A. Suzuki, Suzuki coupling reaction J. Chem. Soc., *Chem. Commun.* **1979**, 19, 866.

S7   A. Sanzone, S. Mattiello, G. M. Garavaglia, A. M. Calascibetta, C. Ceriani, M. Sassi, L. Beverina, *Green Chem.* **2019**,21, 4400.

S8   T. Ishiyama, M. Murata and N. Miyaura, *J. Org. Chem.* **1995**, 60, 23, 7508.

S9   C. Niebel, Y. Kim, C. Ruzi, J. Karpinska, B. Chattopadhyay, G. Schweicher, A. Richard, V. Lemaur, Y. Olivier, J. Cornil, A. R. Kennedy, Y. Diao, W. Lee, S. Mannsfeld, Z. Baoc, Y. H. Geerts, *J. Mater. Chem. C*, **2015**, 3, 674.

12. Apendix

12.1 Supporting information of chapter 4

The supporting information of chapter 4 is available in online. [S1]
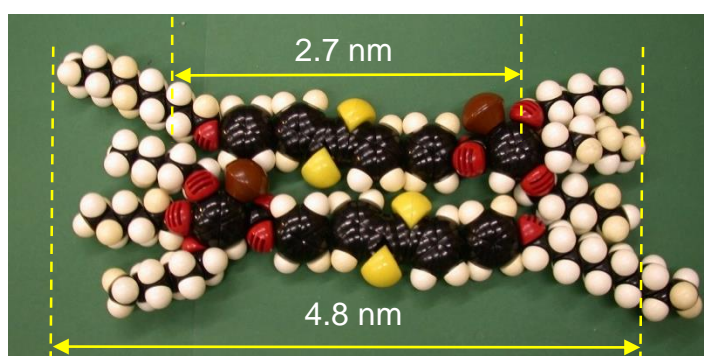
Figure S4.1 Space filling CPK model showing the molecular dimensions of **B10**.
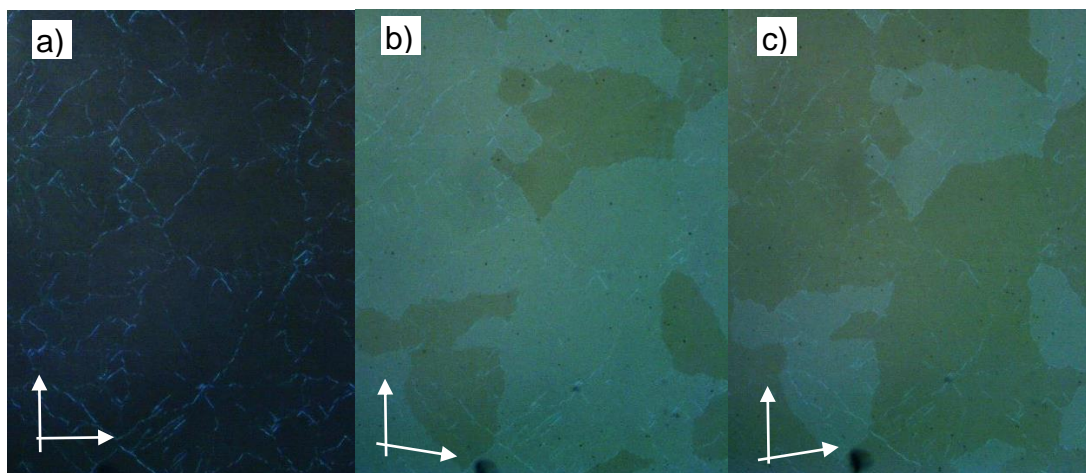
Figure S4.2 Textures of the crystalline mesophase of **B22** at 20 ℃: a) between crossed polarizers and b, c) between slightly uncrossed polarizers rotated in opposite directions, indicating a conglomerate type helical crystalline mesophase.

12.2 Supporting information of chapter 5

The supporting information of chapter 5 is published and available online. [S2]

12.3 Supporting information of chapter 6

12.3.1 DSC traces and transition temperatures
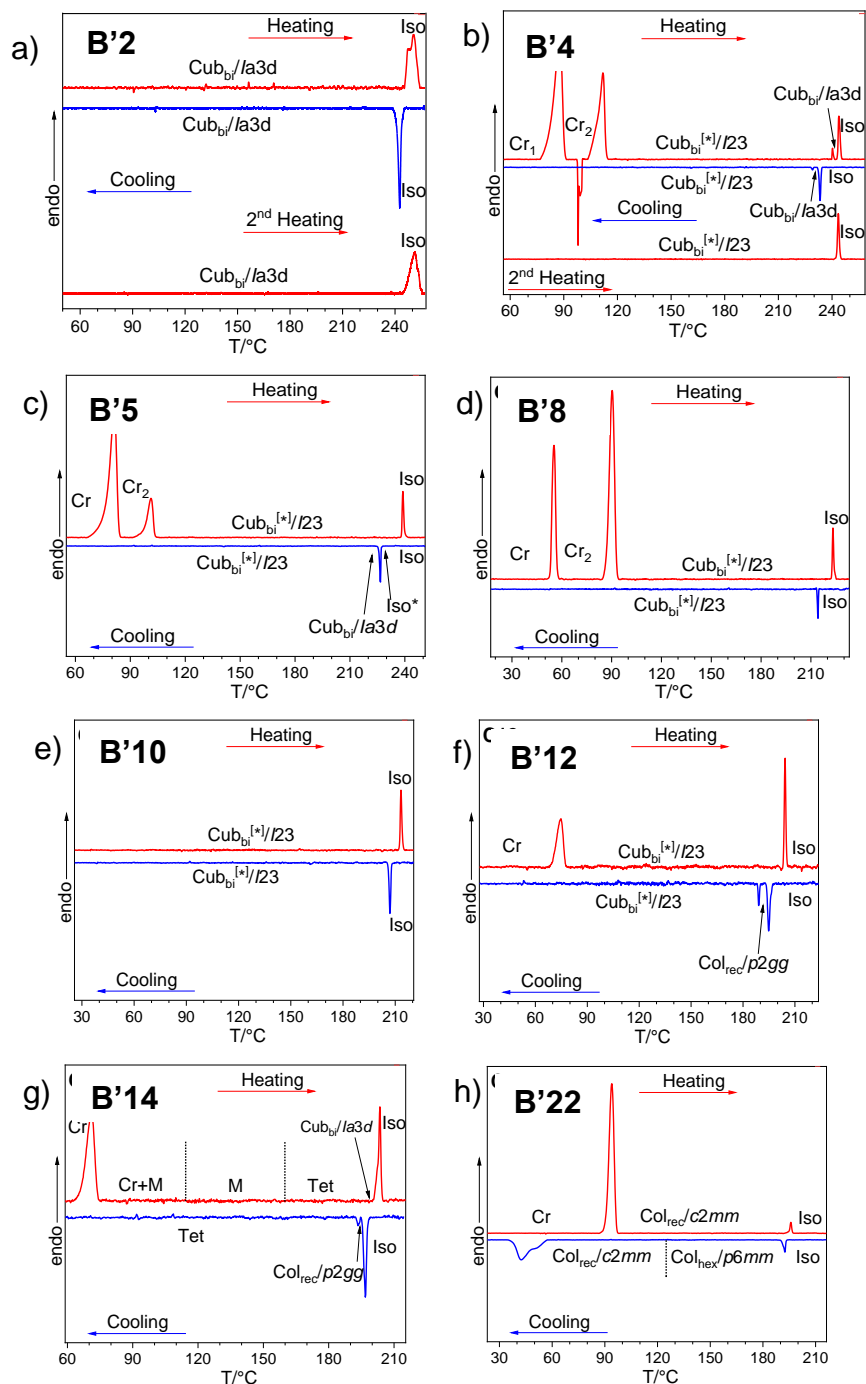
Figure S6.1 DSC traces of compounds **B'2** – **B'22** (10 K·min⁻¹); transitions without enthalpy were determined by POM or XRD.
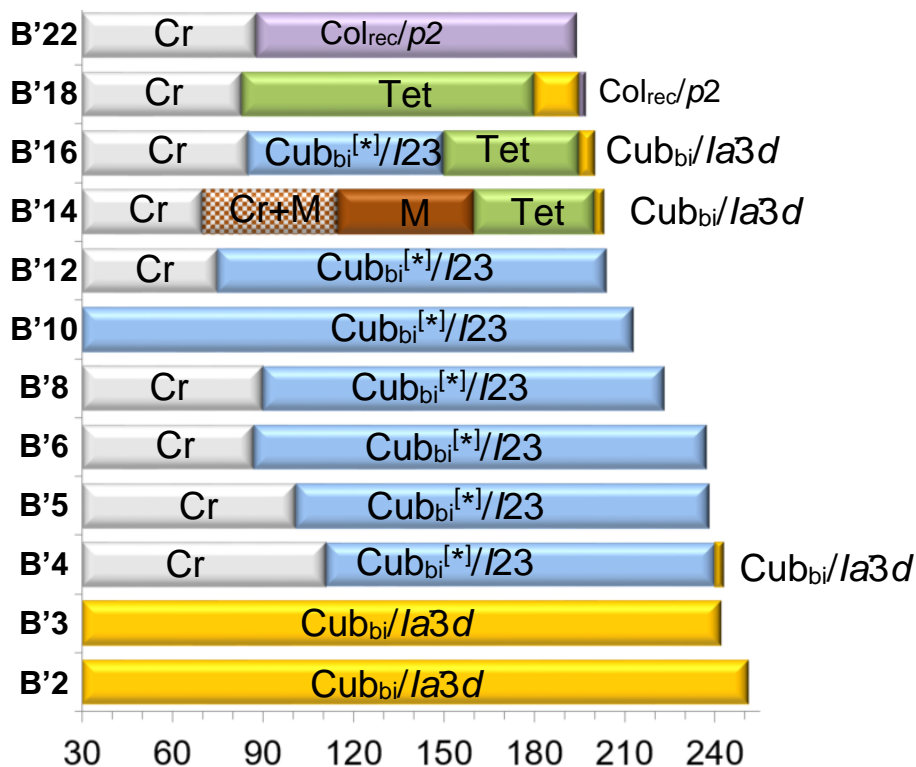
Figure S6.2 Phases and phase transitions observed in the first heating scan (rate 10 K min^{-1}).

12.3.2 XRD data and structural data
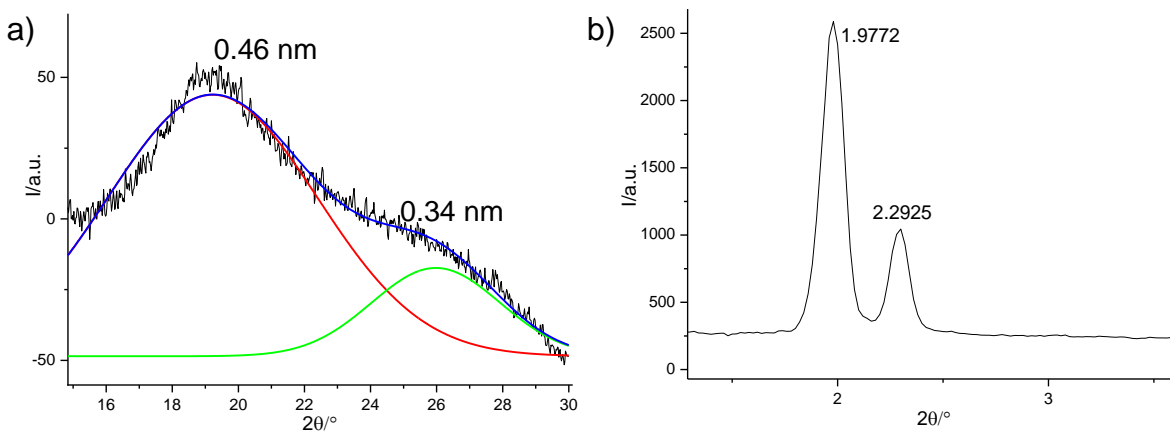
Figure S6.3 a) WAXS and b) SAXS diffractograms of the Cub$_{bi}$/$Ia3d$ of **B'2** at 180 °C.
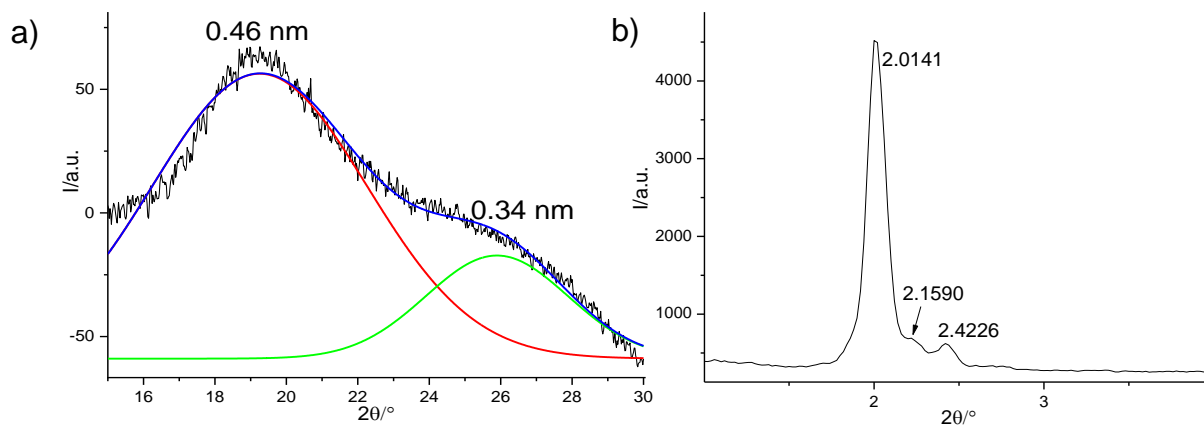
Figure S6.4 a) WAXS and b) SAXS diffractograms of the Cub$_{bi}$/*Ia3d* of **B'5** at 180 °C.
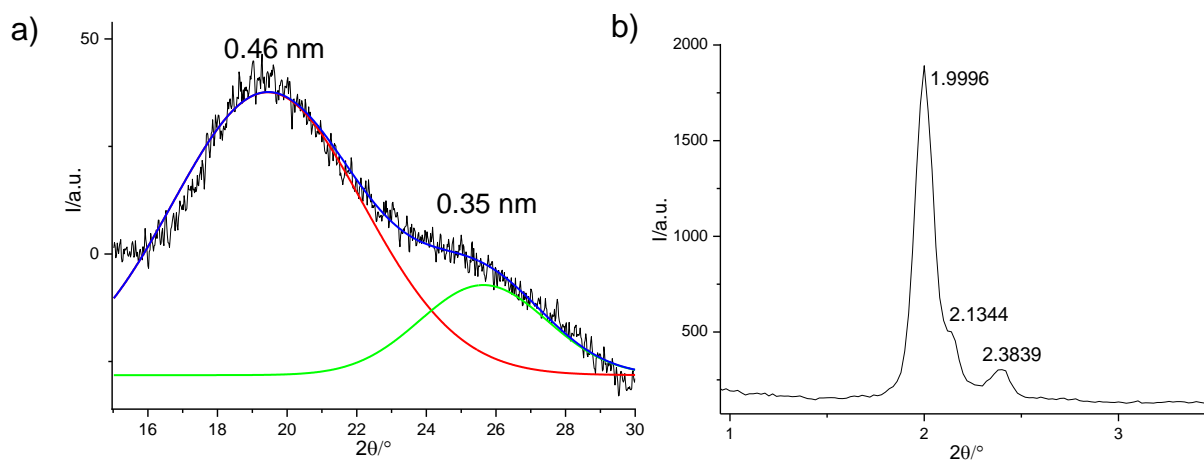
Figure S6.5 a) WAXS and b) SAXS diffractograms of the Cub$_{bi}$[*]/*I*23 of **B'8** at 180°C.
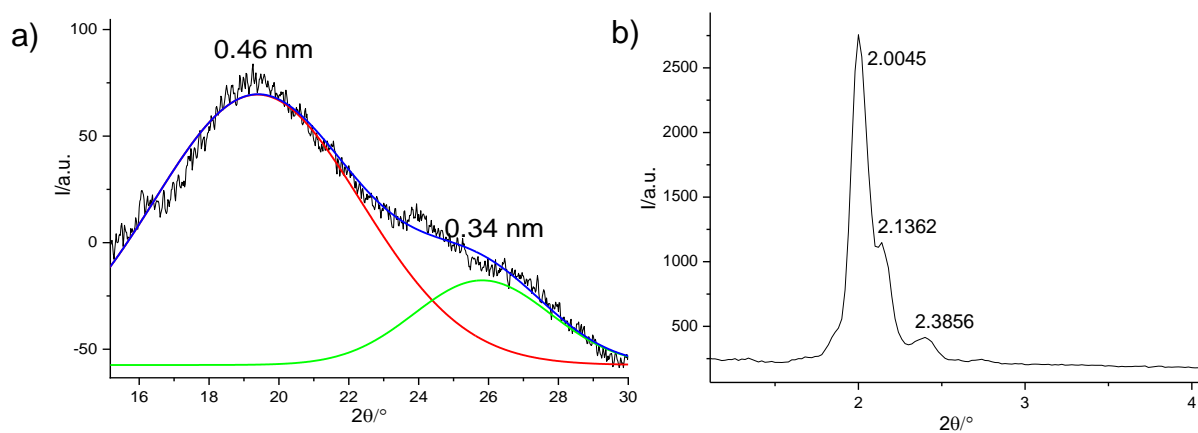
Figure S6.6 a) WAXS and b) SAXS diffractograms of the Cub$_{bi}$[*]/*I*23 of **B'10** at 180°C.

Table S6.1 Experimental and calculated *d*-spacings of *Ia*3*d* phase of **B'2** at 180 ℃**.**

$2\theta/°$	$\theta/°$	d_{obs}/nm	d_{calc}/nm	*hkl*	Δ
1.977	0.989	4.468	4.468	211	0.00
2.293	1.146	3.854	3.869	220	0.02
19.242	9.621	0.461		diff	

Cub$_{bi}$/*Ia*3*d*: *a* = 10.94 nm

Table S6.2 Experimental and calculated *d*-spacings of *I*23 phase of **B'8** at 180 ℃**.**

$2\theta/°$	$\theta/°$	d_{obs}/nm	d_{calc}/nm	*hkl*	Δ
2.000	1.000	4.418	4.418	321	0.00
2.134	1.067	4.139	4.133	400	0.01
2.384	1.192	3.706	3.696	420	0.01
19.454	9.727	0.456		diff	

Cub$_{bi}$[*]/*I*23: *a* = 16.53 nm

Table S6.3 Experimental and calculated *d*-spacings of *I*23 phase of **B'10** at 180 ℃**.**

$2\theta/°$	$\theta/°$	d_{obs}/nm	d_{calc}/nm	*hkl*	Δ
2.005	1.002	4.407	4.407	321	0.00
2.136	1.068	4.136	4.122	400	0.00
2.386	1.193	3.703	3.687	420	0.00
19.350	9.675	0.459		diff	

Cub$_{bi}$[*]/*I*23: *a* = 16.49 nm

12.4 Supporting information of chapter 7

12.4.1 DSC traces and transition temperatures
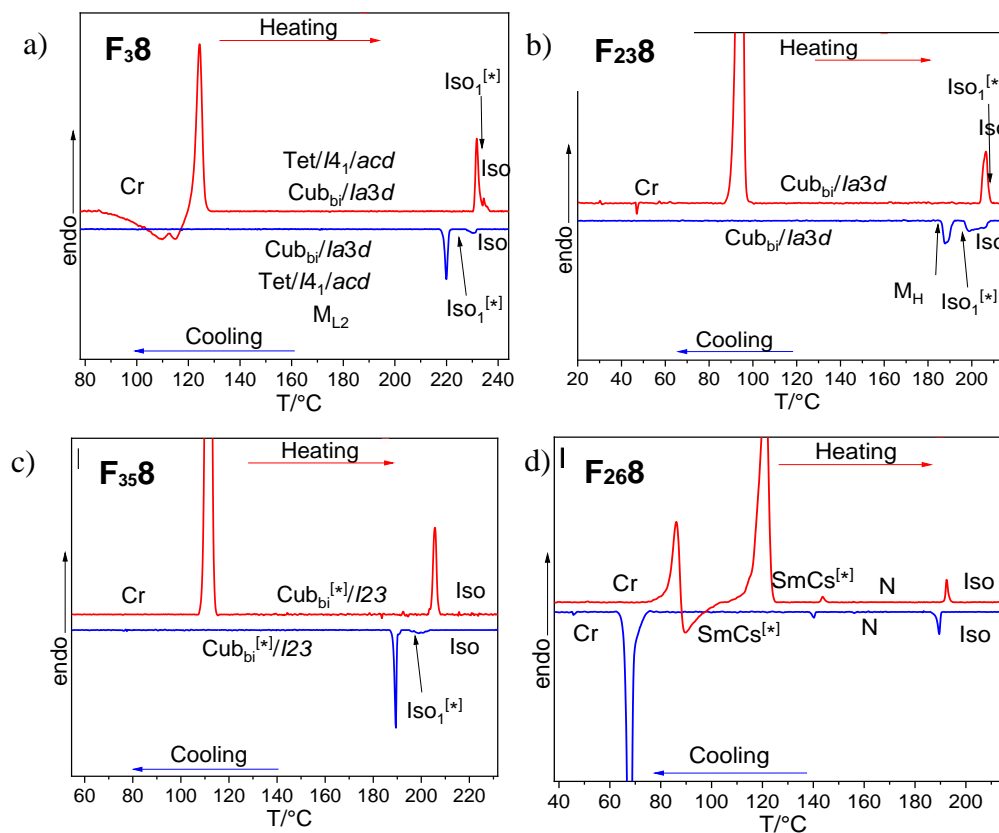
Figure S7.1 DSC traces of compounds **F$_X$8** (10 K·min^{-1}); transitions without enthalpy were determined by POM or XRD.

12.4.2 XRD data
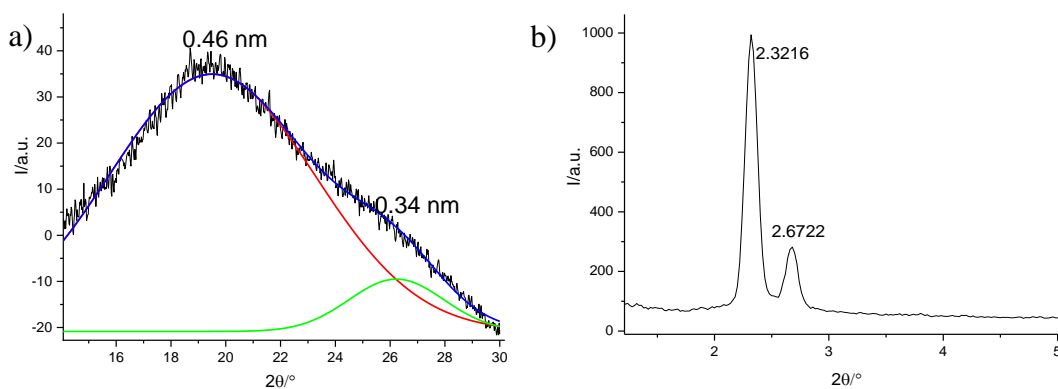
Figure S7.2 a) WAXS and b) SAXS diffractograms of the Cub$_{bi}$/$Ia\overline{3}d$ of **F$_{23}$** at 150 °C
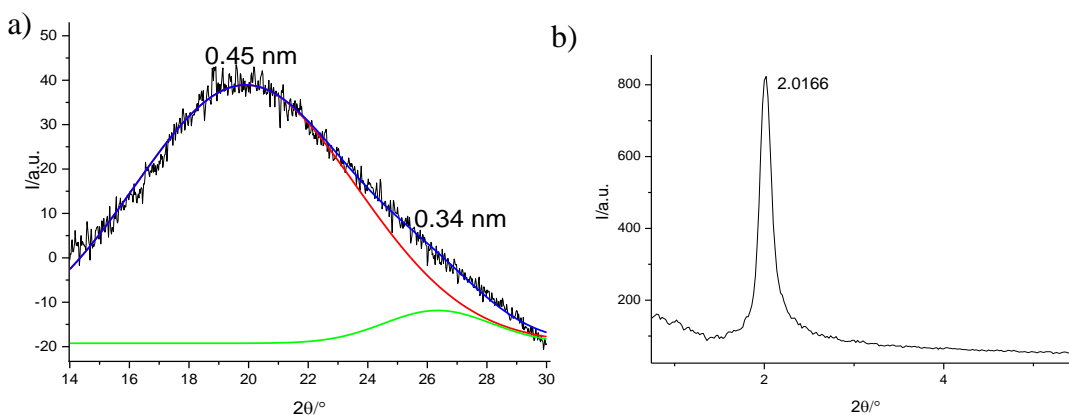
Figure S7.3 a) WAXS and b) SAXS diffractograms of the SmC of $F_{26}8$ at 130°C.
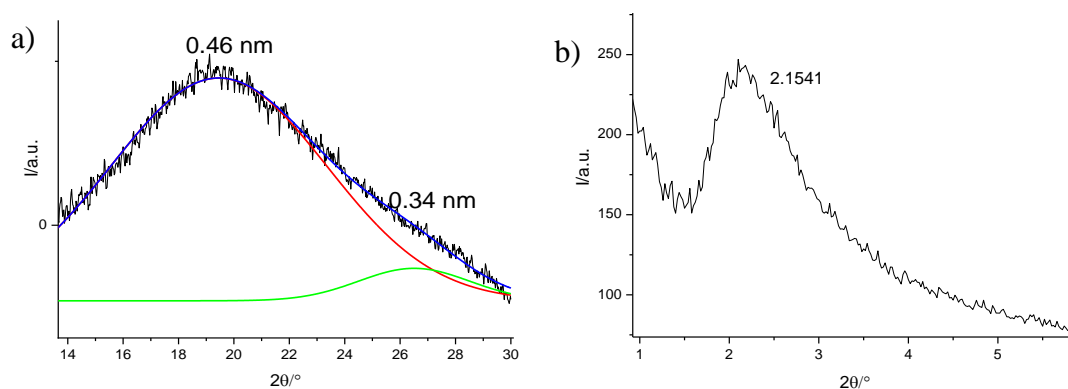
Figure S7.4 a) WAXS and b) SAXS diffractograms of the N of $F_{26}8$ at 180 °C.
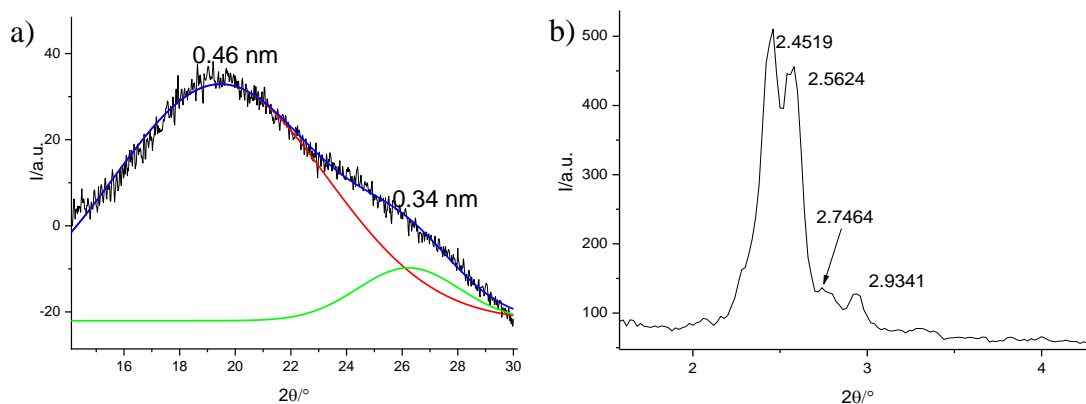
Figure S7.5 a) WAXS and b) SAXS diffractograms of the Cub$_{bi}$[*]/$I23$ of $F_{35}8$ at 150 °C.

Table S7.1 Experimental and calculated d-spacings for Cub$_{bi}$/$Ia\overline{3}d$ of $F_{23}8$

$2\theta/°$	$\theta/°$	d_{obs}/nm	d_{calc}/nm	hkl	Δ
2.322	1.161	3.805	3.805	211	0.00
2.672	1.336	3.306	3.295	220	0.01
19.448	9.724	0.456		diff	

Cub/$Ia3d$: a = 9.32 nm at 150 °C

Table S7.2 Experimental and calculated d-spacings for SmCs[*] of **F$_{26}$8**

$2\theta/°$	$\theta/°$	d_{obs}/nm	d_{calc}/nm	hkl	Δ
2.017	1.008	4.381	4.381	10	0.00
19.822	9.911	0.448		diff	

Sm: d = 4.38 nm at 130 °C

Table S7.3 Experimental and calculated d-spacings for SmCs[*] of **F$_{26}$8**

$2\theta/°$	$\theta/°$	d_{obs}/nm
2.154	1.077	4.101
19.427	9.714	0.457

N: d = 4.10 nm at 180 °C

Table S7.4 Experimental and calculated d-spacings for Cub$_{bi}$[*]/$I$23 of **F$_{35}$8**

$2\theta/°$	$\theta/°$	d_{obs}/nm	d_{calc}/nm	hkl	Δ
2.452	1.226	3.603	3.603	321	0.00
2.562	1.281	3.448	3.370	400	0.08
2.746	1.373	3.217	3.177	411	0.04
2.934	1.467	3.011	3.014	420	0.00
19.527	9.763	0.455		diff	

Cub$_{bi}$[*]/$I$23: a = 13.48 nm at 150 °C

12.5 Supporting information of chapter 8

12.5.1 DSC traces and transition temperatures
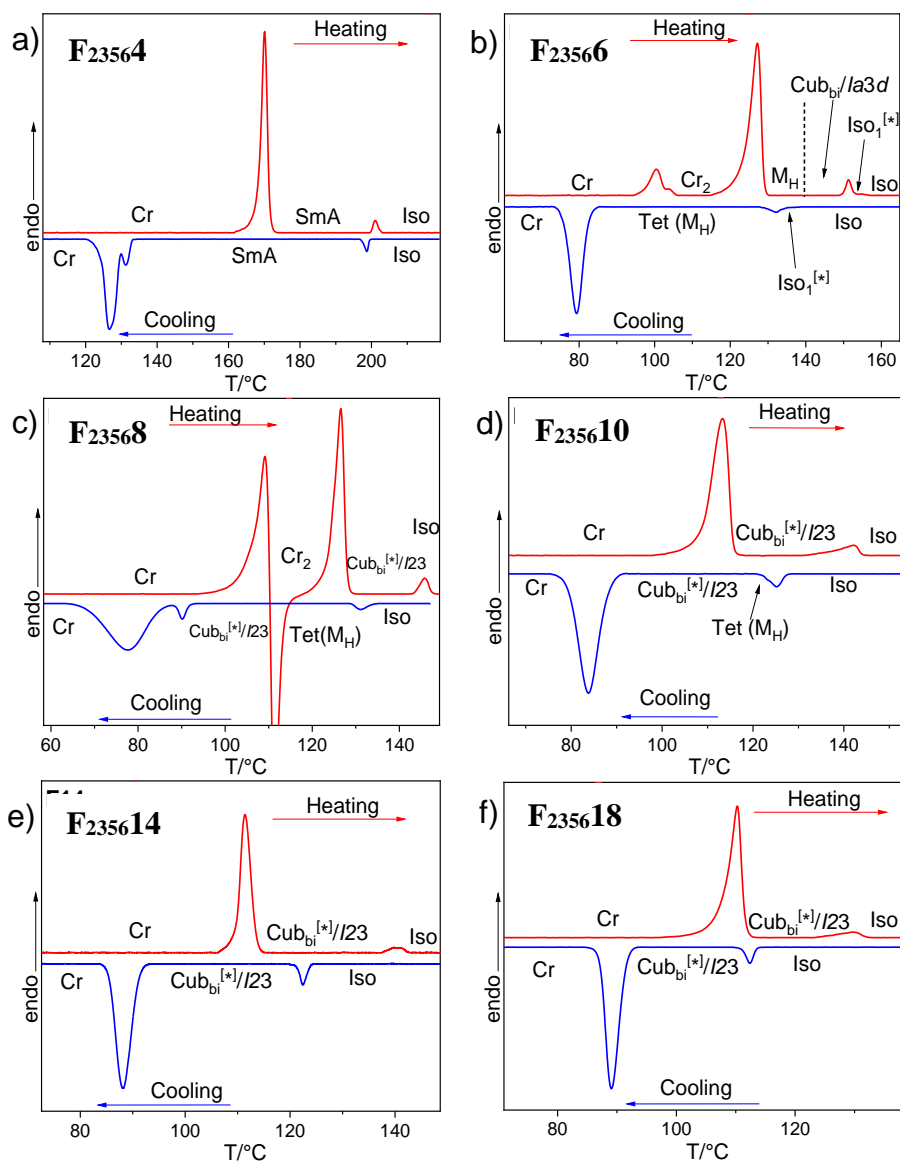
Figure S8.1 DSC traces of compounds $F_{2356}4 - F_{2356}18$ (10 K·min^{-1}); transitions without enthalpy were determined by POM or XRD.
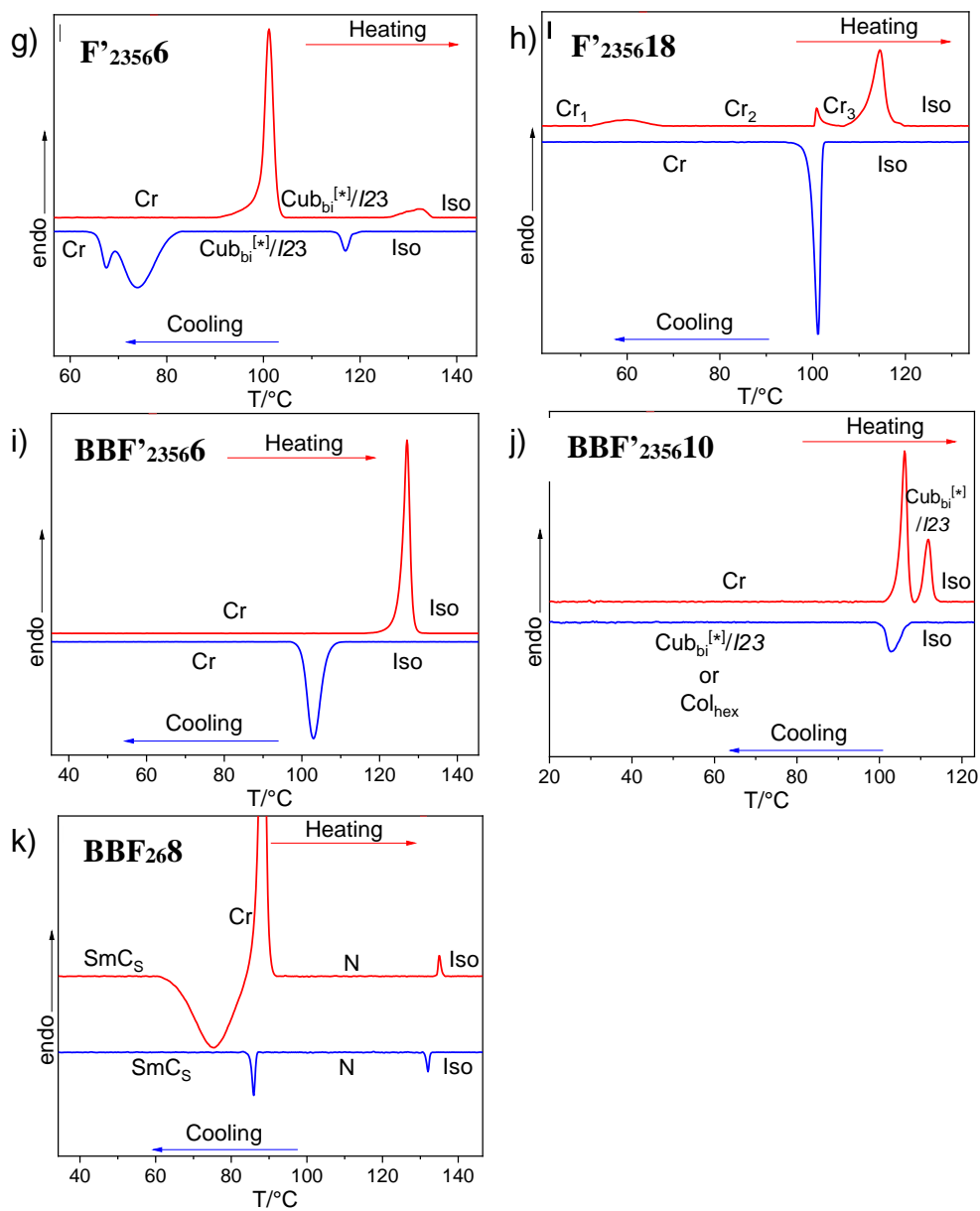
Figure S8.1 (continue). DSC traces of compounds **F'$_{2356}$6, F'$_{2356}$18, BBF'$_{2356}$6, BBF'$_{2356}$10 and BBF$_{26}$8** (10 K·min^{-1}); transitions without enthalpy were determined by POM or XRD.
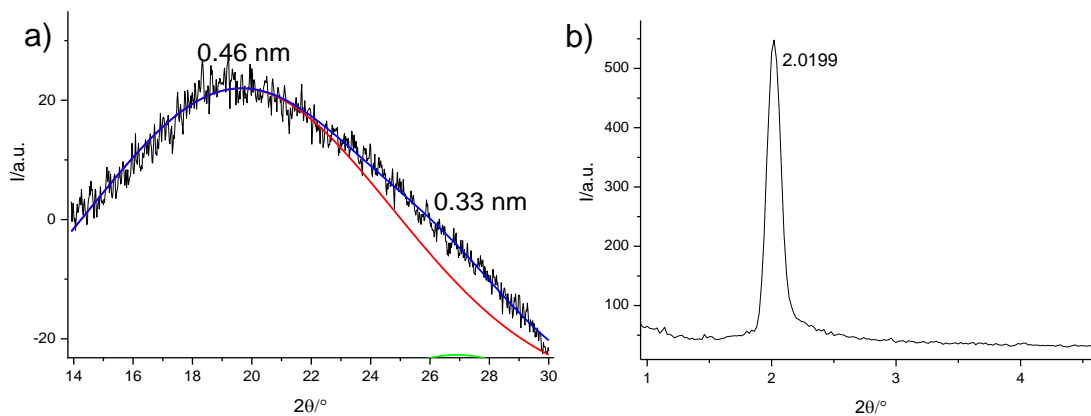
12.5.2 XRD data

Figure S8.2 a) WAXS and b) SAXS diffractograms of the SmA phase of **F$_{2356}$4** at 180 °C.
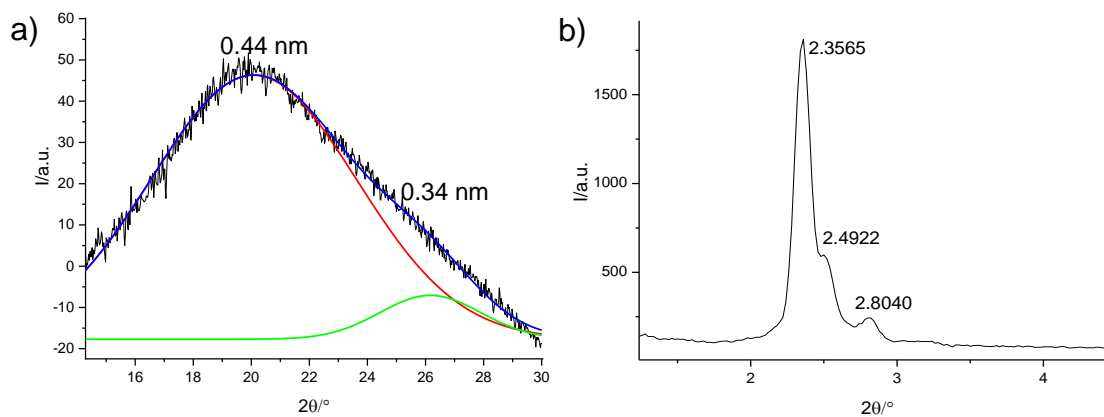
Figure S8.3 a) WAXS and b) SAXS diffractograms of the Cub$_{bi}$[*]/*I*23 of **F$_{2356}$14** at 120 °C.
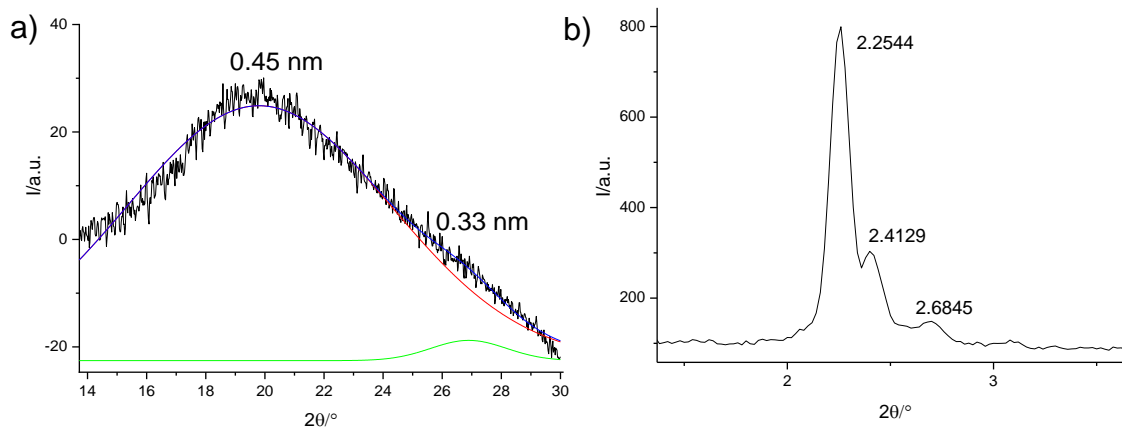
Figure S8.4 a) WAXS and b) SAXS diffractograms of the Cub$_{bi}$[*]/*I*23 of **F$_{2356}$18** at 110 °C.
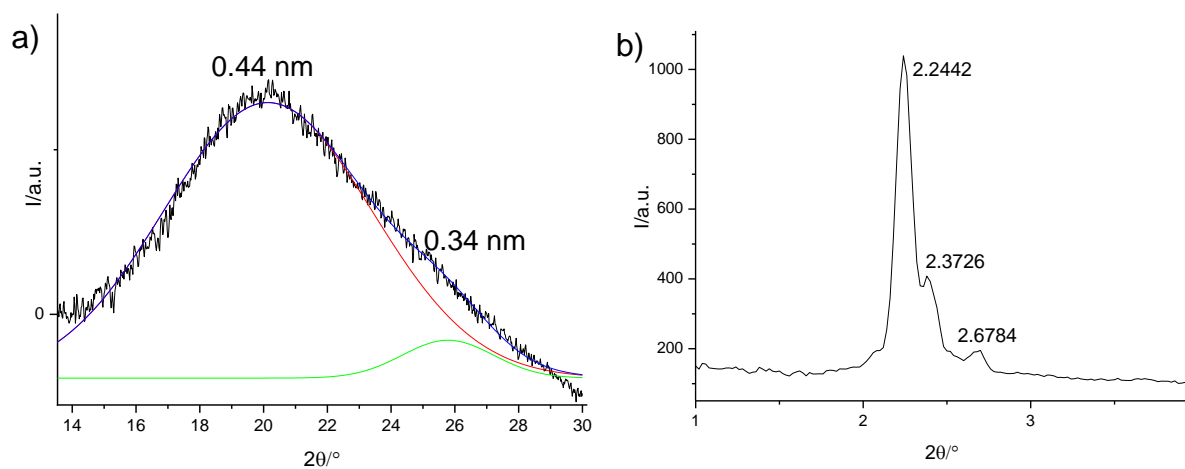
Figure S8.5 a) WAXS and b) SAXS diffractograms of the $\text{Cub}_{\text{bi}}^{[*]}/I23$ of **F'$_{2356}$6** at 120 °C.
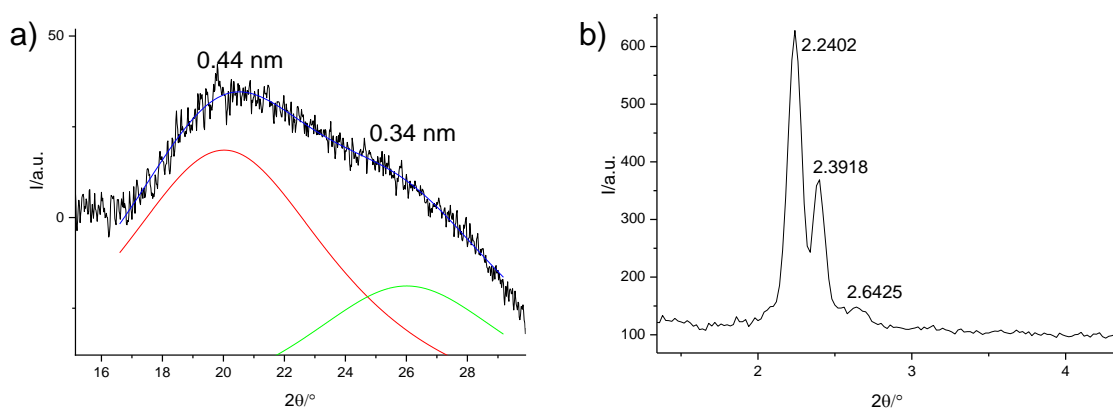
Figure S8.6 a) WAXS and b) SAXS diffractograms of the $\text{Cub}_{\text{bi}}^{[*]}/I23$ of **BBF'$_{2356}$10** at 108 °C.
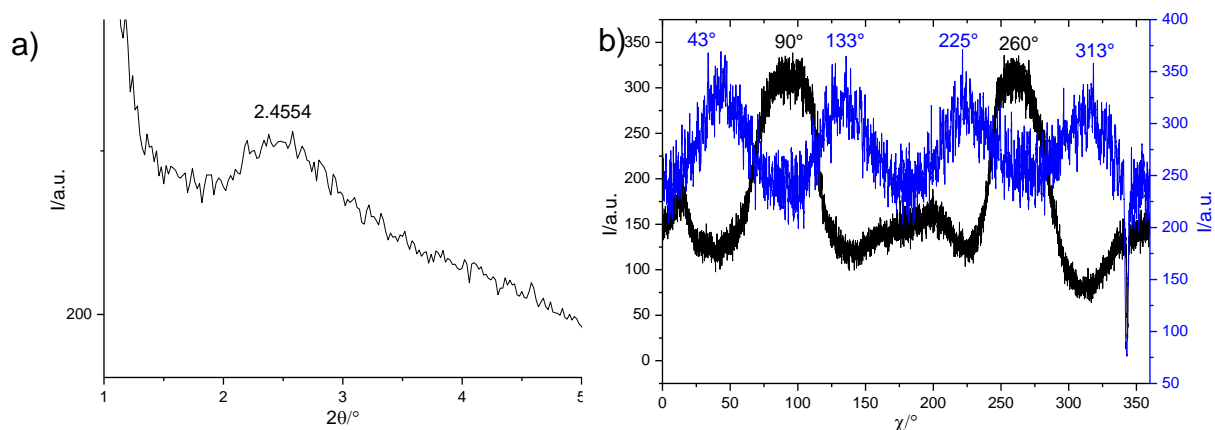
Figure S8.7 a) SAXS diffractogram and b) chi scan of the N_{cybC} phase of **BBF$_{26}$8** at 120 °C.
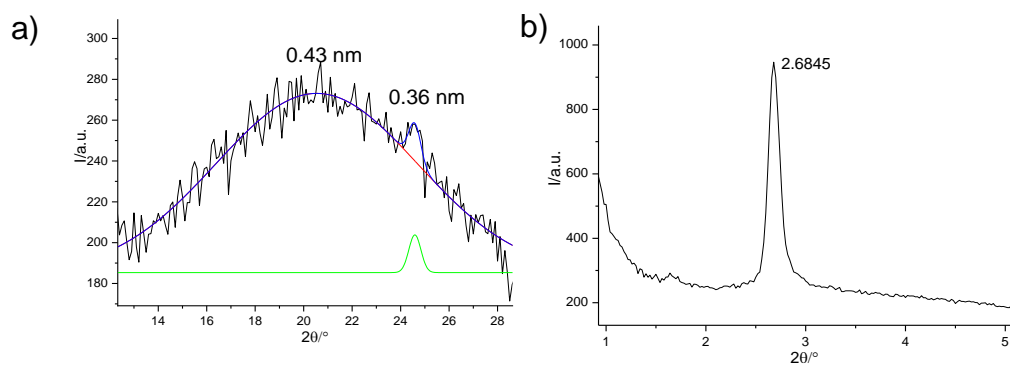
Figure S8.8 a) WAXS and b) SAXS diffractograms of the SmC$_S$ phase of **BBF$_{26}$8** at 70 °C.
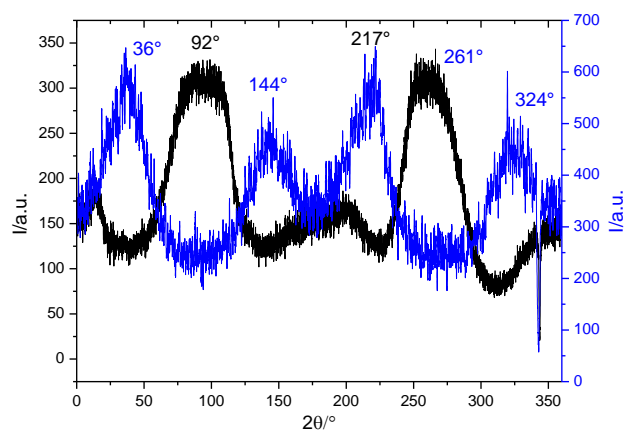
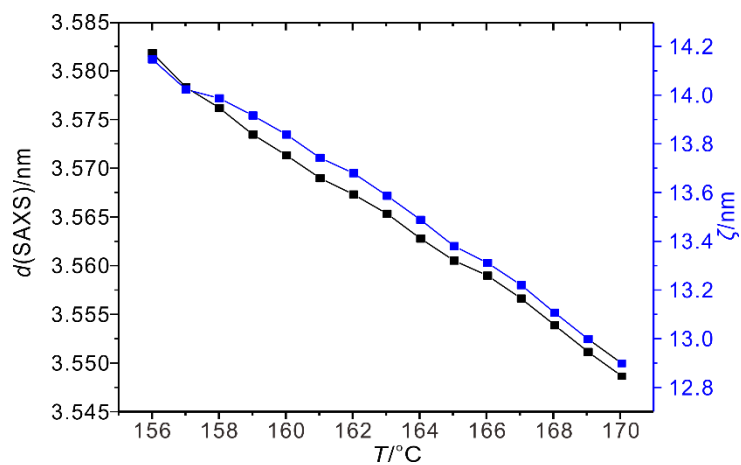**Figure S8.9** Chi scan of the SmC$_S$ phase of **BBF$_{26}$8** at 70 °C.

Figure S8.10 *d*-spacings and correlation length of **F$_{2356}$6** upon heating.

Table S8.1 Experimental and calculated d-spacings for SmA of $F_{2356}4$ at 180 °C

$2\theta/°$	$\theta/°$	d_{obs}/nm	d_{calc}/nm	hkl	Δ
2.020	1.010	4.374	4.374	10	0.00
19.775	9.888	0.449		diff	

➔ **Sm:** d = **4.37 nm**

Table S8.2 Experimental and calculated d-spacings of $Cub_{bi}^{[*]}/I23$ for $F_{2356}14$ at 120 °C

$2\theta/°$	$\theta/°$	d_{obs}/nm	d_{calc}/nm	hkl	Δ
2.357	1.178	3.749	3.749	321	0.00
2.492	1.246	3.545	3.507	400	0.04
2.804	1.402	3.151	3.137	420	0.01
19.982	9.991	0.444		diff	

➔ **$Cub_{bi}^{[*]}/I23$:** a = **14.03 nm**

Table S8.3 Experimental and calculated d-spacings of $Cub_{bi}^{[*]}/I23$ for $F_{2356}18$ at 110 °C

$2\theta/°$	$\theta/°$	d_{obs}/nm	d_{calc}/nm	hkl	Δ
2.254	1.127	3.919	3.919	321	0.00
2.413	1.206	3.661	3.666	400	0.01
2.685	1.342	3.291	3.279	420	0.01
19.710	9.855	0.450		diff	

➔ **$Cub_{bi}^{[*]}/I23$:** a = **14.66 nm**

Table S8.4 Experimental and calculated d-spacings of $Cub_{bi}^{[*]}/I23$ for $F'_{2356}6$ at 120 °C

$2\theta/°$	$\theta/°$	d_{obs}/nm	d_{calc}/nm	hkl	Δ
2.244	1.122	3.937	3.937	321	0.00
2.373	1.186	3.724	3.683	400	0.04
2.678	1.339	3.298	3.294	420	0.00
20.145	10.072	0.441		diff	

➔ **$Cub_{bi}^{[*]}/I23$:** a = **14.73 nm**

Table S8.5 Experimental and calculated d-spacings of $Cub_{bi}^{[*]}/I23$ for $BBF'_{2356}10$ at 108 °C

$2\theta/°$	$\theta/°$	d_{obs}/nm	d_{calc}/nm	hkl	Δ	
2.240	1.120	3.944	3.944	321	0.00	
2.392	1.196	3.694	3.689	400	0.01	
2.643	1.321	3.343	3.300	420	0.04	
20.025	10.012	0.443		Diff1		
26.010	13.005	0.343		Diff2		

➔ **$Cub_{bi}^{[*]}/I23$:** a = **14.76 nm**

Table S8.6 Experimental and calculated d-spacings of N_{cybC} phase for $BBF_{26}8$ at 120 °C

$2\theta/°$	$\theta/°$	d_{obs}/nm
2.455	1.228	3.598

➔ **N_{cybC}:** d = **3.60 nm, Tilt:45°**

Figure S8.7 Experimental and calculated d-spacings of of SmC$_S$ phase for **BBF$_{26}$8** at 70 °C

$2\theta/°$	$\theta/°$	d_{obs}/nm
2.685	1.342	3.291
20.682	10.341	0.429

→ **SmC: d = 3.29 nm, Tilt: 55°**

12.5.3 Additional textures

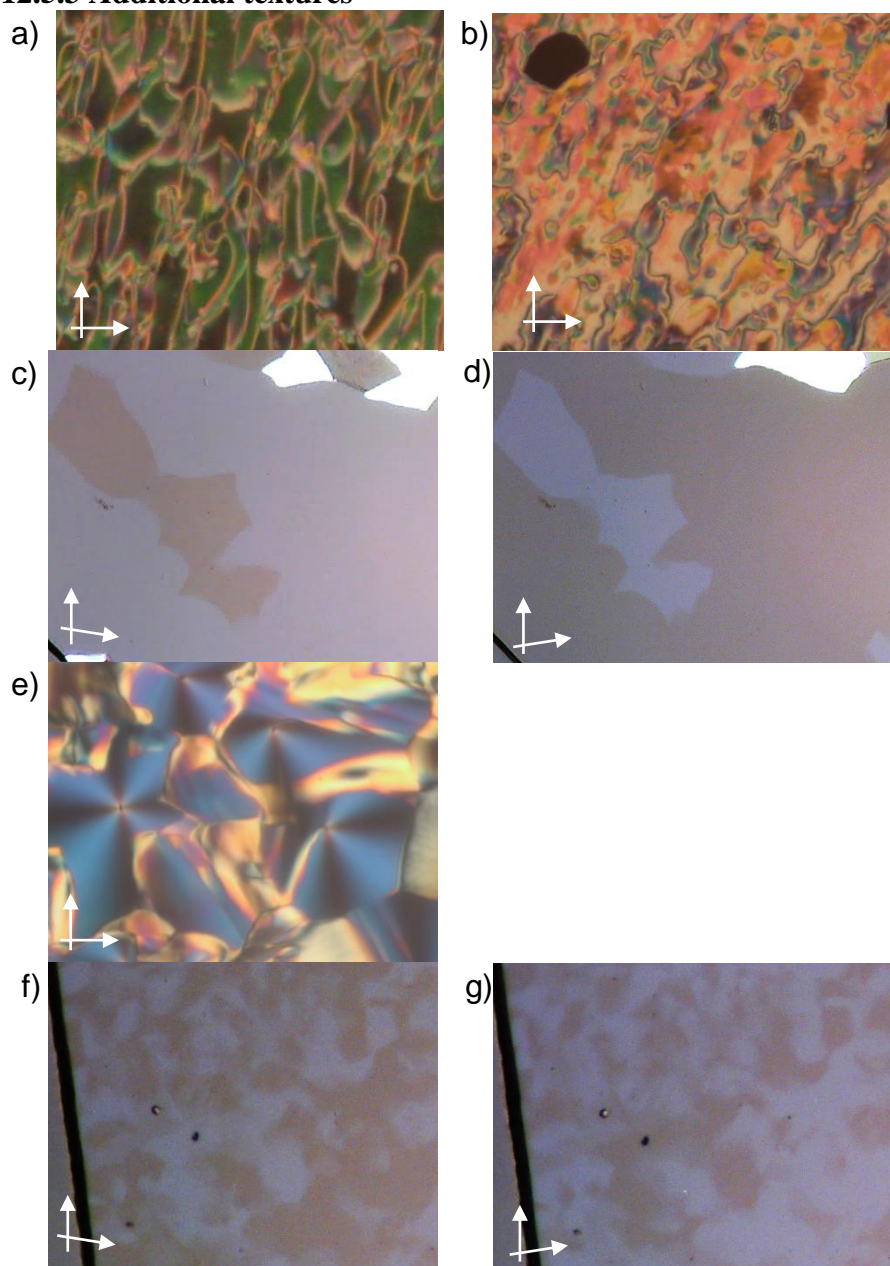**Figure S8.11** additional textures; (a) transition from SmC$_s^{[*]}$ to Cub$_{bi}$/*Ia*3*d* phase at 87 °C on heating for **BF'$_{26}$8**; (b) transition from M$_H$ to Cub$_{bi}^{[*]}$/*I*23 phase for at 117 °C on cooling for **F$_{2356}$10**; (c,d) Col$_{hex}$ at 105 °C after fast cooling and (e-g) Cub$_{bi}^{[*]}$/*I*23 after 5 mins at 105 °C for **BBF'$_{2356}$10**.
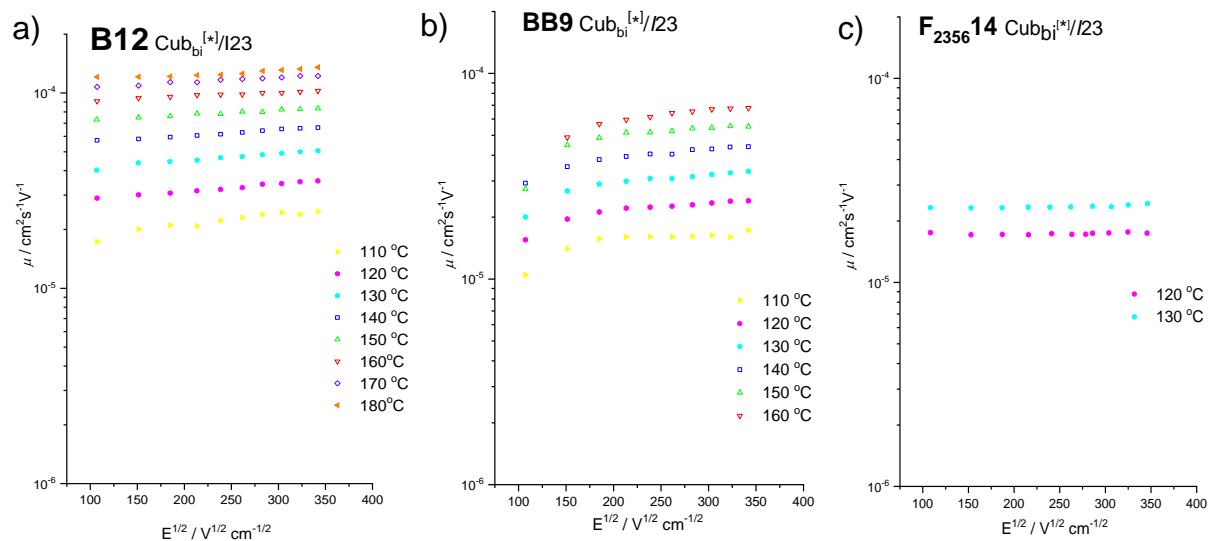
12.5.4 Additional TOF data

Figure S8.12 Field dependence of the charge carrier mobility on temperature as measured on cooling for the $Cub_{bi}^{[*]}/I23$ phases of compounds **B12**, **BB9** and **F$_{2356}$14**.
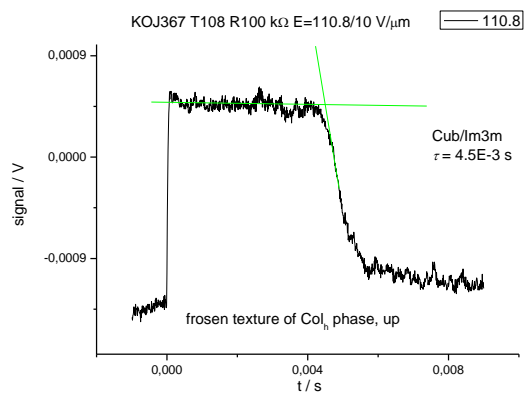

Figure S8.13 ToF transients of holes of the $Cub_{bi}^{[*]}/I23$ phase for **BBF'$_{2356}$10.**

12.6 Supporting information of chapter 9
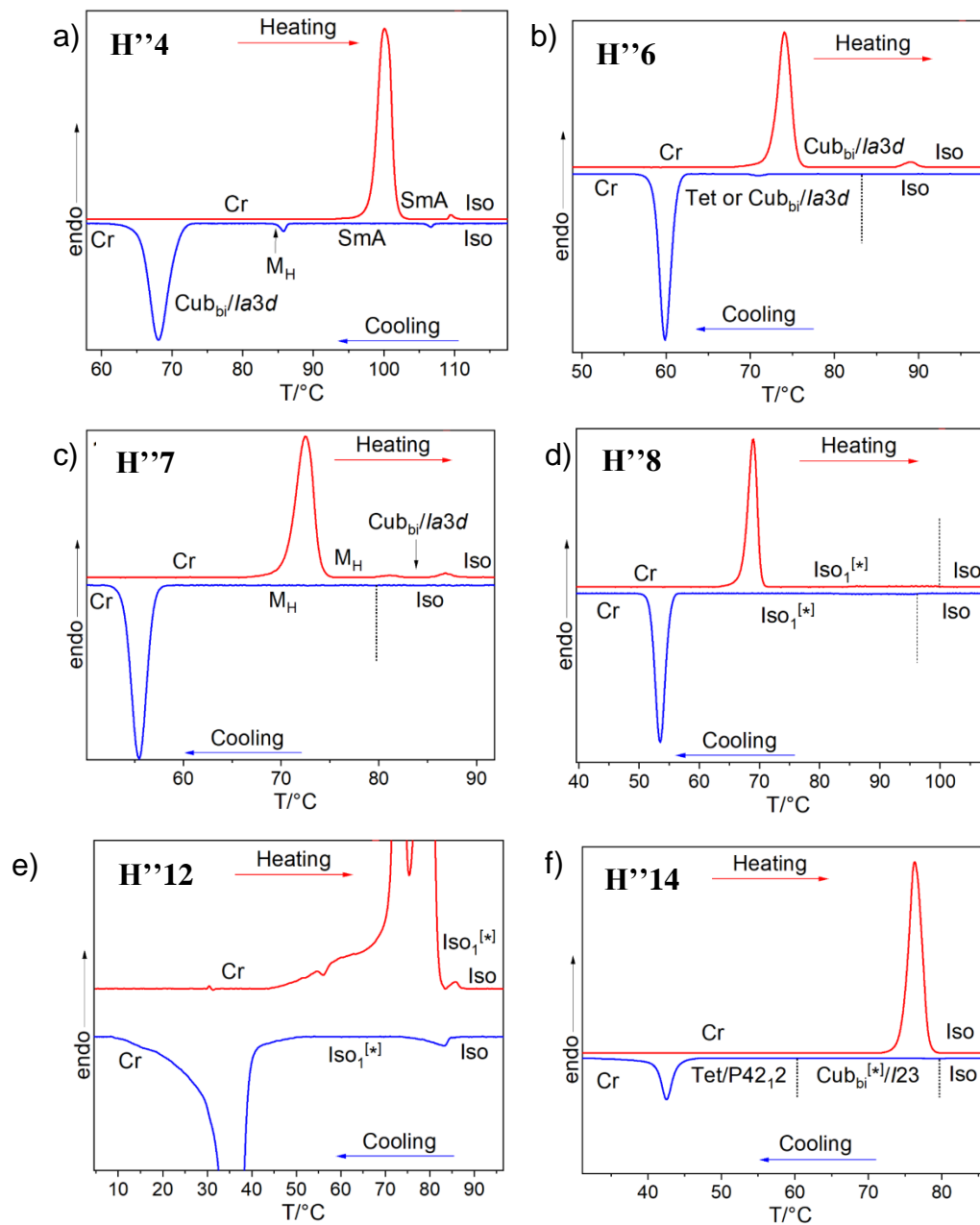
12.6.1 DSC traces and transition temperatures

Figure S9.1 DSC traces (10K·min^{-1}) compounds **H''4-H''14**

Figure S9.1 (continued). DSC traces (10K·min⁻¹) compounds **H''18**, **H'4-H'18**
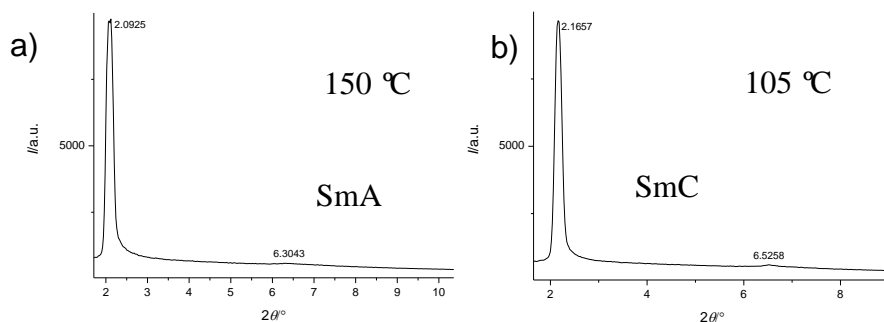
12.6.2 XRD data and structural data

Figure S9.2 SAXS diffractograms of the a) SmA and the b) SmC of **H'4**.

Table S9.1 Experimental and calculated *d*-spacing, relative integrated intensities for the SmA phase for **H'4**.

$2\theta/°$	$\theta/°$	d_{obs}/nm	d_{calc}/nm	*hkl*	Δ
2.093	1.046	4.222	4.222	10	0.00
6.304	3.152	1.402	1.407	30	0.01
19.445	9.722	0.456		diff	

➔ **SmA:** *d* = **4.22 nm** (150 °C)

Table S9.2 Experimental and calculated *d*-spacing, relative integrated intensities for the SmC phase for **H'4**.

$2\theta/°$	$\theta/°$	d_{obs}/nm	d_{calc}/nm	*hkl*	Δ
2.166	1.083	4.079	4.079	10	0.00
6.526	3.263	1.354	1.360	30	0.01
19.677	9.839	0.451		diff	

➔ **SmC:** *d* = **4.08 nm** (105 °C)

Table S9.3 Experimental and calculated *d*-spacing, relative integrated intensities for the Iso_1[*]

$2\theta/°$	$\theta/°$	d_{obs}/nm
2.558	1.279	3.454
2.492	1.246	3.545
2.470	1.235	3.577
2.421	1.211	3.649
2.375	1.188	3.720
2.343	1.172	3.771
2.295	1.148	3.849
2.268	1.134	3.895
2.233	1.117	3.956
2.208	1.104	4.001
2.173	1.087	4.066
2.145	1.073	4.119
2.107	1.054	4.193

2.083	1.042	4.241
2.055	1.028	4.299
2.042	1.021	4.326

Table S9.4 Changes of correlation length and FWHM with temperature.

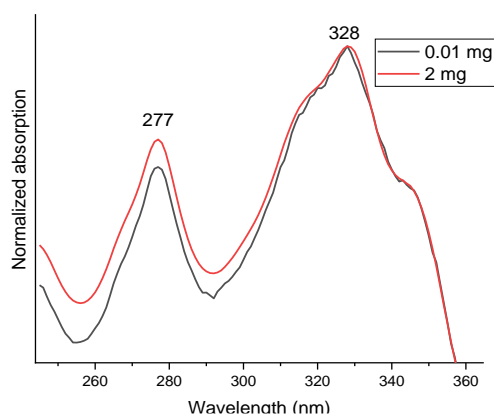| T (°C)	FWHM (°)	Correlation length (nm)
130	1.56	19.7
125	1.39	19.9
120	1.26	21.3
115	1.02	24.6
110	0.98	24.1
105	0.9	25.3
100	0.85	25.3
95	0.74	28.2
90	0.64	31.5
85	0.62	31.7
80	0.58	32.7
75	0.56	33.0
70	0.53	33.7
65	0.52	33.7
60	0.5	34.2
55	0.5	33.8

Figure S9.3 Normalized absorption curve with highest and lowest concentration.

References

1   O. Kwon, X. Cai, W. Qu, F. Liu, J. Szydłowska, E. Gorecka, M. J. Han, D. K. Yoon S. Poppe and C. Tschierske, *Adv. Funct. Mater*, **2021**, 2102271

2   O. Kwon, X. Cai, A. Saeed, F. Liu, S. Poppe and C. Tschierske, *Chem. Comm.* **2021**, d1cc01922h.

Curriculum Vitae

Personal Data

Name	Ohjin Kwon
Date of Birth	29.01.1985
Place of Birth	Seoul
Nationality	Republic of Korea
Marital Status	Married

Education

Mar. 2017 – Present	PhD candidate, Institute of Organic Chemistry, Martin Luther University Halle-Wittenberg, Supervisor: Prof. Dr. Tschierske
Oct. 2014 – Dec. 2016	Master Degree, Polymer Materials Science Master Program, Martin Luther University Halle-Wittenberg, Supervisor: Prof. Dr. Tschierske
Mar. 2010 – Feb. 2012	Bachelor Degree, Polymer Science and Engineering, Sungkyunkwan University
Mar. 2003 – Feb. 2007	Associate Degree, Web Master Course, Yeojoo Institute of Technology

Work Experience

Mar. 2017 – Present	Organic chemist, Martin Luther University Halle-Wittenberg
Jan. 2012 – Nov. 2013	Chemical fiber engineer, Kolon Fashion Material, Inc
Dec. 2008 – Feb. 2010	Production worker, YoungJin Textile, Inc

Publications

May 2021	**O. Kwon,** X. Cai, W. Qu, F. Liu, J. Szydłowska, E. Gorecka, M. J. Han, D. K. Yoon, S. Poppe, C. Tschierske**,** *Adv. Funct. Mater.* **2021**, 2102271.

June 2021   **O. Kwon,** X. Cai, A. Saeed, F. Liu, S. Poppe, C. Tschierske, *Chem. Comm.* **2021**, d1cc01922h.

Conference contributions

Mar. 2018   **O. Kwon**, S. Poppe, M. Poppe, M. Wagner, C. Kerzig, F. Liu, C. Tschierske, *45th German Liquid Crystal Conference* **2018**, Luxemburg, Oral presentation.

July 2018   **O. Kwon**, F. Liu, C. Tschierske, *27th International Liquid Crystal Conference* **2018**, Kyoto, Poster presentation.

June 2019   **O. Kwon**, Y. Cao, F. Liu, C. Tschierske, *15th European Conference on Liquid Crystals* **2019**, Wroclaw, Oral presentation.

Other Experience

Aug. 2004 – Aug. 2006   Military service,
Ministry of national defense of the Republic of Korea

Awards

July 2018   Poster Award,
International Liquid Crystal Conference 2018

Aug. 2016   STIBET Degree Scholarship for International Students
Deutscher Akademischer Austauschdienst (DAAD)

Halle (Saale), den 15.06.2021

Ohjin Kwon

Eidesstattliche Erklärung

Hiermit erkläre ich an Eides statt, dass ich die vorliegende Arbeit selbständig und nur unter Verwendung der angegebenen Quellen und Hilfsmittel angefertigt habe. Wörtlich oder inhaltlich übernommene Stellen sind als solche gekennzeichnet.

Diese Arbeit wurde bisher an keiner anderen Universität oder Hochschule vorgelegt. Des Weiteren bestätige ich, dass ich mich zu keinem früheren Zeitpunkt um den Doktorgrad beworben habe.

Halle (Saale), den 15.06.2021

Ohjin Kwon